BioMed Research International

Animal Models of Human Pathology 2013

Guest Editors: Monica Fedele, Oreste Gualillo, and Andrea Vecchione

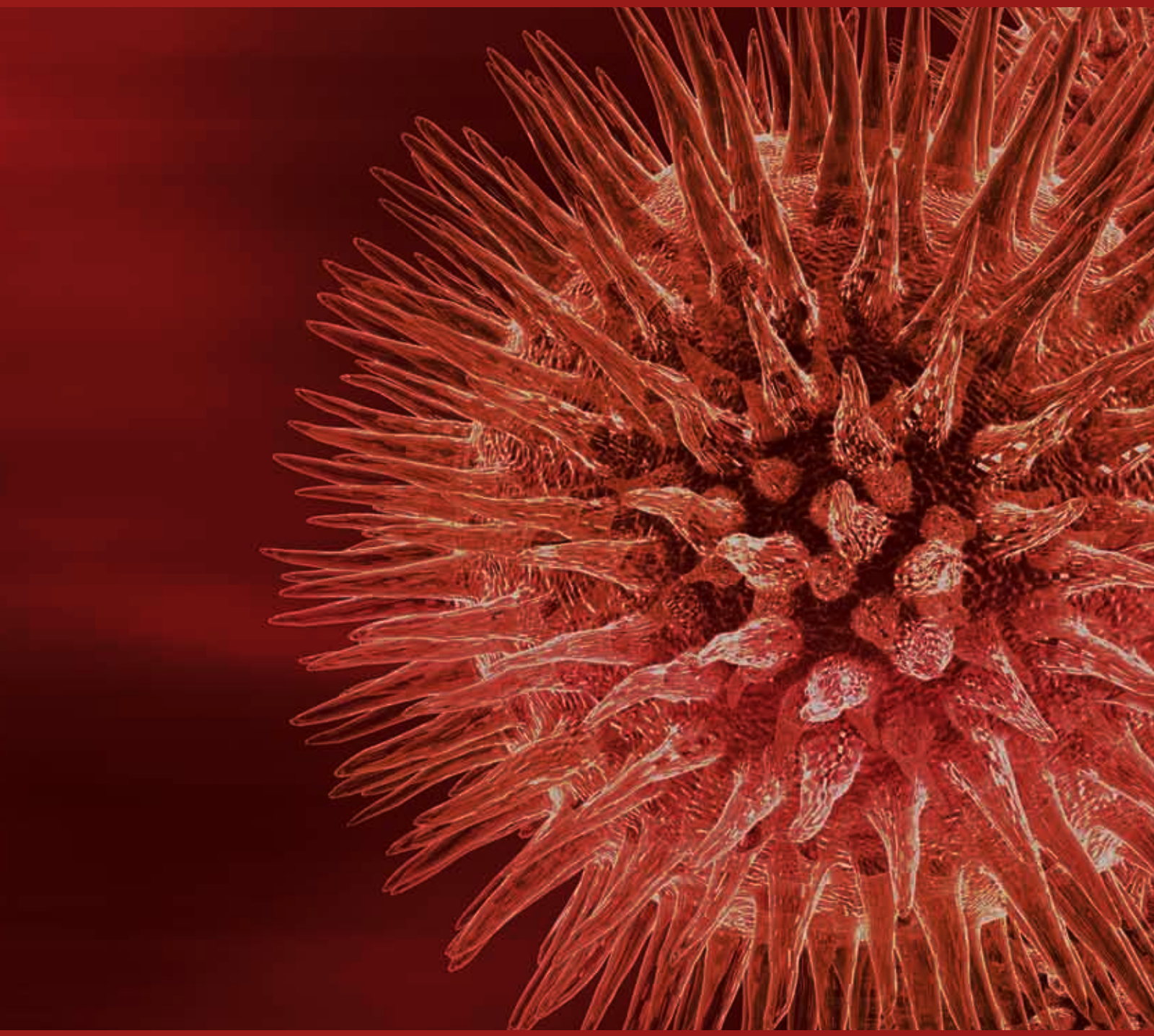

Animal Models of Human Pathology 2013

BioMed Research International

Animal Models of Human Pathology 2013

Guest Editors: Monica Fedele, Oreste Gualillo,
and Andrea Vecchione

Contents

Hindawi Publishing Corporation
BioMed Research International
Volume 2014, Article ID 861424, 2 pages
http://dx.doi.org/10.1155/2014/861424

Editorial

Animal Models of Human Pathology 2013

Monica Fedele,[1] Oreste Gualillo,[2] and Andrea Vecchione[3]

[1] *Institute of Experimental Endocrinology and Oncology (IEOS), CNR, 80131 Naples, Italy*
[2] *Santiago University Clinical Hospital IDIS, 15706 Santiago de Compostela, Spain*
[3] *Human Cancer Genetics Program, Division of Pathology, Comprehensive Cancer Center, The Ohio State University, Columbus, OH 43216, USA*

Correspondence should be addressed to Monica Fedele; mfedele@unina.it

Received 31 December 2013; Accepted 31 December 2013; Published 20 February 2014

Despite the success of biomedical engineering that made it possible to reproduce *in vitro* whole organ systems, biological processes are complex and cannot be replaced or properly simulated *in vitro* or *in silico*. Therefore, medicine still needs *in vivo* studies in whole organisms to ensure that the scientific demonstrations are as close as possible to human life.

In this special issue we collected six reviews and nine research articles describing studies using animals as disease models. In particular, you will read about the development and use of animal models for new therapeutic strategies, as well as for the development of the scientific understanding, related to different human pathologies, including cancer, autism, osteoarthritis, cardiovascular diseases, secondary lymphedema, metabolic syndrome, and abnormal scarring.

Several contributions focus on cancer: M. Lamberti et al. discuss about the different mechanisms of cardiotoxicity induced by antiblastic drugs assessed using animal models; S. Bimonte et al. review the role of morphine in primary tumor growth in animal models, focusing upon invasiveness and development of metastasis; the same group also presents a nice contribution showing, in an orthotopic mouse model of pancreatic cancer, that curcumin has a great potential in treatment of human pancreatic cancer, through the modulation of NF-κB pathway; M. Carvalho et al. review the role of T-lymphocytes in breast cancer, both in human and canine models; C. Calixto-Campos et al. describe a novel model of cancer pain for pathophysiological studies and pharmacological screening.

Four research articles are interested in the topic of cardiovascular diseases: N. E. Beltran et al. analyze the gastric tissue damage induced by ischemia, using a bioimpedance confocal endomicroscopy; G. Biondi-Zoccai et al. report the design and ensuing application of a novel porcine experimental model of closed-chest chronic ischemia, suitable for biomedical research, mimicking postmyocardial infarction heart failure; T. Spata et al. tackle the development of a platelet-induced coronary occlusion in a large animal, such as the sheep; Y. Cheng et al. show, in ovariectomized rats, that estradiol attenuates the decreased hippocampal neurogenesis produced by poststroke depression.

A new promising therapy for the autism is reviewed by A. C. Santini et al. who describe the treatment with the NMDAR glycine site against GLYX-13 for the therapy in autistic children, whereas the metabolic syndrome is the topic of V. Venkatesan et al. who evaluate the pancreatic features in a peculiar obese rat model (WNIN/Ob), showing that several cofounding factors in the pancreatic milieu take part to a profound state of inflammation in pancreas, leading to the onset of obesity/insulin resistance, which get worsened with age.

Finally, three papers describe animal models for three different human pathologies: B. F. Seo et al. review the current status of animal models of keloid and hypertrophic scarring; H. S. Park et al. show interesting data sets in creating an improved rodent hindlimb model of secondary lymphedema; M. Moreau et al. optimize the dog model of experimental osteoarthritis and show how the combination of this model with the dog model of naturally-occurring osteoartritis has the potential to be translated to the human condition, offering

the opportunity to investigate structural and functional benefits of disease modifying strategies.

We hope that the articles in this special issue will be of interest to the scientific community, providing new elements for the study and treatment of some human diseases.

Lastly, we would like to thank all the authors for their efforts and all the reviewers for their critical notes useful to improve the papers.

Monica Fedele
Oreste Gualillo
Andrea Vecchione

Review Article

Animal Models in Studies of Cardiotoxicity Side Effects from Antiblastic Drugs in Patients and Occupational Exposed Workers

Monica Lamberti,[1] Giancarlo Giovane,[1] Elpidio M. Garzillo,[1] Franca Avino,[2] Antonia Feola,[3] Stefania Porto,[3] Vincenzo Tombolini,[4,5] and Marina Di Domenico[3,6]

[1] *Department of Experimental Medicine, Section of Hygiene, Occupational Medicine and Forensic Medicine, Area of Occupational Medicine, Second University of Naples, Via L. De Crecchio 7, 80138 Naples, Italy*
[2] *National Institute for the Study and Treatment of Cancer, Foundation "G. Pascale", Via Mariano Semmola, 80131 Napoli, Italy*
[3] *Department of Biochemistry, Biophysics and General Pathology, Second University of Naples, Via L. De Crecchio 7, 80138 Naples, Italy*
[4] *Department of Radiology, Oncology and Pathological Anatomy Sciences, University of Rome, "La Sapienza", Piazzale Aldo Moro 5, 00185 Rome, Italy*
[5] *Spencer-Lorillard Foundation, University of Rome, "La Sapienza", Piazzale Aldo Moro 5, 00185 Rome, Italy*
[6] *Sbarro Institute for Cancer Research and Molecular Medicine, Center for Biotechnology, Building Suite 431, 1900 North 12th Street, Philadelphia, PA 19122, USA*

Correspondence should be addressed to Marina Di Domenico; marina.didomenico@unina2.it

Received 31 July 2013; Revised 29 October 2013; Accepted 7 November 2013; Published 19 February 2014

Academic Editor: Monica Fedele

Cardiotoxicity is an important side effect of cytotoxic drugs and may be a risk factor of long-term morbidity for both patients during therapy and also for staff exposed during the phases of manipulation of antiblastic drugs. The mechanism of cardiotoxicity studied in vitro and in vivo essentially concerns the formation of free radicals leading to oxidative stress, with apoptosis of cardiac cells or immunologic reactions, but other mechanisms may play a role in antiblastic-induced cardiotoxicity. Actually, some new cytotoxic drugs like trastuzumab and cyclopentenyl cytosine show cardiotoxic effects. In this report we discuss the different mechanisms of cardiotoxicity induced by antiblastic drugs assessed using animal models.

1. Introduction

Many anticancer drugs have, as side effect, the risk of severe cardiotoxicity by a cumulative, dose-dependent toxicity for both patients during therapy and also for healthcare workers during the phases of manipulation of antiblastic drugs (Table 1). In fact, several scientific studies have shown that in exposed workers the presence of several cardiotoxic drugs like doxorubicin, epirubicin, cyclophosphamide, and 5-fluourouracil was often identified in urine [1, 2]. Cardiotoxicity effects include small changes in blood pressure as well as arrhythmias and cardiomyopathy [3]. Mechanisms of cardiotoxicity by antiblastic drugs comprise cellular damage, with the formation of free oxygen radicals and the induction of immunogenic reactions with the presence of antigen presenting cells in the heart [4]. Early and late onset cardiac effects are reported; the first effect can be acute, subacute, or chronically progressive [5]. Acute or subacute cardiotoxicity effects of antiblastic drugs are rare; they occur during or immediately following infusion and are usually transient (e.g., electrocardiographic abnormalities such as nonspecific ST-T changes and QT prolongation, pericarditis-myocarditis syndrome, and ventricular dysfunction with congestive heart failure) [6]. The late effect generally starts within one year after the beginning of antiblastic therapy with chronic cardiac abnormalities and can progress to overt cardiac disease.

Table 1: Effects of antiblastic drugs on heart.

Drugs	CHF*	ECG change	Bradycardia	Ischemia	Arrythmias	Myo/pericarditis	Hypotension	Hypertension
Anthracyclines	++	++			+	+		
Trastuzumab	++							
5-FU	+	+		++	+			
Cisplatin		++		++				++
Bleomycin		+				+		
Cyclophosphamide	+++	++				++		
Methotrexate		+					+	
Doxorubicin	+	+						+
Taxoids (paclitaxel)		++	+	+	++		+	
Mitoxantrone					+		+	
TKIs (sorafenib, sunitinib, etc.)	+++							++

*CHF: congestive heart failure.

However a sudden atrial fibrillation was observed at the third week of chemotherapy administration in patients with myotonic dystrophy [7]. The clinical symptoms may include all signs of cardiomyopathy with electrophysiologic changes, decrease of left ventricular function, changes in exercise-stress capacity, and overt signs of congestive heart failure [8]. During administration of taxoids, as paclitaxel, combined or with cisplatin, various cardiac disturbances, like brady- and tachyarrhythmias, atrioventricular and bundle branch blocks, and cardiac ischemia were reported [9]. Evidence of hypotension is also described, probably correlated to hypersensitivity reaction. A combination of doxorubicin and paclitaxel administration in rats is correlated to an increase of myocardial necrosis compared with those treated with DOX alone [10].

5-Fluorouracil (5-FU) has direct toxic effects on vascular endothelium that involves endothelial nitric oxide synthase and leads to coronary spasms and endothelium-independent vasoconstriction via protein kinase C [11, 12]. Cardiotoxicity effects of 5-FU include cardiac arrhythmias, silent myocardial ischemia, angina, congestive heart failure, and even sudden death [13]. Various neoadjuvant chemoradiation therapies of squamous cell carcinoma are reported in the literature. They consisted of a combination between radiotherapy treatments and mitomycin-C and 5-fluorouracil [14]. A recent large meta-analysis shows that notwithstanding ongoing improvements in chemotherapy treatments, anthracyclines still represent a considerable risk of cardiotoxicity [15].

Other cytotoxic drugs that have been reported to be cardiotoxic are capecitabine, mitoxantrone, cisplatin, and newer drugs, like the monoclonal antibody trastuzumab or melphalan, fludarabine, mitomycin, busulfan, mechlorethamine and dacarbazine [16]. New generation of tyrosine kinase inhibitors (TKIs), like sorafenib and sunitinib, are associated with direct cardiotoxicity [17]. Since the antiblastic-induced cardiotoxicity is generally irreversible, it is crucial to detect the myocardial injury at its earliest possible stage; for this reason several experimental studies on cell cultures or animal models have been carried out.

Results on toxic effects of antiblastic drugs in various species were found extremely variable. Not only does the LD50 vary from species to species [18] but the qualitative character of the pharmacodynamic action of the drug also is equally varied [19]; therefore we can only partially compare precisely the dose and the toxic effects of antiblastic drugs between the model and the human animal model.

The major point of attack may be either the central nervous system or the heart. The rabbit is a representative animal showing cardiac responses [20], while in the dog [21] effects on central nervous system are the main response; rhesus monkey produces mixed-type responses [22]. However, despite the large number of investigations made, the results obtained in animal models are still hard to be translated to humans; therefore there is a critical need for continued translational research and animal studies to improve our understanding of the molecular mechanisms that underlie the cardiac dysfunction of antiblastic drugs.

2. Mechanisms of Cardiotoxicity

2.1. Role of Oxidative Stress. Antiblastic drugs, as most of xenobiotics, are generally metabolized through the NADPH-cytochrome P450 system in order to increase their solubility in urine. In particular, doxorubicin could be substrate of several oxidoreductases like NADH-dehydrogenase of mitochondrial complex I and various cytoplasmic oxidoreductases, including xanthine oxidase. The oxidoreductive reaction starts with a single electron transfer from NADPH to doxorubicin forming a semiquinone radical that is complexed with iron ion in a ferrous form; this complex is responsible for the oxygen reduction, thus producing a superoxide ion [8]. The superoxide free radicals generated in mitochondria have cardiolipin as a preferential target. Cardiolipin is a major phospholipid component of the inner mitochondrial membrane and is required for the activity of respiratory chain. It is rich in polyunsaturated fatty acids and is particularly susceptible to peroxidative injury [23]; furthermore, evidence has been reported showing a strong affinity of doxorubicin for cardiolipin [24]. The drug-phospholipid complex formation leads to an inhibition of mitochondrial enzymes involved in oxidative phosphorylation. The mitochondrial membrane damage can also generate the inactivation of key transporters involved in ion homeostasis. Thus, the well-known cardiotoxicity of anthracycline could simply explain considering the fact that the cardiac tissue is rich in mitochondria. However, other factors are involved in anthracycline cardiotoxicity among which the relative lower amount of antioxidant defenses of heart compared with other tissues. It should be also considered that when the levels of free radicals increase, the apoptotic cascade is activated by cytochrome c being released from the damaged mitochondria, thus triggering apoptosis. Vásquez-Vivar et al. [25] have shown that doxorubicin binds to the reductase domain of endothelial nitric oxide synthase causing an increase in superoxide and a decrease in nitric oxide formation.

2.2. Role of Cytokines. Anthracyclines produce a drug-related systemic inflammation which has been found to be mediated by interleukins [26]. In particular, interleukin-1beta (IL-1beta) has been implicated in this mechanism. Doxorubicin induces a systemic increase in IL-1beta and other inflammatory cytokines, chemokines, and growth factors including TNF-alpha, IL-6, CXCL1/Gro-alpha, CCL2/MCP-1, granulocyte colony stimulating factor, and CXCL10/IP-10. Studies on mice deficient in IL-1 receptor demonstrate that IL-1 signaling plays a role in the increase of IL-6 and GCSF induced by doxorubicin. The IL-1beta release required the expression of caspase-1, NLRP3, and the adaptor protein ASC indicating that inflammation is mediated by the NLRP3 inflammasome. The molecular mechanisms by which anthracyclines trigger IL-1beta release are not completely understood; however the undesirable consequences of anthracyclines due to their inflammatory activity that complicate chemotherapy may be reduced by suppressing the actions of IL-1beta. It has been also showed that the administration of anthracyclines to mice having cancer stimulates the secretion of tumor necrosis factor alpha (TNF-alpha) in neoplastic tissue [27].

The antineoplastic effects of anthracyclines could be partially due to a local immune response that involves several distinct subsets of T lymphocytes and dendritic cells. However, the blockage of the TNF-alpha/TNF receptor system did not influence the antineoplastic effects of doxorubicin against MCA205 fibrosarcomas growing in C57BL/6 mice, F244 sarcomas developing in 129/Sv hosts, and H2N100 mammary carcinomas in BALB/c mice. These findings show that, in contrast to other cytokines, TNF-alpha is not required to elicit anticancer immune responses. Aluise and coworkers [28] demonstrate that doxorubicin oxidizes plasma APOA1 that, in turn, enhances macrophage TNF-alpha release contributing to a possible TNF-alpha-mediated toxicity. Furthermore they produced evidence that reducing agent 2-mercaptoethane sulfonate blocks this mechanism suggesting that this antioxidant could reduce systemic side effects of doxorubicin.

Doxorubicin has been also showed to be a potent inducer of apoptosis in both cardiomyocytes H9c2 and osteosarcoma tumor cells U2OS; however, caspase activation and kinetics take place with significant differences between the two cell lines [29]. In fact, apoptosis is accompanied by relevant changes in levels of TNF-alpha receptor in H9c2 cardiomyocytes but not in U2OS cells. Moreover, treatment with exogenous TNF-alpha strongly increases the apoptotic effect of doxorubicin in H9c2 cardiomyocytes but not in U2OS cells. The function of TNF receptors I and II is differently affected by doxorubicin which induces in H9c2 cells an increase in the death domain-containing TNFR-1 protein levels and a decrease in the survival domain-containing TNFR-2 protein levels. These findings demonstrate a balance between proapoptotic and antiapoptotic signaling pathways in the cardiomyocyte survival after TNF stimulation showing a relevant role of TNF-alpha receptor-mediated signaling in cardiotoxicity induced by anthracyclines.

2.3. Calcium Homeostasis. Another aspect to be considered is the effect of anthracyclines on the role played by mitochondria in calcium homeostasis [30]. In fact the drug-induced malfunction of transporters involved in ion homeostasis can lead to a loss of mitochondrial calcium loading capacity which is observed in several in vitro and in vivo models [31, 32]. Alterations in calcium transport can lead to tissue damage impairing the cardiac contraction. In vitro experiments demonstrate that doxorubicin treatment produces an irreversible decrease in mitochondrial calcium loading capacity. Moreover, anthracyclines could stimulate "in vitro" the release of calcium from isolated sarcoplasmic reticulum. In rodent models a decrease of calcium loading capacity together with alterations in cardiac mitochondrial function has been observed [33]. Verapamil, a calcium blocking agent, shows a protective effect against doxorubicin cardiotoxicity [34]. The antagonizing effect could be due to the ability of verapamil to inhibit the intracellular calcium overload. Contradictory results, however, arise from experiments showing an increase of cardiotoxicity when doxorubicin was given in combination with verapamil [35]. A possible explanation for this discrepancy could be due to the capacity of verapamil to inhibit the function of P-glycoprotein and therefore may increase intracellular cytotoxic drug concentrations. Other authors found that the additive cardiotoxicity of verapamil was due to its selective inhibition of cardiac actin gene [36], an effect which was also demonstrated with doxorubicin alone. Tagliaferri and coworkers [37] found side effects on heart electric conductance following infusion of high dose verapamil incorporated into cytotoxic chemotherapy. Several symptoms like premature ventricular beats, and mild and transient hypotension were observed. Hypokalemia was also detected probably as a consequence of transient activation of the renin-angiotensin system.

2.4. Metabolite Theory. To overcome the cardiotoxic effect of anthracyclines the use of antioxidants have been suggested [38, 39], however antioxidants has proven to be useful in delaying or preventing chronic cardiotoxicity in rodents [40] but not in dogs [41] or sheep [42]. For patients, contradictory results have been reported showing positive [43, 44] or no [45] effect. Taking into account these discrepancies, a new hypothesis has been made on the evidence that chronic cardiomyopathy develops after conversion of doxorubicin to the corresponding secondary alcohol metabolite doxorubicinol [46]. This metabolite is formed after the reduction of carbonyl group on the C-13 side chain; the reaction is probably mediated by cytoplasmic oxidoreductases [47]. The secondary alcohol metabolite production is suggested by several lines of evidence: (i) in rodents, after anthracycline treatment, a decline of cardiac function usually is observed when alcohol metabolite reachs its maximum levels in the heart [48]; (ii) overexpression of human carbonyl reductase in transgenic mice heart produces an accelerated development of cardiomyopathy [49]; (iii) modified anthracyclines with resistance to reduction of carbonyl moiety produce a less severe chronic cardiotoxicity in rats [50]. Due to their chemical structures, secondary alcohol metabolites are considerably less effective than their parent drugs at producing oxygen radicals, probably for their reduced affinity for quinone reductases [51]. However, secondary alcohol metabolites are several times more potent at inactivating membrane ATPases [52] and cytoplasmic aconitase/iron regulatory protein 1 [53]. The evidence that secondary alcohol metabolites can be involved in chronic cardiomyopathy suggested the hypothesis that the clinical use of anthracyclines could be improved by reducing their conversion to secondary alcohol. This goal could be reached in at least two ways: (i) a chemical modification of drugs to produce less alcohol metabolites and (ii) a development of inhibitors of reductases which are responsible for transformation of ketone/aldehyde moiety to alcohol. Obviously the investigations on the inhibitors have to consider possible differences in specificity and affinity between the reductases of humans and those of laboratory animals used to verify the protective efficacy of these inhibitors.

Recently [54] an effect of glutamine against oxidative damage due to doxorubicin has been reported. The free radicals produced by doxorubicin result in a decrease of

glutathione (GSH) and a depletion of superoxide dismutase in cardiac muscle [55]. It seems that glutamine has a protective role in the myocardial cell by upregulating GSH and also by inducing the synthesis of heat shock protein 72 [56]. This protein is known to protect the myocardium against hypoxic/ischemic injury. Furthermore, the induction of heat shock protein 27 has been shown to be protective against cardiac injury induced by doxorubicin [57]. Glutamine also appears to be a potent inducer of myocardial HSP 72 in an in vivo rat model. Recently evidence has been produced indicating that glutamine can preserve the level of high-energy phosphate in myocardial tissue and prevent the stress-dependent accumulation of lactate, including ischemia/reperfusion injury [58].

It is now well assessed that anthracyclines possess the ability to bind covalently to DNA; the bind is strictly dependent on the availability of formaldehyde [59]. In fact, formaldehyde supplies the carbon required for the N–C–N linkage necessary for the adduct formation with DNA. The resulting adduct is further stabilized by the formation of hydrogen bond with the complementary strand of DNA to crosslink the DNA duplex resulting in stabilization of the local region of DNA.

Doxorubicin is also known to intercalate itself into the DNA, with the inhibition of both DNA and RNA polymerase, thus blocking DNA replication and RNA transcription [60]. Recently it has been reported that doxorubicin is capable of intercalating with not only nuclear DNA but also mitochondrial DNA [61].

2.5. Tyrosine Kinase Inhibitors. Recent years have seen significant progress in cancer therapy through the development of "targeted therapies", in particular those using TKIs directed against certain tyrosine kinases whose abnormal activity triggers cancer development and progression through cell proliferation and neoangiogenesis. Multikinase inhibitors have been widely used alone and in combination with other drugs in cancer therapies for different tumor types [62, 63]. Unfortunately, due to their large spectra of action, these inhibitors are also associated with toxicity to the heart [64, 65]. For example, sunitinib inhibits a number of growth factor receptors regulating both tumor cell proliferation/survival and tumor angiogenesis including vascular endothelial growth factor receptors, platelet-derived growth factor receptors α and β, c-Kit, FLT3, CSF1R, and RET [66]. However, care should be taken when cardiotoxicity in humans and animal models is compared. In fact it has been reported [67] that while the TKIs pazopanib, sunitinib and sorafenib, showed cardiotoxic effects in humans, studies in animal model failed to show cardiac toxicities for all of these TKIs. TKIs can be divided into two general classes: (i) humanized monoclonal antibodies directed against the tyrosine kinase receptor or their ligands and (ii) small molecules interacting with kinases inhibiting their activity. The use of both classes of TKIs revealed a relatively high rate of adverse cardiac events in the clinic, with systolic dysfunction and resultant heart failure as one of the most common and important side effects. TKIs are frequently used for the treatment of renal-cell carcinoma, gastrointestinal stromal tumors, and other tumor types in which these drugs are still under investigation. It seems that TKIs have as target AMPK which is a critical kinase controlling the balance between ATP and AMP levels [66]. Following conditions of energy stress, AMPK may act as a metabolic switch, increasing energy generation and inhibiting anabolic pathways. Studies on animals treated with sunitinib suggest that together with a potential misregulation in AMPK signaling a possible role is played by mitochondrial dysfunction leading to alterations in cardiac energy homeostasis. Most probably sunitinib induces a cardiac dysfunction that could be dependent on the simultaneous inhibition of multiple signaling pathways all of which are necessary for the preservation of cardiac function and which could play a pivotal role in the increased cardiac stress such as hypertension [68].

3. Other Cardiotoxicity Mechanisms

3.1. Taxoids. Paclitaxel is formulated in a cremophor EL vehicle to enhance the drug solubility and it is suggested that the vehicle and not the cytotoxic drug itself is responsible for the cardiac disturbances. However, the cardiac rhythm disturbances are not reported with use of other drugs containing cremophor EL such as cyclosporine [69, 70]. The possible mechanism by which cremophor EL would cause cardiotoxicity is massive histamine release. Indeed, stimulation of histamine receptors in cardiac tissue in animal studies has resulted in conduction disturbances and arrhythmias. An alternative explanation for paclitaxel induced cardiotoxicity could be the induction of cardiac muscle damage by affecting subcellular organelles. Enhanced cardiac toxicity has been found in combined therapy of paclitaxel and doxorubicin. A similar effect has been shown for epirubicin. Docetaxel shows no increase in cardiac toxicity when combined with doxorubicin.

3.2. Cyclophosphamide and Ifosfamide. High dose cyclophosphamide is used in transplant regimens and is associated with acute cardiotoxicity such as cardiac decompensation as well as fatal cardiomyopathy. Acute reversible decrease in systolic function has been described. Ifosfamide cardiotoxicity is reported in only a single study. The pathogenesis is not fully understood but an increase in free oxygen radicals seems to play a role in oxazaphosphorine induced cardiotoxicity. This increase would be mediated by elevated intracellular levels of the actual cytotoxic metabolite phosphoramide mustard [71].

3.3. Cisplatin. Several factors have been suggested to be involved like vascular damage, alterations in platelet aggregation, and hypomagnesemia [72]. In experiments on animal platelets, cisplatin was able to trigger platelet aggregation and/or enhance thromboxane formation by platelets. Activation of an arachidonic pathway in platelets by cisplatin seemed to be involved [73].

3.4. Trastuzumab. Trastuzumab is a monoclonal antibody directed against the HER2 receptor protein on breast cancer

cells and it has been used alone or in combination with other chemotherapeutic agents. Cardiac toxicity associated to trastuzumab seems to be similar with the congestive heart failure observed with anthracycline therapy [74].

4. Concluding Remarks

In the context of modern cancer chemotherapeutics, cancer survivors are living longer and being exposed to potential comorbidities related to noncancer side effects of such treatments as cardiotoxicity. These same toxic effects can also be detected in healthcare worker exposed during the manipulation of chemotherapy because several studies have identified the presence of drugs such as doxorubicin, epirubicin, cyclophosphamide, and 5-fluorouracil in these subjects. These side effects can be cause of severe morbidity and even mortality, so knowledge about their incidence and mechanism is important. The authors have reevaluated in the different articles available in the scientific literature the possible causes of cardiotoxicity due to administration of antiblastic drugs by using animal models. In fact, animal models have historically been unable to predict human response to drugs and this is the basis for their widespread use in human toxicity testing. The mechanisms of action described in the literature are different, such as, the oxidative stress for doxorubicin and misregulation in AMPK signaling by TKI. These results disclose a new scenario for prevention of heart complications.

We are now, in fact, able to identify specific early biomarker of chemotherapy cardiotoxicity, discovered on animal models, and to develop supportive therapies to reduce or eliminate the appearance of these side effects in humans.

Conflict of Interests

The authors declare that there is no conflict of interests regarding the publication of this paper.

References

[1] T. H. Connor, G. DeBord, J. R. Pretty et al., "Evaluation of antineoplastic drug exposure of health care workers at three university-based US cancer centers," *Journal of Occupational and Environmental Medicine*, vol. 52, no. 10, pp. 1019–1027, 2010.

[2] M. Pieri, L. Castiglia, P. Basilicata, N. Sannolo, A. Acampora, and N. Miraglia, "Biological monitoring of nurses exposed to doxorubicin and epirubicin by a validated liquid chromatography/fluorescence detection method," *The Annals of Occupational Hygiene*, vol. 54, no. 4, pp. 368–376, 2010.

[3] K. J. Schimmel, D. J. Richel, R. B. van den Brink, and H. J. Guchelaar, "Cardiotoxicity of cytotoxic drugs," *Cancer Treatment Reviews*, vol. 30, no. 2, pp. 181–191, 2004.

[4] Y. J. Kang, "Molecular and cellular mechanisms of cardiotoxicity," *Environmental Health Perspectives*, vol. 109, supplement 1, pp. 27–34, 2001.

[5] H. Broder, R. A. Gottlieb, and N. E. Lepor, "Chemotherapy and cardiotoxicity," *Reviews in Cardiovascular Medicine*, vol. 9, no. 2, pp. 75–83, 2008.

[6] C. Dechant, M. Baur, R. Bock et al., "Acute reversible heart failure caused by coronary vasoconstriction due to continuous 5-fluorouracil combination chemotherapy," *Case Reports in Oncology*, vol. 5, no. 2, pp. 296–301, 2012.

[7] L. Montella, M. Caraglia, R. Addeo et al., "Atrial fibrillation following chemotherapy for stage IIIE diffuse large B-cell gastric lymphoma in a patient with myotonic dystrophy (Steinert's disease)," *Annals of Hematology*, vol. 84, no. 3, pp. 192–193, 2005.

[8] F. S. Carvalho, A. Burgeiro, R. Garcia, A. J. Moreno, R. A. Carvalho, and P. J. Oliveira, "Doxorubicin-induced cardiotoxicity: from bioenergetic failure and cell death to cardiomyopathy," *Medicinal Research Reviews*, vol. 34, no. 1, pp. 106–135, 2014.

[9] J. B. Vermorken, "The integration of paclitaxel and new platinum compounds in the treatment of advanced ovarian cancer," *International Journal of Gynecological Cancer*, vol. 11, supplement s1, pp. 21–30, 2001.

[10] S. Y. Saad, T. A. Najjar, and M. Alashari, "Cardiotoxicity of doxorubicin/paclitaxel combination in rats: effect of sequence and timing of administration," *Journal of Biochemical and Molecular Toxicology*, vol. 18, no. 2, pp. 78–86, 2004.

[11] M. Lamberti, M. Caraglia, S. Zappavigna et al., "Evaluation in vitro of the cardiotoxic effects of 5-fluorouracil for the prevention of cardiovascular damage in health workers occupationally exposed," *Giornale Italiano di Medicina del Lavoro ed Ergonomia*, vol. 33, no. 3, supplement, pp. 298–302, 2011.

[12] M. Lamberti, S. Porto, M. Marra et al., "5-Fluorouracil induces apoptosis in rat cardiocytes through intracellular oxidative stress," *Journal of Experimental & Clinical Cancer Research*, vol. 31, article 60, 2012.

[13] B. B. Hasinoff, "The cardiotoxicity and myocyte damage caused by small molecule anticancer tyrosine kinase inhibitors is correlated with lack of target specificity," *Toxicology and Applied Pharmacology*, vol. 244, no. 2, pp. 190–195, 2010.

[14] M. Indinnimeo, A. Impagnatiello, G. D'Ettorre et al., "Buschke-Löwenstein tumor with squamous cell carcinoma treated with chemo-radiation therapy and local surgical excision: report of three cases," *World Journal of Surgical Oncology*, vol. 11, article 231, 2013.

[15] M. Lotrionte, G. Biondi-Zoccai, A. Abbate et al., "Review and meta-analysis of incidence and clinical predictors of anthracycline cardiotoxicity," *The American Journal of Cardiology*, vol. 112, no. 12, pp. 1980–1984, 2013.

[16] V. Brower, "Cardiotoxicity debated for anthracyclines and trastuzumab in breast cancer," *Journal of the National Cancer Institute*, vol. 105, no. 12, pp. 835–836, 2013.

[17] V. Chintalgattu, M. L. Rees, J. C. Culver et al., "Coronary microvascular pericytes are the cellular target of sunitinib malate-induced cardiotoxicity," *Science Translational Medicine*, vol. 5, no. 187, p. 187ra69, 2013.

[18] M. Wasowska, I. Oszczapowicz, J. Wietrzyk et al., "Influence of the structure of new anthracycline antibiotics on their biological properties," *Anticancer Research*, vol. 25, no. 3, pp. 2043–2048, 2005.

[19] R. Danesi, S. Fogli, A. Gennari, P. Conte, and M. Del Tacca, "Pharmacokinetic-pharmacodynamic relationships of the anthracycline anticancer drugs," *Clinical Pharmacokinetics*, vol. 41, no. 6, pp. 431–444, 2002.

[20] E. Jirkovský, O. Lenčová-Popelová, M. Hroch et al., "Early and delayed cardioprotective intervention with dexrazoxane each show different potential for prevention of chronic anthracycline cardiotoxicity in rabbits," *Toxicology*, vol. 311, no. 3, pp. 191–204, 2013.

[21] S. Gillings, J. Johnson, A. Fulmer, and M. Hauck, "Effect of a 1-hour IV infusion of doxorubicin on the development of cardiotoxicity in dogs as evaluated by electrocardiography and echocardiography," *Veterinary Therapeutics*, vol. 10, no. 1-2, pp. 46–58, 2009.

[22] D. Beulz-Riche, J. Robert, C. Menard, and D. Ratanasavanh, "Metabolism of methoxymorpholino-doxorubicin in rat, dog and monkey liver microsomes: comparison with human microsomes," *Fundamental and Clinical Pharmacology*, vol. 15, no. 6, pp. 373–378, 2001.

[23] M. Tokarska-Schlattner, M. Dolder, I. Gerber, O. Speer, T. Wallimann, and U. Schlattner, "Reduced creatine-stimulated respiration in doxorubicin challenged mitochondria: particular sensitivity of the heart," *Biochimica et Biophysica Acta*, vol. 1767, no. 11, pp. 1276–1284, 2007.

[24] M. A. Parker, V. King, and K. P. Howard, "Nuclear magnetic resonance study of doxorubicin binding to cardiolipin containing magnetically oriented phospholipid bilayers," *Biochimica et Biophysica Acta*, vol. 1514, no. 2, pp. 206–216, 2001.

[25] J. Vásquez-Vivar, P. Martasek, N. Hogg, B. S. Masters, K. A. Pritchard Jr., and B. Kalyanaraman, "Endothelial nitric oxide synthase-dependent superoxide generation from adriamycin," *Biochemistry*, vol. 36, no. 38, pp. 11293–11297, 1997.

[26] K. A. Sauter, L. J. Wood, J. Wong, M. Iordanov, and B. E. Magun, "Doxorubicin and daunorubicin induce processing and release of interleukin-1β through activation of the NLRP3 inflammasome," *Cancer Biology and Therapy*, vol. 11, no. 12, pp. 1008–1016, 2011.

[27] Y. Ma, T. Yamazaki, H. Yang et al., "Tumor necrosis factor is dispensable for the success of immunogenic anticancer chemotherapy," *Oncoimmunology*, vol. 2, no. 6, Article ID e24786, 2013.

[28] C. D. Aluise, S. Miriyala, T. Noel et al., "2-Mercaptoethane sulfonate prevents doxorubicin-induced plasma protein oxidation and TNF-α release: implications for the reactive oxygen species-mediated mechanisms of chemobrain," *Free Radical Biology and Medicine*, vol. 50, no. 11, pp. 1630–1638, 2011.

[29] E. Chiosi, A. Spina, A. Sorrentino et al., "Change in TNF-α receptor expression is a relevant event in doxorubicin-induced H9c2 cardiomyocyte cell death," *Journal of Interferon and Cytokine Research*, vol. 27, no. 7, pp. 589–597, 2007.

[30] H. A. Gambliel, B. E. Burke, B. J. Cusack et al., "Doxorubicin and C-13 deoxydoxorubicin effects on ryanodine receptor gene expression," *Biochemical and Biophysical Research Communications*, vol. 291, no. 3, pp. 433–438, 2002.

[31] M. Verma, N. Shulga, and J. G. Pastorino, "Sirtuin-4 modulates sensitivity to induction of the mitochondrial permeability transition pore," *Biochimica et Biophysica Acta*, vol. 1827, no. 1, pp. 38–49, 2013.

[32] A. Ascensão, J. Lumini-Oliveira, N. G. Machado et al., "Acute exercise protects against calcium-induced cardiac mitochondrial permeability transition pore opening in doxorubicin-treated rats," *Clinical Science*, vol. 120, no. 1, pp. 37–49, 2011.

[33] C. Richard, S. Ghibu, S. Delemasure-Chalumeau et al., "Oxidative stress and myocardial gene alterations associated with doxorubicin-induced cardiotoxicity in rats persist for 2 months after treatment cessation," *The Journal of Pharmacology and Experimental Therapeutics*, vol. 339, no. 3, pp. 807–814, 2011.

[34] F. Rossi, W. Filippelli, S. Russo, A. Filippelli, and L. Berrino, "Cardiotoxicity of doxorubicin: effects of drugs inhibiting the release of vasoactive substances," *Pharmacology and Toxicology*, vol. 75, no. 2, pp. 99–107, 1994.

[35] T. Budde, J. Haney, S. Bien et al., "Acute exposure to doxorubicin results in increased cardiac P-glycoprotein expression," *Journal of Pharmaceutical Sciences*, vol. 100, no. 9, pp. 3951–3958, 2011.

[36] H. Akimoto, N. A. Bruno, D. L. Slate, M. E. Billingham, S. V. Torti, and F. M. Torti, "Effect of verapamil on doxorubicin cardiotoxicity: altered muscle gene expression in cultured neonatal rat cardiomyocytes," *Cancer Research*, vol. 53, no. 19, pp. 4658–4664, 1993.

[37] P. Tagliaferri, P. Correale, M. Mottola et al., "Cardiovascular monitoring of drug-resistant lymphoma patients treated with epoch chemotherapy plus high dose verapamil in continuous-infusion," *Oncology Reports*, vol. 1, no. 2, pp. 341–344, 1994.

[38] H. Jacobs, R. Peters, G. J. den Hartog, W. J. van der Vijgh, A. Bast, and G. R. Haenen, "Identification of the metabolites of the antioxidant flavonoid 7-mono-O-(β-hydroxyethyl)-rutoside in mice," *Drug Metabolism and Disposition*, vol. 39, no. 5, pp. 750–756, 2011.

[39] S. Arunachalam, S. Y. Kim, S. H. Lee et al., "Davallialactone protects against adriamycin-induced cardiotoxicity *in vitro* and *in vivo*," *Journal of Natural Medicines*, vol. 66, no. 1, pp. 149–157, 2012.

[40] A. M. Osman, S. E. Al-Harthi, O. M. Alarabi et al., "Chemosensetizing and cardioprotective effects of resveratrol in doxorubicin-treated animals," *Cancer Cell International*, vol. 13, article 52, 2013.

[41] E. H. Herman, V. J. Ferrans, C. E. Myers, and J. F. Van Vleet, "Comparison of the effectiveness of (+/−)-1,2-bis(3,5-dioxopiperazinyl-1-yl)propane (ICRF-187) and N-acetylcysteine in preventing chronic doxorubicin cardiotoxicity in beagles," *Cancer Research*, vol. 45, no. 1, pp. 276–281, 1985.

[42] A. Carbone, P. J. Psaltis, A. J. Nelson et al., "Dietary omega-3 supplementation exacerbates left ventricular dysfunction in an ovine model of anthracycline-induced cardiotoxicity," *Journal of Cardiac Failure*, vol. 18, no. 6, pp. 502–511, 2012.

[43] A. Bast, G. R. Haenen, A. M. Bruynzeel, and W. J. van der Vijgh, "Protection by flavonoids against anthracycline cardiotoxicity: from chemistry to clinical trials," *Cardiovascular Toxicology*, vol. 7, no. 2, pp. 154–159, 2007.

[44] C. D. Aluise, D. St Clair, M. Vore, and D. A. Butterfield, "*In vivo* amelioration of adriamycin induced oxidative stress in plasma by gamma-glutamylcysteine ethyl ester (GCEE)," *Cancer Letters*, vol. 282, no. 1, pp. 25–29, 2009.

[45] C. Myers, R. Bonow, S. Palmeri et al., "A randomized controlled trial assessing the prevention of doxorubicin cardiomyopathy by N-acetylcysteine," *Seminars in Oncology*, vol. 10, no. 1, supplement 1, pp. 53–55, 1983.

[46] G. Minotti, S. Licata, A. Saponiero et al., "Anthracycline metabolism and toxicity in human myocardium: comparisons between doxorubicin, epirubicin, and a novel disaccharide analogue with a reduced level of formation and [4Fe-4S] reactivity of its secondary alcohol metabolite," *Chemical Research in Toxicology*, vol. 13, no. 12, pp. 1336–1341, 2000.

[47] O. S. Bains, M. J. Karkling, T. A. Grigliatti, R. E. Reid, and K. W. Riggs, "Two nonsynonymous single nucleotide polymorphisms of human carbonyl reductase 1 demonstrate reduced *in vitro* metabolism of daunorubicin and doxorubicin," *Drug Metabolism and Disposition*, vol. 37, no. 5, pp. 1107–1114, 2009.

[48] P. S. Mushlin, B. J. Cusack, R. J. Boucek Jr., T. Andrejuk, X. Li, and R. D. Olson, "Time-related increases in cardiac concentrations of doxorubicin could interact with doxorubicin to depress myocardial contractile function," *British Journal of Pharmacology*, vol. 110, no. 3, pp. 975–982, 1993.

[49] G. L. Forrest, B. Gonzalez, W. Tseng, X. Li, and J. Mann, "Human carbonyl reductase overexpression in the heart advances the development of doxorubicin-induced cardiotoxicity in transgenic mice," *Cancer Research*, vol. 60, no. 18, pp. 5158–5164, 2000.

[50] R. Cirillo, G. Sacco, S. Venturella, J. Brightwell, A. Giachetti, and S. Manzini, "Comparison of doxorubicin-and MEN 10755-induced long-term progressive cardiotoxicity in the rat," *Journal of Cardiovascular Pharmacology*, vol. 35, no. 1, pp. 100–108, 2000.

[51] P. G. Gervasi, M. R. Agrillo, A. Lippi, N. Bernardini, R. Danesi, and M. Del Tacca, "Superoxide anion production by doxorubicin analogs in heart sarcosomes and by mitochondrial NADH dehydrogenase," *Research Communications in Chemical Pathology and Pharmacology*, vol. 67, no. 1, pp. 101–115, 1990.

[52] R. J. Boucek Jr., R. D. Olson, D. E. Brenner, E. M. Ogunbunmi, M. Inui, and S. Fleischer, "The major metabolite of doxorubicin is a potent inhibitor of membrane-associated ion pumps: a correlative study of cardiac muscle with isolated membrane fractions," *The Journal of Biological Chemistry*, vol. 262, no. 33, pp. 15851–15856, 1987.

[53] G. Minotti, R. Ronchi, E. Salvatorelli, P. Menna, and G. Cairo, "Doxorubicin irreversibly inactivates iron regulatory proteins 1 and 2 in cardiomyocytes: evidence for distinct metabolic pathways and implications for iron-mediated cardiotoxicity of antitumor therapy," *Cancer Research*, vol. 61, no. 23, pp. 8422–8428, 2001.

[54] K. Gaurav, R. K. Goel, M. Shukla, and M. Pandey, "Glutamine: a novel approach to chemotherapy-induced toxicity," *Indian Journal of Medical and Paediatric Oncology*, vol. 33, no. 1, pp. 13–20, 2012.

[55] S. I. Glushkov, S. A. Kutsenko, T. M. Novikova, and V. V. Axenov, "Glutathione metabolism in rat cardiac tissues in acute doxorubicin-induced intoxication," *Voprosy Onkologii*, vol. 51, no. 1, pp. 108–112, 2005.

[56] H. Xue, D. Slavov, and P. E. Wischmeyer, "Glutamine-mediated dual regulation of heat shock transcription factor-1 activation and expression," *The Journal of Biological Chemistry*, vol. 287, no. 48, pp. 40400–40413, 2012.

[57] L. Liu, X.-J. Zhang, B. Qian, X.-Y. Min, and Y.-L. Cheng, "Heat shock protein 27 attenuated doxorubicin-induced myocardial damage by reducing cardiomyocyte apoptosis, mitochondria damage and protein carbonylation," *Zhonghua Xin Xue Guan Bing Za Zhi*, vol. 36, no. 11, pp. 1021–1026, 2008.

[58] P. E. Wischmeyer, D. Jayakar, U. Williams et al., "Single dose of glutamine enhances myocardial tissue metabolism, glutathione content, and improves myocardial function after ischemia-reperfusion injury," *Journal of Parenteral and Enteral Nutrition*, vol. 27, no. 6, pp. 396–403, 2003.

[59] R. A. Forrest, L. P. Swift, B. J. Evison et al., "The hydroxyl epimer of doxorubicin controls the rate of formation of cytotoxic anthracycline-DNA adducts," *Cancer Chemotherapy and Pharmacology*, vol. 71, no. 3, pp. 809–816, 2013.

[60] O. Tacar, P. Sriamornsak, and C. R. Dass, "Doxorubicin: an update on anticancer molecular action, toxicity and novel drug delivery systems," *Journal of Pharmacy and Pharmacology*, vol. 65, no. 2, pp. 157–170, 2013.

[61] N. Ashley and J. Poulton, "Mitochondrial DNA is a direct target of anti-cancer anthracycline drugs," *Biochemical and Biophysical Research Communications*, vol. 378, no. 3, pp. 450–455, 2009.

[62] C. F. Greineder, S. Kohnstamm, and B. Ky, "Heart failure associated with sunitinib: lessons learned from animal models," *Current Hypertension Reports*, vol. 13, no. 6, pp. 436–441, 2011.

[63] M. Caraglia, G. Giuberti, M. Marra et al., "Oxidative stress and ERK1/2 phosphorylation as predictors of outcome in hepatocellular carcinoma patients treated with sorafenib plus octreotide LAR," *Cell Death and Disease*, vol. 2, no. 4, article e150, 2011.

[64] A. Y. Khakoo, P. P. Liu, T. Force et al., "Cardiotoxicity due to cancer therapy," *Texas Heart Institute Journal*, vol. 38, no. 3, pp. 253–256, 2011.

[65] T. Force, D. S. Krause, and R. A. Van Etten, "Molecular mechanisms of cardiotoxicity of tyrosine kinase inhibition," *Nature Reviews Cancer*, vol. 7, no. 5, pp. 332–344, 2007.

[66] R. Kerkela, K. C. Woulfe, J.-B. Durand et al., "Sunitinib-induced cardiotoxicity is mediated by off-target inhibition of AMP-activated protein kinase," *Clinical and Translational Science*, vol. 2, no. 1, pp. 15–25, 2009.

[67] B. Yang and T. Papoian, "Tyrosine kinase inhibitor (TKI)-induced cardiotoxicity: approaches to narrow the gaps between preclinical safety evaluation and clinical outcome," *Journal of Applied Toxicology*, vol. 32, no. 12, pp. 945–951, 2012.

[68] D. Hannani, C. Locher, T. Yamazaki et al., "Contribution of humoral immune responses to the antitumor effects mediated by anthracyclines," *Cell Death and Differentiation*, vol. 21, no. 1, pp. 50–58, 2014.

[69] E. Senkus and J. Jassem, "Cardiovascular effects of systemic cancer treatment," *Cancer Treatment Reviews*, vol. 37, no. 4, pp. 300–311, 2011.

[70] A. Pieniążek, J. Czepas, J. Piasecka-Zelga, K. Gwoździński, and A. Koceva-Chyła, "Oxidative stress induced in rat liver by anticancer drugs doxorubicin, paclitaxel and docetaxel," *Advances in Medical Sciences*, vol. 58, no. 1, pp. 104–111, 2013.

[71] K. Kandylis, M. Vassilomanolakis, S. Tsoussis, and A. P. Efremidis, "Ifosfamide cardiotoxicity in humans," *Cancer Chemotherapy and Pharmacology*, vol. 24, no. 6, pp. 395–396, 1989.

[72] J. Nuver, E. C. De Haas, Z. M. Van, J. A. Gietema, and C. Meijer, "Vascular damage in testicular cancer patients: a study on endothelial activation by bleomycin and cisplatin *in vitro*," *Oncology Reports*, vol. 23, no. 1, pp. 247–253, 2010.

[73] F. Zhang, G. Suarez, J. Sha, J. C. Sierra, J. W. Peterson, and A. K. Chopra, "Phospholipase A2-activating protein (PLAA) enhances cisplatin-induced apoptosis in HeLa cells," *Cellular Signalling*, vol. 21, no. 7, pp. 1085–1099, 2009.

[74] M. Bonifazi, M. Franchi, M. Rossi et al., "Trastuzumab-related cardiotoxicity in early breast cancer: a cohort study," *The Oncologist*, vol. 18, no. 7, pp. 795–801, 2013.

Review Article

A Role for T-Lymphocytes in Human Breast Cancer and in Canine Mammary Tumors

Maria Isabel Carvalho,[1] Isabel Pires,[1] Justina Prada,[1] and Felisbina L. Queiroga[2,3,4]

[1] *CECAV, Department of Veterinary Sciences, University of Trás-os-Montes and Alto Douro, 5001-801 Vila Real, Portugal*
[2] *Department of Veterinary Sciences, University of Trás-os-Montes and Alto Douro, 5001-801 Vila Real, Portugal*
[3] *Center for the Study of Animal Sciences (CECA), University of Porto, Porto, 4480 Vila do Conde, Portugal*
[4] *Center for Research and Technology of Agro-Environment and Biological Sciences (CITAB), University of Trás-os-Montes and Alto Douro, 5001-801 Vila Real, Portugal*

Correspondence should be addressed to Felisbina L. Queiroga; fqueirog@utad.pt

Received 27 April 2013; Accepted 18 November 2013; Published 2 February 2014

Academic Editor: Monica Fedele

Chronic inflammation in the tumor microenvironment has a prominent role in carcinogenesis and benefits the proliferation and survival of malignant cells, promoting angiogenesis and metastasis. Mammary tumors are frequently infiltrated by a heterogeneous population of immune cells where T-lymphocytes have a great importance. Interestingly, similar inflammatory cell infiltrates, cytokine and chemokine expression in humans and canine mammary tumors were recently described. However, in both species, despite all the scientific evidences that appoint for a significant role of T-lymphocytes, a definitive conclusion concerning the effectiveness of T-cell dependent immune mechanisms has not been achieved yet. In the present review, we describe similarities between human breast cancer and canine mammary tumors regarding tumor T-lymphocyte infiltration, such as relationship of TILs and mammary tumors malignancy, association of ratio CD4+/ CD8+ T-cells with low survival rates, promotion of tumor progression by Th2 cells actions, and association of great amounts of Treg cells with poor prognostic factors. This apparent parallelism together with the fact that dogs develop spontaneous tumors in the context of a natural immune system highlight the dog as a possible useful biological model for studies in human breast cancer immunology.

1. Introduction

The mammalian immune system comprises a coordinated and finely controlled series of interactions involving cells and molecules and has an essential role on species survival and adaptation all over the years [1]. The immune system has the important task of distinguishing between "self" and "nonself," providing protection against foreign pathogens, maintaining at the same time tolerance to self-antigens [2, 3].

Cancer is a progressive process that arises from a well-defined step where somatic cells acquire activating (oncogenes) or deactivating (tumor suppressor genes) mutations [4, 5]. All types of cancer are caused by the progressive and uncontrolled growth of transformed cells and the control of this disease requires the ablation and destruction of all the malignant cells without damaging the patient. To attain this assignment the own body has to distinguish between the cells of the tumor and other cellular counterparts [3, 6]. However, unfortunately, many tumors continue to grow progressively and expand, which demonstrates that immune system is not always effective and fails on its protective role against tumor development [3, 7].

Decades of intensive investigation left clear that the interplay between immunity and cancer is complex [8]. One example of this high complexity is the phenomena of "*Cancer Immunoediting*." Cancer cells constantly modulate the host antitumor immune response in a process called *immunoediting*. During this process, the balance between antitumor and tumor-promoting immunity can be tilted to protect against the neoplasia development or, on the contrary, to support tumor growth. Immunoediting is characterized as a three-phase process including *elimination phase*

(immunosurveillance), *equilibrium phase*, and *escape phase* [5]. Therefore, the immune system can release factors that promote neoplastic cells survivor, growth, and invasion. Thus, paradoxically, immune system acts as an extrinsic tumor-suppressor but can also promote cancer initiation, promotion, and progression [9].

2. Chronic Inflammation and Cancer

The role of chronic inflammation in cancer was first proposed by Rudolf Virchow in 1863, when he observed the presence of leucocytes in neoplastic tissues. Virchow postulated that an inflammatory milieu promotes a cellular environment that drives the initiation and development of carcinogenesis (reviewed in [10, 11]).

Inflammatory responses play a crucial role at different stages of tumor development [12, 13]. Innate immune cells that infiltrate tumors participate in an extensive and dynamic crosstalk with cancer cells and some of the molecular events that mediate this dialog have been revealed [6, 14]. The most relevant molecular mechanisms include increased production of proinflammatory mediators, such as cytokines, chemokines, reactive oxygen intermediates, increased expression of oncogenes, COX-2 (cyclooxygenase-2), 5-LOX (5-lipoxygenase), and MMPs (matrix metalloproteinases), and proinflammatory transcription factors such as NF-κB (nuclear factor κB), STAT3 (signal transducer and activator of transcription 3), AP-1 (activator protein 1), and HIF-1α (hypoxia-inducible factor 1α). These proinflammatory mediators potentiate tumor cell proliferation, transformation, metastasis, invasion, angiogenesis, chemoresistance, and radioresistance [11, 15–17].

So, *why does inflammation potentiate cancer development rather than protect against it?* In fact, chronic inflammation is considered important in the promotion of cellular proliferation and cancer progression by enhancing angiogenesis and tissue invasion [5, 13], releasing products that promote carcinogenesis in nearby cells and accelerating genetic mutations through a state of malignancy [7]. Finally, through cancer-derived products, immune and regulatory cells are recruited and the weak tumor antigenicity subverts immune cells in order to support cancer progression [5, 18].

3. Adaptive Immunity and Cancer Development: A Role for T-Lymphocytes

In neoplastic lesions, the role of infiltrating T-lymphocytes is often paradoxical. Despite the evidence that the responses of T-lymphocyte can destroy tumor cells "in situ," these responses appear to be frequently ineffective in the elimination of the established cancer [19, 20]. In fact, patients with cancer present a deficient immune response to tumor antigens. However, this deficient immune response is clearly different from immunosuppression observed in patients receiving high doses of corticosteroids and/or chemotherapy. The term "immune dysfunction" seems the most appropriate to describe the changes observed. The mechanisms that support this "immune disorder" include *barriers that prevent recognition of the tumor by immune cells and also lymphocyte dysfunction* [21].

The *barriers that prevent recognition of the tumor* by immune cells include several mechanisms such as sequestration of tumor associated antigens and major histocompatibility complex (MHC) molecules, loss of costimulatory molecules and other molecules required by cytotoxic T-cells. These mechanisms represent a barrier for the total elimination of tumor [19, 22, 23]. In respect to the *lymphocyte dysfunction* that seems to be present in cancer patients, a tumor-directed immune response involving cytotoxic CD8+ T-cells, T helper 1 (Th1) cells, and natural killer (NK) cells appears to protect against tumor development and progression. Contrarily, the immune responses that involves B-cells, the activation of chronic humoral immunity and/or a T helper 2 (Th2) polarized response and polarized innate inflammatory cells in the tumor, can promote tumor development and progression. This balance between a protective cytotoxic response and a harmful humoral or Th2 response can be regulated systemically by the general immune status of the individual [20, 24].

In this context, the question that arises is *what is the reason why the responses mediated by CD8+ cytotoxic T-lymphocytes are not effective in eradicating the tumor and how can the CD4+ T-cells be involved in neoplastic progression of this disease?*

A part of the response has already been described above and is related to tumor escape mechanisms from cytotoxic CD8+ T-cells action. Another important mechanism appears to be related to the polarity of the responses of CD4+ T-cells in relation to the primary site of cancer and/or their distant metastases [24] and the imbalance of the normal ratio of Th1/Th2 cells [25].

CD4+ T-cells are activated in response to soluble factors and can be classified into categories, Th1 and Th2. After stimulation, the Th1 cells secrete interferon gamma (IFNg), transforming growth factor beta (TGFβ), tumor necrosis factor alpha (TNF), and interleukin 2 (IL-2). These cytokines cooperate with the functions of cytotoxic CD8+ T-cells, producing a tumoricidal activity. In contrast, Th2 cells express interleukin (IL) 4, 5, 6, 10, and 13 that induce anergy of T-cells and loss of cytotoxicity, while increasing the humoral immunity (lymphocyte B function). Thus, Th1 cell responses benefit antitumor immunity, whereas Th2 cell responses produce a down-regulation of antitumor cell mediated immunity and increase the humoral protumourigenic responses [24, 26, 27].

Although the immune dysfunction in patients with cancer is now better understood with the perception of Th1 and Th2 regulation, what is responsible for this dysfunction remains to be determined. One possibility is that the number of Th1 cells or their precursors are reduced, decreasing one line of defense against cancer progression and metastasis. Another possibility is the important role played by *regulatory T-cells* and *immature myeloid cells* in the antitumor immune suppression observed in patients with breast cancer and other type of neoplasms [25, 28].

Regulatory T-cells (Treg cells) are a distinct group of lymphocytes with immunosuppressive properties that usually maintain immune tolerance [29]. Treg cell suppressive

activity is beneficial by restricting T cell response against self-antigens and preventing inflammatory and autoimmune diseases. In cancer, their inhibitory role in limiting immune response against "pseudo-self antigens" from tumor origin avoids an effective antitumoral immune response and often culminates into negative outcomes for the patient. These cells may play an important deleterious role in cancer immunopathology due to their potent suppressive activity of both T-cell activation and effector functions [20, 30, 31].

Immature myeloid cells express MHC class I molecules suggesting that they can induce cytotoxic T-cells anergy by binding to T-cell receptor (TCR) complex in absence of costimulatory signals [32, 33].

In the last years, a new subset of CD4+ (helper) T-cells, termed *Th17 cells*, has been characterized. Th17 subset secretes IL-17, IL-21, and IL-22 and plays critical roles in the pathogenesis of inflammatory and autoimmune diseases, as well as in host protection against pathogens. Although some data suggest the importance of Th17 cells for tumor immunity, conclusions regarding the functional role of Th17 cells remain controversial [34–36]. Even though some studies indicate that mouse Th17 cells support a positive anti-cancer immunity, the Th17 cells with intratumoral location are probably responsible for chronic tissue inflammation and appear to have a tumor-promoting effect [35, 37, 38].

4. T-Lymphocytes and Human Breast Cancer: Friends or Foes?

In humans, the study of the inflammatory infiltrate, mainly T-lymphocytes, has been subject of great interest associated not only with breast cancer [19, 23, 39], but also with other types of neoplasias, including seminoma [40, 41], melanoma [42, 43], colorectal [44, 45], cervical [46], ovarian [47, 48], urothelial [49], and gastric cancer [50].

In breast cancer, an important role has been attributed to inflammatory cells, as well as cytokines produced by them. A large number of observations suggest that inflammatory cells are not "innocent spectators," but, contrarily, they might conspire with the tumor cells favoring tumor development and progression [8]. However, the prognostic significance of infiltrating T-lymphocytes is still subject to considerable debate [24, 51], because no definitive conclusions have been reached so far. The T-lymphocytes infiltrate appear, according to some researchers, associated with a better prognosis, whereas in other cases is related to a decline in overall survival. Table 1 illustrates some of the most relevant studies in this area in the last two decades.

More recently, investigations that focus on understanding the functions of Treg cells and Th17 cells in mammary carcinogenesis have been published; however, the results of the various studies are also quite controversial [69–71].

Lee and collaborators [69] investigated, by immunohistochemistry, whether the presence of FOXP3-positive Treg cells was associated with prognostic factors, such as stage or histologic grade. FOXP3-positive Treg cells were, in this study, an independent prognostic factor for overall survival and progression free survival. The improved survival times were associated with highly infiltrating FOXP3-positive Treg cells.

Another study, on the contrary, showed that the increased number of Foxp3 Treg cells was significantly correlated with lymph node metastasis and immunopositivity for Ki-67, which indicates a probable relationship with a worse prognosis. [70].

Wang and colleagues assessed the Th17 and Treg cells by flow cytometry and observed that Th17 and Treg cells accumulation in the tumor microenvironment of breast cancer occurred in early stages of disease. With tumor progression, Th17 cell infiltration gradually decreased and there was accumulation of Treg cells [71]. So, this last study indicates that an increase in the number of Treg cells is associated with tumor progression.

The apparent controversy among distinct studies emphasizes the need for further research on this topic. A clear understanding about the role of T-lymphocytes in breast cancer is essential for the development of new therapeutic strategies in a near future.

5. T-Lymphocyte Infiltrate in Canine Mammary Tumors

Canine mammary tumors are a spontaneous neoplasia that occurs frequently in the clinical practice [72, 73]. Despite the high number of studies published on this subject in the last decades, little is known about the role of tumor inflammatory infiltrate in cancer development and/or progression. In dogs, the first studies focused on inflammation and cancer have been performed in other type of tumors including transmissible venereal sarcoma [74], benign oral papilloma [75], cutaneous histiocytoma [76], and seminomas [77]. Studies investigating the role of inflammation in canine mammary tumors were only recently published (Table 2) [78–83].

In canine transmissible venereal sarcoma, the quantity of T-lymphocytes is higher in the group of tumors that exhibit spontaneous regression or stable growth, comparatively with the tumors that exhibit a progressive growth [74]. In canine oral papilloma, similar to humans [84], the maximum number of T-cells that infiltrate the tumor occurs during rapid tumor regression [75]. In canine cutaneous histiocytoma, in the same way, a lymphocytic infiltrate represents the morphological expression of one antitumor immune response, which correlates with observations of spontaneous regression "in vivo" [76, 85]. In turn, in canine seminomas [77], in accordance with what occurs in human seminomas [40, 41], infiltrating lymphoid cells consist mainly in T-lymphocytes, especially CD8+ cells, which means that the reaction of the body against neoplastic cells is mainly cytotoxic. This, together with the number of MHC I positive cells and a high amount of antigen presenting cells observed, suggests, according to the authors, that inflammatory cells exhibit a role in antitumor response [77]. This might explain the biological behavior of these tumors that rarely metastasize and the favorable prognosis that often presents. Interestingly, in 2007, Horiuchi and collaborators [86] refer that in animals with cancer, a smaller amount of Th1 cells and a significant

Table 1: Studies of a generalized lymphocytic infiltration in human breast cancer.

Author	Year	Patients (*n*)	Analysis	Location	Type	Comments
Aaltomaa and Lipponen [52]	1992	489	Semiquantitative (none/mild-moderate-severe)	Peritumoral Intratumoral	Lymphocytic infiltration	Better prognosis, positive correlation with the lack of regional lymph nodes involvement, with a smaller diameter of the tumor, with a lower histologic grade and with a larger time free of disease
Carlomagno et al. [53]	1995	1257	Semiquantitative (absent/present)	Peritumoral	Lympho-plasmacytic infiltration	Poorer overall survival in multivariate survival analysis in particularly patients with grade I and II
Ménard et al. [54]	1997	1919	Semiquantitative (absent/present)	Intratumoral	Lymphoid infiltration	Better overall survival in patients <40 years of age, no significant association in patients >40 in multivariate survival analysis
Marsigliante et al. [55]	1999	90	Quantitative (computerised counting)	Intratumoral	T-lymphocyte infiltration	CD3+ TILs was directly correlated to age, lymph node negative patients had tumors infiltrated by fewer CD4+ TILs with respect to lymph node positive patients
Georgiannos et al. [56]	2003	60	Semiquantitative (0 = none; 1 = rare cells; 2 = moderate numbers; and 3 = many positive cells)	Intratumoral	Lymphocytic infiltration	A significant association was found between the intensity of TIL and the number of positive nodes
Campbell et al. [25]	2005	84 patients 26 healthy volunteers	The flow cytometry analysis was performed using CELLQuest software (BD Biosciences)	Peripheral blood and bone marrow aspirates	Peripheral blood lymphocytes	The percentages of both CD4+ and CD8+ cells were significantly lower in patients with breast cancer compared to healthy controls. A correlation was observed between number of micrometastases in the bone marrow and T cell responsiveness
Lee et al. [57]	2006	679	Semiquantitative (none-mild-moderate-severe)	Peritumoral Intratumoral	General inflammation infiltrate	Better recurrence-free survival and overall survival in multivariate survival analysis
Macchetti et al. [19]	2006	23	Flow cytometry quantitative analysis	Intratumoral	Lymphocytic infiltration	In the patients with lymph node metastasis, an increased mean percentage of tumor infiltrating CD4+ T-cells, but not CD8+ T-cells was observed and was correlated with worse prognosis
Al Murri et al. [58]	2008	168	Quantitative analysis	Peritumoral Intratumoral	CD4 and CD8	No significant association
Calabrò et al. [59]	2009	155	Quantitative analysis microarray based screening for Li-associated genes		Lymphocytic infiltration	Poorer overall survival in ER+ patients and better overall survival in ER− patients
Rakha et al. [60]	2009	1597	Semiquantitative (mild-severe)	Peritumoral Intratumoral	General inflammation	Better recurrence-free survival and overall survival
Rody et al. [61]	2009	1263	Quantitative analysis	Peritumoral Intratumoral	CD3	Better recurrence free survival in cases who had HER-2+
Matkowski et al. [62]	2009	88	Semiquantitative (percentage of positive stained cells: 0 = none, 1 = up to 33%, 2 = 33–66%, 3 = more than 66%; intensity of the lymphocytic infiltrate: 1-low, 2-moderate, 3-high)	Intratumoral	Lymphocytic infiltration	In early breast cancer the presence of CD8+ and CD4+ cells was correlated with lymph node involvement and unfavorable prognosis
Baker et al. [63]	2011	1953	Quantitative analysis (TMA)	Peritumoral Intratumoral	CD8	Better cancer-specific survival in only high grade ER− tumor in multivariate survival analysis whereas poorer cancer specific survival in low grade ER+ tumor in univariate analysis

Table 1: Continued.

Author	Year	Patients (n)	Analysis	Location	Type	Comments
Ladoire et al. [64]	2011	162	Semiquantitative (none-mild-moderate-severe)	Peritumoral Intratumoral	CD8	Better recurrence-free survival after chemotherapy CD8/FOXP3 ratio independent predictive factor associated with improved recurrence-free and overall survival after chemotherapy
Liu et al. [65]	2011	1270	Quantitative analysis	Peritumoral Intratumoral	CD8	No significant association
Mahmoud et al. [66]	2011	1334	Quantitative analysis (TMA)	Peritumoral Intratumoral	CD8	Better cancer-specific survival in multivariate survival analysis. Better recurrence free survival and cancer specific survival in only ER− in univariate survival analysis. Whereas no significant association in ER+
West et al. [67]	2011	255	Quantitative analysis microarray based on information in the BioGPS gene portal	Intratumoral	Lymphocytic infiltration	TIL that express cytotoxic markers was strongly associated with favorable outcome after anthracycline based treatment of ER− breast cancer patients
Ruffell et al. [68]	2012	20	Flow cytometry, immunohistochemistry, and confocal immunofluorescence quantitative analysis	Intratumoral	Leukocyte infiltration	Tumors from breast cancer patients treated with neoadjuvant chemotherapy contained an increased CD8/CD4 T-cell ratio compared with tumors removed from patients treated primarily by surgery alone

Table 2: Studies of T-lymphocytic infiltrate in Canine mammary tumors (CMT).

Author	Year	Patients (*n*)	Type	Comments
Estrela-Lima et al. [78]	2010	51	T-lymphocyte infiltration	Animals with high proportions of CD4+ and low CD8+ T-cells had lower survival rates
Kim et al. [79]	2010	58	T-lymphocyte infiltration	Association between the expression of TILs, cytokines, and mutation of BRCA1 suggests that all of these factors may play a role in tumor progression
Carvalho et al. [80]	2011	57	T-lymphocyte infiltration	Tendency for an association of a higher number of CD3+ TILs and a shorter overall survival. CD3+ T-lymphocytes in the adnexal nontumoral mammary gland revealed a statistically significant relationship with overall survival
Saeki et al. [81]	2012	140	Lymphocytic infiltration	Relationship of TILs and canine mammary tumors malignancy
Kim et al. [82]	2012	37	Regulatory T-cells (Treg)	The number of Treg cells is increased in tumors with poor prognostic factors, such as high histological grade, lymphatic invasion, and necrosis
Kim et al. [83]	2013	47	Lymphocytic infiltration	Intense lymphocyte infiltration was associated with aggressive histologic features (higher histologic grade; lymphatic invasion)

larger amount of Th2 cells, compared to healthy ones, was observed. Considering that Th2 cells have an action that promotes tumor progression, these results have come refute what is already known in human works and relaunch the interest in this subject in dogs.

In canine mammary tumors, as previously stated, there are only a very limited number of studies, all of them recently published, that focus on effect of T-lymphocytes infiltrate and malignancy [78–83]. In malignant mammary tumors, abundant lymphocyte infiltrates are frequently found, but the characteristics associated with lymphocyte infiltration in these tumors remain largely unknown. As in humans, the controversy among distinct reports remains an important issue to be clarified (Table 2).

According to Estrela-Lima and collaborators [78], lymphocytes represent the predominant cell type in the tumor infiltrate. The relative percentage of CD4+ T-cells was significantly greater in metastasized tumors, while the percentage of CD8+ T-cells was higher in cases without metastasis. Consequently, the CD4+/CD8+ ratio was significantly increased in cases with metastasis and was associated to lower survival rates. Authors defend that the intensity of lymphocytic infiltrate and the CD4+/CD8+ ratio may represent important survival prognostic biomarkers for canine mammary carcinomas.

In one study performed by Kim and colleagues [79], immunohistochemistry, immunoblotting, and reverse transcriptase-polymerase chain reaction were used to evaluate tumor infiltrating lymphocytes (TILs) and the presence of related cytokines, as well as the expression of breast cancer susceptibility gene-1 (BRCA1). The results of this study revealed a correlation between expression of interleukin (IL)-1 and IL-6 and tumor metastasis. An association among the expression of TILs, cytokines, and mutation of BRCA1 was also verified, suggesting that all of these factors may play a role in tumor progression.

In another study developed by our team [80], CD3+ T-lymphocytes were evaluated in three distinct areas: within the tumor, in the periphery of the tumor and in the adnexal non-tumoral mammary gland. We observed a tendency towards an association of a higher number of CD3+ tumor infiltrating T-lymphocytes and a shorter overall survival. However, interestingly, only for CD3+ T-lymphocytes in the adnexal non-tumoral mammary gland, a statistically significant relationship was observed, with a higher number of lymphocytes conferring a reduced overall survival. This could indicate that CD3+ T-lymphocytes in adnexal non-tumoral mammary gland were implicated in tumor progression and survival, showing that its protumourigenic immune responses may somehow be the starting point for the growth and progression of tumor cells.

Saeki and collaborators [81] accessed the number of tumor infiltrating T-lymphocytes, B-lymphocytes, and antigen presenting cells by immunohistochemistry. As a result, the authors found a statistically significant increase in the number of intratumoral T-lymphocytes in malignant tumors compared with benign ones. The results of this study indicate a positive relationship between a high number of TILs and increased canine mammary tumors malignancy.

Very recently, Kim and colleagues [83] demonstrated, by immunohistochemistry, that the degree of lymphocyte infiltration was significantly higher in canine mammary carcinomas with lymphatic invasion and high histologic grade, suggesting the importance of lymphocytes on tumor aggressiveness and greater malignant behavior.

Treg cells, whose activity is closely associated with the transcription factor FOXP3, have a suppressive action on T-lymphocytes antitumor responses [87, 88]. In dog, there are few studies that focus on the action of Treg cells in tumor development and progression [82, 89–91]. Dogs with cancer had increased numbers of Treg cells in their peripheral blood and tumor-draining lymph nodes compared to healthy animals [89].

In dog mammary tumors, a recent study by Kim and Colleagues [82] described abundant Treg cells associated with high histological grade and lymphatic invasion. The number of Treg cells infiltrating intratumoral areas was markedly increased in tumors with poor prognostic factors, such as

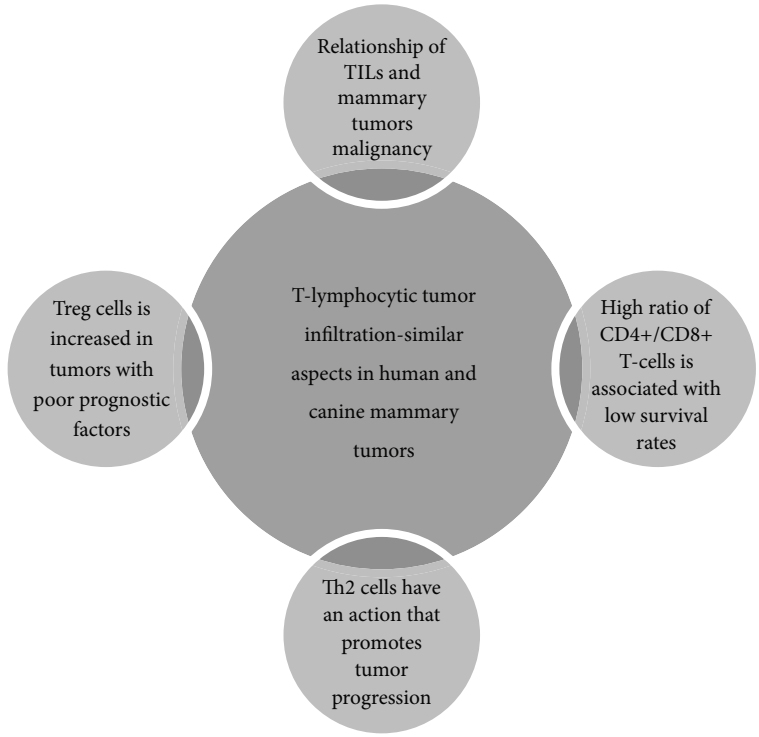

Figure 1: Similarities between human breast cancer and canine mammary tumors regarding tumor T-lymphocyte infiltration.

high histological grade of malignancy, presence of lymphatic invasion, and presence of tumoral necrosis. These findings suggest that Treg cells might play a key role in canine mammary tumors progression. Furthermore, the amount of intratumoral Treg cells may provide a new prognostic factor when assessing survival times, which may in turn lead to the development of new immunologic therapies.

The studies described above, concerning canine mammary tumors, describe results that are in agreement with those from studies already published in human breast cancer which may be an indication of similar cancer immunologic aspects between the two species (Figure 1).

6. Final Remarks

The dog has been proposed, by various authors and throughout several decades, as a model for the study of spontaneous malignancies in humans. This hypothesis is supported by the knowledge that development of spontaneous tumors in dogs and humans is a phenomenon highly incident, sharing many features: histological appearance, tumor genetics, molecular targets, biological behavior, and response to conventional therapy [92–94]. The recent sequencing of the canine genome and the evidence of its similarity to the human counterpart emphasized even more the dog as an attractive model for cancer research [73, 95, 96].

Breast cancer remains a major clinical challenge with considerable mortality both in humans and dogs [72, 97]. Scientific evidences support that, in both species, alterations of inflammatory components within the tumoral microenvironment have a significant role during important steps of carcinogenesis. Additionally, dogs develop spontaneous tumors in the context of a natural immune system [94] which make them an attractive and viable target for immune therapeutic modulation [5, 8, 80, 97, 98].

In the present review, we describe similarities between human breast cancer and canine mammary tumors regarding tumor T-lymphocyte infiltration, such as relationship of TILs and mammary tumors malignancy, association of ratio CD4+/CD8+ T-cells with low survival rates, promotion of tumor progression by Th2 cells actions, and association of great amounts of Treg cells with poor prognostic factors.

We believe that the current state of knowledge could be the basis for a broader and deeper discussion concerning the role of inflammation in dog tumors, especially in canine mammary cancer. Nevertheless, it remains to be clarified the role of the inflammatory infiltrate in tumors of high biological aggressiveness and thus elucidate the T-cell subtypes implicated in the progression of these neoplasms. The identification of specific subtypes and the clarification of the involved pathways, may serve as a basis for the establishment of new therapeutic strategies. In this sense, the development of an active immunization throughout the design of new anticancer-vaccines is expected both in humans and dogs.

In human breast cancer, it was already postulated that vaccination could induce an expansion of CD8+ cytotoxic T-lymphocytes capable of rejecting tumor cells via recognition of tumor-associated antigenic epitopes, located on the surface of cancer cells [99, 100]. The development of anti-cancer

vaccines may lead to the establishment of immunological memory, thereby preventing tumor recurrence with potential advantages in inducing antitumor immune responses in both species [11]. Dogs with mammary cancer develop metastatic disease in a shorter time compared with the humans, due to their smaller longevity which make them particularly good models for study the metastatic process and thus testing new therapeutic modalities [73, 94]. The similarities pointed out in this review support the use of dog with mammary cancer as a reliable biological model to study human breast cancer immunology, providing an attractive opportunity for therapeutic clinical studies in the scope of comparative oncology.

Conflict of Interests

The authors declare that there is no conflict of interests regarding the publication of this paper.

Acknowledgments

The work was supported partially by the Strategic Research Project Pest OE/AGR/UI0772/2011 and by a PhD scholarship SFRH/BD/78771/2011 both financed by the Portuguese Foundation for Science and Technology (FCT).

References

[1] R. J. Prestwich, F. Errington, P. Hatfield et al., "The immune system—is it relevant to cancer development, progression and treatment?" *Clinical Oncology*, vol. 20, no. 2, pp. 101–112, 2008.

[2] R. Medzhitov, "Origin and physiological roles of inflammation," *Nature*, vol. 454, no. 7203, pp. 428–435, 2008.

[3] K. E. de Visser, A. Eichten, and L. M. Coussens, "Paradoxical roles of the immune system during cancer development," *Nature Reviews Cancer*, vol. 6, no. 1, pp. 24–37, 2006.

[4] L. M. Coussens and Z. Werb, "Inflammatory cells and cancer: think different!," *Journal of Experimental Medicine*, vol. 193, no. 6, pp. F23–F26, 2001.

[5] M. D. Vesely, M. H. Kershaw, R. D. Schreiber, and M. J. Smyth, "Natural innate and adaptive immunity to cancer," *Annual Review of Immunology*, vol. 29, pp. 235–271, 2011.

[6] K. E. de Visser and L. M. Coussens, "The inflammatory tumor microenvironment and its impact on cancer development," *Contributions to Microbiology*, vol. 13, pp. 118–137, 2006.

[7] D. Hanahan and R. A. Weinberg, "Hallmarks of cancer: the next generation," *Cell*, vol. 144, no. 5, pp. 646–674, 2011.

[8] A. Ben-Baruch, "Host microenvironment in breast cancer development. Inflammatory cells, cytokines and chemokines in breast cancer progression: reciprocal tumor-microenvironment interactions," *Breast Cancer Research*, vol. 5, no. 1, pp. 31–36, 2003.

[9] M. C. Mihm Jr., C. G. Clemente, and N. Cascinelli, "Tumor infiltrating lymphocytes in lymph node melanoma metastases: a histopathologic prognostic indicator and an expression of local immune response," *Laboratory Investigation*, vol. 74, no. 1, pp. 43–47, 1996.

[10] S. Demaria, E. Pikarsky, M. Karin et al., "Cancer and inflammation: promise for biologic therapy," *Journal of Immunotherapy*, vol. 33, no. 4, pp. 335–351, 2010.

[11] G. Sethi, M. K. Shanmugam, L. Ramachandran, A. P. Kumar, and V. Tergaonkar, "Multifaceted link between cancer and inflammation," *Bioscience Reports*, vol. 32, no. 1, pp. 1–15, 2012.

[12] O. J. Finn, "Molecular origins of cancer: cancer immunology," *The New England Journal of Medicine*, vol. 358, no. 25, pp. 2704–2715, 2008.

[13] W. B. Morrison, "Inflammation and cancer: a comparative view," *Journal of Veterinary Internal Medicine*, vol. 26, no. 1, pp. 18–31, 2012.

[14] S. I. Grivennikov, F. R. Greten, and M. Karin, "Immunity, inflammation, and cancer," *Cell*, vol. 140, no. 6, pp. 883–899, 2010.

[15] B. B. Aggarwal, S. Shishodia, S. K. Sandur, M. K. Pandey, and G. Sethi, "Inflammation and cancer: how hot is the link?" *Biochemical Pharmacology*, vol. 72, no. 11, pp. 1605–1621, 2006.

[16] B. B. Aggarwal and P. Gehlot, "Inflammation and cancer: how friendly is the relationship for cancer patients?" *Current Opinion in Pharmacology*, vol. 9, no. 4, pp. 351–369, 2009.

[17] F. Balkwill and A. Mantovani, "Cancer and inflammation: implications for pharmacology and therapeutics," *Clinical Pharmacology and Therapeutics*, vol. 87, no. 4, pp. 401–406, 2010.

[18] T. Hagemann, T. Lawrence, I. McNeish et al., "'Re-educating' tumor-associated macrophages by targeting NF-κB," *Journal of Experimental Medicine*, vol. 205, no. 6, pp. 1261–1268, 2008.

[19] A. H. Macchetti, H. R. C. Marana, J. S. Silva, J. M. de Andrade, A. Ribeiro-Silva, and S. Bighetti, "Tumor-infiltrating CD4+ T lymphocytes in early breast cancer reflect lymph node involvement," *Clinics*, vol. 61, no. 3, pp. 203–208, 2006.

[20] G. Curigliano, "Immunity and autoimmunity: revising the concepts of response to breast cancer," *Breast*, vol. 20, supplement 3, pp. S71–S74, 2011.

[21] J. Finke, S. Ferrone, A. Frey, A. Mufson, and A. Ochoa, "Where have all the T cells gone? Mechanisms of immune evasion by tumors," *Immunology Today*, vol. 20, no. 4, pp. 158–160, 1999.

[22] A. J. Marrogi, A. Munshi, A. J. Merogi et al., "Study of tumor infiltrating lymphocytes and transforming growth factor-beta as prognostic factors in breast carcinoma," *International Journal of Cancer*, vol. 74, pp. 492–501, 1997.

[23] B. Sheu, W. Kuo, R. Chen, S. Huang, K. Chang, and S. Chow, "Clinical significance of tumor-infiltrating lymphocytes in neoplastic progression and lymph node metastasis of human breast cancer," *Breast*, vol. 17, no. 6, pp. 604–610, 2008.

[24] D. G. DeNardo and L. M. Coussens, "Inflammation and breast cancer. Balancing immune response: crosstalk between adaptive and innate immune cells during breast cancer progression," *Breast Cancer Research*, vol. 9, no. 4, article 212, 2007.

[25] M. J. Campbell, J. Scott, H. T. Maecker, J. W. Park, and L. J. Esserman, "Immune dysfunction and micrometastases in women with breast cancer," *Breast Cancer Research and Treatment*, vol. 91, no. 2, pp. 163–171, 2005.

[26] S. Goto, M. Sato, R. Kaneko, M. Itoh, S. Sato, and S. Takeuchi, "Analysis of Th1 and Th2 cytokine production by peripheral blood mononuclear cells as a parameter of immunological dysfunction in advanced cancer patients," *Cancer Immunology Immunotherapy*, vol. 48, no. 8, pp. 435–442, 1999.

[27] M. J. M. Gooden, G. H. de Bock, N. Leffers, T. Daemen, and H. W. Nijman, "The prognostic influence of tumour-infiltrating lymphocytes in cancer: a systematic review with meta-analysis," *British Journal of Cancer*, vol. 105, no. 1, pp. 93–103, 2011.

[28] A. Mantovani, F. Marchesi, C. Porta, A. Sica, and P. Allavena, "Inflammation and cancer: breast cancer as a prototype," *Breast*, vol. 16, supplement 2, pp. 27–33, 2007.

[29] H. von Boehmer and C. Daniel, "Therapeutic opportunities for manipulating T(Reg) cells in autoimmunity and cancer," *Nature Reviews Drug Discovery*, vol. 12, pp. 51–63, 2013.

[30] S. Sakaguchi, K. Wing, Y. Onishi, P. Prieto-Martin, and T. Yamaguchi, "Regulatory T cells: how do they suppress immune responses?" *International Immunology*, vol. 21, no. 10, pp. 1105–1111, 2009.

[31] C. Tanchot, M. Terme, H. Pere et al., "Tumor-infiltrating regulatory T cells: phenotype, role, mechanism of expansion in situ and clinical significance," *Cancer Microenvironment*, vol. 6, no. 2, pp. 147–157, 2013.

[32] B. Almand, J. I. Clark, E. Nikitina et al., "Increased production of immature myeloid cells in cancer patients: a mechanism of immunosuppression in cancer," *Journal of Immunology*, vol. 166, no. 1, pp. 678–689, 2001.

[33] S. Ostrand-Rosenberg and P. Sinha, "Myeloid-derived suppressor cells: linking inflammation and cancer," *Journal of Immunology*, vol. 182, no. 8, pp. 4499–4506, 2009.

[34] K. S. Sfanos, T. C. Bruno, C. H. Maris et al., "Phenotypic analysis of prostate-infiltrating lymphocytes reveals T H17 and Treg skewing," *Clinical Cancer Research*, vol. 14, no. 11, pp. 3254–3261, 2008.

[35] F. Martin, L. Apetoh, and F. Ghiringhelli, "Controversies on the role of Th17 in cancer: a TGF-beta-dependent immunosuppressive activity?" *Trends in Molecular Medicine*, vol. 18, no. 12, pp. 742–749, 2012.

[36] J. Ye, R. S. Livergood, and G. Peng, "The role and regulation of human Th17 cells in tumor immunity," *The American Journal of Pathology*, vol. 182, pp. 10–20, 2013.

[37] I. Kryczek, M. Banerjee, P. Cheng et al., "Phenotype, distribution, generation, and functional and clinical relevance of Th17 cells in the human tumor environments," *Blood*, vol. 114, no. 6, pp. 1141–1149, 2009.

[38] S. V. Novitskiy, M. W. Pickup, A. E. Gorska et al., "TGF-beta receptor II loss promotes mammary carcinoma progression by Th17 dependent mechanisms," *Cancer Discovery*, vol. 1, pp. 430–441, 2011.

[39] H. Kuroda, J. Tamaru, G. Sakamoto, K. Ohnisi, and S. Itoyama, "Immunophenotype of lymphocytic infiltration in medullary carcinoma of the breast," *Virchows Archiv*, vol. 446, no. 1, pp. 10–14, 2005.

[40] E. Yakirevich, O. Lefel, Y. Sova et al., "Fractalkine expression in human renal inflammation," *Journal of Pathology*, vol. 196, no. 1, pp. 85–90, 2002.

[41] S. R. Hadrup, O. Brændstrup, G. K. Jacobsen et al., "Tumor infiltrating lymphocytes in seminoma lesions comprise clonally expanded cytotoxic T cells," *International Journal of Cancer*, vol. 119, no. 4, pp. 831–838, 2006.

[42] F. Piras, R. Colombari, L. Minerba et al., "The predictive value of CD8, CD4, CD68 and human leukocyte antigen-D-related cells in the prognosis of cutaneous malignant melanoma with vertical growth phase," *Cancer*, vol. 104, no. 6, pp. 1246–1254, 2005.

[43] R. C. Taylor, A. Patel, K. S. Panageas, K. J. Busam, and M. S. Brady, "Tumor-infiltrating lymphocytes predict sentinel lymph node positivity in patients with cutaneous melanoma," *Journal of Clinical Oncology*, vol. 25, no. 7, pp. 869–875, 2007.

[44] F. Pagès, A. Berger, M. Camus et al., "Effector memory T cells, early metastasis, and survival in colorectal cancer," *The New England Journal of Medicine*, vol. 353, no. 25, pp. 2654–2666, 2005.

[45] J. Galon, A. Costes, F. Sanchez-Cabo et al., "Type, density, and location of immune cells within human colorectal tumors predict clinical outcome," *Science*, vol. 313, no. 5795, pp. 1960–1964, 2006.

[46] S. J. Piersma, E. S. Jordanova, M. I. E. van Poelgeest et al., "High number of intraepithelial CD8+ tumor-infiltrating lymphocytes is associated with the absence of lymph node metastases in patients with large early-stage cervical cancer," *Cancer Research*, vol. 67, no. 1, pp. 354–361, 2007.

[47] L. Zhang, J. R. Conejo-Garcia, D. Katsaros et al., "Intratumoral T cells, recurrence, and survival in epithelial ovarian cancer," *The New England Journal of Medicine*, vol. 348, no. 3, pp. 203–213, 2003.

[48] M. Tomšová, B. Melichar, I. Sedláková, and I. Šteiner, "Prognostic significance of CD3+ tumor-infiltrating lymphocytes in ovarian carcinoma," *Gynecologic Oncology*, vol. 108, no. 2, pp. 415–420, 2008.

[49] P. Sharma, Y. Shen, S. Wen et al., "CD8 tumor-infiltrating lymphocytes are predictive of survival in muscle-invasive urothelial carcinoma," *Proceedings of the National Academy of Sciences of the United States of America*, vol. 104, no. 10, pp. 3967–3972, 2007.

[50] H. E. Lee, S. W. Chae, Y. J. Lee et al., "Prognostic implications of type and density of tumour-infiltrating lymphocytes in gastric cancer," *British Journal of Cancer*, vol. 99, no. 10, pp. 1704–1711, 2008.

[51] Z. M. Mohammed, J. J. Going, J. Edwards, and D. C. McMillan, "The role of the tumour inflammatory cell infiltrate in predicting recurrence and survival in patients with primary operable breast cancer," *Cancer Treatment Reviews*, vol. 38, pp. 943–955, 2012.

[52] S. Aaltomaa and P. Lipponen, "Prognostic factors in breast-cancer (review)," *International Journal of Oncology*, vol. 1, pp. 153–159, 1992.

[53] C. Carlomagno, F. Perrone, R. Lauria et al., "Prognostic significance of necrosis, elastosis, fibrosis and inflammatory cell reaction in operable breast cancer," *Oncology*, vol. 52, no. 4, pp. 272–277, 1995.

[54] S. Ménard, G. Tomasic, P. Casalini et al., "Lymphoid infiltration as a prognostic variable for early-onset breast carcinomas," *Clinical Cancer Research*, vol. 3, no. 5, pp. 817–819, 1997.

[55] S. Marsigliante, L. Biscozzo, A. Marra et al., "Computerised counting of tumour infiltrating lymphocytes in 90 breast cancer specimens," *Cancer Letters*, vol. 139, no. 1, pp. 33–41, 1999.

[56] S. N. Georgiannos, A. Renaut, A. W. Goode, and M. Sheaff, "The immunophenotype and activation status of the lymphocytic infiltrate in human breast cancers, the role of the major histocompatibility complex in cell-mediated immune mechanisms, and their association with prognostic indicators," *Surgery*, vol. 134, no. 5, pp. 827–834, 2003.

[57] A. H. S. Lee, C. E. Gillett, K. Ryder, I. S. Fentiman, D. W. Miles, and R. R. Millis, "Different patterns of inflammation and prognosis in invasive carcinoma of the breast," *Histopathology*, vol. 48, no. 6, pp. 692–701, 2006.

[58] A. M. Al Murri, M. Hilmy, J. Bell et al., "The relationship between the systemic inflammatory response, tumour proliferative activity, T-lymphocytic and macrophage infiltration, microvessel density and survival in patients with primary operable breast cancer," *British Journal of Cancer*, vol. 99, no. 7, pp. 1013–1019, 2008.

[59] A. Calabrò, T. Beissbarth, R. Kuner et al., "Effects of infiltrating lymphocytes and estrogen receptor on gene expression and

prognosis in breast cancer," *Breast Cancer Research and Treatment*, vol. 116, no. 1, pp. 69–77, 2009.

[60] E. A. Rakha, M. Aleskandarany, M. E. El-Sayed et al., "The prognostic significance of inflammation and medullary histological type in invasive carcinoma of the breast," *European Journal of Cancer*, vol. 45, no. 10, pp. 1780–1787, 2009.

[61] A. Rody, U. Holtrich, L. Pusztai et al., "T-cell metagene predicts a favorable prognosis in estrogen receptor-negative and HER2-positive breast cancers," *Breast Cancer Research*, vol. 11, no. 2, article R15, 2009.

[62] R. Matkowski, I. Gisterek, A. Halon et al., "The prognostic role of tumor-infiltrating CD4 and CD8 T lymphocytes in breast cancer," *Anticancer Research*, vol. 29, no. 7, pp. 2445–2451, 2009.

[63] K. Baker, J. Lachapelle, I. Zlobec, T. A. Bismar, L. Terracciano, and W. D. Foulkes, "Prognostic significance of CD8+ T lymphocytes in breast cancer depends upon both oestrogen receptor status and histological grade," *Histopathology*, vol. 58, no. 7, pp. 1107–1116, 2011.

[64] S. Ladoire, G. Mignot, S. Dabakuyo et al., "In situ immune response after neoadjuvant chemotherapy for breast cancer predicts survival," *Journal of Pathology*, vol. 224, no. 3, pp. 389–400, 2011.

[65] F. Liu, R. Lang, J. Zhao et al., "CD8+ cytotoxic T cell and FOXP3+ regulatory T cell infiltration in relation to breast cancer survival and molecular subtypes," *Breast Cancer Research and Treatment*, vol. 130, no. 2, pp. 645–655, 2011.

[66] S. M. A. Mahmoud, E. C. Paish, D. G. Powe et al., "Tumor-infiltrating CD8+ lymphocytes predict clinical outcome in breast cancer," *Journal of Clinical Oncology*, vol. 29, no. 15, pp. 1949–1955, 2011.

[67] N. R. West, K. Milne, P. T. Truong, N. Macpherson, B. H. Nelson, and P. H. Watson, "Tumor-infiltrating lymphocytes predict response to anthracycline-based chemotherapy in estrogen receptor-negative breast cancer," *Breast Cancer Research*, vol. 13, no. 6, article R126, 2011.

[68] B. Ruffell, A. Au, H. S. Rugo, L. J. Esserman, E. S. Hwang, and L. M. Coussens, "Leukocyte composition of human breast cancer," *Proceedings of the National Academy of Sciences of the United States of America*, vol. 109, no. 8, pp. 2796–2801, 2012.

[69] S. Lee, E. Y. Cho, Y. H. Park, J. S. Ahn, and Y. H. Im, "Prognostic impact of FOXP3 expression in triple-negative breast cancer," *Acta Oncologica*, vol. 52, no. 1, pp. 73–81, 2013.

[70] S. T. Kim, H. Jeong, O. H. Woo et al., "Tumor-infiltrating lymphocytes, tumor characteristics, and recurrence in patients with early breast cancer," *American Journal of Clinical Oncology*, vol. 36, no. 3, pp. 224–231, 2013.

[71] J. Wang, D. Cai, B. Ma, G. Wu, and J. Wu, "Skewing the balance of regulatory T-cells and T-helper 17 cells in breast cancer patients," *Journal of International Medical Research*, vol. 39, no. 3, pp. 691–701, 2011.

[72] K. U. Sorenmo, R. Rasotto, V. Zappulli, and M. H. Goldschmidt, "Development, anatomy, histology, lymphatic drainage, clinical features, and cell differentiation markers of canine mammary gland neoplasms," *Veterinary Pathology*, vol. 48, no. 1, pp. 85–97, 2011.

[73] F. L. Queiroga, T. Raposo, M. I. Carvalho, J. Prada, and I. Pires, "Canine mammary tumours as a model to study human breast cancer: most recent findings," *In Vivo*, vol. 25, no. 3, pp. 455–465, 2011.

[74] J. Pérez, M. J. Day, and E. Mozos, "Immunohistochemical study of the local inflammatory infiltrate in spontaneous canine transmissible venereal tumour at different stages of growth," *Veterinary Immunology and Immunopathology*, vol. 64, no. 2, pp. 133–147, 1998.

[75] P. K. Nicholls, P. F. Moore, D. M. Anderson et al., "Regression of canine oral papillomas is associated with infiltration of CDA+ and CD8+ lymphocytes," *Virology*, vol. 283, no. 1, pp. 31–39, 2001.

[76] G. L. Cockerell and D. O. Slauson, "Patterns of lymphoid infiltrate in the canine cutaneous histiocytoma," *Journal of Comparative Pathology*, vol. 89, no. 2, pp. 193–203, 1979.

[77] V. Grieco, M. Rondena, S. Romussi, D. Stefanello, and M. Finazzi, "Immunohistochemical characterization of the leucocytic infiltrate associated with canine seminomas," *Journal of Comparative Pathology*, vol. 130, no. 4, pp. 278–284, 2004.

[78] A. Estrela-Lima, M. S. S. Araújo, J. M. Costa-Neto et al., "Immunophenotypic features of tumor infiltrating lymphocytes from mammary carcinomas in female dogs associated with prognostic factors and survival rates," *BMC Cancer*, vol. 10, article 256, 2010.

[79] J.-H. Kim, C.-H. Yu, J.-Y. Yhee, K.-S. Im, and J.-H. Sur, "Lymphocyte infiltration, expression of interleukin (IL)-1, IL-6 and expression of mutated breast cancer susceptibility gene-1 correlate with malignancy of canine mammary tumours," *Journal of Comparative Pathology*, vol. 142, no. 2-3, pp. 177–186, 2010.

[80] M. I. Carvalho, I. Pires, J. Prada, and F. L. Queiroga, "T-lymphocytic infiltrate in canine mammary tumours: clinic and prognostic implications," *In Vivo*, vol. 25, no. 6, pp. 963–969, 2011.

[81] K. Saeki, Y. Endo, K. Uchida, R. Nishimura, N. Sasaki, and T. Nakagawa, "Significance of tumor-infiltrating immune cells in spontaneous canine mammary gland tumor: 140 cases," *Journal of Veterinary Medical Science*, vol. 74, no. 2, pp. 227–230, 2012.

[82] J. H. Kim, J. H. Hur, S. M. Lee, K. S. Im, N. H. Kim, and J. H. Sur, "Correlation of Foxp3 positive regulatory T cells with prognostic factors in canine mammary carcinomas," *Veterinary Journal*, vol. 193, pp. 222–227, 2012.

[83] J. H. Kim, S. K. Chon, K. S. Im, N. H. Kim, and J. H. Sur, "Correlation of tumor-infiltrating lymphocytes to histopathological features and molecular phenotypes in canine mammary carcinoma: a morphologic and immunohistochemical morphometric study," *Canadian Journal of Veterinary Research*, vol. 77, pp. 142–149, 2013.

[84] G. Knowles, B. W. O'Neil, and M. S. Campo, "Phenotypical characterization of lymphocytes infiltrating regressing papillomas," *Journal of Virology*, vol. 70, no. 12, pp. 8451–8458, 1996.

[85] I. Pires, F. L. Queiroga, A. Alves, F. Silva, and C. Lopes, "Decrease of E-cadherin expression in canine cutaneous histiocytoma appears to be related to its spontaneous regression," *Anticancer Research*, vol. 29, no. 7, pp. 2713–2717, 2009.

[86] Y. Horiuchi, A. Hanazawa, Y. Nakajima et al., "T-helper (Th) 1/Th2 imbalance in the peripheral blood of dogs with malignant tumor," *Microbiology and Immunology*, vol. 51, no. 11, pp. 1135–1138, 2007.

[87] S. Gupta, K. Joshi, J. D. Wig, and S. K. Arora, "Intratumoral FOXP3 expression in infiltrating breast carcinoma: its association with clinicopathologic parameters and angiogenesis," *Acta Oncologica*, vol. 46, no. 6, pp. 792–797, 2007.

[88] D. Mougiakakos, A. Choudhury, A. Lladser, R. Kiessling, and C. C. Johansson, "Regulatory T cells in cancer," *Advances in Cancer Research*, vol. 107, pp. 57–117, 2010.

[89] B. J. Biller, R. E. Elmslie, R. C. Burnett, A. C. Avery, and S. W. Dow, "Use of FoxP3 expression to identify regulatory T cells in healthy dogs and dogs with cancer," *Veterinary Immunology and Immunopathology*, vol. 116, no. 1-2, pp. 69–78, 2007.

[90] B. J. Biller, A. Guth, J. H. Burton, and S. W. Dow, "Decreased ratio of CD8+ T cells to regulatory T cells associated with decreased survival in dogs with osteosarcoma," *Journal of Veterinary Internal Medicine*, vol. 24, no. 5, pp. 1118–1123, 2010.

[91] J. H. Kim, S. K. Chon, K. S. Im, N. H. Kim, K. W. Cho, and J. H. Sur, "Infiltrating Foxp3+ regulatory T cells and histopathological features in canine classical and spermatocytic seminomas," *Reproduction in Domestic Animals*, vol. 48, pp. 218–222, 2013.

[92] R. Kumaraguruparan, D. Prathiba, and S. Nagini, "Of humans and canines: immunohistochemical analysis of PCNA, Bcl-2, p53, cytokeratin and ER in mammary tumours," *Research in Veterinary Science*, vol. 81, no. 2, pp. 218–224, 2006.

[93] M. C. Paoloni and C. Khanna, "Comparative oncology today," *Veterinary Clinics of North America*, vol. 37, no. 6, pp. 1023–1032, 2007.

[94] P. Uva, L. Aurisicchio, J. Watters et al., "Comparative expression pathway analysis of human and canine mammary tumors," *BMC Genomics*, vol. 10, article 135, 2009.

[95] K. Lindblad-Toh, C. M. Wade, T. S. Mikkelsen et al., "Genome sequence, comparative analysis and haplotype structure of the domestic dog," *Nature*, vol. 438, no. 7069, pp. 803–819, 2005.

[96] F. Joy, S. Basak, S. K. Gupta, P. J. Das, S. K. Ghosh, and T. C. Ghosh, "Compositional correlations in canine genome reflects similarity with human genes," *Journal of Biochemistry and Molecular Biology*, vol. 39, no. 3, pp. 240–246, 2006.

[97] A. Ben-Baruch, "Breast cancer progression: a "Vicious Cycle" of pro-malignancy activities is mediated by inflammatory cells, chemokines and cytokines," in *Integration/Interaction of Oncologic Growth*, pp. 189–217, Springer, Amsterdam, The Netherlands, 2005.

[98] F. Balkwill and A. Mantovani, "Inflammation and cancer: back to Virchow?" *The Lancet*, vol. 357, no. 9255, pp. 539–545, 2001.

[99] G. Curigliano, G. Spitaleri, E. Petri et al., "Breast cancer vaccines: a clinical reality or fairy tale?" *Annals of Oncology*, vol. 17, no. 5, pp. 750–762, 2006.

[100] B. Acres, J. Limacher, and J. Bonnefoy, "Discovery and development of therapeutic cancer vaccines," *Current Opinion in Drug Discovery and Development*, vol. 10, no. 2, pp. 185–192, 2007.

Review Article

Glix 13, a New Drug Acting on Glutamatergic Pathways in Children and Animal Models of Autism Spectrum Disorders

Annamaria Chiara Santini,[1] Giovanna Maria Pierantoni,[2] Raffaele Gerlini,[2] Rosamaria Iorio,[3] Yinka Olabinjo,[4] Alfonso Giovane,[3] Marina Di Domenico,[3] and Carla Sogos[1]

[1] *Dipartimento di Pediatria e Neuropsichiatria Infantile, Università di Roma La Sapienza, Via dei Sabelli 108, 00185 Roma, Italy*
[2] *Dipartimento di Medicina Molecolare e Biotecnologie Mediche, Università di Napoli Federico II, Via Pansini 5, 80131 Napoli, Italy*
[3] *Dipartimento di Biochimica, Biofisica e Patologia Generale, Seconda Università degli Studi di Napoli, Via De Crecchio 7, 80138 Napoli, Italy*
[4] *Dipartimento di Medicina, Chirurgia e Neuroscienze, Università di Siena, Policlinico Santa Maria alle Scotte, Viale Mario Bracci 16, 53100 Siena, Italy*

Correspondence should be addressed to Annamaria Chiara Santini; chiara1290@hotmail.it and Carla Sogos; carla.sogos@uniroma1.it

Received 31 July 2013; Accepted 9 December 2013; Published 30 January 2014

Academic Editor: Andrea Vecchione

Recently standardized diagnostic instruments have been developed in diagnostic and therapeutic procedures for Autism Spectrumv Disorders (ASD). According to the DSM-5 criteria, individuals with ASD must show symptoms from early childhood. These symptoms are communication deficits and restricted, repetitive patterns of behaviour. It was recently described by Bioinformatic analysis that 99 modified genes were associated with human autism. Gene expression patterns in the low-line animals show significant enrichment in autism-associated genes and the NMDA receptor gene family was identified among these. Using ultrasonic vocalizations, it was demonstrated that genetic variation has a direct impact on the expression of social interactions. It has been proposed that specific alleles interact with a social reward process in the adolescent mouse modifying their social interaction and their approach toward each other. In this review we report that the monoclonal antibody-derived tetrapeptide GLYX-13 was found to act as an N-methyl-D-aspartate receptor modulator and possesses the ability to readily cross the blood brain barrier. Treatment with the NMDAR glycine site partial agonist GLYX-13 rescued the deficit in the animal model. Thus, the NMDA receptor has been shown to play a functional role in autism, and GLYX-13 shows promise for the treatment of autism in autistic children.

1. Introduction

Autism Spectrum Disorders (ASD) are diseases driven by abnormalities in reciprocal social interaction (SI) and by the limited and repetitive behaviours (American Psychiatric Association, 1994). In developing infants, the evolution of social behaviours and the ability to share affect with other people have been previously described [1]. Meltzoff showed that the interactions between infants and their caregivers suggest the child's ability to respond to the emotions of those around him [2, 3]. Kanner said that children with autism were "like in a shell, happiest when left alone, acted as if people were'nt [sic] there and failed to develop the usual amount of social awareness" [4]. What is really frustrating, for the reliability of behavioural diagnosis, is that for autism a specific biomarker has not yet been identified. It is well known that a central network in the pathology of psychiatric disorders is represented by glutamatergic signalling, through N-methyl-D-aspartic acid (NMDA) receptor [5]. This receptor is activated by glutamate when specific D-serine or glycine coagonists occupy its allosteric site [6]. Glycine is considered the main coagonist in the spinal cord and in the hindbrain, and it has a high affinity for extrasynaptic NMDARs. D-serine is the main coagonist in the forebrain

[7], and it is characterized by a high affinity for synaptic NMDARs. In several brain regions (hippocampus, thalamus, and neocortex), NMDA receptor glycine/D-serine site is normally not saturated [8, 9] and, in this light, it was shown that the treatments of coagonists produce a modulation of affective behaviours in animal models [10].

Several mutations or allelic variants, that can influence brain development and behaviour, have been found in autism. Animal models have been employed to underline psychobiological determinants and early epigenetic influence [11]. In particular, juvenile mice are a popular species for genetic research [10] as well as in a more naturalistic context [12]. It was recently described that Bioinformatic analyses of 99 modified genes were associated with human autism. Gene expression patterns in the low-line animals show significant enrichment in autism-associated genes and the NMDA receptor gene family was identified among these. Recently, the monoclonal antibody-derived tetrapeptide GLYX-13 was found to act as an N-methyl-D-aspartate receptor modulator and it possesses the ability to readily cross the blood brain barrier. Treatment with the NMDAR glycine site partial agonist GLYX-13 rescued the deficit in the animal model. Thus, the NMDA receptor has been shown to play a functional role in autism, and GLYX-13 shows promise for the treatment of autism in autistic children.

2. GLYX 13, DMG, and NMDA Signaling

N-methyl-D-aspartate glutamate receptors (NMDARs) are involved in Ca^{2+} influx into neurons and are important to synaptic plasticity. When these receptors are uncontrolled they may trigger events that cause neuronal degeneration and death. This receptor-ionophore complex is functionally involved in modulating normal synaptic transmission, synaptic plasticity, and excitotoxicity in the central nervous system. Unlike other ligand-gated ion channels, the N-methyl-D-aspartate receptor-ionophore complex has a unique feature since it requires two distinct recognition sites by glutamate and glycine for its activation. Although the stoichiometry of native NMDARs is still uncertain, recombinant NMDARs appear to consist of at least one NR1 and one NR2 subunits, and most evidence now suggests that NMDARs assemble as tetramers containing 2 NR1 and 2 NR2 subunits. Many glutamate receptors have been found in the central nervous system but the glycine site of NMDA receptor possesses the distinctive ability to be strychnine-insensitive. Because of this specificity and the number of clinically relevant functions in which the NMDA receptors are involved, its glycine site is a potentially important target for drug development. Therefore, a noticeable increase occurred in the exploitation of pharmacological agents that interact selectively with the glycine binding site. For example, glycine and D-serine were found to be helpful in reducing some of the negative symptoms of schizophrenia [13] when used to augment antipsychotic therapeutics. The partial agonist, D-cycloserine (DCS), has been shown to have cognitive-enhancing properties in vivo. However, these compounds show desensitization after chronic administration. An increasing number of glycine site modulators have been described as appearing to have therapeutical potential. In 1991 was produced a monoclonal antibody, B6B21, that significantly elevates long-term potentiation when applied to CA1 pyramidal cell apical dendrites in rat hippocampus [14]. This antibody was found to bind at strychnine-insensitive glycine sites thus demonstrating its direct binding to N-methyl-D-aspartate receptors. In 2005, the B6B21 was transformed into a family of small peptides called Glyxins [15]. The GLYX-13, a tetrapeptide (TPPT-amide) originating from that antibody, was found to act as a NMDA receptor modulator similar to the partial agonist D-cycloserine and potentiates learning when administered intravenously to rats undergoing hippocampus-dependent trace eyeblink conditioning. Pharmacological and electrophysiological experiments demonstrate that GLYX-13 modulates the NMDA receptor in a glycine-like manner as a partial agonist. On the other hand, it is still unclear if GLYX-13 precisely mimics the action of the monoclonal antibody B6B21 from which it is derived. It is likely that GLYX-13 acts on a different site that indirectly affects glycine binding. Data obtained from behavioral studies suggest that systemic administration of peptides acting as NMDA receptor modulators can facilitate hippocampus-dependent learning. GLYX-13 administration in rats showed enhancements of hippocampus-dependent trace eyeblink conditioning that were similar to those obtained with the antibody B6B21 and with D-cycloserine, the partial agonist of the glycine site on the NMDA receptor. It is worthy to note that chronic administration of DCS can lead to desensitization and the monoclonal antibody B6B21 does not cross the blood brain barrier; instead GLYX-13 easily crosses the blood brain barrier making it a good candidate for clinical use as a cognitive enhancer.

3. Genetic Variation Influence in Autistic Animal Models

Knockouts in gene-targeted mice have been produced. They carry mutations in genes that have been associated with a SDA [16]. Genetic correlations include allelic variants of fragile-X [17]. Allelic variants have been found to be associated with ASD and gene-targeted mice can be generated to study development of receptor mechanisms in order to evaluate potential therapeutic strategy. Other evidences have been shown in fragile X mouse models, and several other strains, most notably the BTBR mouse, underline the importance of animal model in autism research [18]. Several evidences show a genetic predisposition to autism that involves a reduced expression of gene coding for Hepatocyte growth factor receptor (HGFR), also known as mesenchymal-epithelial transition factor (MET). In particular a 2-fold decrease in MET promoter activity and altered binding of specific transcription factor was observed in 204 autism families [19]. A critical step is to continue to push for more nuanced measures of mouse socialability, including the capacity to express emotion and to respond to emotional expressions of others. Several studies [20, 21] demonstrated that prepubescent mice from the B6 strain are particularly prosocial, whereas age-matched BALB mice are less reactive to social ability. Interestingly, adult mice from these two genetic backgrounds

appear to be much less distinct than juvenile mice in terms of their SI [22, 23].

According to Panksepp et al. [24], genetic variation has a direct impact on the expression of SI which can be divided into the following: (i) sniffing or snout contact with the head/neck/mouth area, (ii) sniffing or snout contact with the flank area, (iii) direct contact with the anogenital area, (iv) social pursuit within one body-length as the stimulus mouse moved continuously throughout the cage, and (v) social grooming. SI were evaluated by ultrasonic vocalizations and related underlying reward. The authors also proposed that specific alleles are involved in a social reward process in the adolescent mouse, modifying SI and to approach each other.

4. GLYX-13 Treatment in Animal Models

Adolescent as well as young mammals exhibit a characteristic form of SI known as social play behaviour or rough-and-tumble play. This form of social behaviour is considered a fundamental step for the development of social and cognitive skills. Hence, in order to study disorders of neural development, young rats are generally used as animal model. In fact, young rats exhibit the highest rates of social rough-and-tumble play behavior from among all species tested [25]. During testing, animals are videotaped and high frequency ultrasonic vocalizations were recorded. In fact, several researches on rat brain have shown a correlation between high frequency ultrasonic vocalizations (USVs) and anticipatory affective states. More precisely, long low-frequency (approximately 22 kHz) USVs occur during anticipation of punishment or avoidance behavior, whereas short high frequency (approximately 50 kHz) USVs typically occur during anticipation of reward or approach behavior. Thus, long 22 kHz USVs may be an indicator of negative activation state, whereas short 50 kHz USVs may instead indicate a state of positive activation [26]. Thus, USVs recording can be used to assay the rat emotional state as consequence of drug administration. This type of animal model was used to study the effect of GLYX 13 in autism. An animal model that displays analogous symptoms of autism was created using rats that show low rates of prosocial ultrasonic vocalizations (i.e., frequency modulated 50 kHz USVs) in response to rough-and-tumble play behavior. According to Moskal the low-line animals used for the experimental study found that lower rates of play-induced prosocial ultrasonic vocalizations correlate to an increased proportion of monotonous ultrasonic vocalizations compared to randomly bred animals [27]. The low-line selection was also screened by microarray gene expression and significant gene changes in brain regions in low-line animals were found compared to nonselectively bred random-line animals. The administration of GLYX-13 at a dose of 50 mg/kg (s.c.) significantly increased rates of play-induced pro-social USVs and significantly decreased the proportion of total USVs that are monotonous (i.e., pure tone whistles without any detectible frequency modulation) [28].

5. A New Candidate Drug in Autistic Children

ASDs cover a heterogeneous group of neurodevelopmental disorders defined behaviourally by three core disturbances: marked deficits in interpersonal SI, disrupted verbal and nonverbal communication, and restricted repetitive and stereotyped patterns of behaviour and interests [29, 30]. The ASD phenotype includes the classical or typical autistic disorder (AD), Asperger syndrome (AS) characterized by no general delay in language or cognitive development, and pervasive developmental disorders not otherwise specified (PDD-NOS), which is a milder condition that includes some, but not all, of the symptoms associated with classic autism. Once considered a rare clinical entity, autism is now considered common, with the most recent prevalence estimate being around 1 in 150 [31, 32]. In the scientific literature, there is varying support for a wide spectrum of hypotheses regarding the causes of autism: from studies showing that genes play a greater role in the risk for autism than in any other common neuropsychiatric disorder [33] to studies implicating disruptive environmental factors during neurodevelopment in genetically susceptible individuals [34]. Nevertheless, it is becoming increasingly obvious that a single cause or unifying theory is unlikely to account for what is now better referred to as "the autisms" [35, 36]. According to DSM-V, autism spectrum disorders (ASDs) can be diagnosed in a patient in early childhood with persistent deficits in social communication and SI. Autism is also manifested as deficits in social emotional reciprocity, deficits in nonverbal communicative behaviours, and deficits in developing and maintaining relationships. The patient has to be characterized by restricted, repetitive patterns of behaviour, interests, or activities. A paper aimed to compare the joint engagement of children with autism, children with Down syndrome, and their typically developing peers indicated that autism and Down syndrome often affect a young child's joint engagement experiences during social interactions with a caregiver [37]. Children with autism rarely coordinated attention to a shared object as normal developing peers do. In contrast, children in the Down syndrome group readily shared events with their partners but they were less likely to attend to symbols during these periods.

No specific biomarker for autism has been identified yet in order to improve the reliability of behavioural diagnosis. It was shown that the GABA system is related to pathophysiology of autism [38]. The exact pathophysiology of autism is yet unknown but the N-methyl-D-aspartate receptor (NMDAR) has received great attention as a possibility of treatment. In order to study its implications in this disorder, animal models have been used. A rat model has been developed for autism features such as social and communication deficits and repetitive and restrictive behaviours. Evidences previously described include dysfunction of NMDARs; as is known genetic risk factors suggest that its hypofunction is involved in pathogenesis. The NMDAR pathway could become a target for the development of a variety of therapeutic drugs as glycine site modulators. In fact, it is involved in learning and memory formation and also in a number of neuropathologies [39]. NMDAR role is validated by the effects obtained upon D-cycloserine treatment. D-cycloserine is an antibiotic and a partial agonist at NMDA; its significant improvement in social withdrawal has been shown and it has been proposed as a treatment for autism by several authors. Posey et

al. described the effects of DCS on the Autism Spectrum Disorder symptoms [40]. The therapeutic program consisted of a single-blind placebo lead-in phase about the treatment of 10 drug-free subjects (5–27 years old) with autistic disorder. Three different doses of D-cycloserine were used and patients followed for two weeks. Measures used for subject ratings included the Clinical Global Impression (CGI) scale and Aberrant Behavior Checklist. On the highest dose, subjects enrolled for this therapeutic approach had statistically significant improvement in social withdrawal. Adverse effects reported included motor tics and increased echolalia in two subjects. Priestley et al. [41] suggested that partial agonists at glycine site may be better therapeutic candidates: acting as weak agonists, they would facilitate receptor activation without creating the risk of overactivating the receptors and acting as antagonists, they would allow normal synaptic transmission to take place while simultaneously suppressing receptor hyperactivity, through the NMDA signaling.

6. Concluding Remarks

GLYX 13 belongs to a new class of NMDAR glycine site modulators with therapeutic potential and could have a clinical value. Several studies have reported that important peptides derived from monoclonal antibody have been created for therapeutic approach. In order to provide useful novel therapeutics in autism, the mimetic peptide GLYX-13 has been produced and is added to the list of CDR-derived functional peptides (complementary determining regions). Recent studies show that GLYX-13 readily crosses the blood brain barrier and modulates the NMDA receptor in a glycine-like way decreasing the deficit in animal models and giving hope for the treatment of autism in children. Burgdorf et al. [42] showed that this drug can be used in association with ketamine and produced antidepressant-like effect. These treatments are currently in a Phase II clinical development program for treatment-resistant depression. Several reports explain how NMDA receptors are involved in neuropsychiatric disorder, as well as development of symptoms for schizophrenia. However, open questions concerning the molecular mechanism of NMDAR dysfunction yet remain.

Conflict of Interests

The authors declare that there is no conflict of interests regarding the publication of this paper.

References

[1] G. Markova and M. Legerstee, "Contingency, imitation, and affect sharing: foundations of infants' social awareness," *Developmental Psychology*, vol. 42, no. 1, pp. 132–141, 2006.

[2] R. Feldman, "Parent-infant synchrony: biological foundations and developmental outcomes," *Current Directions in Psychological Science*, vol. 16, no. 6, pp. 340–345, 2007.

[3] A. N. Meltzoff, "The 'like me' framework for recognizing and becoming an intentional agent," *Acta Psychologica*, vol. 124, no. 1, pp. 26–43, 2007.

[4] L. Kanner, "Autistic disturbances of affective contact," *Nervous Child*, vol. 2, pp. 217–250, 1943.

[5] J. T. Coyle, "Glutamate and schizophrenia: beyond the dopamine hypothesis," *Cellular and molecular neurobiology*, vol. 26, no. 4–6, pp. 365–384, 2006.

[6] P. M. Kim, H. Aizawa, P. S. Kim et al., "Serine racemase: activation by glutamate neurotransmission via glutamate receptor interacting protein and mediation of neuronal migration," *Proceedings of the National Academy of Sciences of the United States of America*, vol. 102, no. 6, pp. 2105–2110, 2005.

[7] M. Martina, N. V. Krasteniakov, and R. Bergeron, "D-Serine differently modulates NMDA receptor function in rat CA1 hippocampal pyramidal cells and interneurons," *Journal of Physiology*, vol. 548, no. 2, pp. 411–423, 2003.

[8] V. Baptista and W. A. Varanda, "Glycine binding site of the synaptic NMDA receptor in subpostremal NTS neurons," *Journal of Neurophysiology*, vol. 94, no. 1, pp. 147–152, 2005.

[9] A. C. Basu, G. E. Tsai, C.-L. Ma et al., "Targeted disruption of serine racemase affects glutamatergic neurotransmission and behavior," *Molecular Psychiatry*, vol. 14, no. 7, pp. 719–727, 2009.

[10] V. Labrie, T. Lipina, and J. C. Roder, "Mice with reduced NMDA receptor glycine affinity model some of the negative and cognitive symptoms of schizophrenia," *Psychopharmacology*, vol. 200, no. 2, pp. 217–230, 2008.

[11] S. M. Pellis and M. McKenna, "What do rats find rewarding in play fighting?—an analysis using drug-induced non-playful partners," *Behavioural Brain Research*, vol. 68, no. 1, pp. 65–73, 1995.

[12] M. E. Ritchie and G. E. Belovsky, "Sociality of Columbian ground squirrels in relation to their seasonal energy intake," *Oecologia*, vol. 83, no. 4, pp. 495–503, 1990.

[13] S. E. Lakhan, M. Caro, and N. Hadzimichalis, "NMDA receptor activity in neuropsychiatric disorders," *Front Psychiatry*, vol. 4, p. 52, 2013.

[14] R. Haring, P. K. Stanton, M. A. Scheideler, and J. R. Moskal, "Glycine-like modulation of N-methyl-D-aspartate receptors by a monoclonal antibody that enhances long-term potentiation," *Journal of Neurochemistry*, vol. 57, no. 1, pp. 323–332, 1991.

[15] J. R. Moskal, A. G. Kuo, C. Weiss et al., "GLYX-13: a monoclonal antibody-derived peptide that acts as an N-methyl-D-aspartate receptor modulator," *Neuropharmacology*, vol. 49, no. 7, pp. 1077–1087, 2005.

[16] X.-Q. Liu, A. D. Paterson, and P. Szatmari, "Genome-wide linkage analyses of quantitative and categorical autism subphenotypes," *Biological Psychiatry*, vol. 64, no. 7, pp. 561–570, 2008.

[17] A. Zhang, C.-H. Shen, S. Y. Ma, Y. Ke, and A. E. Idrissi, "Altered expression of Autism-associated genes in the brain of Fragile X mouse model," *Biochemical and Biophysical Research Communications*, vol. 379, no. 4, pp. 920–923, 2009.

[18] J. L. Silverman, S. S. Tolu, C. L. Barkan, and J. N. Crawley, "Repetitive self-grooming behavior in the BTBR mouse model of autism is blocked by the mGluR5 antagonist MPEP," *Neuropsychopharmacology*, vol. 35, no. 4, pp. 976–989, 2010.

[19] D. B. Campbell, J. S. Sutcliffe, P. J. Ebert et al., "A genetic variant that disrupts MET transcription is associated with autism," *Proceedings of the National Academy of Sciences of the United States of America*, vol. 103, no. 45, pp. 16834–16839, 2006.

[20] S. S. Moy, J. J. Nadler, N. B. Young et al., "Social approach in genetically engineered mouse lines relevant to autism," *Genes, Brain and Behavior*, vol. 8, no. 2, pp. 129–142, 2009.

[21] G. M. V. Sankoorikal, K. A. Kaercher, C. J. Boon, J. K. Lee, and E. S. Brodkin, "A mouse model system for genetic analysis of sociability: C57BL/6J versus BALB/cJ inbred mouse strains," *Biological Psychiatry*, vol. 59, no. 5, pp. 415–423, 2006.

[22] E. S. Brodkin, A. Hagemann, S. M. Nemetski, and L. M. Silver, "Social approach-avoidance behavior of inbred mouse strains towards DBA/2 mice," *Brain Research*, vol. 1002, no. 1-2, pp. 151–157, 2004.

[23] E. S. Brodkin, "BALB/c mice: low sociability and other phenotypes that may be relevant to autism," *Behavioural Brain Research*, vol. 176, no. 1, pp. 53–65, 2007.

[24] J. B. Panksepp, K. A. Jochman, J. U. Kim et al., "Affiliative behavior, ultrasonic communication and social reward are influenced by genetic variation in adolescent mice," *PLoS ONE*, vol. 2, no. 4, article e351, 2007.

[25] K. M. Harmon, H. C. Cromwell, J. Burgdorf et al., "Rats selectively bred for low levels of 50 kHz ultrasonic vocalizations exhibit alterations in early social motivation," *Developmental Psychobiology*, vol. 50, no. 4, pp. 322–331, 2008.

[26] J. Burgdorf, R. A. Kroes, J. R. Moskal, J. G. Pfaus, S. M. Brudzynski, and J. Panksepp, "Ultrasonic vocalizations of rats (Rattus norvegicus) during mating, play, and aggression: behavioral concomitants, relationship to reward, and self-administration of playback," *Journal of Comparative Psychology*, vol. 122, no. 4, pp. 357–367, 2008.

[27] J. R. Moskal, J. Burgdorf, R. A. Kroes, S. M. Brudzynski, and J. Panksepp, "A novel NMDA receptor glycine-site partial agonist, GLYX-13, has therapeutic potential for the treatment of autism," *Neuroscience and Biobehavioral Reviews*, vol. 35, no. 9, pp. 1982–1988, 2011.

[28] J. Burgdorf, J. R. Moskal, S. M. Brudzynski, and J. Panksepp, "Rats selectively bred for low levels of play-induced 50kHz vocalizations as a model for Autism Spectrum Disorders: a role for NMDA receptors," *Behavioural Brain Research*, vol. 251, pp. 18–24, 2013.

[29] F. R. Volkmar and D. Pauls, "Autism," *The Lancet*, vol. 362, no. 9390, pp. 1133–1141, 2003.

[30] B. Jackson, "The revised diagnostic and statistical manual of the American Psychiatric Association," *American Journal of Psychiatry*, vol. 127, no. 1, pp. 65–73, 1970.

[31] Autism and Developmental Disabilities Monitoring Network Surveillance Year 2002 Principal Investigators, "Centers for Disease Control and Prevention. Prevalence of autism spectrum disordersautism and developmental disabilities monitoring network, 14 sites, United States, 2002," *MMWR Surveillance Summaries*, vol. 56, pp. 12–28, 2007.

[32] G. Baird, E. Simonoff, A. Pickles et al., "Prevalence of disorders of the autism spectrum in a population cohort of children in South Thames: the Special Needs and Autism Project (SNAP)," *The Lancet*, vol. 368, no. 9531, pp. 210–215, 2006.

[33] A. R. Gupta and M. W. State, "Recent advances in the genetics of autism," *Biological Psychiatry*, vol. 61, no. 4, pp. 429–437, 2007.

[34] A. M. Persico and T. Bourgeron, "Searching for ways out of the autism maze: genetic, epigenetic and environmental clues," *Trends in Neurosciences*, vol. 29, no. 7, pp. 349–358, 2006.

[35] D. H. Geschwind and P. Levitt, "Autism spectrum disorders: developmental disconnection syndromes," *Current Opinion in Neurobiology*, vol. 17, no. 1, pp. 103–111, 2007.

[36] F. Happé, A. Ronald, and R. Plomin, "Time to give up on a single explanation for autism," *Nature Neuroscience*, vol. 9, no. 10, pp. 1218–1220, 2006.

[37] L. B. Adamson, R. Bakeman, D. F. Deckner, and M. Romski, "Joint engagement and the emergence of language in children with autism and down syndrome," *Journal of Autism and Developmental Disorders*, vol. 39, no. 1, pp. 84–96, 2009.

[38] D. Dhossche, H. Applegate, A. Abraham et al., "Elevated plasma gamma-aminobutyric acid (GABA) levels in autistic youngsters: stimulus for a GABA hypothesis of autism," *Medical Science Monitor*, vol. 8, no. 8, pp. PR1–PR6, 2002.

[39] A. E. Evins, E. Amico, T. A. Posever, R. Toker, and D. C. Goff, "D-Cycloserine added to risperidone in patients with primary negative symptoms of schizophrenia," *Schizophrenia Research*, vol. 56, no. 1-2, pp. 19–23, 2002.

[40] D. J. Posey, D. L. Kem, N. B. Swiezy, T. L. Sweeten, R. E. Wiegand, and C. J. McDougle, "A pilot study of D-cycloserine in subjects with autistic disorder," *American Journal of Psychiatry*, vol. 161, no. 11, pp. 2115–2117, 2004.

[41] T. Priestley, G. R. Marshall, R. G. Hill, and J. A. Kemp, "L-687,414, a low efficacy NMDA receptor glycine site partial agonist *in vitro*, does not prevent hippocampal LTP *in vivo* at plasma levels known to be neuroprotective," *British Journal of Pharmacology*, vol. 124, no. 8, pp. 1767–1773, 1998.

[42] J. Burgdorf, X. L. Zhang, K. L. Nicholson et al., "GLYX-13, a NMDA receptor glycine-site functional partial agonist, induces antidepressant-like effects without ketamine-like side effects," *Neuropsychopharmacology*, vol. 38, no. 5, pp. 729–742, 2013.

Hindawi Publishing Corporation
BioMed Research International
Volume 2013, Article ID 617569, 19 pages
http://dx.doi.org/10.1155/2013/617569

Research Article

Obesity, Insulin Resistance, and Metabolic Syndrome: A Study in WNIN/Ob Rats from a Pancreatic Perspective

Vijayalakshmi Venkatesan,[1] Soundarya L. Madhira,[1] Venkata M. Malakapalli,[1] Maniprabha Chalasani,[1] Sarfaraz N. Shaik,[1] Vasudevan Seshadri,[2] Venkaiah Kodavalla,[3] Ramesh R. Bhonde,[4] and Giridharan Nappanveettil[5]

[1] *Department of Biochemistry/Stem Cell Research, National Institute of Nutrition, Indian Council of Medical Research, Jamai-Osmania (P.O), Hyderabad, Andhra Pradesh 500007, India*
[2] *Laboratory 12, National Center for Cell Sciences, NCCS Complex, Pune University Campus, Ganeshkhind, Pune, Maharashtra 411007, India*
[3] *Division of Community Studies, National Institute of Nutrition, Hyderabad, Andhra Pradesh 500007, India*
[4] *Manipal Institute of Regenerative Medicine, GKVK Post, Bellary Road, Allalasandra, Yelahanka, Bangalore, Karnataka 560065, India*
[5] *National Center for Laboratory Animal Sciences, National Institute of Nutrition, Hyderabad, Andhra Pradesh 500007, India*

Correspondence should be addressed to Vijayalakshmi Venkatesan; v.venkateshan@gmail.com

Received 16 July 2013; Revised 9 November 2013; Accepted 11 November 2013

Academic Editor: Oreste Gualillo

Alterations in pancreatic milieu to adapt to physiological shifts occurring in conditions of obesity and metabolic syndrome (MS) have been documented, though mechanisms leading to such a state have remained elusive so far. The data presented here tries to look at the gravity of metabolic insult during the early and prolonged phases of obesity/insulin resistance (IR) depicted in WNIN/Ob strain of rats—an obese euglycemic mutant rat model developed indigenously at our institute which is highly vulnerable for a variety of degenerative diseases. The present results *in situ* show the participation of several confounding factors in the pancreatic milieu that collectively coprecipitates for a state of profound inflammation in the pancreas (among Mutant compared to Lean/Control) which gets worsened with age. These include hypertrophy, macrophage infiltration (CD11b/TNFα/IL6), apoptosis, β-cell vacuolation, hyperinsulinemia (HI), and stress markers (RL-77/HSP104/TBARS) all of which correlated well with indices for obesity (2-3 fold), IR (1.5-3 fold), and HI (2-3 fold). Further, supportive data was also obtained from *in vitro* studies using islet cell cultures amongst phenotypes. Taken together, these results advocate that inflammation was the major precipitating factor to cause islet cell dysfunctions (*in situ* and *in vitro*) in these Mutant rats compared to their Lean littermates and parental Control.

1. Introduction

Obesity with insulin resistance (IR) forms a major part of metabolic syndrome (MS) and its co-precipitation with etiological factors has been shown to cause dysregulation of several dynamic processes, thereby predisposing the organism to long-term micro- and macro-vascular complications [1]. Interestingly, animal models (ob/ob and db/db mice and Zucker and Koletsky rats) have greatly helped our understanding of the pathophysiology associated with MS, although the mechanism(s) remain(s) obscure [2]. WNIN/Ob rat strain (Mutant) is a new entrant to the list of obese animal models and is derived indigenously from the Wistar rat strain of our institute (WNIN), maintained at our institute in an inbred status since 1920. WNIN/Ob, which arose spontaneously from WNIN in 1997, is euglycemic and portrays features of obesity/IR with distinct clinical and biochemical features like hyperinsulinemia (HI), hypertriglyceridemia, and hypercholesterolemia along with hyperphagia, polydipsia, polyuria, and proteinuria akin to other obese model systems [3]. Interestingly, this is the biggest obese rat strain (1.4 Kgs) so far recorded in literature, and is leptin resistant with unaltered leptin or its receptor coding sequences and the strain exhibits three distinct phenotypes:

homozygous lean (+/+), heterozygous carrier (+/−), and homozygous obese (−/−), in a typical Mendelian ratio of 1 : 2 : 1. The mode of inheritance is autosomal incomplete dominance. Attempts to localize the mutation in this model system are in progress and a recent study from our institute has localized the observed unilocus mutation to exist in a 4.3 cM region with flanking markers D5Rat256 and D5Wox37 on chromosome 5 upstream of the leptin receptor [4]. These Mutants stand apart from other similar models, due to the presence of "kinky tail" in heterozygous carriers (+/−) and in homozygous obese (−/−) phenotypes. Apart from obesity, these Mutants show a variety of degenerative diseases, as they cross one year, like breast tumors and lipomas, cataract and retinal degenerations (in 20%), hypertension [5], osteoporosis, polycystic ovaries, kidney damage, impaired immunity, and accelerated aging with the life span of Mutants reduced to 1.5 years, while a normal rat lives up to 3–3.5 years [6].

The impetus obtained from our published data using adipose tissue (AT) [7] and bone marrow derived mesenchymal stem cells (BM-MSCs) [8] from these animals supported an *in situ* inflammation with obesity as a predominant metabolic lesion. The metabolic interrelationships and cross-talks (cytokines) contributed from skeletal muscle (SM) and AT have been shown to be decisive for the maintenance of glucose homeostasis [9] and dysregulations have been shown to influence the β-cell functions and integrity [10]. It is to be noted here that β-cells of the pancreas have an inherent weak antioxidant system as compared to any organ [11] and with persistent IR [3], hyperglycemia, and obesity or HI could predispose the organism to long-term secondary complications [12, 13] vis-à-vis β-cell dysfunctions [12].

We hypothesize that WNIN/Ob rats (Mutants) with their inherent phenotypic features would form an ideal model to assess the gravity of metabolic insult both at early and prolonged (chronic) phases seen with age (1, 6, and 12 months). In the present study we have compared homozygous obese rats (WNIN/Ob (−/−)) (Mutants) with their age matched homozygous lean (WNIN/Ob (+/+)) littermates (Leans) and parental (WNIN) controls (Controls) for all the parameters (islet cell architecture, inflammation, and islet cell functions) studied in *in situ* (tissue) and *in vitro* (primary islet cell cultures). This is primarily to understand the early and chronic phases of the metabolic insult which has been reported with these Mutants and is appreciable with age (1, 6, and 12 months).

2. Material and Methods

2.1. Animals. Experimental procedures were in compliance with the principles of laboratory animal care and approved by the Institutional Ethical Committee on Animal Experiments, Hyderabad, India. Male rats, six per strain, (Mutant, Lean, and Control) matched for age (1, 6, and 12 months) were obtained from an inbred colony of the National Centre for Laboratory Animal Sciences (NCLAS) facility at our institute. To understand the effect of accelerated aging on the pathophysiology of MS in the 12-month Mutant rats, we have made a comparison of 12-month Mutants with two-year-old (24-month) Control rats in few critical metabolic parameters. The animals were given normal rat chow with water *ad libitum*. They were maintained under optimal conditions of 12 hr light/dark cycles, with temperature (20 ± 2°C) with relative humidity (50 ± 10%) kept constant. Prior to the day of euthanization, animals were fasted overnight to normalize any differences in feeding patterns and to minimize experimental variations.

2.2. Physiological Parameters. Anthropometric measurements (body/pancreatic tissue weights), blood glucose [7], insulin (plasma/tissue) [11, 14] and IR indices—Homeostasis Model of Assessment for Insulin Resistance (HOMA-IR) and Quantitative Insulin Sensitivity Check Index (QUICKI) were measured as described previously [8]. Thiobarbituric acid reacting species (TBARS), a marker of global oxidative stress/lipid peroxidation, were measured in plasma/pancreatic tissue as per our earlier protocol [15].

2.3. Tissue Morphometry. Pancreatic tissues (formalin fixed and paraffin embedded) of 6–8 μm thickness were processed for hematoxylin and eosin (H&E), and immunofluorescence including TUNEL assay [7, 16, 17]. H&E stained sections were used for studying islet morphology (islet size, β-cell vacuolation, and AT/macrophage infiltration), and images were captured using an inverted microscope (TE2000S, Nikon, Japan) with ACT2U software (version 1.7, Nikon, Japan).

2.4. Immunofluoresence. Immunostaining of the pancreatic sections was performed as described previously [8, 16]. In brief, pancreatic sections were blocked with 4% horse serum and incubated overnight at 4°C using either 1 : 100 dilution of primary antibodies for mouse antihuman insulin (Sigma, USA), rabbit antihuman glucagon (Santa Cruz, USA), goat antihuman PDX-1 (Santa Cruz, USA), rabbit polyclonal antihuman HSP104 (gift), mouse polyclonal anti-RL-77 (gift, National Centre for Cell Sciences, Pune, India), or 1 : 400 dilution of rabbit polyclonal anti-IL-6 (Abcam, USA). After repeated washes, the sections were incubated with secondary antibodies (1 : 200 dilution) for anti-mouse FITC (Insulin/RL-77), anti-rabbit Texas Red (glucagon) (Santa Cruz, USA), anti-goat Texas Red (Pdx-1), anti-rabbit Cy3 (HSP104) (Jackson's Laboratories, USA), and anti-rabbit Alexa 568 (IL-6). After several more washes the sections were mounted using DAPI (Vectashield, Vector Laboratories, USA). Antigen retrieval for the nuclear transcription factor Pdx-1 was performed by treating tissue sections with 2 N HCl for 1 hr at room temperature. Similarly, dual fluorescence for CD11b and TNFα was carried out using FITC conjugated mouse anti-rat CD11b (BD Biosciences, USA) and PE hamster anti-rat TNFα (BD Biosciences, USA) at 1 : 100 dilution. Immunostaining of pancreatic sections of 24-month-old WNIN rats was performed for insulin, glucagon, CD11b, TNFα, IL-6, and Pdx-1 as described above. The images were captured using 405 (DAPI), 488 (FITC), 514 (Cy3), 561

(PE/568), and 594 (Texas red) lasers using a confocal microscope (Leica SP5, Leica Microsystems, Germany) with Leica Advanced Fluorescence (LAF) software (Leica Microsystems, Germany). The fluorescence intensities were calculated as relative fluorescent units (RFU) (relative to isotype control) using the LAF software and represented as RFU per unit area. All images were captured using Leica Advanced Fluorescence software (Mannheim, Germany) in Leica Confocal Microscope SP5 series (Mannheim, Germany) at a magnification of 400x unless otherwise specified. An asterisk (*) indicates a significance of $P < 0.05$ by ANOVA compared to Control and ($) represents the statistical significance ($P < 0.05$ by ANOVA) compared to the phenotype at 1 month. Values have been represented as Mean ± SE ($n = 6$) from three independent experiments performed in duplicate.

β-cell mass was calculated from the insulin stained sections, captured using LAF software as mentioned above [18] at a final magnification of 200x. Area of β-cells was determined by quantifying the cross-sectional area occupied by β-cells to the total cross-sectional area of the tissue (in all multiple fields per slide) and represented as a product of the cross-sectional area of β-cells/total tissue and the weight of the pancreatic tissue before fixation. Total tissue area was corrected for the unstained area inside the fat cells, by tracing the region occupied by fat cells in the H&E stained specimens (at a final magnification of 200x).

2.5. TUNEL Assay. Apoptosis was studied using DeadEnd Fluorometric TUNEL assay kit (Promega, USA) as per the manufacturer's protocol. Apoptotic cells were visualized with FITC positive nuclei and images were captured using 405 and 488 lasers under a confocal microscope using LAF software. TUNEL assay was also performed on 24-month-old Control pancreatic tissue sections. Apoptotic index (AI) was calculated as the ratio of number of TUNEL positive nuclei to the total number of nuclei per islet [19].

2.6. Gene Expression Analysis. The methodology for semi-quantitative reverse transcription polymerase chain reaction (sq-RT-PCR) used was similar to the procedures reported earlier by us [8]. Total RNA (from ~100 mg of pancreatic tissue) was isolated using TriReagent (Sigma, USA) and cDNA was prepared from 2 μg of total RNA using enhanced avian myeloblastosis virus reverse transcriptase enzyme (Sigma, USA) and amplified with JumpStart AccuTaq LA DNA Polymerase (Sigma, USA). Primers were designed with the aid of PrimerQuest software (Integrated DNA technologies, Coralville, IA). PCR was carried out to analyze the expression of *Insulin-1* (sense: caatcatagaccatcagcaagc; antisense: tttattcattgcagaggggtgg), *Pdx-1* (sense: tacaaggacccgtgcgcatt; antisense: tcaagttgagcatcactgcc), and *β-actin* (sense: tgtgatggtgggaatgggtcag; antisense: tttgatgtcacgcacgatttcc). Amplicons were resolved electrophoretically (1.2% agarose gel), visualized in GelDoc (BioRad, Italy), and quantitated by densitometric analysis using QuantityOne software (BioRad, Italy). Results have been normalized against the house keeping gene *β-actin*.

Quantitative real-time PCR was performed for each sample in triplicate using a CFX 96 Touch Real-Time PCR system (BioRad, Italy) in a 96-well PCR plate (BioRad, Italy). Each assay (20 μL total volume) contained nuclease-free water (11 μL-12 μL), cDNA template (conc—2 ng/μL), gene-specific primers (conc—4.5 pm/μL), and 5 μL SYBR green PCR Master Mix (KAPA Biosystems, South Africa). The cycling conditions were enzyme activation at 95°C for 30 s; 40 cycles of 95°C for 30 s (denaturation); and *Pdx-1* at 60°C and *Insulin-1* at 58°C for 30 s (annealing) with a single fluorescence measurement at 72°C for 30 s (dissociation curve). Specificity of the PCR products was confirmed by the melting curve program with temperatures in the range of 60 to 95°C with a heating rate of 0.5 to 0.05°C/s and a continuous fluorescence measurement. Relative differences in gene expression between groups (Mutant, Lean, and Control—aged 1, 6, and 12 months) are represented as fold change using $2^{\Delta\Delta CT}$ method as per the protocol of Dussault and Pouliot [20].

2.7. In Vitro Assays

Islet Isolation, Primary Cell Cultures, Viability, and Functional Assays. Islets were isolated under sterile conditions from all the three phenotypes (Mutant, Lean, and Control) as per our published protocol [14]. Keeping in view the fact that Mutants have 47% fat in their body which interferes with the islet integrity and cell yield by forming a viscous jelly-like material when compared to their age matched parental Controls, we had optimized conditions for islet cell isolation with minimal viscous material and maximum islet yield and functional response (primary islet cell cultures) using differential collagenase digestion [14]. Briefly, pancreas were collected under sterile conditions, minced and subjected to collagenase digestion using either 0.5 mg/mL for Mutants or 1 mg/mL for Lean/Control. The digestion mixture also contained 2 mg/mL soy bean trypsin inhibitor (Sigma, USA) and 2% BSA fraction V (Sigma, USA). All steps were performed at optimal temperature (37 ± 1.5°C) and pH (7.0 or 7.7–7.9) [21] and digestion (turbidity appearance) was stopped with the addition of chilled RPMI-1640 containing 10% FCS (1 : 3 ratio) in order to prevent islet necrosis during isolation [22]. The digests were washed (3x), and islet-cell-enriched fractions were seeded in RPMI-1640 medium with 10% FBS with antibiotics (Invitrogen, USA). After a period of 24–48 hrs, the islets were harvested by handpicking for *in vitro* assays including viability by MTT (3-(4,5-dimethylthiazol-2-yl)-2,5-diphenyl tetrazolium bromide) assay [23] and islet cell integrity by dithizone (DTZ) staining (Sigma, USA) [14], and images were captured with a Nikon inverted microscope using ACT-2U software. Insulin secretion assay was carried out from the primary islet cell cultures of Mutant, Lean, and Control phenotypes at basal (5.5 mmol/L) followed by high glucose (16.5 mmol/L) challenge as described earlier [8, 14]. Similarly, insulin secretion assay to assess islet cell function was also performed from islets (primary islet cell cultures) derived from 24-month-old Control rats [14].

2.8. Ultrastructural Analysis. For ultrastructural studies, the primary islet cell cultures of only 12-month-old animals (Mutant, Lean, and Control) presenting increased degenerative changes [3, 6, 24] were processed for both scanning electron microscopy (SEM) [25] (performed at 5 to 10 KV in S3400N, Hitachi, Japan) and transmission electron microscopy (TEM) [26] (performed at 75 KV in H-600, Hitachi, Japan), respectively.

2.9. Statistics. Descriptive statistics (Mean/SE) were calculated for all the samples using SPSS version 15.0 software and values have been represented as Mean ± SE ($n = 6$). To compare between the phenotypes, analysis of variance (ANOVA) followed by post hoc tests (LSD/Dunnett's C test) was carried out based on Levene's test for equality of error variances. Bivariate correlation analysis (2-tailed) for better understanding of the correlation between metabolic, anthropometric, and physiological parameters was performed using the same software (SPSS version 15.0) for a better understanding of the correlation between these parameters. $P < 0.05$ was considered statistically significant for all the measurements. Data have been computed from three independent experiments carried out in duplicate for tissue morphometry, immunofluoresence, PCR, and ultrastructural analyses and from six animals per group for all anthropometric/physiological analyses.

3. Results

3.1. Physiological Parameters

3.1.1. Body Weight/Pancreatic Weight. A significant increase in the body weight of Mutants, which increased with age (1, 6, and 12 months) to a tune of 4–7-fold ($P < 0.05$) compared to their Leans and Controls, was observed (Figure 1(a)). In similar lines, pancreatic weights were also increased in Mutants by 2-fold when compared to their Leans and Controls at all age groups (Figure 1(b)). However, both body weights and pancreatic weights were almost comparable between Leans and Controls with age (Figures 1(a) and 1(b)).

3.1.2. Glucose and Insulin (Plasma and Tissue Insulin). The animals were euglycemic [6] in all age groups with fasting blood glucose (FBG) in the range of 3.9–6.1 mmoles/L. The plasma and tissue insulin levels were almost similar during the early age, that is, at 1 month, amongst phenotypes, but with age Mutants demonstrated a significant increase in both plasma (HI) and tissue insulin levels being appreciable at 6 months (compared to Leans (by 3.03- and 1.10-fold) and Controls (by 3.70- and 2.82-fold)) and 12 months (compared to Leans (by 5.51- and 1.71-fold) and Controls (by 3.77- and 1.39-fold)), respectively (Figures 1(c) and 1(j)). The plasma (2.13±0.52) and tissue insulin (5.36±0.75) levels measured in 24-month-old Control rats were, however, found to be lower than those observed in 12-month Controls.

3.1.3. Oxidative Stress (Malonaldehyde Measurements). TBARS signifying global oxidative stress indices were also upregulated significantly ($P < 0.05$) in Mutants at all ages which was reflected both in plasma (Figure 1(f)) and pancreatic tissue (Figure 1(k)) levels compared to their Leans and Controls.

3.1.4. Measurement of IR. We observed a significant increase in HOMA-IR (Figure 1(d)) supported by a significant decrease in QUICKI (Figure 1(e)) among Mutants at 6 and 12 months but not at 1 month suggesting an increase in IR with age. However Lean and Control rats remained insulin sensitive as reflected by IR Indices. Based on the HOMA-IR and QUICKI indices calculated 24-month-old Control rats also showed IR (1.21 and 0.32, resp.) as an age dependent effect similar to Mutant rats.

3.2. Morphometric Studies. H&E staining of Mutant pancreatic tissues at 6 and 12 months of age demonstrated a marked hypertrophy with large and irregular islets (Figure 1(g)), β-cell vacuolation (Figure 1(h)), and disruption in the outer collagenous layer as compared to the intact morphology of the islets noted with Leans and Controls (Figures 1(g) and 1(h)). Further, evidence for an increased vasculature, intraislet vacuolation, and fat infiltration into the exocrine region was also predominant in Mutant pancreas when compared to its Lean and Control (Figure 1(g)). However the morphology was more or less similar to the early age group of 1 month studied amongst the phenotypes (Figures 1(g)-1(h)).

As shown in Figure 1(i), Mutant pancreas showed increase in islet size measured using ACT2U software (Nikon microscope), which was significant among Mutants by 1.25-, 1.54-, and 1.35-fold compared to Leans and by 1.40-, 1.38-, and 1.54-fold compared to their Controls at 1, 6, and 12 months (Figure 1(i)). However, the differences observed in islet size between Leans and Controls were not statistically significant. Islet size among 24-month Controls was found to be 320.45 ± 15.02 μm, in line with the trends expected with 12-month Mutants.

3.3. Immunofluoresence. Immunostaining of pancreatic tissues with insulin and glucagon amongst the phenotypes demonstrated a central core of insulin positive β-cells surrounded by a peripheral mantle of glucagon positive α-cells at all the ages studied (Figures 2(a)–2(d)). As depicted in Figure 2(f), insulin immunopositive cells expressed as RFU per unit (relative to isotype controls (Figure 2(e))) were significantly higher in Mutants at 1, 6, and 12 months compared to Leans (by 1.72-, 3.31-, and 1.27-fold) and Controls (by 2.74-, 3.03-, and 1.42-fold), respectively, substantiating HI/increased tissue insulin levels observed. However, similar levels of insulin positivity (RFU per unit area) were observed among Lean and Control with age (Figures 2(a)–2(d) and 2(f)). Among the 24-month Controls, RFU per unit area for insulin was found to be 30.75 ± 2.6.

Interestingly, glucagon positive cells (RFU per unit area relative to isotype controls (Figure 2(e))) were also increased in Mutant pancreas, both at an early phase, that is, 1 month, (RFU = 19.32) and midphase, that is, 6 months, (RFU = 16.04) unlike at 12 months (RFU = 14.68) which showed a

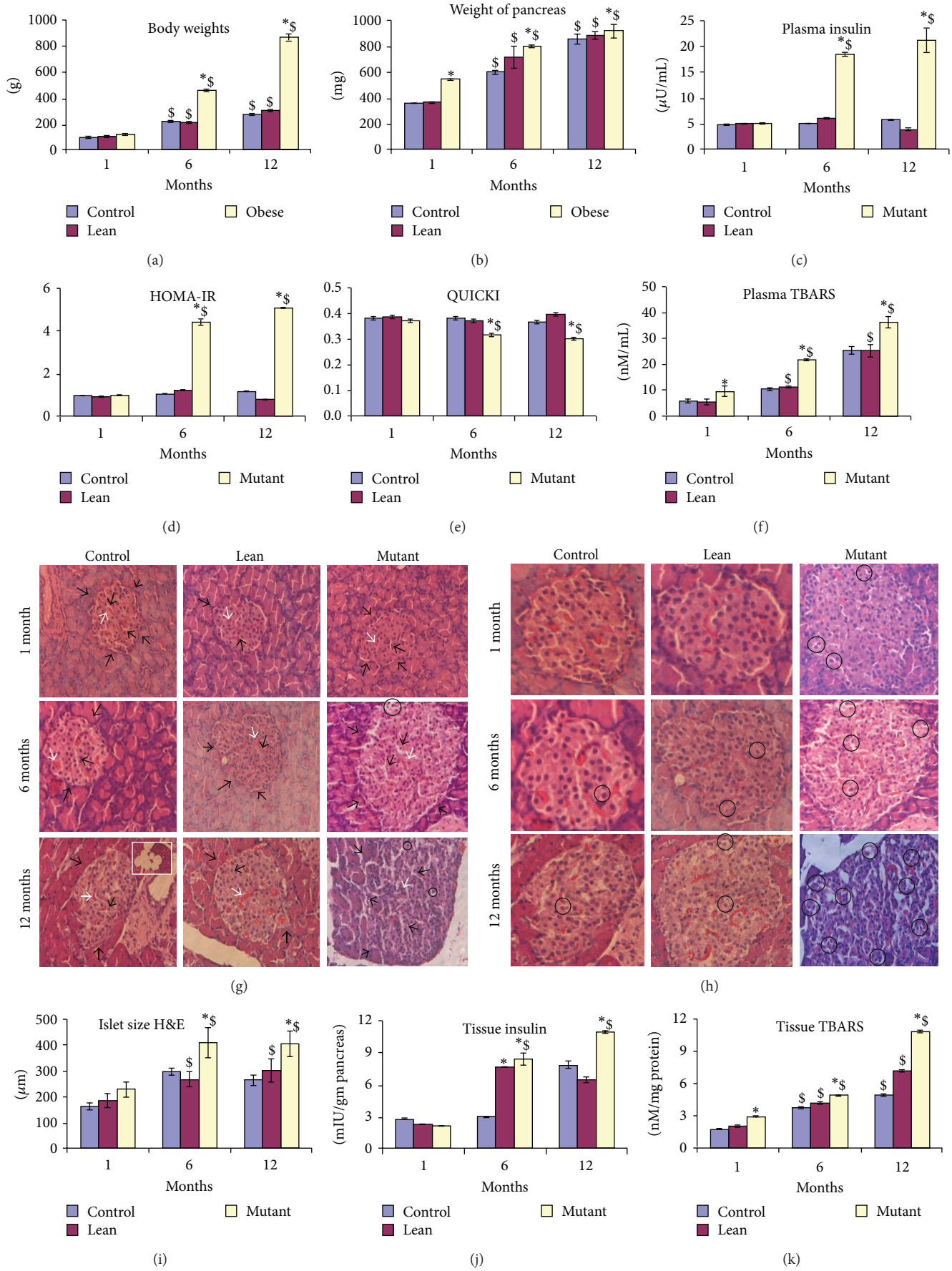

Figure 1: Continued.

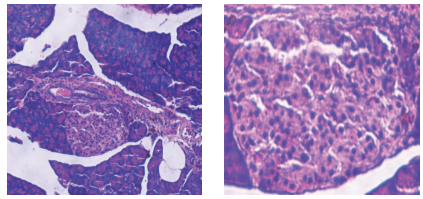

(l)

Physiological parameters	Value
Body weight (g)	350 ± 12.86
Pancreas weight (mg)	655 ± 20.84
FBG (mg/dL)	82 ± 3.2
FPI (μU/mL)	2.13 ± 0.52
Islet size (μm)	320.45 ± 15.02

(m)

Figure 1: Physiological, biochemical and structural analysis. The figure shows anthropometric measurements such as (a) body weights and (b) pancreatic tissue weights; metabolic measurements such as (c) plasma insulin, (d) insulin resistance indices (HOMA-IR), (e) QUICKI, and (f) global oxidative stress levels by plasma TBARS. Histological studies of H&E stained pancreata revealed hypertrophied islets with irregular morphology (black arrows) and increased vascular supply (white arrow head) with widened intraislet connective tissue septa (black arrow head) seen more with Mutants and with age compared to their Lean, and Control phenotypes. Insight shows the intrapancreatic tissue fat infiltration with age (g). These islets among Mutant phenotypes also demonstrated β-cell vacuolation (black bold circles) in the islet region compared to that from Lean and Control (h). All images were captured using ACT2U software (Nikon, Japan) attached to Nikon TE2000S Microscope (Nikon, Japan) at magnification of 200x (g) and 400x (h). Islet size was quantified using ACT2U software (Nikon, Japan) and represented graphically as Mean ± SE ($n = 6$) among Mutant, Lean, and Control with age (i). Mutants showed an increase in islet size and correlated well with increased tissue insulin (j) and oxidative stress (k) compared to Lean and Control and with age. Figure 1 also depicts histological comparison between the pancreatic islets between 24-month-old Control rats and 12-month-old Mutant rats showing hypertrophied islets with irregular morphology, increased vascular supply with widened intraislet connective tissue septa, intrapancreatic tissue fat infiltration, and β-cell vacuolation. Parameters such as body weight, pancreatic weight, FBG, FPI, and islet size of 24-month-old Control rats have also been indicated (m). An asterisk (*) represents significance ($P < 0.05$ by ANOVA) compared to Control and ($) indicates significance ($P < 0.05$ by ANOVA) compared to the same phenotype at 1 month.

decrease. Leans and Controls were almost comparable at all ages (Figures 2(a)–2(d) and 2(g)). However, the levels among 24-month Controls were found to be 10.37 ± 1.6, which was similar to the levels observed among 12-month Mutants.

Further, insulin/glucagon ratio (*per se* indices) indicating the relative percentage of β-/α-cells was also significant ($P < 0.05$) at the higher age group (12 months) among Mutant compared to its Lean and Control, further denoting HI (Figure 2(h)).

β-cell mass was also calculated [18] by quantifying the cross-sectional area occupied by β-cells to the total cross-sectional area of the tissue (in all multiple fields per slide) from the phenotypes. Mutants showed an increase in β-cell mass at 1 and 6 months compared to their Leans and Controls. However, at 12 months, β-cell mass of Mutant was decreased which is probably attributed to increased degenerative effects (hypertrophy and apoptosis). Comparison of β-cell mass between Leans and Controls (Figure 2(i)) does show a consistence in tune with the observed islet cell size.

Immunostaining of the pancreatic tissue sections with insulin and PDX-1 demonstrated decreased PDX-1 intensities (RFU per unit area compared to isotype control (Figure 7(e))) (Figures 7(a)–7(f)).

3.3.1. Inflammatory (CD11b, TNFα, and IL-6) and Stress Markers. As shown in Figure 3(a), HSP-104 localization (cytosolic region) in islets was significantly increased in Mutants at all ages (12 months > 6 months > 1 month) when compared to that in Leans and Controls. Although Leans tend to show an increase for HSP-104 (RFU per unit area with reference to isotype control (Figure 3(c))) compared to Controls, this was not statistically significant (Figures 3(a) and 3(d)). On similar lines, Mutant islets also demonstrated increased localization of endoplasmic reticulum (ER) stress protein RL-77 (RFU per unit area with reference to isotype control (Figure 3(e))) compared to Lean and Control (Figures 3(b) and 3(f)).

Figures 4(a)–4(e) depict dual immunofluoresence for CD11b/TNFα (RFU per unit area with reference to isotype control (Figure 4(c))), that is, relative percentage of macrophages/mast cells/inflammatory protein *in situ* which was significantly upregulated in Mutants with age. However, Leans and Controls showed few immunopositive cells for CD11b/TNFα in comparison to Mutants with age (Figures 4(a)–4(e)). In addition, increased IL-6 immunolocalization with increasing age was seen amongst Mutant pancreatic islets (Figures 4(f)–4(i)).

3.3.2. Apoptosis/TUNEL Assay. Age dependent increase in apoptosis was evident amongst the phenotypes, that is, Mutants, Leans, and Controls, but the quantitative increase in AI was more predominant in Mutants (Figure 5(a)) compared to that in Leans (by 1.20-, 2.84-, and 15.77-fold) and Controls (by 5.16-, 5.67-, and 9.98-fold) (Figure 5(d)), respectively. Interestingly, apoptotic rate was increased among 12-month Mutants by 3.70-fold compared to that of 24-month Controls (Figure 5(b)) as compared to its negative control (Figure 5(c)).

3.4. Gene Expression Analysis. mRNA for *Insulin* was significantly upregulated only at 6 months in Mutants against the data obtained from plasma and tissue insulin, which showed an increase in insulin levels at all the ages (12 months > 6 months > 1 month). The expression levels were, however, comparable in Leans and Controls as reflected by the densitometric analysis (Figure 6(a)).

Pdx-1 homeobox transcription factor required for β-cell functions and regulation of insulin secretion was significantly

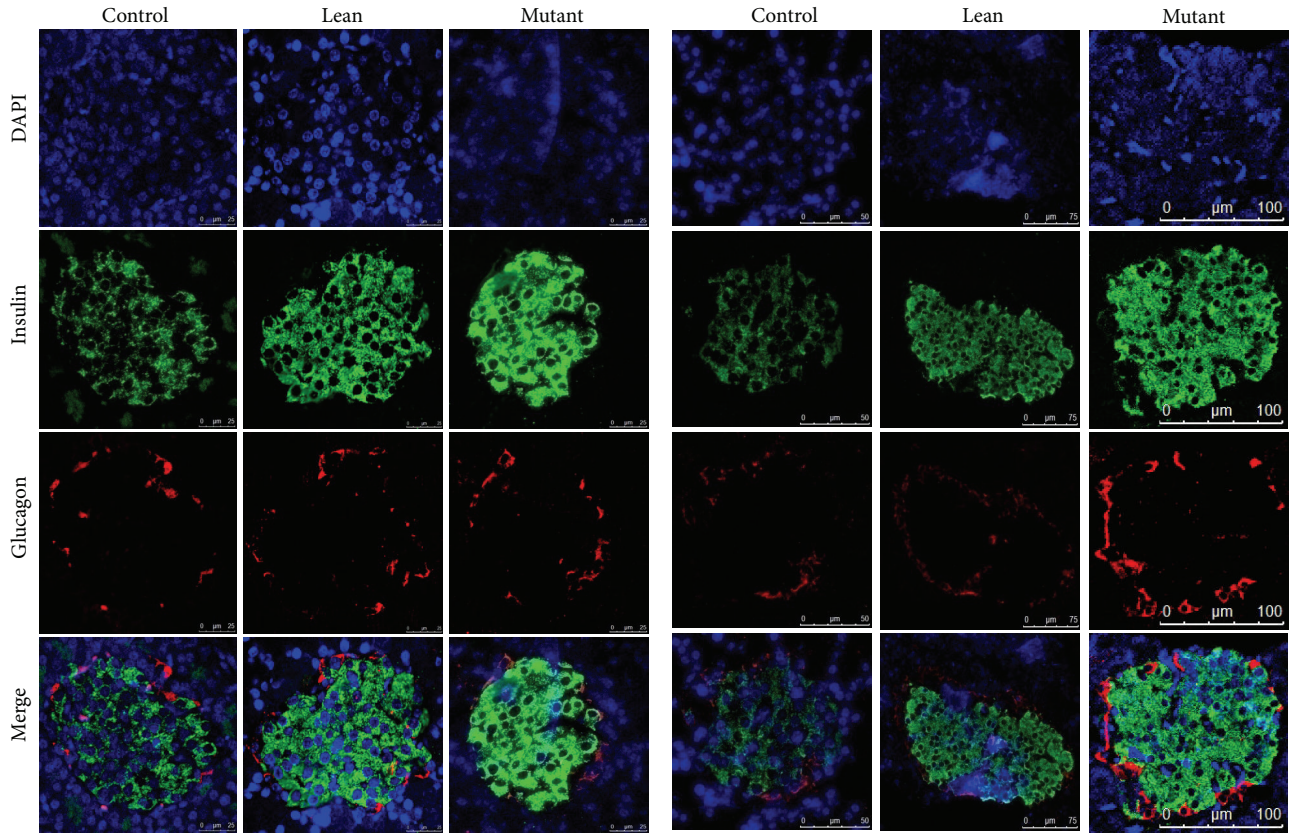

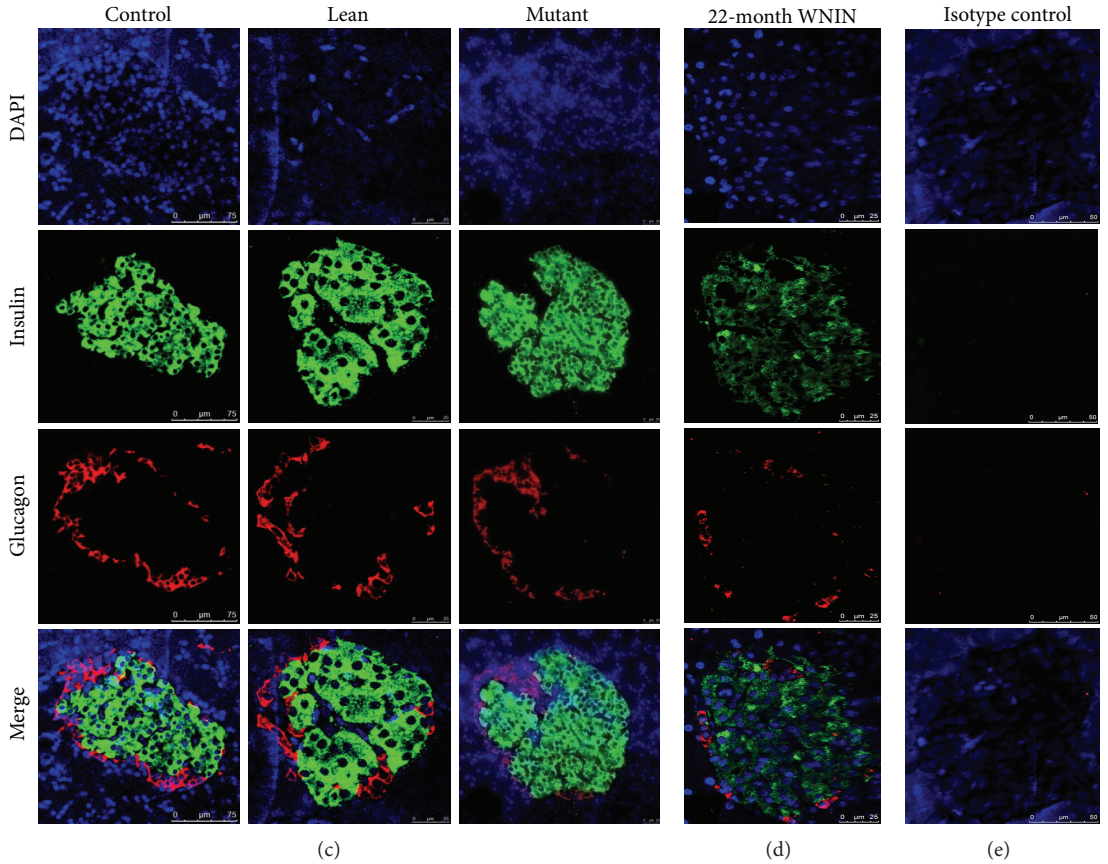

Figure 2: Continued.

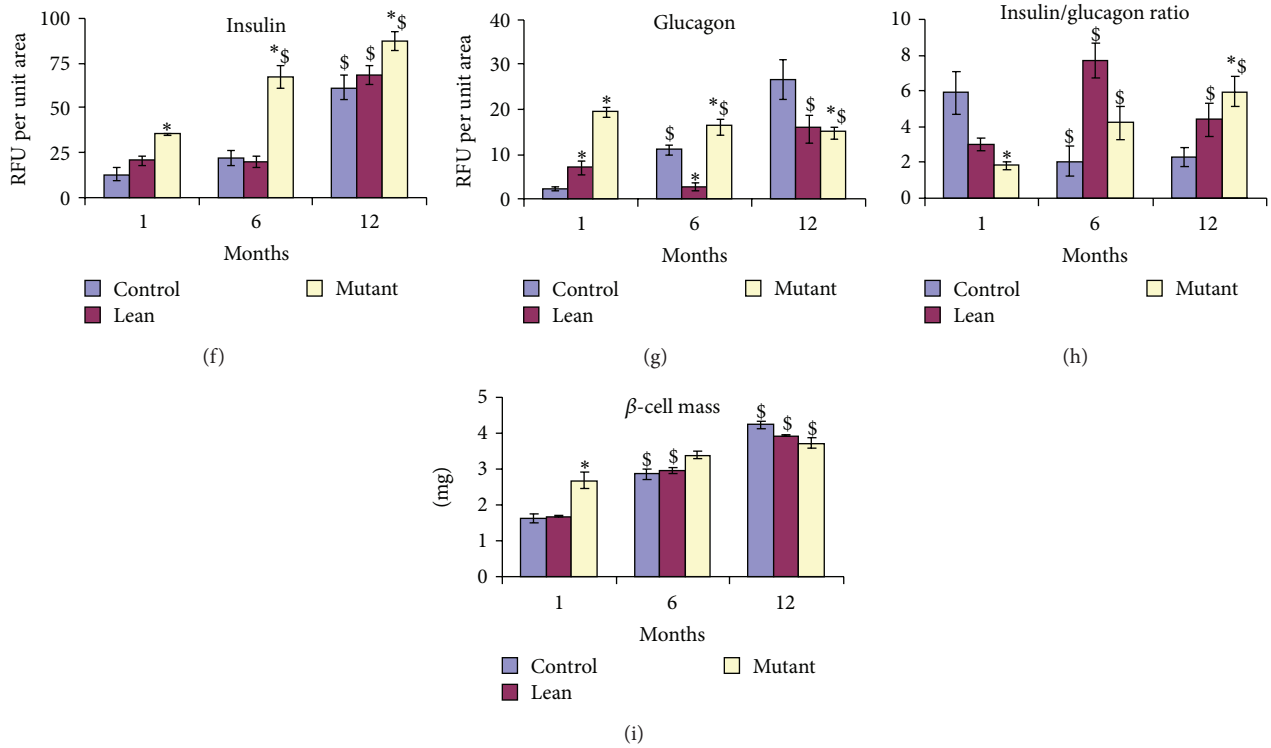

FIGURE 2: Immunostaining for insulin and glucagon. Immunolocalization of islets for β-cell marker insulin (green) and α-cell marker glucagon (red), counterstained with 4′,6-diamidino-2-phenylindole (DAPI) (nuclear stain) (blue), showed increased insulin immunostaining among Mutants compared to Lean and Control and with age from 1 month (a) to 6 months (b) and 12 months (c) and showed a comparison with 24-month-old (2 yr) Controls (d). Isotype control is also represented (e). Quantitative fluorescence measurements as relative fluorescence units (RFU) for (f) insulin, (g) glucagon, (h) insulin to glucagon ratio, and (i) β-cell mass were calculated from insulin stained areas. An asterisk (*) represents significance ($P < 0.05$ by ANOVA) compared to Control and ($) indicates significance ($P < 0.05$ by ANOVA) compared to the same phenotype at 1 month.

downregulated in Mutants at both 6 and 12 months with a peak expression seen at 1 month (Figure 6(b)).

Quantitative data generated from RT-PCR further substantiated increased expression of *Insulin* gene among Mutants, being more pronounced at 6–12 months of age compared with their Lean littermates (values have been normalized against their Controls) (Figure 6(c)). In line with our qRT-PCR data, *Pdx-1* expression in Mutants showed downregulation with age (1 month > 6 months > 12 months) with a peak expression at 1 month. Interestingly, *Pdx-1* expression was down regulated in 6–12-month-old Leans when compared with that of their Mutants (age matched/littermates) with a peak expression at 1 month as compared to its Mutant (values have been normalized against their Controls) (Figure 6(d)).

3.5. Primary Islet Cell Cultures

3.5.1. Viability. MTT assay demonstrated an increase in viability during the early phase, that is, 1 month, and declined with age, suggestive of age dependent effects—Mutants (86%, 75%, and 60%), Lean (85%, 80%, and 74%), and Control (98%, 95%, and 85%) corresponding to 1, 6, and 12 months. However, the islet cell integrity was not altered with age and showed >85% intactness, as assessed from the DTZ stained (deep crimson red) islet cell clusters (Figure 8(a) (insights)).

3.5.2. Insulin Secretion Assay. As given in Figure 8(c), Mutants at all the age groups, that is, 1, 6, and 12 months, were hyperinsulinemic as evidenced by an increase in their basal insulin levels similar to our earlier observations of increased insulin levels in both plasma and tissue (Figures 1(c) and 1(j)). However, when Mutant islets were challenged with high glucose concentrations (16.5 mmol/L), insulin secretion was almost absent or was nonresponsive unlike Leans and Controls which elicited a better secretory response under the same conditions. The ratio of basal/challenge secretion, depicting the islet cell functions, was also high in Mutant islets, compared to its Lean and Control counterparts (Figure 8(c)). As a positive control to 12-month Mutants, we have also calculated the ratio of basal/challenge secretion, from the 24-month Control rats (ratio = 1.03), with higher basal insulin secretion levels (24.75 ± 2.86) than when challenged with high glucose (24.13 ± 3.12), and the islets were nonresponsive similar to the findings from 12-month-old Mutant rats (Figure 8(c)).

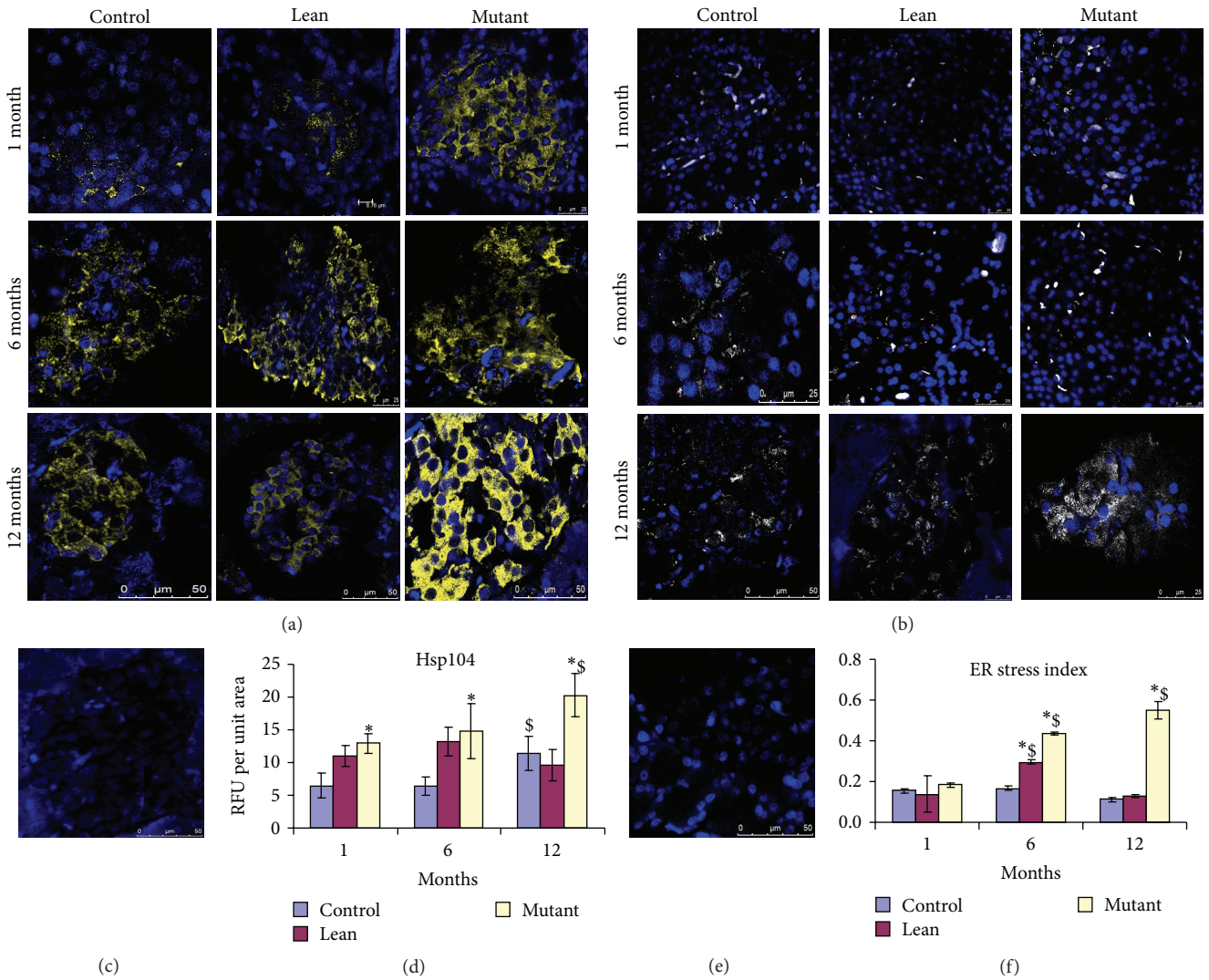

Figure 3: Cellular stress responses. Immunostaining of pancreatic sections for cellular stress protein, HSP-104 (yellow—pseudocolor for Cy3) (a) and endoplasmic reticulum stress protein RL-77 (green) (b) demonstrate an increased cellular stress (HSP104 and RL-77) among Mutants compared to Lean and Control and with age. Isotype controls for HSP-104 (c) and RL-77 (e) have also been depicted and with corresponding RFU for HSP-104 (d) and RL-77 (f). An asterisk (*) represents significance ($P < 0.05$ by ANOVA) compared to Control and ($) indicates significance ($P < 0.05$ by ANOVA) compared to the same phenotype at 1 month.

3.5.3. Ultrastructural Studies (SEM/TEM). SEM data revealed spherical and globular pancreatic β-cells amongst the phenotypes, but fine perforations with ruffles on the islet surface were more prominent with Mutant islets, as Lean and Control islets demonstrated a smooth surface with no such perforations (Figure 8(b)).

On similar lines, TEM photographs showed electron dense spherical secretory granules for insulin among Leans and Controls, while Mutants showed a comparatively less number of the secretory granules with distinct degranulation and vacuolation in the islet region (Figure 8(b)).

3.6. Correlation Analysis. Bivariate 2-tailed correlation analysis of metabolic health measures such as HOMA-IR and QUICKI with other physiological parameters revealed a significant correlation between IR indices-HOMA-IR and QUICKI, with body weight, pancreatic tissue weight, FPG, FPI, plasma and tissue TBARS, tissue insulin levels, islet size, and islet AI at $P < 0.01$. These results have been summarized in Table 1.

4. Discussion

The present study demonstrates for the first time an age dependent (1–12 months) increase in hypertrophy, inflammation, and β-cell dysfunctions with significant degranulation of the insulin secreting cells in the pancreas from Mutants (obesity/IR/HI) which otherwise show distinct features of obesity and IR [7]. These observations are noteworthy in view of the recent reports defining obesity and IR as a state of

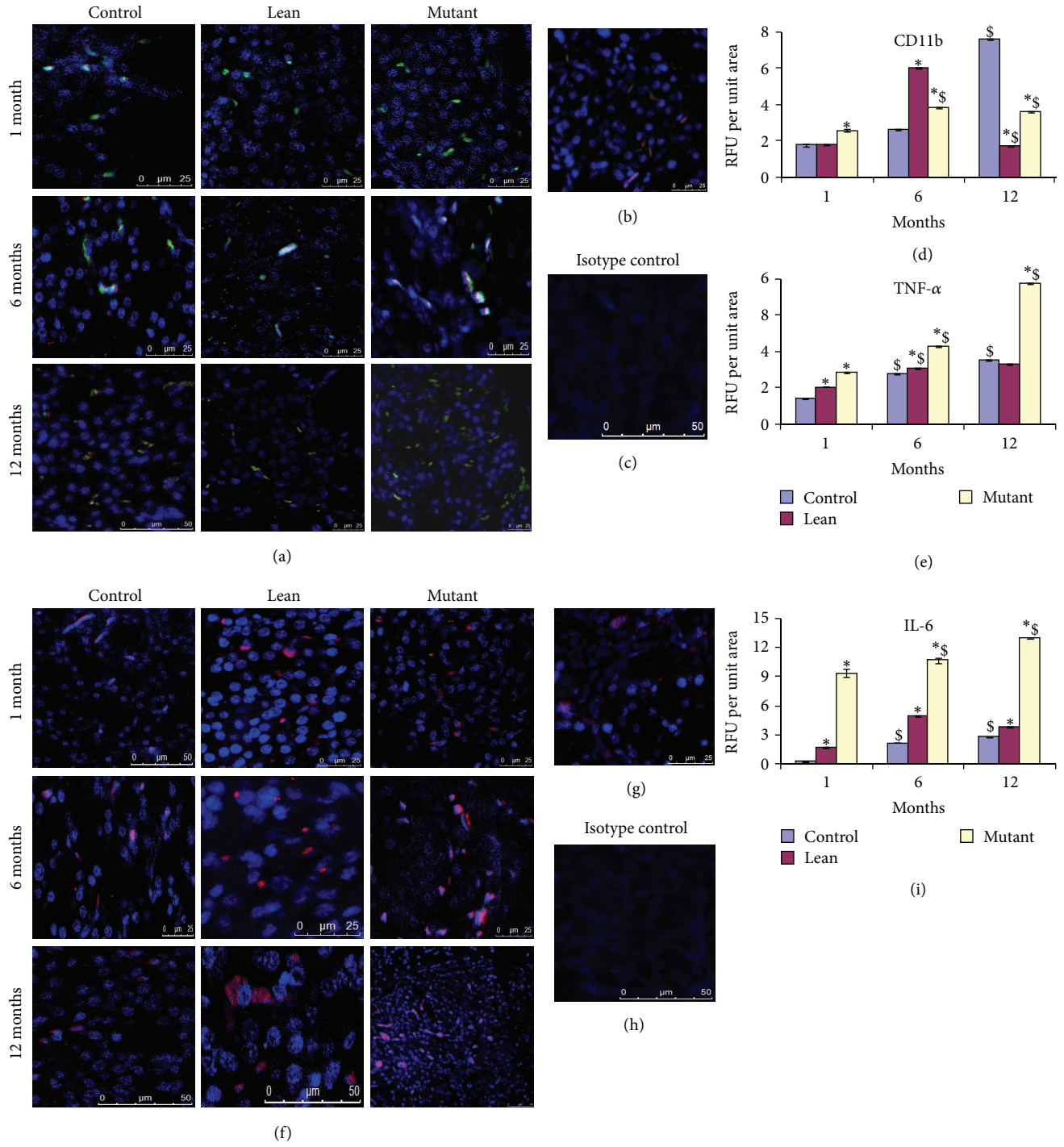

Figure 4: Inflammatory stress responses. Immunofluoresence staining of pancreatic sections for inflammatory markers shown by colocalization (yellow) with macrophage marker CD11b (green) and proinflammatory cytokine for TNFα (red) shows more CD11b/TNFα colocalization with Mutant pancreas (a) compared to Lean and Control and comparable with (b) 24 months older in age Control; (c) represents its isotype control. (d and e) represent RFU for CD11b and TNFα, respectively, amongst phenotypes. Mutant pancreas also showed an increase in (f) IL-6, compared to its Lean and Control, and was similar to (g) 24-month Control; (h) represents isotype control and (i) RFU for IL-6 amongst phenotypes. An asterisk (*) represents significance ($P < 0.05$ by ANOVA) compared to Control and ($) indicates significance ($P < 0.05$ by ANOVA) compared to the same phenotype at 1 month.

Table 1: Correlation matrix of anthropometric versus physiological parameters.

		Body weights	Pancreas weights	HOMA-IR	QUICKI	FPG	FPI	Plasma TBARS	Tissue TBARS	Tissue insulin	Islet size	Apoptotic index
Body weights	Pearson correlation	1										
	Sig. (2-tailed)	.										
Pancreas weights	Pearson correlation	0.700**	1									
	Sig. (2-tailed)	0.000	.									
HOMA-IR	Pearson correlation	0.893**	0.501**	1								
	Sig. (2-tailed)	0.000	0.000	.								
QUICKI	Pearson correlation	—	—	—	1							
		0.678**	0.372**	0.765**								
	Sig. (2-tailed)	0.000	0.006	0.000	.							
FPG	Pearson correlation	0.339*	0.123	0.431**	—	1						
					0.397**							
	Sig. (2-tailed)	0.012	0.376	0.001	0.003	.						
FPI	Pearson correlation	0.884**	0.494**	0.995**	—	0.408**	1					
					0.751**							
	Sig. (2-tailed)	0.000	0.000	0.000	0.000	0.002	.					
Plasma TBARS	Pearson correlation	0.818**	0.837**	0.626**	—	0.294*	0.601**	1				
					0.519**							
	Sig. (2-tailed)	0.000	0.000	0.000	0.000	0.031	0.000	.				
Tissue TBARS	Pearson correlation	0.917**	0.821**	0.669**	—	0.178	0.658**	0.874**	1			
					0.482**							
	Sig. (2-tailed)	0.000	0.000	0.000	0.000	0.199	0.000	0.000	.			
Tissue insulin	Pearson correlation	0.812**	0.827**	0.710**	—	0.221	0.702**	0.778**	0.800**	1		
					0.572**							
	Sig. (2-tailed)	0.000	0.000	0.000	0.000	0.108	0.000	0.000	0.000	.		
Islet size	Pearson correlation	0.765**	0.700**	0.749**	—	0.275*	0.725**	0.696**	0.699**	0.702**	1	
					0.549**							
	Sig. (2-tailed)	0.000	0.000	0.000	0.000	0.044	0.000	0.000	0.000	0.000	.	
Apoptotic index	Pearson correlation	0.924**	0.554**	0.971**	—	0.367**	0.964**	0.657**	0.745**	0.733**	0.760**	1
					0.736**							
	Sig. (2-tailed)	0.000	0.000	0.000	0.000	0.006	0.000	0.000	0.000	0.000	0.000	.

The table shows the correlation analysis between metabolic health parameters and physiological parameters and demonstrates a strong correlation of HOMA-IR and QUICKI with body weights, pancreas weights, plasma and tissue insulin levels, and plasma and tissue TBARS levels ($n = 54$). The table also shows the correlation analysis for other metabolic and physiological parameters ($n = 54$). FBG: fasting blood glucose, FPI: fasting plasma insulin, HOMA-IR: homeostasis model of assessment for insulin, QUICKI: quantitative insulin sensitivity check index, TBARS: thiobarbituric acid reacting species.

**Correlation is significant at the 0.01 level (2-tailed).

*Correlation is significant at the 0.05 level (2-tailed).

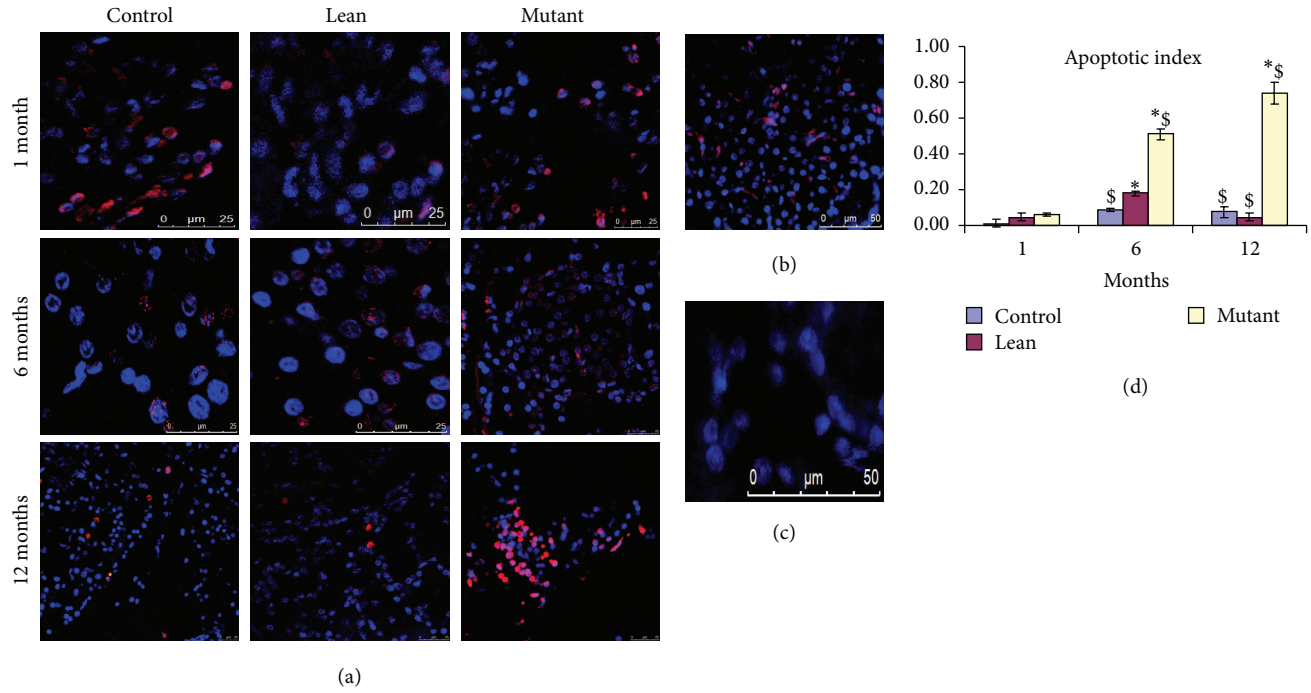

Figure 5: Apoptosis (TUNEL assay). Apoptosis detected by TUNEL assay shows red (pseudocolor) nuclei (counterstained with DAPI (blue). Mutants showed an increase in (a) apoptosis as compared to Lean and Control and apoptotic index (b) and it is comparable with 24-month-old Controls; (c) represent its negative control. Quantitatively, AI was significantly higher in (d) Mutants compared to Lean and Control and with age. Mean ± SE ($n = 6$). An asterisk (*) represents significance ($P < 0.05$ by ANOVA) compared to Control and ($) indicates significance ($P < 0.05$ by ANOVA) compared to the same phenotype at 1 month.

profound inflammation and oxidative stress [24]. Interestingly, the present evidence for an early onset of degenerative-like changes was very much appreciable in Mutants which show features of "kinky tail," a rare trait [3], overweight (Figures 1(a)-1(b)), tissue hypertrophy/hyperplasia (Figures 1(g)–1(i)), inflammation (Figure 4), and apoptosis (Figure 5). These changes very much complement the chronic inflammatory conditions and related metabolic disorders [1] well illustrated in this animal model (Table 1). Several etiological factors such as environmental, genetic, and epigenetic factors [1] in addition to IR have been shown to alter the functions of adipose and muscle tissues eventually causing altered glucose homeostasis [9] and thereby impairing islet cell functions and integrity, a phenomenon well noted in T2D [10].

Using cellular, molecular, and morphological approaches, we have been able to demonstrate the coprecipitation of several confounding factors in Mutant pancreas noted by extensive vascularization (Figures 1(g) and 1(h)), interlobular septa with fat accumulation (Figures 1(g) and 1(h)), increased macrophage infiltration (CD11b) (Figures 4(a)–4(e)), and proinflammatory cytokines (TNFα and IL-6) (Figures 4(a)–4(i)) when compared to its Lean and Control. Inflammation as an intrinsic mechanism to facilitate towards islet dysfunction has been well correlated with frank diabetes and hyperglycemia in T1D [27], obese T2D [28], and T2D with IR [28], unlike our present model system demonstrating euglycemia with obesity/IR [3, 6] suggestive of the preclinical scenario in human subjects [29]. Earlier studies from our institute have shown an altered immune status in the WNIN Mutant rats (WNIN/Ob and WNIN/GR-Ob) in terms of percentages of splenic $CD8^+$ T cytotoxic cells in males and splenic $CD3^+$ T lymphocytes and $CD4^+$ T helper cells in females, respectively, and in response to vaccination [30, 31]. CD11b studied here is a macrophage marker that is highly expressed as a surface marker of activation on resting monocytes along with others such as CD11c and HLADR [32] which correlates with the increased macrophage and T-cell activation among Mutants and with age. This is further confirmed from the observed increased expression of inflammatory cytokines, IL-6 and TNFα, released by activated macrophages. TNFα has been implicated as a key molecule to facilitate insulin-mediated glucose uptake at peripheral tissues [33] and the increased expression of TNF-α (Figures 4(a)–4(e)) could however be partly responsible for the marked increase in macrophage infiltration (Figures 4(a)–4(e)) and IL-6 expression that we have observed from the Mutant pancreas (Figures 4(f)–4(i)). Indeed, TNFα has been reported to upregulate IL-6 in murine pancreatic islets [34] and IL-6 has been shown to be infiltrated in islets both before and during immune infiltration in NOD mice suggesting its pathogenic role, closely correlating to target β-cells [35]. Further, overexpression studies in NOD mice have also demonstrated the interplay of IL-6 with proinflammatory cytokines (e.g., TNFα) leading to β-cell dysfunction [35]. Increased localization of CD11b with a concomitant upregulated expression of downstream inflammatory markers IL-6 and TNFα observed here in the Mutant pancreatic islets unequivocally demonstrates an activated macrophage phenotype in the pancreatic islets/tissue and

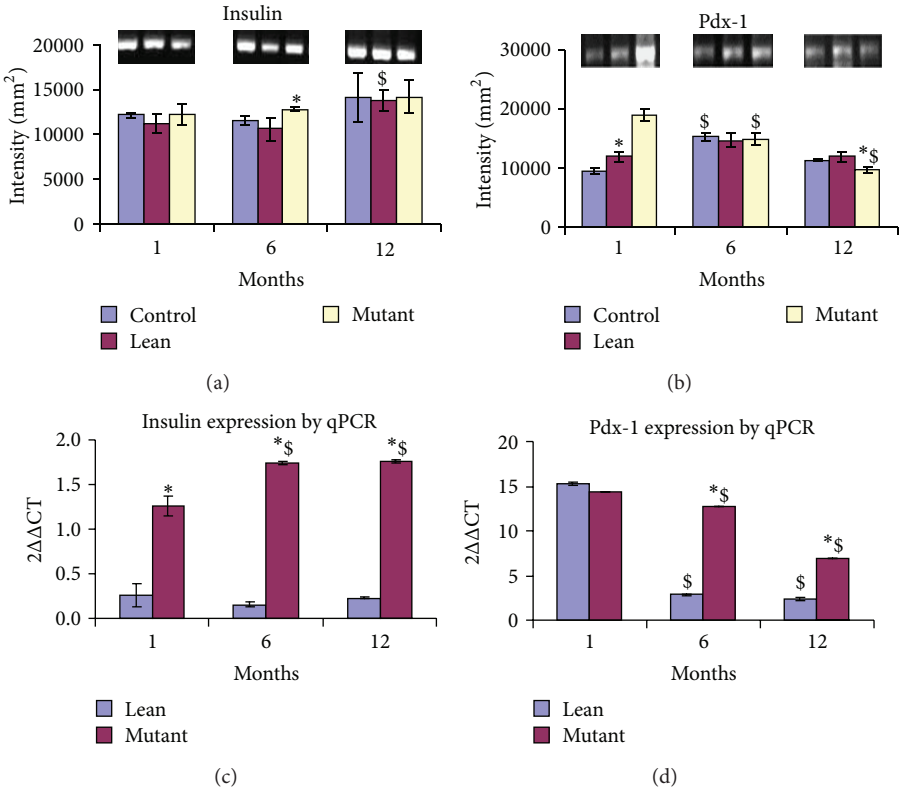

Figure 6: Gene expression (semiquantitative and real-time PCR) mRNA levels for (a) *Insulin-1* were increased in Mutants with age as compared to their phenotypes. However (b) *Pdx-1* expression was downregulated with age (1 > 6 > 12 months). Gel images have been represented for (a) *Insulin-1* and (b) *Pdx-1*. In line with semiquantitative data, mRNA transcripts were upregulated for (c) *Insulin-1* in Mutants with age as compared to their phenotypes. In similar lines (d) *Pdx-1* expression was downregulated with age (1 > 6 > 12 months). The values have been represented as $2^{-\Delta\Delta CT}$ against Control. Statistical significance ($P < 0.05$ by ANOVA) has been represented as compared to Control by an asterisk (*) and as compared to younger age by ($).

is probably responsible for the localized pancreatic tissue inflammation among Mutants which gets worsened with the severity of disease (obesity) and with age. These observations are in line with the observations on human subjects [36, 37] and other animal models such as ob/ob and db/db mice, fa/fa rats, and obese diabetic Wistar fatty rats [31].

The inciting events that cause systemic inflammation and IR, the two cardinal features of the MS, remain unknown. According to one school of thought, factors secreted by hypertrophied mature adipocytes (within white adipose tissue (WAT))/the intraexocrine fat [35] (Figure 1(g)) could be one such causative agent or it could be due to chemokines secreted by fat cells (monocyte chemoattractant protein-1, leptin, etc.,) normally overexpressed in obesity [38, 39]. In addition, leptin is known to have pleiotropic effects on immune cell activity by (a) promoting macrophage phagocytosis; (b) increasing secretion of proinflammatory cytokines such as TNF-α (early), IL-6 (late), and IL-1 by macrophages; (c) increasing expression of surface markers of activation HLADR, CD11b, and CD11c on monocytes; (d) stimulating monocyte, proliferation and upregulating the expression of CD38, CD69, CD25 (IL-2 receptor a-chain), and CD71 (transferrin receptor) (activation markers); (e) stimulating chemotaxis of polymorphonuclear cells by producing ROS; and (f) playing a role in NK cell development, differentiation, proliferation, activation, and cytotoxicity [39–41]. Although the mechanism(s) are obscure, we have shown an increased infiltration of macrophages within the pancreas [35] with prolonged obesity (12 > 6 > 1 months) and this was correlating with indices for obesity (2-3-fold)/IR (1.5–3-fold)/HI (2-3-fold) for Mutants [42] as compared to their Leans and Controls (Figure 1). The fact that inflammation is the central mechanism operating in both obesity and IR [43] has been demonstrated from our earlier findings (6 months old) in AT [7] and BM-MSCs [8] from the same animal model. In similar lines transcriptional profiling analysis from obese mice also correlated with adiposity and infiltration of macrophages [44]. With advancing age, the pancreas in such genetic models could undergo alterations such as hypertrophy, fibrotic-like changes, and fatty infiltration because of oxidative damage (Figures 1(f) and 1(k)). However, the pancreas in Leans and Controls showed mild (a) hypertrophy (Figures 1(g) and 1(h)), (b) fibrotic-like changes (Figures 1(g) and 1(h)), and (c) intermittent scanty macrophages (Figures 4(a)–4(e)) which could be related to the aging process [3, 45]. The sequel of events reported here, for example, (a) increased insulin immunolocalization (Figures 2(a)–2(f)), (b) increased insulin to glucagon ratio

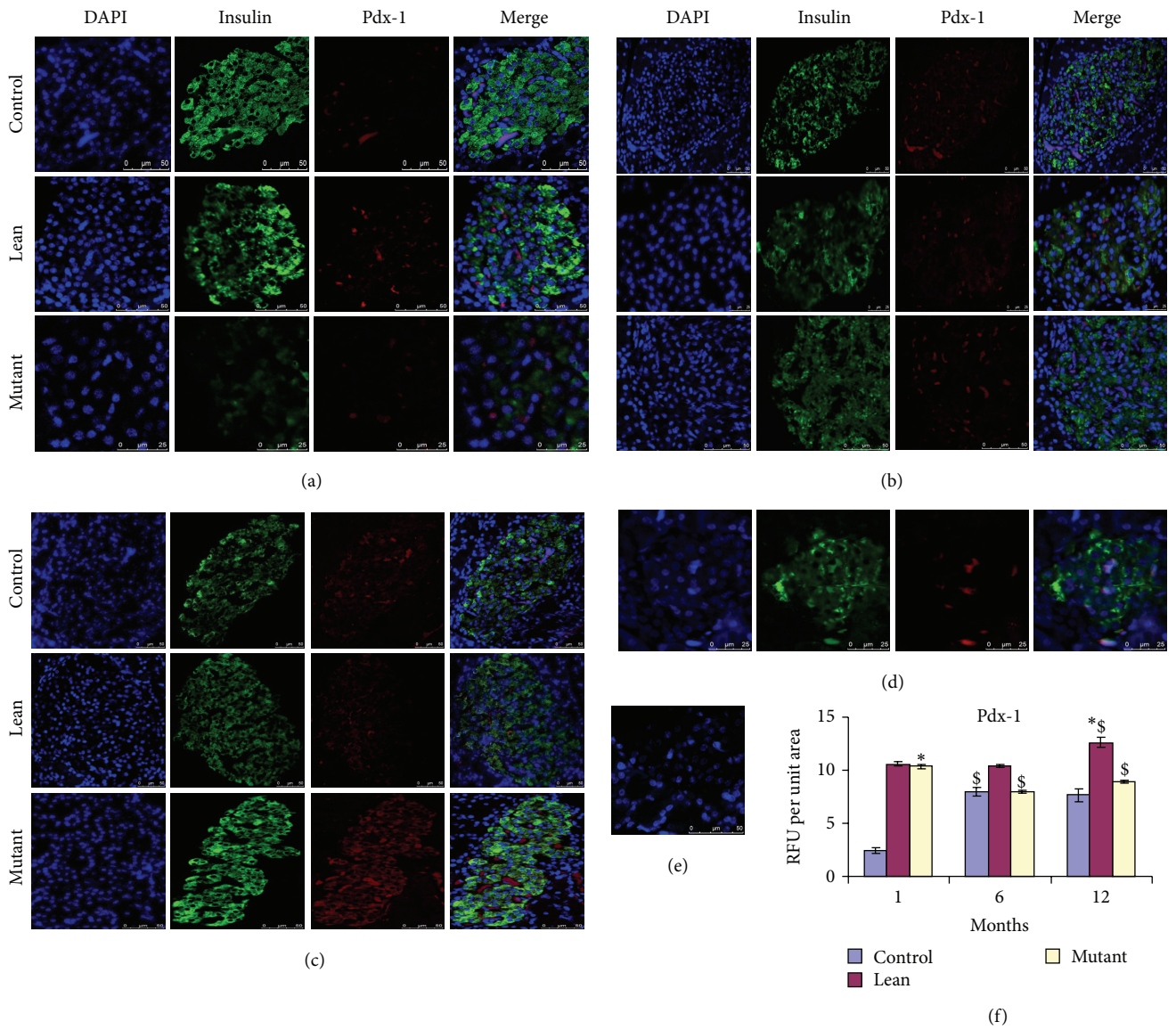

FIGURE 7: Immunolocalization of insulin and Pdx-1. Pdx-1 (red) shows increased nuclear localization in (a) 1-month Mutants followed by (b) 6-month Mutants and (c) 12-month Mutants compared with their Leans and Controls among insulin (green) positive β-cells. The localization was almost similar between 12-month Mutants and (d) older age (24-month) Controls. RFU has been represented (e) amongst phenotypes. Statistical significance ($P < 0.05$ by ANOVA) has been represented compared to Control by an asterisk (*) and compared to younger age by ($).

(Figure 2(h)), (c) mRNA levels of *Insulin* (Figures 6(a) and 6(c)), (d) downregulation of *Pdx-1* expression (Figures 6(b) and 6(d)), (e) HI (Figure 1(c)), and (f) increase in β-cell size/β-cell volume (Figure 2(i)) [46], advocates for *in situ* inflammation with Mutants, which probably accounts for β-cell dysfunction. Studies have demonstrated a decreased expression and/or DNA binding activities of MafA and PDX-1 in diabetes and chronic hyperglycemia which present a gradual deterioration of pancreatic β-cell function [47]. *Pdx-1* is known to control the expression of two key genes-*Insulin* and *Glut-2* which are required for the integrity and function of islet cells. *Pdx-1* is a common transcription factor required for β-cell development, differentiation, function, and pancreatic regeneration. The vulnerability of PDX-1 to the oxidative stress (suppression) has been well demonstrated both *in vitro* in HIT cells 36 and *in vivo* in the partially pancreatectomized rats exposed to chronic hyperglycemia [11, 48].

Pancreatic β-cells are constantly exposed to a great demand for insulin production, and ER has been reported to play a critical role towards preserving β-cell functions and differentiation [49, 50]. It is of utmost importance to note that β-cells have weak inherent antioxidant systems compared to other organs in the body making them highly vulnerable to the deleterious effects of oxidative stress [11]. Addressing these issues, we have demonstrated with age an

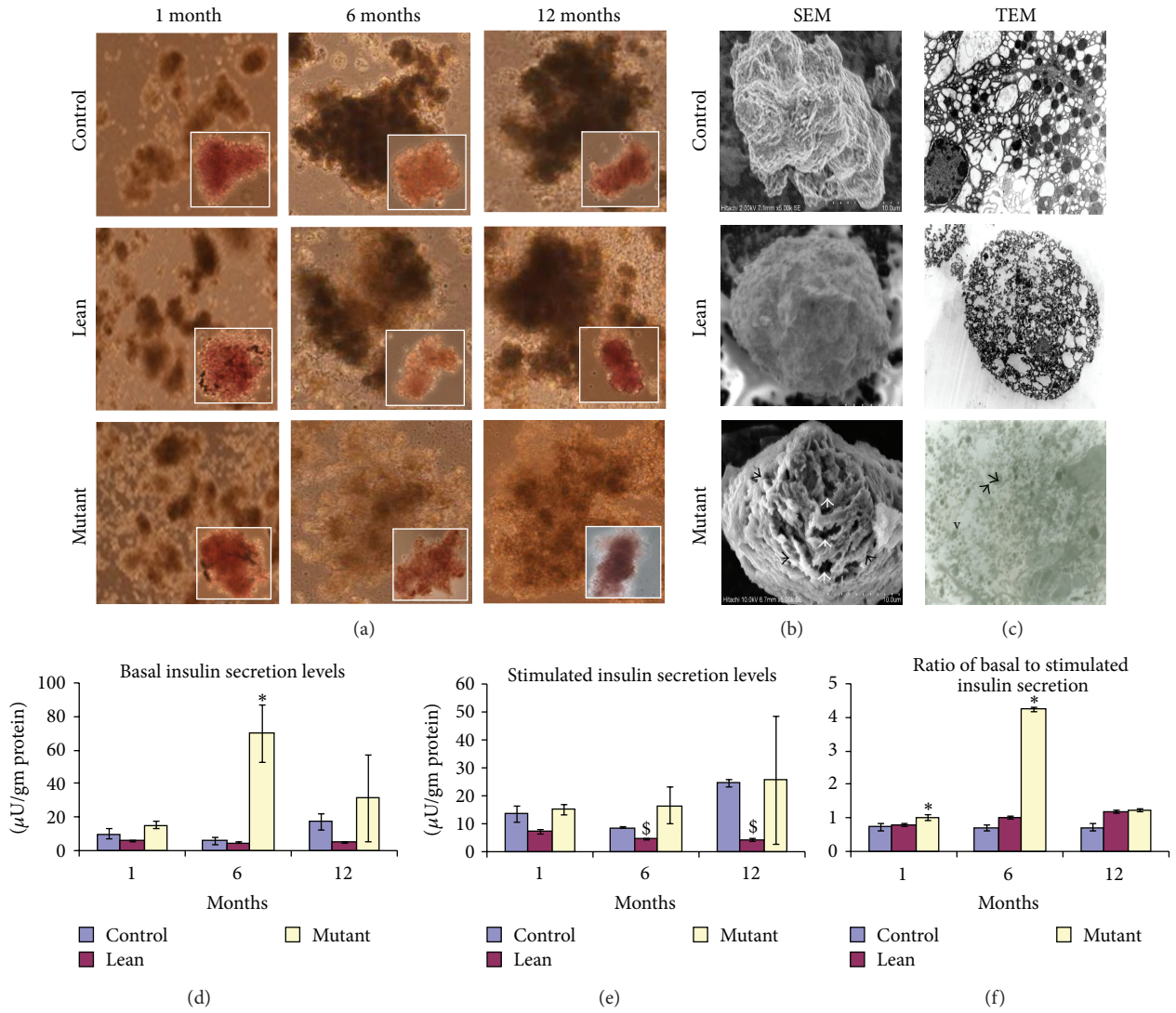

Figure 8: Insulin secretion assay and ultrastructural studies on primary islet cell cultures. (a) Bright field images of primary islet cultures isolated from Mutant, Lean, and Control at 1, 6, and 12 months. Insights show the DTZ stained islets (magnification of 100x). (b) shows the ultrastructural studies of 12-month Mutant phenotypes by scanning (SEM) and (c) transmission electron microscopy (TEM). As shown in the figures Mutants showed less integrity with a ruptured outer collagenous layer (black arrows) and perforations (white arrow heads) (SEM), degranulation of insulin crystals, large less electron dense secretory granules (arrow head), and vacuolation (v) (TEM) compared to their Lean and Control. Insulin secretion measured from 250 islets: (d) basal (5.5 mmol/L glucose), (e) stimulated (16.5 mmol/L glucose), and (f) basal to stimulated insulin secretion, shows impaired insulin secretion with challenge (16.5 mmol/L glucose) from Mutants with age as compared to their Leans and Controls. However, Mutants showed higher basal insulin levels with age.

increase in RL-77 (ER stress) (Figures 3(b), 3(e), and 3(f)), TBARS (Figures 1(f) and 1(k)), and HSP-104 (Figures 3(a), 3(c), and 3(d)) in these Mutants (compared to their Leans and Controls) with a concomitant increase in expression of stress proteins including ER [51] and HSPs [15, 50, 52]. In similar lines *in vitro* experiments, using insulinoma cells [53] and primary islet cells [53] also demonstrates pancreatic β-cell dysregulation or death [54] with upregulation of UPR genes. As shown in Figure 5, age dependent degenerative changes and apoptosis (TUNEL assay) seem to have played an important role in increased β-cell vacuolation (12 months > 6 months > 1 month) in Mutants (Figures 1(g) and 1(h)). Interestingly, the accelerated aging process has been a well-documented phenomenon in these Mutants with their average life span shortened to 1.5 yrs compared to 2.5–3 years seen in Controls and Leans [3] and the phenomenal increase in episodes of cataract [6, 55], cancers [6], infertility [56], and immune dysfunction [30] playing a critical role to shorten their lifespan as given in Figure 9.

To obtain further insights underlying altered pancreatic milieu, we next examined functional responses (with age) and ultrastructural changes (only 12 months) using primary islet cell cultures isolated from these phenotypes. Mutant islets depicted inflammatory milieu evidenced by their

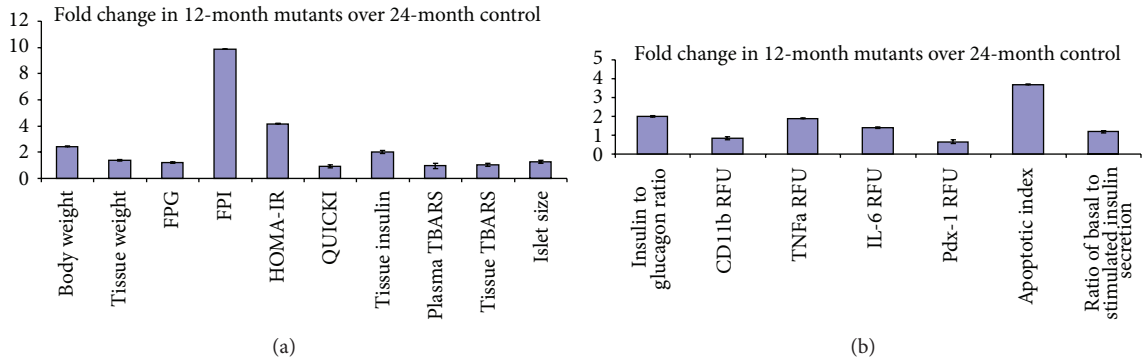

Figure 9: Comparison between 12-month Mutants and 24-month Control rats (metabolic and physiological). Data shows comparison of metabolic and physiological parameters as compared to 24-month old Control rats. Panel (a) depicts fold change for body and pancreatic tissue weights, fasting plasma glucose (FPG), fasting plasma insulin (FPI), homeostasis model assessment for insulin resistance (HOMA-IR), quantitative insulin sensitivity check index (QUICKI), tissue insulin, plasma and tissue thiobarbituric acid reacting species (TBARS), and islet size. Panel (b) depicts the fold change for insulin to glucagon ratio, inflammatory marker (CD11b, TNFα, and IL-6) fluorescent intensities, PDX-1 expression, apoptotic index, and ratio of basal to stimulated insulin secretory levels.

nonresponsiveness to high glucose challenge (16.5 mmol/L) >6 and 12 months (Figure 8(c)) [57]. The perturbations noted with functional responses of islets to glucose challenge could be a multifactorial effect and can be attributed to a reduced threshold of the β-cells under chronic conditions [58] and islet hypertrophy [59] or can be due to the functional loss of insulin receptor [60], hypertriglyceridemia [61], inflammation [6], hyperleptinemia [62], oxidative stress [63], and IR [29]. Higher basal insulin levels (5.5 mmol/L glucose) observed with Mutant islets at all ages (1/6/12 months) (Figure 8(c)) could probably be noted as a compensatory response initiated by β-cells resulting in HI [45] or by insulin hypersecretion under substimulatory conditions [61, 62].

Ultrastructural analysis of the primary islet cells (12 months) revealed significant inflammatory/apoptotic responses in Mutants evidenced by a disrupted outer collagenous layer (SEM) and this data was complemented with TEM findings for increased islet cell degranulation evidenced in Mutant islets (Figure 8(b)). Interestingly, data generated from model systems such as Zucker fatty rats [64] and sand rats [65] have advocated for an increased macrophage accumulation [66] and IL-6 expression [66] in β-cells themselves [38], contributing to islet cell impairments suggestive of a prediabetic state [51]. Systemic elevation of IL-6 cytokine in obesity has been identified as the risk/predictive factor for development of T2D [35] akin to our present observations. Further, *in vitro* studies [35] show that increased expression of IL-6 renders inhibition of glucose-stimulated insulin secretion [35], albeit that results have not been consistent.

Interestingly we have attempted here to integrate and correlate metabolic health measures of HOMA-IR and QUICKI amongst the phenotypes (Table 1) with other measures such as body weight, fasting plasma glucose, fasting plasma insulin, pancreatic tissue TBARS, islet size, and islet apoptotic index. to arrive at a significant correlation of metabolic insult to be associated with the Mutant trait, as compared with its Lean and Control.

5. Conclusions

Our findings *in situ* and *in vitro* authenticate the use of WNIN/Ob Mutant model as an optimal system for studying MS (obesity/IR/T2D) and its complications which are increasing worldwide at an alarming rate. These findings pave the way to explore the efficacy and feasibility of using these mutant rats as a valuable resource (model systems) in the management of obesity and metabolic syndrome.

Conflict of Interests

The authors declare that they have no conflict of interests.

Authors' Contribution

Dr. Vijayalakshmi Venkatesan designed the experiment and prepared the paper. Mrs. Soundarya Madhira carried out the *in situ* characterizations and prepared the draft. Mr. Venkata Malakapalli carried out gene expression studies. Mrs. Maniprabha Chalasani worked on the immunohistochemistry for all the markers given in the paper. Dr. Sarfaraz Nawaz prepared the islet cell cultures and prepared samples for ultrastructural analysis. Dr. Vasudevan Sheshadri contributed the endoplasmic reticulum component of the paper, including the antibody contribution. Dr. Venkaiah Kodavalla gave the entire feedback on statistical applications to the study. Dr. Ramesh Bhonde contributed his expertise towards islet cell virology, including inflammation. Dr. Giridharan Nappanveetil was responsible for the development of WNIN mutant obese rats and collaborated in the present study.

Acknowledgments

The authors wish to thank the Director of the National Institute of Nutrition, Indian Council of Medical Research (Flagship Project), Hyderabad, for extending grant support to execute this work. They also thank Dr. NV Giridharan and

Dr. P Suresh, the former and present, respectively, person in charge of NCLAS, for extending support to carry out the animal experiments. They deeply acknowledge help extended by Dr. P. Uday Kumar (Pathology Head) and his team for providing them with tissue sections.

References

[1] M. Qatanani and M. A. Lazar, "Mechanisms of obesity-associated insulin resistance: many choices on the menu," *Genes and Development*, vol. 21, no. 12, pp. 1443–1455, 2007.

[2] W. T. Cefalu, "Animal models of type 2 diabetes: clinical presentation and pathophysiological relevance to the human condition," *ILAR Journal*, vol. 47, no. 3, pp. 186–198, 2006.

[3] N. V. Giridharan, "Animal models of obesity and their usefulness in molecular approach to obesity," *Indian Journal of Medical Research*, vol. 108, pp. 225–242, 1998.

[4] R. R. Kalashikam, K. K. Battula, V. Kirlampalli, J. M. Friedman, and G. Nappanveettil, "Obese locus in WNIN/obese rat maps on chromosome 5 upstream of leptin receptor," *PLoS ONE*, vol. 8, no. 10, Article ID e77679, 2013.

[5] N. V. Giridharan, P. Sailaja, and N. Harishankar, "A new obese rat model to study obesity and cardiovascular risks," *Proceedings of CMJ Journal*, vol. 96, 2010.

[6] N. Harishankar, P. U. Kumar, B. Sesikeran, and N. Giridharan, "Obesity associated pathophysiological & histological changes in WNIN obese mutant rats," *Indian Journal of Medical Research*, vol. 134, no. 9, pp. 330–340, 2011.

[7] S. L. Madhira, G. Nappanveethl, V. Kodavalla, and V. Venkatesan, "Comparison of adipocyte-specific gene expression from WNIN/Ob mutant obese rats, lean control, and parental control," *Molecular and Cellular Biochemistry*, vol. 357, pp. 217–225, 2011.

[8] S. L. Madhira, S. S. Challa, M. Chalasani et al., "Promise(s) of mesenchymal stem cells as an in vitro model system to depict pre-diabetic/diabetic milieu in WNIN/GR-Ob mutant rats," *PLoS ONE*, vol. 7, no. 10, Article ID e48061, 2012.

[9] G. Kewalramani, P. J. Bilan, and A. Klip, "Muscle insulin resistance: assault by lipids, cytokines and local macrophages," *Current Opinion in Clinical Nutrition and Metabolic Care*, vol. 13, no. 4, pp. 382–390, 2010.

[10] C. Wang, Y. Guan, and J. Yang, "Cytokines in the progression of pancreatic β-cell dysfunction," *International Journal of Endocrinology*, vol. 2010, Article ID 515136, 10 pages, 2010.

[11] S. G. Kiran, R. K. Dorisetty, M. R. Umrani et al., "Pyridoxal 5′ phosphate protects islets against streptozotocin-induced beta-cell dysfunction- in vitro and in vivo," *Experimental Biology and Medicine*, vol. 236, no. 4, pp. 456–465, 2011.

[12] R. Kikkawa, "Chronic complications in diabetes mellitus," *British Journal of Nutrition*, vol. 84, no. 2, pp. S183–S185, 2000.

[13] T. Mitsuhashi, K. Hibi, M. Kosuge et al., "Relation between hyperinsulinemia and nonculprit plaque characteristics in nondiabetic patients with acute coronary syndromes," *JACC: Cardiovascular Imaging*, vol. 4, no. 4, pp. 392–401, 2011.

[14] V. Venkatesan, M. Chalsani, S. S. Nawaz, R. R. Bhonde, S. S. Challa, and G. Nappanveettil, "Optimization of condition(s) towards establishment of primary islet cell cultures from WNIN/Ob mutant rat," *Cytotechnology*, vol. 64, no. 2, pp. 139–144, 2012.

[15] A. Chairmandurai, S. Kanappa, K. Vadrevu, U. Putcha, and V. Venkatesan, "Recombinant human epidermal growth factor alleviates gastric antral ulcer induced by naproxen: a non-steroidal anti inflammatory drug," *Gastroenterology Research*, vol. 3, pp. 1918–2813, 2010.

[16] R. K. Dorisetty, S. G. Kiran, M. R. Umrani, S. Boindala, R. R. Bhonde, and V. Venkatesan, "Immunolocalization of nestin in pancreatic tissue of mice at different ages," *World Journal of Gastroenterology*, vol. 14, no. 46, pp. 7112–7116, 2008.

[17] G. Gobe, "Identification of apoptosis in kidney tissue sections," *Methods in Molecular Biology*, vol. 466, pp. 175–192, 2009.

[18] D. T. Finegood, M. D. McArthur, D. Kojwang et al., "β-Cell mass dynamics in Zucker diabetic fatty rats: rosiglitazone prevents the rise in net cell death," *Diabetes*, vol. 50, no. 5, pp. 1021–1029, 2001.

[19] K. Mishima, A. P. Mazar, A. Gown et al., "A peptide derived from the non-receptor-binding region of urokinase plasminogen activator inhibits glioblastoma growth and angiogenesis in vivo in combination with cisplatin," *Proceedings of the National Academy of Sciences of the United States of America*, vol. 97, no. 15, pp. 8484–8489, 2000.

[20] A.-A. Dussault and M. Pouliot, "Rapid and simple comparison of messenger RNA levels using real-time PCR," *Biological Procedures Online*, vol. 8, no. 1, pp. 1–10, 2006.

[21] M. M. Amoli, R. Moosavizadeh, and B. Larijani, "Optimizing conditions for rat pancreatic islets isolation," *Cytotechnology*, vol. 48, no. 1–3, pp. 75–78, 2005.

[22] Y.-F. Cui, M. Ma, G.-Y. Wang, D.-E. Han, B. Vollmar, and M. D. Menger, "Prevention of core cell damage in isolated islets of Langerhans by low temperature preconditioning," *World Journal of Gastroenterology*, vol. 11, no. 4, pp. 545–550, 2005.

[23] S. S. Challa, G. S. Kiran, R. R. Bhonde, and V. Venkatesan, "Enhanced neogenic potential of Panc-1 cells supplemented with human umbilical cord blood serum-An alternative to FCS," *Tissue and Cell*, vol. 43, no. 4, pp. 266–270, 2011.

[24] H. Xu, G. T. Barnes, Q. Yang et al., "Chronic inflammation in fat plays a crucial role in the development of obesity-related insulin resistance," *Journal of Clinical Investigation*, vol. 112, no. 12, pp. 1821–1830, 2003.

[25] L. Singotamu and P. M. Chary, "Scanning electron microscope studies on genetically modified (GM) crops–G.M. cotton fiber (Gossypium herbaceum)," *Scanning*, vol. 27, no. 3, pp. 160–161, 2005.

[26] V. Vijayalakshmi and P. D. Gupta, "Role of transglutaminase in keratinization of vaginal epithelial cells in oestrous cycling rats," *Biochemistry and Molecular Biology International*, vol. 43, no. 5, pp. 1041–1049, 1997.

[27] M. Cnop, N. Welsh, J.-C. Jonas, A. Jörns, S. Lenzen, and D. L. Eizirik, "Mechanisms of pancreatic β-cell death in type 1 and type 2 diabetes: many differences, few similarities," *Diabetes*, vol. 54, no. 2, pp. S97–S107, 2005.

[28] J. A. Ehses, A. Perren, E. Eppler et al., "Increased number of islet-associated macrophages in type 2 diabetes," *Diabetes*, vol. 56, no. 9, pp. 2356–2370, 2007.

[29] C.-H. Hsieh, Y.-J. Hung, C.-Z. Wu et al., "Insulin resistance & secretion in subjects with normal fasting plasma glucose," *Indian Journal of Medical Research*, vol. 124, pp. 527–534, 2006.

[30] P. Bandaru, H. Rajkumar, and G. Nappanveettil, "Altered or impaired immune response upon vaccination in WNIN/Ob rats," *Vaccine*, vol. 29, no. 16, pp. 3038–3042, 2011.

[31] P. Bandaru, H. Rajkumar, and G. Nappanveettil, "The impact of obesity on immune response to infection and vaccine: an insight into plausible mechanisms," *Endocrinology & Metabolic Syndrome*, vol. 2, p. 113, 2013.

[32] C. Sánchez-Pozo, J. Rodriguez-Baño, A. Domínguez-Castellano, M. A. Muniain, R. Goberna, and V. Sánchez-Margalet, "Leptin stimulates the oxidative burst in control monocytes but attenuates the oxidative burst in monocytes from HIV-infected patients," *Clinical and Experimental Immunology*, vol. 134, no. 3, pp. 464–469, 2003.

[33] L. Rui, V. Aguirre, J. K. Kim et al., "Insulin/IGF-1 and TNF-α stimulate phosphorylation of IRS-1 at inhibitory Ser307 via distinct pathways," *Journal of Clinical Investigation*, vol. 107, no. 2, pp. 181–189, 2001.

[34] M. Chentouf, G. Dubois, C. Jahannaut et al., "Excessive food intake, obesity and inflammation process in Zucker fa/fa rat pancreatic islets," *PLoS ONE*, vol. 6, no. 8, Article ID e22954, 2011.

[35] O. P. Kristiansen and T. Mandrup-Poulsen, "Interleukin-6 and diabetes: the good, the bad, or the indifferent?" *Diabetes*, vol. 54, no. 2, pp. S114–S124, 2005.

[36] D. C. Nieman, S. L. Nehlsen-Cannarella, D. A. Henson et al., "Immune response to obesity and moderate weight loss," *International Journal of Obesity*, vol. 20, no. 4, pp. 353–360, 1996.

[37] D. O'Shea, T. J. Cawood, C. O'Farrelly, and L. Lynch, "Natural killer cells in obesity: impaired function and increased susceptibility to the effects of cigarette smoke," *PloS ONE*, vol. 5, no. 1, Article ID e8660, 2010.

[38] J.-P. Bastard, M. Maachi, C. Lagathu et al., "Recent advances in the relationship between obesity, inflammation, and insulin resistance," *European Cytokine Network*, vol. 17, no. 1, pp. 4–12, 2006.

[39] C. Procaccini, E. Jirillo, and G. Matarese, "Leptin as an immunomodulator," *Molecular Aspects of Medicine*, vol. 33, no. 1, pp. 35–45, 2012.

[40] P. Bandaru, H. Rajkumar, V. P. Upadrasta, and G. Nappanveettil, "Role of leptin in immune dysfunction in WNIN obese rats," *Endocrinology & Metabolic Syndrome*, vol. 2, p. 116, 2013.

[41] V. de Rosa, C. Procaccini, G. Calì et al., "A key role of leptin in the control of regulatory T cell proliferation," *Immunity*, vol. 26, no. 2, pp. 241–255, 2007.

[42] H. K. Vincent and A. G. Taylor, "Biomarkers and potential mechanisms of obesity-induced oxidant stress in humans," *International Journal of Obesity*, vol. 30, no. 3, pp. 400–418, 2006.

[43] P. A. Tataranni and E. Ortega, "A burning question: does an adipokine-induced activation of the immune system mediate the effect of overnutrition on type 2 diabetes?" *Diabetes*, vol. 54, no. 4, pp. 917–927, 2005.

[44] K. E. Wellen and G. S. Hotamisligil, "Obesity-induced inflammatory changes in adipose tissue," *Journal of Clinical Investigation*, vol. 112, no. 12, pp. 1785–1788, 2003.

[45] Y. Saisho, A. E. Butler, E. Manesso, D. Elashoff, R. A. Rizza, and P. C. Butler, "β-cell mass and turnover in humans: effects of obesity and aging," *Diabetes Care*, vol. 36, pp. 111–117, 2013.

[46] D. A. Nugent, D. M. Smith, and H. B. Jones, "A review of islet of Langerhans degeneration in rodent models of type 2 diabetes," *Toxicologic Pathology*, vol. 36, no. 4, pp. 529–551, 2008.

[47] H. Kaneto, T.-A. Matsuoka, S. Kawashima et al., "Role of MafA in pancreatic β-cells," *Advanced Drug Delivery Reviews*, vol. 61, no. 7-8, pp. 489–496, 2009.

[48] D. Kawamori, Y. Kajimoto, H. Kaneto et al., "Oxidative stress induces nucleo-cytoplasmic translocation of pancreatic transcription factor PDX-1 through activation of c-Jun NH2-terminal kinase," *Diabetes*, vol. 52, no. 12, pp. 2896–2904, 2003.

[49] K. L. Lipson, S. G. Fonseca, S. Ishigaki et al., "Regulation of insulin biosynthesis in pancreatic beta cells by an endoplasmic reticulum-resident protein kinase IRE1," *Cell Metabolism*, vol. 4, no. 3, pp. 245–254, 2006.

[50] R. J. Kaufman, S. H. Back, B. Song, J. Han, and J. Hassler, "The unfolded protein response is required to maintain the integrity of the endoplasmic reticulum, prevent oxidative stress and preserve differentiation in β-cells," *Diabetes, Obesity and Metabolism*, vol. 12, no. 2, pp. 99–107, 2010.

[51] U. Özcan, Q. Cao, E. Yilmaz et al., "Endoplasmic reticulum stress links obesity, insulin action, and type 2 diabetes," *Science*, vol. 306, no. 5695, pp. 457–461, 2004.

[52] S. Thanumalayan, M. Laxmi Narasu, and V. Venkatesan, "Down regulation of suppressor of potassium transport defect 3 (SKD3) in testis of nonobese diabetic (NOD) mice," *Indian Journal of Veterinary Pathology*, vol. 32, pp. 242–245, 2008.

[53] D. A. Cunha, P. Hekerman, L. Ladrière et al., "Initiation and execution of lipotoxic ER stress in pancreatic β-cells," *Journal of Cell Science*, vol. 121, no. 14, pp. 2308–2318, 2008.

[54] W. Quan, Y.-M. Lim, and M.-S. Lee, "Role of autophagy in diabetes and endoplasmic reticulum stress of pancreatic β-cells," *Experimental and Molecular Medicine*, vol. 44, no. 2, pp. 81–88, 2012.

[55] G. B. Reddy, V. Vasireddy, M. N. A. Mandal et al., "A novel rat model with obesity-associated retinal degeneration," *Investigative Ophthalmology and Visual Science*, vol. 50, no. 7, pp. 3456–3463, 2009.

[56] N. Harishankar, P. Ravinder, K. M. Nair, and N. Giridharan, "Infertility in WNIN obese mutant rats-causes?" *ISRN Endocrinol*, vol. 2011, Article ID 863403, 7 pages, 2011.

[57] M. Y. Donath, M. Böni-Schnetzler, H. Ellingsgaard, and J. A. Ehses, "Islet inflammation impairs the pancreatic B-ceII in type 2 diabetes," *Physiology*, vol. 24, no. 6, pp. 325–331, 2009.

[58] N.-G. Chen, T. M. Tassava, and D. R. Romsos, "Threshold for glucose-stimulated insulin secretion in pancreatic islets of genetically obese (ob/*ob*) mice is abnormally low," *Journal of Nutrition*, vol. 123, no. 9, pp. 1567–1574, 1993.

[59] K. Kaneko, K. Ueki, N. Takahashi et al., "Class IA phosphatidylinositol 3-kinase in pancreatic β cells controls insulin secretion by multiple mechanisms," *Cell Metabolism*, vol. 12, no. 6, pp. 619–632, 2010.

[60] Y.-L. Ding, Y.-H. Wang, W. Huang et al., "Glucose intolerance and decreased early insulin response in mice with severe hypertriglyceridemia," *Experimental Biology and Medicine*, vol. 235, no. 1, pp. 40–46, 2010.

[61] H.-E. Kim, S.-E. Choi, S.-J. Lee et al., "Tumour necrosis factor-α-induced glucose-stimulated insulin secretion inhibition in INS-1 cells is ascribed to a reduction of the glucose-stimulated Ca2+ influx," *Journal of Endocrinology*, vol. 198, no. 3, pp. 549–560, 2008.

[62] J. Seufert, "Leptin Effects on Pancreatic β-Cell Gene Expression and Function," *Diabetes*, vol. 53, no. 1, pp. S152–S158, 2004.

[63] L. P. Roma, S. M. Pascal, J. Duprez, and J. C. Jonas, "Mitochondrial oxidative stress contributes differently to rat pancreatic islet cell apoptosis and insulin secretory defects after prolonged culture in a low non-stimulating glucose concentration," *Diabetologia*, vol. 55, pp. 2226–2237, 2012.

[64] R. Alemzadeh and K. M. Tushaus, "Modulation of adipoinsular axis in prediabetic Zucker diabetic fatty rats by diazoxide," *Endocrinology*, vol. 145, no. 12, pp. 5476–5484, 2004.

[65] G. Üçkaya, P. Delagrange, A. Chavanieu et al., "Improvement of metabolic state in an animal model of nutrition-dependent type 2 diabetes following treatment with S 23521, a new glucagon-like peptide 1 (GLP-1) analogue," *Journal of Endocrinology*, vol. 184, no. 3, pp. 505–513, 2005.

[66] M. Y. Donath, M. Böni-Schnetzler, H. Ellingsgaard, P. A. Halban, and J. A. Ehses, "Cytokine production by islets in health and diabetes: cellular origin, regulation and function," *Trends in Endocrinology and Metabolism*, vol. 21, no. 5, pp. 261–267, 2010.

Hindawi Publishing Corporation
BioMed Research International
Volume 2013, Article ID 938047, 7 pages
http://dx.doi.org/10.1155/2013/938047

Research Article

A Nonthoracotomy Myocardial Infarction Model in an Ovine Using Autologous Platelets

Tyler Spata,[1] Daniel Bobek,[1] Bryan A. Whitson,[1] Sampath Parthasarathy,[1] Peter J. Mohler,[1] Robert S. D. Higgins,[1] and Ahmet Kilic[1,2]

[1] *The Ohio State University Wexner Medical Center, Columbus, OH 43210, USA*
[2] *Division of Cardiac Surgery, Department of Surgery, The Ohio State University Wexner Medical Center, 410 W. 10th Avenue, N-831 Doan Hall, Columbus, OH 43210, USA*

Correspondence should be addressed to Ahmet Kilic; ahmet.kilic@osumc.edu

Received 3 July 2013; Accepted 15 November 2013

Academic Editor: Andrea Vecchione

Objective. There is a paucity of a biological large animal model of myocardial infarction (MI). We hypothesized that, using autologous-aggregated platelets, we could create an ovine model that was reproducible and more closely mimicked the pathophysiology of MI. *Methods*. Mepacrine stained autologous platelets from male sheep ($n = 7$) were used to create a myocardial infarction via catheter injection into the mid-left anterior descending (LAD) coronary artery. Serial daily serum troponin measurements were taken and tissue harvested on post-embolization day three. Immunofluorescence microscopy was used to detect the mepacrine-stained platelet-induced thrombus, and histology performed to identify three distinct myocardial (infarct, peri-ischemic "border zone," and remote) zones. *Results*. Serial serum troponin levels (μg/mL) measured 0.0 ± 0.0 at baseline and peaked at 297.4 ± 58.0 on post-embolization day 1, followed by 153.0 ± 38.8 on day 2 and 76.7 ± 19.8 on day 3. Staining confirmed distinct myocardial regions of inflammation and fibrosis as well as mepacrine-stained platelets as the cause of intravascular thrombosis. *Conclusion*. We report a reproducible, unique model of a biological myocardial infarction in a large animal model. This technique can be used to study acute, regional myocardial changes following a thrombotic injury.

1. Introduction

Myocardial infarction (MI) resulting from coronary arterial disease is the number one cause for mortality in the United States. It is estimated that roughly 785,000 people in the United States will have a new MI in 2012 with an additional 470,000 having a recurrent MI [1, 2]. Early diagnosis and treatment of myocardial infarction is crucial with optimal outcomes in patients seeking immediate medical attention [3].

Currently, there are several large animal models used to study myocardial infarction; however, they deviate significantly from the biological pathophysiology of human MI [4–6]. In our present experiments, we illustrate the use of autologous-aggregated platelets to create an ovine model of MI that is reproducible and more akin to the natural MI process in humans.

2. Materials and Methods

All studies were conducted with approval by the Institutional Animal Care and Use Committee (IACUC) at Ohio State University (Study number: 2012A00000040). Adult male Dorsett sheep weighing between 50–70 kg were used for this study ($n = 7$). Strict adherence was kept to the Guide for the Care and Use of Laboratory Animals of the National Institutes of Health.

2.1. Mepacrine Labeled Platelet Aggregates. Autologous platelet aggregates were made by collecting 200 mL of venous

blood 24 hours prior to the embolization procedure. The blood was drawn in a sterile fashion, centrifuged at 200 ×g for the supernatant, then 1500 ×g for platelet isolation. Platelets were stabilized with a buffer (pH 6.5) consisting of 6.85 mM citric acid, trisodium salt in saline [4]. Mepacrine (10 mM) in phosphate buffered saline (PBS) was used to stain the platelets for 1 hour prior to the embolization experiment and to confirm presence of platelet induced thrombus in infracted tissue. The platelets were then stored in 15 mM Trizma and saline buffer (pH 7.4) as a thrombus was then created by adding 25 μL of thrombin to the platelets in a 3 mL syringe. The syringe was then wrapped in aluminum foil to limit further enzymatic reaction and stored at $^{+}4^{\circ}$C for creation of the thrombus for injection the following day. The mepacrine-stained platelets were verified in the tissue under a Zeiss LSM 510 Confocal Microscope with Argon-2 laser at 488-nm excitation with 500–530-nm BP filter at 63x.

2.2. Serum Troponin Levels. Serum was collected daily at baseline and at postprocedure day 1, 2, and 3 for troponin level assessment [7]. A volume of 0.25 mL of plasma was processed in the Ohio State University Chemistry Lab (Columbus, OH) for troponin levels (μg/mL) at each time point (ADVIA Centaur XP Immunoassay System, Global Siemens Healthcare Sector, Germany).

2.3. Embolization Procedure. All animals were sedated, and all attempts were made to minimize animal discomfort as previously described [4]. A right lateral decubitus position was utilized with the left neck being clipped, prepped, and draped in standard sterile, surgical fashion.

To minimize potentially fatal arrhythmias and provide hemodynamic support during the peri-infarct period, intravenous inotropic (epinephrine at 0.25 mcg/kg/hr) and antiarrhythmic (lidocaine at 2 mg/hr) medications were used [8].

The left carotid artery was surgically exposed, and an introducer sheath (8F Axcess, Argon Medical Devices, Athens, TX) was placed. Subsequently, under fluoroscopic guidance (GE-OEC 9800 Plus, Salt Lake City, UT) a Wiseguide 8 French AL-1 guide catheter (Boston Scientific, Maple Grove, MN) was placed into the left main coronary artery. Five-20 cc of Omnipaque (iohexol) Injection Contrast (350 mgI/mL, GE Healthcare Inc., Princeton, NJ) was used for preembolization verification of the coronary anatomy, and all images were digitally stored. A Bard, Tru-Trac 4 mm × 2 cm balloon catheter (Covington, GA) was positioned in the mid-left anterior descending (LAD) coronary artery. A balloon catheter was inflated to 2–4 atmospheres using an Encore 26 inflation device (Boston Scientific, Cork, Ireland) to temporarily occlude the LAD and to prevent reflux during the infusion. Aggregated platelets (1.5 mL) were infused through the balloon catheter guide wire lumen to infarct the LAD. Subsequently, 5 mL of nonheparanized saline was used to flush the catheter, and then the balloon was deflated after 30 seconds.

Continuous electrocardiograms and arterial line hemodynamic monitoring was carried out with a postembolization angiogram verifying occlusion of the mid-LAD. The epinephrine and lidocaine drips were weaned over a period of twenty minutes. The incision was then closed, and the animal was allowed to recover.

2.4. Procurement Procedure. On post-embolization day 3, the sheep underwent a 5th intercostal space left thoracotomy, and a cardiectomy was performed [4]. Standard double-staining technique was utilized for infarct size measurement with imaging software readily available (ImageJ 1.46r, Wayne Rasband, National Institutes of Health, Bethesda, MD) [5]. Different regions of the left ventricle that were harvested including the (1) infarct zone, (2) peri-ischemic border zone, and (3) remote zones were identified. The infarct zone was identified by location of the mepacrine-staining thrombus injection on the animal's respective angiogram as well as the grossly stained myocardium after the tissue harvest (i.e., significant fibrosis present, pale myocardial surface, and thinning of the myocardium wall). The peri-ischemic border zone was identified as the area between 0.5 and 2.0 cm away from the edge of grossly stained myocardium. The remote zone was identified by being at least 3 cm away from the edge of grossly infracted tissue. All regions were verified by histological and staining techniques.

2.5. Statistical Analysis. All measurements are expressed as mean ± standard error of the mean. A repeated measures analysis of variance (ANOVA) was used to compare the serial daily intragroup troponin-level trends following embolization. A retrospective power analysis was performed to evaluate the power of the study and verify the sample size. Calculations were performed by using IBM SPSS Statistics for Windows, Version 19.0 (IBM Corp., Released 2010, Armonk, NY).

3. Results

3.1. Reproducibility of Infarction. Five of seven animals survived resulting in a twenty-eight percent attrition rate secondary to lethal arrhythmias and/or cardiogenic shock. The other five animals survived to completion of the study. All animals had significant ST elevation in the continuous single lead electrocardiogram monitoring during the procedure as illustrated in Figure 1. Additionally, a single distinct episode of myocardial injury was verified with serial daily serum troponin levels showing a peak level at postembolization day 1 of 297.4 ± 58.0 μg/mL (see Table 1).

A representative angiogram of pre- and post-embolization with corresponding infarct size at post-embolization day 3 is shown in Figure 2. The catheter directed embolization was carried out at the mid to distal one-third of the LAD, and double staining technique revealed an infarct size of 35.8 ± 3.5% of the left ventricular free wall.

3.2. Histology. Hematoxylin and eosin staining as well as Masson's trichrome staining confirmed three distinct regions of myocardial cell hypertrophy, inflammation, and apoptosis. The regions of (a) noninfarcted zone (>3 cm from the region of infarct), (b) peri-ischemic border zone (defined as within

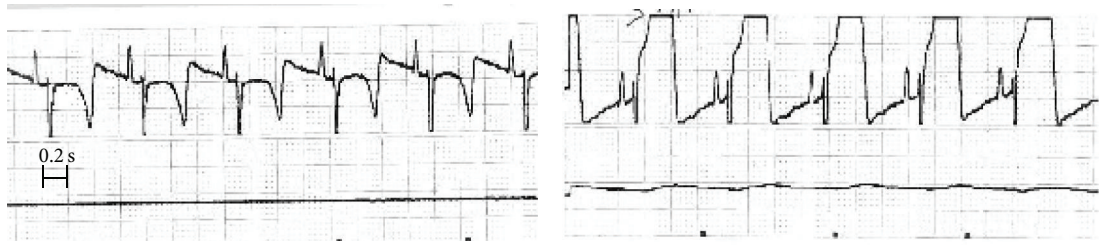

One large box length = 0.2 s

(a) Baseline ECG

(b) 3-minute Postembolization ECG

Figure 1: Electrocardiogram (ECG) readings during embolization. Myocardial infarction verification through electrocardiogram changes. Representative electrocardiogram (ECG) readings from Lead II during the embolization procedure in one animal showing (a) baseline, or preembolization ECG showing absence of ischemia, and (b) 3 minute-post embolization showing "tombstone" or significantly elevated ST segments consistent with a large anterior infarction.

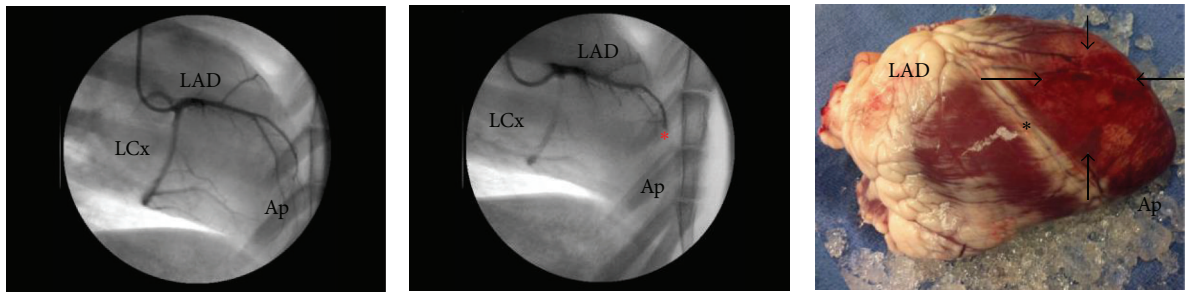

LAD: left anterior descending artery
LCx: left circumflex artery
Ap: apex

(a) Preembolization Angiogram

LAD: left anterior descending artery
LCx: left circumflex artery
Ap: apex

(b) Postembolization Angiogram

LAD: left anterior descending artery
LCx: left circumflex artery
Ap: apex

(c) Final pathological. Specimen

Figure 2: Pre- and postembolization angiograms and infarct area at cardiectomy. Illustrative example of embolization and corresponding area of infarctionat cardiectomy. (a) Preembolization angiogram showing the relationship of the nativeovine coronary anatomy and selection of embolization target of the LAD. (b) Area of thrombus formation immediately postembolization (note that $*$ corresponds to the location of embolization injection). (c) Final pathology showing the corresponding area of infarction (note that $*$ once again shows area of embolization with arrows demarcating the area effected by infarction).

0.5–2.0 cm of the gross edge of ischemic tissue), and (c) the infarct zone are illustrated in Figure 3. The remote zone myocardium shows little to no inflammatory cells present. Within the peri-ischemic border zone, there is an area of demarcation between the presence of inflammatory cells and tissue spared of inflammation and ischemia. The infarcted area has little viable cardiomyocytes present on postembolization day 3. Immunofluorescence verifies the presence of intravascular mepacrine-stained platelets as the cause of thrombosis as seen in Figure 4.

Table 1: Serial serum troponin levels.

	Baseline	Day #1 Post-embolization	Day #2 Post-embolization	Day #3 Post-embolization
Troponin (μg/mL)	0.0 ± 0.0	297.4 ± 58.0*	153.0 ± 38.8*	76.7 ± 19.8*

Troponin levels during baseline and daily post-embolization (mean ± standard deviation). Troponin levels peaked within twenty-four hours post-embolization and started decreasing towards baseline. ($n = 5$, $^*P < 0.05$).

4. Discussion

4.1. Current Models and Their Limitations. Large animal models make it more challenging to provide a direct ischemic event in the myocardium without either a thoracotomy with direct ligation or embolization using synthetic, nonbiological beads [6]. Indeed, the currently available models of heart failure are initiated by either (1) rapid-ventricular pacing induction, (2) aortic banding, (3) intracoronary injection of ethyl alcohol [9], (4) intracoronary balloon occlusion [10], or (5) surgical occlusion of coronary arteries [11]. Other ways to induce catheter-based ischemia include ameroid constrictors and coiling/gelfoam in addition to cryonecrosis within the coronary artery after a thoracotomy [6]. All of these methods deviate significantly from the normal mechanisms of human MI [4].

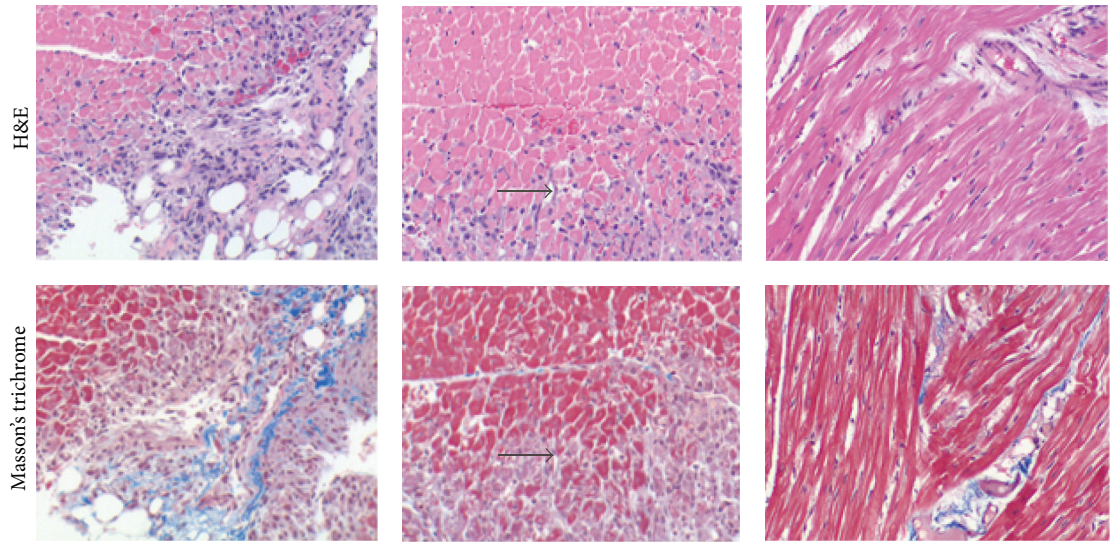

H&E: Hematoxylin and eosin. (a) Infarct zone

H&E: Hematoxylin and eosin. (b) Border zone

H&E: Hematoxylin and eosin. (c) Remote zone

Figure 3: Histological analysis highlighting the three distinct zones of myocardium post-embolization. Representative regional myocardial histology (20x magnification). (a) Infarct tissue showing significant area of inflammation (H&E) and fibrosis (Masson's trichrome), (b) border zone myocardium showing the transition (delineated by blocked arrows) between normal myocytes (top) and ischemic tissue (bottom), and (c) remote zone showing normal myocardial cell structure and no fibrosis.

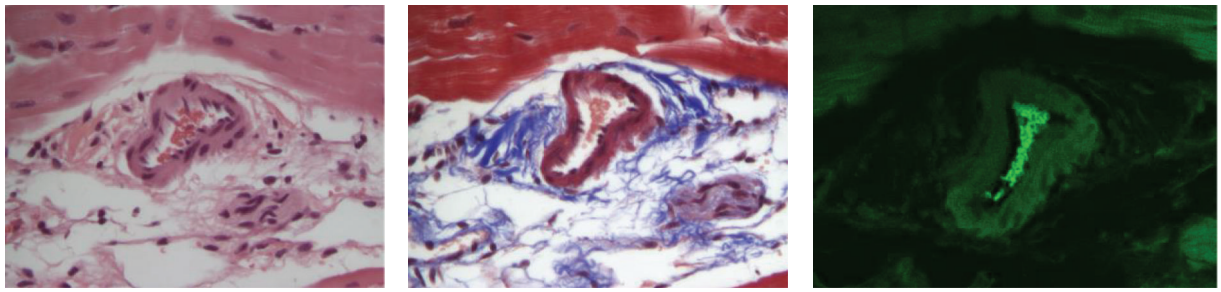

H&E: Hematoxylin and eosin. (a) H&E

H&E: Hematoxylin and eosin. (b) Masson's trichrome

H&E: Hematoxylin and eosin. (c) Immunofluorescence

Figure 4: Intravascular thrombus confirmation with mepacrine-labeled platelets. Representative intravascular thrombus secondary to mepacrine-labeled platelet embolization (magnification 63x). (a) H&E showing inflammation and intravascular thrombus. (b) Masson's trichrome showing early fibrosis and organization of immature collagen deposition. (c) Immunohistochemistry showing intravascular presence of mepacrine labeled platelets.

Although the direct coronary artery ligation model is widely used in large animals, MI in humans is due to a thromboembolic event and not a direction ligation of a coronary artery with an accompanying surgical trauma. Other less invasive animal models (i.e., injection of polystyrene beads into the coronary artery causing myocardial injury to the left-ventricle) have more closely mimicked the human pathophysiologic process; however, the use of foreign materials, such as the polystyrene beads, can potentially stimulate an exaggerated inflammatory response making it a less than ideal model for study [4]. Recent research has shown that platelets in the thromboembolic events do trigger initial inflammatory reactions with microembolization after myocardial injury [12]. With our alternative, nonsurgical model of permanent coronary artery occlusion, we can more closely recreate the thromboembolic phenomenon that occurs during the human MI. In addition, the ability to localize and reproduce the area of injury gives us the ability to study not only the global cardiac changes but also the local changes that occur after an MI.

4.2. Current Study on the Ovine Model. Our current, non-thoracotomy strategy of accomplishing myocardial infarction should enable us to more closely explore the cellular and molecular pathways underlying an acute MI. It is essential

to improve our current preclinical models to gain a better understanding of the human pathophysiology. This approach is important in order to accurately develop a relevant pathophysiologic model for clinical therapeutic evaluations. Unfortunately, there currently is a paucity of a biologic large animal model of an acute MI. Mice models of myocardial ischemia and heart failure are most commonly employed due to cost efficiency and availability; however, these models do not necessarily translate into the human condition.

Various different species of large animals (i.e., dogs, pigs, and sheep) have been used to explore myocardial disease. Amongst the large animal models, the ovine model has been shown to more closely mimic human coronary arterial anatomy [6, 13]. The sheep are superior to canines in the manner with which the heart behaves towards coronary arterial injury [14] and are less arrhythmogenic than pigs to myocardial infarction [15].

Sheep, however, do have some significant variability in the distribution of their left circumflex artery, leading to significant variation in infarct sizes [16]. Our group had previously reported on the efficacy of repeated embolizations to the left circumflex artery to induce heart failure [4]. Subsequently, we have noted that the left anterior descending (LAD) artery tends to be less variable and hence have elected to modify our techniques to create a more reproducible model of an acute myocardial infarction using the LAD as the target for biological embolization. Previous ovine models of postinfraction heart failure through the ligation of either the distal LAD or the diagonal branches off of the LAD have shown reproducible results. This has been attributed to the consistent territory of myocardium supplied by this artery as well as the lack of collateral vascularity [16–18].

Various studies have been performed to evaluate the importance of how different regions of the heart are affected by a myocardial infarction. After a localized infarction, there is an increase in regional remodeling strain as a result of increased myocardial apoptosis and regional contractile dysfunction [19]. Multiple regional coronary ligations have been shown as a model to mimic global ischemic cardiomyopathy [20].

Clinically, various studies have shown the importance of not only regional but also global cardiac changes that occur after a localized myocardial infarction, governed by local changes in blood flow as well as global changes in adjacent myocardium [21]. The heart must undergo a variety of complex pathways, especially in ways to heal from the infarction [22–24]. Such cardiac remodeling pathways as calcium-handling [25–28], inflammation [28–31], angiogenesis [28, 31], hypertrophy [26, 30, 32], and cell survival/apoptosis [25, 26, 29–32] are still being studied in how the myocardial compensates to episodes of ischemia with the eventual development of heart failure. The only way to better study these regional changes is to develop a large animal model that closely mimics the human myocardial infarction pathophysiology.

4.3. Limitations. There are limitations to this study. The ovine left coronary anatomy does have some variation; the different anatomical configurations include (1) origin of where left circumflex branches result in a short left main coronary artery, (2) complex angles amongst the left main coronary artery requiring longer procedure duration, and (3) high bifurcation to an LAD diagonal branch that provides significant blood flow to the left anteroseptal area of the heart (and thus making the heart more prone to malignant arrhythmias). Our goal was to place the embolization catheter/balloon past the last prominent diagonal branch of the LAD to prevent occlusion of the branch and better localize the area of ischemia. However, the LAD diagonal variability results in a variation of the amount of myocardial ischemia resulted from the embolization. The previous model [4] used the left circumflex artery in order to provide adequate myocardial tissue on the anterior portion of the heart for future studies with left-ventricular assist devices. In addition, although the thrombus size appeared consistent and was measured in a consistent aliquot, the thrombus had an organic appearance making it challenging to quantify absolutely.

4.4. Future Implications. The ideal embolization model should address variations of LAD anatomy to provide consistent areas of occlusion following embolization. Thus, future studies should analyze regional versus global mRNA/protein expression amongst the different myocardial zones following an infraction. Possible therapeutic interventions, including regionally targeted anti-inflammatory, proangiogenic, and antiapoptotic measures, can be tested using this model without the added variability of surgical and/or nonbiological inflammatory insult. As we further test the hypotheses with this model, we move the field closer to an ideal model to study acute human myocardial infarction.

5. Conclusion

Our unique, nonthoracotomy surgical model platform will enable investigators to identify regional as well as global changes that occur after an acute heart attack. These targeted myocardial zones will enable the identification of genetic and protein targets to prevent infarct expansion following an MI. It is our hope that this approach will help to mitigate maladaptive cardiac remodeling and stop the development of ischemic heart failure in future studies.

Conflict of Interests

The authors have no financial relations with commercial identities and no conflict of interests.

Acknowledgment

Statistical evaluation was verified through David P. Way, MEd, Senior Research Associate in the Center for Education and Scholarship, Ohio State University College of Medicine.

References

[1] V. L. Roger, A. S. Go, D. M. Lloyd-Jones et al., "Heart disease and stroke statistics—2011 update: a report from the American Heart Association," *Circulation*, vol. 123, no. 4, pp. e18–e209, 2011.

[2] N. I. Parikh, P. Gona, M. G. Larson et al., "Long-term trends in myocardial infarction incidence and case fatality in the national heart, lung, and blood institute's Framingham heart study," *Circulation*, vol. 119, no. 9, pp. 1203–1210, 2009.

[3] E. M. Antman, D. T. Anbe, P. W. Armstrong et al., "ACC/AHA guidelines for the management of patients with ST-elevation myocardial infarction: a report of the American College of Cardiology/American Heart Association Task Force on Practice Guidelines (Committee to Revise the 1999 Guidelines for the Management of Patients with Acute Myocardial Infarction)," *Journal of the American College of Cardiology*, vol. 44, no. 3, pp. E1–E22, 2004.

[4] P. Kwiatkowski, C. Sai-Sudhakar, A. Philips, S. Parthasarathy, and B. Sun, "Development of a novel large animal model of ischemic heart failure using autologous platelet aggregates," *International Journal of Artificial Organs*, vol. 33, no. 2, pp. 63–71, 2010.

[5] L. H. Michael, M. L. Entman, C. J. Hartley et al., "Myocardial ischemia and reperfusion: a murine model," *American Journal of Physiology—Heart and Circulatory Physiology*, vol. 269, no. 6, pp. H2147–H2154, 1995.

[6] E. Monnet and J. C. Chachques, "Animal models of heart failure: what is new?" *Annals of Thoracic Surgery*, vol. 79, no. 4, pp. 1445–1453, 2005.

[7] A. J. Bakker, J. P. M. C. Gorgels, B. van Vlies et al., "Contribution of creatine kinase MB mass concentration at admission to early diagnosis of acute myocardial infarction," *British Heart Journal*, vol. 72, no. 2, pp. 112–118, 1994.

[8] K. Grauer, "New trends in the pharmacologic management of cardiac arrest," *American Family Physician*, vol. 49, no. 3, pp. 591–600, 1994.

[9] W. Kim, M. H. Jeong, D. S. Sim et al., "A porcine model of ischemic heart failure produced by intracoronary injection of ethyl alcohol," *Heart and Vessels*, vol. 26, no. 3, pp. 342–348, 2011.

[10] G. A. Krombach, S. Kinzel, A. H. Mahnken, R. W. Günther, and A. Buecker, "Minimally invasive close-chest method for creating reperfused or occlusive myocardial infarction in swine," *Investigative Radiology*, vol. 40, no. 1, pp. 14–18, 2005.

[11] E. Gao, Y. H. Lei, X. Shang et al., "A novel and efficient model of coronary artery ligation and myocardial infarction in the mouse," *Circulation Research*, vol. 107, no. 12, pp. 1445–1453, 2010.

[12] J. Liu, X. M. Gao, L. Fang et al., "Novel role of platelets in mediating inflammatory responses and ventricular rupture or remodeling following myocardial infarction," *Arteriosclerosis, Thrombosis, and Vascular Biology*, vol. 31, no. 4, pp. 834–841, 2011.

[13] M. E. Weaver, G. A. Pantely, J. D. Bristow, and H. D. Ladley, "A quantitative study of the anatomy and distribution of coronary arteries in swine in comparison with other animals and man," *Cardiovascular Research*, vol. 20, no. 12, pp. 907–917, 1986.

[14] W. G. Kim, Y. C. Shin, S. W. Hwang, C. Lee, and C. Y. Na, "Comparison of myocardial infarction with sequential ligation of the left anterior descending artery and its diagonal branch in dogs and sheep," *International Journal of Artificial Organs*, vol. 26, no. 4, pp. 351–357, 2003.

[15] J. A. Dixon and F. G. Spinale, "Large animal models of heart failure; a critical link in the translation of basic science to clinical practice," *Circulation*, vol. 2, no. 3, pp. 262–271, 2009.

[16] P. Locatelli, F. D. Olea, O. Mendiz et al., "An ovine model of postinfarction dilated cardiomyopathy in animals with highly variable coronary anatomy," *ILAR Journal*, vol. 52, no. 1, pp. E16–21, 2011.

[17] S. L. Moainie, J. H. Gorman III, T. S. Guy et al., "An ovine model of postinfarction dilated cardiomyopathy," *Annals of Thoracic Surgery*, vol. 74, no. 3, pp. 753–760, 2002.

[18] S. Rabbani, H. Ahmadi, E. Fayazzadeh et al., "Development of an ovine model of myocardial infarction," *ANZ Journal of Surgery*, vol. 78, no. 1-2, pp. 78–81, 2008.

[19] G. K. Yankey, T. Li, A. Kilic et al., "Regional remodeling strain and its association with myocardial apoptosis after myocardial infarction in an ovine model," *Journal of Thoracic and Cardiovascular Surgery*, vol. 135, no. 5, pp. 991.e1–991.e2, 2008.

[20] J. D. Schmitto, S. A. Mokashi, L. S. Lee et al., "A novel, innovative ovine model of chronic ischemic cardiomyopathy induced by multiple coronary ligations," *Artificial Organs*, vol. 34, no. 11, pp. 918–922, 2010.

[21] B. B. Løgstrup, D. E. Høfsten, T. B. Christophersen et al., "Correlation between left ventricular global and regional longitudinal systolic strain and impaired microcirculation in patients with acute myocardial infarction," *Echocardiography*, 2012.

[22] M. Konoplyannikov, K. H. Haider, V. K. Lai, R. P. Ahmed, S. Jiang, and M. Ashraf, "Activation of diverse signaling pathways by ex-vivo delivery of multiple cytokines for myocardial repair," *Stem Cells and Development*, vol. 22, no. 2, pp. 204–215, 2013.

[23] G. Nucifora, M. Bertini, N. A. Marsan et al., "Temporal evolution of left ventricular dyssynchrony after myocardial infarction: relation with changes in left ventricular systolic function," *European Heart Journal*, vol. 13, no. 12, pp. 1041–1046, 2012.

[24] J. A. Dixon, R. C. Gorman, R. E. Stroud et al., "Targeted regional injection of biocomposite microspheres alters post-myocardial infarction remodeling and matrix proteolytic pathways," *Circulation*, vol. 124, supplement 11, pp. S35–S45, 2011.

[25] K. A. Webster, "Mitochondrial membrane permeabilization and cell death during myocardial infarction: roles of calcium and reactive oxygen species," *Future Cardiology*, vol. 8, no. 6, pp. 863–884, 2012.

[26] Y. Zhao, T. Li, X. Wei et al., "Mesenchymal stem cell transplantation improves regional cardiac remodeling ovine infarction," *Stem Cells Translational Medicine*, vol. 1, no. 9, pp. 685–695, 2012.

[27] D. S. Bocalini, L. Dos-Santos, E. L. Antonio et al., "Myocardial remodeling after large infarcts in rat converts post rest-potentiation in force decay," *Arquivos Brasileiros de Cardiologia*, vol. 98, no. 3, pp. 243–251, 2012.

[28] M. Hori and K. Nishida, "Oxidative stress and left ventricular remodelling after myocardial infarction," *Cardiovascular Research*, vol. 81, no. 3, pp. 457–464, 2009.

[29] G. Vilahur, O. Juan-Babot, E. Peña, B. Oñate, L. Casaní, and L. Badimon, "Molecular and cellular mechanisms involved in cardiac remodeling after acute myocardial infarction," *Journal of Molecular and Cellular Cardiology*, vol. 50, no. 3, pp. 522–533, 2011.

[30] M. A. Kolpakov, R. Seqqat, K. Rafiq et al., "Pleiotropic effects of neutrophils on myocyte apoptosis and left ventricular remodeling during early volume overload," *Journal of Molecular and Cellular Cardiology*, vol. 47, no. 5, pp. 634–645, 2009.

[31] R. P. H. Ahmed, K. H. Haider, J. Shujia, M. R. Afzal, and M. Ashraf, "Sonic Hedgehog gene delivery to the rodent heart promotes angiogenesis via iNOS/netrin-1/PKC pathway," *PLoS ONE*, vol. 5, no. 1, Article ID e8576, 2010.

[32] M. Prech, A. Marszałek, J. Schröder et al., "Apoptosis as a mechanism for the elimination of cardiomyocaytes after acute myocardial infarction," *American Journal of Cardiology*, vol. 105, no. 9, pp. 1240–1245, 2010.

Hindawi Publishing Corporation
BioMed Research International
Volume 2013, Article ID 810423, 8 pages
http://dx.doi.org/10.1155/2013/810423

Research Article

Curcumin Inhibits Tumor Growth and Angiogenesis in an Orthotopic Mouse Model of Human Pancreatic Cancer

Sabrina Bimonte,[1] Antonio Barbieri,[1] Giuseppe Palma,[1,2] Antonio Luciano,[1] Domenica Rea,[1] and Claudio Arra[1]

[1] *Istituto Nazionale per lo Studio e la Cura dei Tumori "Fondazione G. Pascale", IRCCS, Via Mariano Semmola, 80131 Naples, Italy*
[2] *Istituto di Endocrinologia e Oncologia Sperimentale del Consiglio Nazionale delle Ricerche, Dipartimento di Biologia e Patologia Cellulare e Molecolare "L. Califano", Università degli Studi di Napoli "Federico II", Via Pansini 5, 80131 Napoli, Italy*

Correspondence should be addressed to Sabrina Bimonte; s.bimonte@istitutotumori.na.it

Received 25 July 2013; Revised 7 October 2013; Accepted 8 October 2013

Academic Editor: Monica Fedele

Pancreatic cancer is a malignant neoplasm originating from transformed cells arising in tissues forming the pancreas. The best chemotherapeutic agent used to treat pancreatic cancer is the gemcitabine. However, gemcitabine treatment is associated with many side effects. Thus novel strategies involving less toxic agents for treatment of pancreatic cancer are necessary. Curcumin is one such agent that inhibits the proliferation and angiogenesis of a wide variety of tumor cells, through the modulation of many cell signalling pathways. In this study, we investigated whether curcumin plays antitumor effects in MIA PaCa-2 cells. *In vitro* studies showed that curcumin inhibits the proliferation and enhances apoptosis of MIA PaCa-2 cells. To test whether the antitumor activity of curcumin is also observed *in vivo*, we generated an orthotopic mouse model of pancreatic cancer by injection of MIA PaCa-2 cells in nude mice. We placed mice on diet containing curcumin at 0.6% for 6 weeks. In these treated mice tumors were smaller with respect to controls and showed a downregulation of the transcription nuclear factor NF-κB and NF-κB-regulated gene products. Overall, our data indicate that curcumin has a great potential in treatment of human pancreatic cancer through the modulation of NF-κB pathway.

1. Introduction

Pancreatic cancer is a malignant neoplasm originating from transformed cells arising in tissues forming the pancreas, and it is now the fourth most common cause of cancer-related deaths in the United States and the eighth worldwide [1]. This pathology leads to an aggressive local invasion and early metastases, and is poorly responsive to treatment with chemotherapy [2]. At present, gemcitabine is the best chemotherapeutic agent available for treatment of pancreatic cancer. However, it is noted that patients with this cancer treated with gemcitabine, showed several side effects and developed drug resistance over time [3]. In order to bypass these problems, novel strategies involving less toxic agents that can sensitize pancreatic cancer cells to chemotherapy are necessary. Curcumin, a component of the spice turmeric (*Curcuma longa*), is one such agent and is not toxic to humans [4]. It has been used for thousands years in Orient as a healing agent for variety of illnesses. Many studies provided evidence that curcumin is an agent with strong inflammatory properties and strong therapeutic potential against many variety of cancer. Curcumin inhibits the cell survival, proliferation, and angiogenesis of a wide variety of tumor cells, through the modulation of various cell signalling pathways, which involve transcription factor, protein kinases, growth factor, and other enzymes. In particular, it has been demonstrated that curcumin modulates the activation of the transcription factor nuclear factor-κB (NF-κB) which, in turn, plays a role in the growth and chemoresistance of pancreatic cancer [5, 6]. It has been showed that NF-κB promotes pancreatic growth by inhibiting apoptosis [7–9]. Additionally it has been demonstrated that NF-κB plays also

several roles in angiogenesis [10], migration, and invasion of pancreatic cells [11]. Curcumin has also been shown to suppress angiogenesis *in vivo* [12–14]. *In vitro* and *in vivo* studies have already demonstrated that curcumin inhibits the growth of human pancreatic cancer cells [15, 16]. Previously, it has been demonstrated that curcumin can potentiates the antitumor activity of gemcitabine in pancreatic cells by downregulating NF-κB-regulated gene products [17].

In this study, we assessed the antitumor activities of curcumin in human pancreatic cancer cell line and MIA PaCa-2 cells by *in vitro* and *in vivo* experiments. *In vitro* data allowed us to demonstrate that curcumin, inhibited the proliferation and enhanced the apoptosis of MIA PaCa-2 cells. *In vivo*, by generation of an orthotopic mouse model of pancreatic cancer, we showed that tumours from mice injected with MIA PaCa-2 cells and placed on diet containing curcumin at 0.6% for 6 weeks were smaller than those observed in controls. We also showed a down regulation of the NF-κB-regulated gene products (cyclin D, VEGF, MMP-9, and IKKα/β). Overall, our data indicate that curcumin has a great potential in treatment of human pancreatic cancer, through the modulation of NF-κB pathway.

2. Materials and Methods

2.1. Materials. Curcumin, (E,E)-1,7-bis (4-Hydroxy-3-methoxyphenyl)-1,6-heptadiene-3,5-dione, Diferuloylmethane, Diferulylmethane, Natural Yellow 3 used for *in vitro* experiments, was obtained from Sigma Aldrich (Piscataway, NJ). The following polyclonal antibodies cyclin D1, MMP-9 and monoclonal antibodies against VEGF were obtained from Santa Cruz Biotechnology (Santa Cruz, CA). Anti-IKKα and anti-IKKβ antibodies were kindly provided by Imgenex (San Diego, CA). The liquid DAB+ Substrate Chromogen System-HRP used for immunocytochemistry was obtained from DakoCytomation (Carpinteria, CA). Penicillin, streptomycin, RPMI 1640, and fetal bovine serum (FBS) were obtained from Invitrogen (Grand Island, NY). Tris, glycine, NaCl, SDS, and bovine serum albumin (BSA) were obtained from Sigma Chemical (St. Louis, MO). Complete feed for mice with curcumin 0.6% (AIN-93G) was purchased by Mucedola (Settimo Milanese, Italy).

2.2. Cell Lines. The pancreatic cancer cell line MIA PaCa-2 transfected with red fluorescent protein (RPF) and MPanc-96 cells was a kind gift from Professor Turco (University of Fisciano, Italy). Panc-1 cells were obtained from the American Type Culture Collection (Manassas, VA). All cell lines were cultured in RPMI 1640 supplemented with 10% FBS, 100 units/mL penicillin, and 100 μg/mL streptomycin.

2.3. Proliferation Assay. The effect of curcumin on cell proliferation was determined by using TACS 3-(4,5-dimethylthiazol-2-yl)-2,5-diphenyltetrazolium bromide (MTT) cell proliferation assay (Trevigen, Githersburg). The cells (2,000 per well) were incubated with or without curcumin, in triplicate in a 96-well plate and then incubated for 2, 4 and 6 days at 37°C. A MTT solution was added to each well and incubated for 2 h at 37°C. An extraction buffer (20% SDS and 50% dimethylformamide) was added, and the cells were incubated overnight at 37°C. The absorbance of the cell suspension was measured at 570 nm using a microplate reader (DAS Technologies, Chantilly, VA). This experiment was repeated twice, and the statistical analysis was performed to obtain the final values.

2.4. Wound-Healing Assay. MIA PaCa-2 cells were seeded at the density of 40×10^3 cells per well into a 6-multiwell plate and cultured in RPMI 1640 medium supplemented with 1% FBS. At the time of confluence, cells were incubated in the absence or presence of curcumin (50 μM) for 48 h after a slit made horizontally with a white tip at the center of each confluent well. Cell invasion on the slit of the confluent well, was assessed at 0, 24, and 48 hours in each condition by light microscopy.

2.5. In Vitro Apoptosis Assay by Flow Cytometry. Cells were washed and suspended in 0.5 mL of PBS, and 1 AL/mL YO-PRO-1, and propidium iodide was added. Cells were incubated for 30 min on ice and analyzed by flow cytometry (FACScan, Becton Dickinson, Franklin Lakes, NJ) by measurements of fluorescence emission at 530 and 575 nm.

The apoptotic cells were stained with the green fluorescent dye YO-PRO-1 while necrotic cells were stained with propidium iodide. The apoptotic fraction was obtained by dividing the number of apoptotic cells by the total number of cells (minimum of 10^4 cells). Data were analyzed using Cell Quest software (Becton Dickinson). All data were reproduced at least thrice in independent experiments.

2.6. Transfection of Small Interfering RNA. MIA PaCa cells in 96-well plates were grown to 50% confluence and transfected with double-stranded siRNA for relA/p65 (form of NF-κB) target sequence (Sense 5′ CCAUCAACUAUGAUGAGUU dTdT 3′, Antisense 3′ dGdTGGUAGUUGAUACUACUCAA 5′) or with a siRNA nonspecific control (Ambion, Austin, TX, cat n.461) in serum-free medium without antibiotic supplements using Hiperfect Transfection Reagent (Qiagen, Inc.). Cells were incubated under these conditions for 48 h and silencing was then confirmed by western blotting analysis.

2.7. NF-κB Activation in Cell and Tumor Samples. To assess NF-κB activation, we performed electrophoresis mobility shift assays (EMSA) on isolated nuclei from pancreatic cancer tumor and cell samples as described previously [17, 18]. Briefly, nuclear extracts prepared from pancreatic cancer cells (1×10^6/mL) and tumor samples were incubated with 32P-end-labeled 45-mer double-stranded NF-κB oligonucleotide (4 μg of protein with 16 fmol of DNA) from the HIV long terminal repeat (5′ -TTGTTACAAGGGACTTTCCG-CTGGGGACTTTCCAGGGAGGCGTGG-3′; indicates NF-κB-binding sites) for 15 min at 37°C. The resulting DNA-protein complex was separated from free oligonucleotide on 6.6% native polyacrylamide gels. A double-stranded mutant oligonucleotide (5′ -TTGTTACAACTCACTTTCCGCTG-CTCACTTTCCAGGGAGGCGTGG-3′) was used to examine the specificity of binding of NF-κB to the DNA. The dried gels were visualized, and radioactive bands were quantitated

using Phosphor Imager (Molecular Dynamics, Sunnyvale, CA) using Image Quant software.

2.8. Mice. Sixteen eight-week-old female upstream to Foxn1 mice were purchased by Harlan, San Pietro al Natisone, and (Italy). Mice were housed five for cage in the standard mice Plexiglas cages and maintained on a 12 h light : 12 h dark cycle (lights on at 7.00 am) in a temperature-controlled room (22 ± 2°C) and with food and water ad libitum at all times. The experimental protocols were in compliance with the European Communities Council directive (86/609/EEC).

2.9. Generation of Orthotopic Mouse Model of Pancreatic Cancer and Experimental Protocol. RFP-transfected MIA PaCa-2 cells were harvested from subconfluent cultures after a brief exposure to 0.25% trypsin. Trypsinization was stopped with medium containing 10% FBS. The cells were washed once in serum-free medium and suspended in PBS. Only suspensions consisting of single cells, with >90% viability, were used for the injections. A total of 16 female Foxn1 nu/nu mice were used in this experiment and maintained in a barrier facility on HEPA-filtered racks. Animals were individually identified using numbered ear tags. All experiments were conducted in a biological laminar flow hood, and all surgical procedures were conducted with strict adherence to aseptic technique. The mice were anesthetized with avertin solution injected intraperitoneally according to their weight. Then mice were prepped with 10% povidone-iodine on the left flank and draped in a sterile fashion. A longitudinal median laparotomy with a xiphopubic incision was made, and the tail of the pancreas is exteriorized gently. A suspension of 5×10^5 MIA PaCa 2-RFP cells in 25 μL of PBS 1X/mouse was injected into the tail of the pancreas by using a 29-gauge needle and a calibrated push button-controlled dispensing device (Becton Dickinson, Franklin Lakes, NJ). To prevent leakage, the injection point was dubbed with sterile cotton. Once haemostasis was confirmed, the tail of the pancreas was returned into the abdomen and the abdominal wound was closed in a single layer using interrupted 5-0 silk sutures (US Surgical, Norwalk, CT) and skin staples. After 2 week of implantation, mice were randomized into the following treatment groups ($n = 6$) on the basis of fluorescent area measured by MacroFluo imaging: (a) untreated mice placed in normal died; (b) curcumin treated mice placed in diet containing curcumin at 0.6%. Tumor volumes were monitored once a week by using MacroFluo and LAS V3.7 software Leica Microsystems s.r.l. (Switzerland, Ltd). Before imaging, mice were anesthetized with Avertin solution. At each imaging time point, the real-time determination of tumor burden was performed by quantifying fluorescent surface area. Graph depicts tumor area means at 35 weeks after tumor cells injection. Therapy was continued for 4 weeks and animals were sacrificed 2 weeks later. Primary tumors in the pancreas were excised, and the final tumor volume was measured as $V = 2/3\pi r3$, where r is the mean of the three dimensions (length, width, and depth). Statistical analysis was performed to detect the final tumor volumes (paired t-test) by Graph Pad Prisme 5.0. Half of the tumor tissue was formalin fixed and paraffin embedded for immunohistochemistry and routine H&E staining. The other half was snap frozen in liquid nitrogen and stored at −80°C. H&E staining confirmed the presence of tumor(s) in each pancreas.

2.10. Preparation of Nuclear Extract from Tumor Samples. Pancreatic tumor tissues (75–100 mg/mouse) from control and experimental mice were prepared as previously described [17]. The supernatant (nuclear extract) was collected and stored at −70°C until use. Protein concentration was determined by the Bradford protein assay with BSA as the standard.

2.11. Immunohistochemical Analysis for VEGF and COX-2 in Tumor Tissue. Pancreatic cancer tumor samples from control and treated mice were embedded in paraffin and fixed with paraformaldehyde. After being washed in PBS, the slides were blocked with protein block solution (DakoCytomation) for 20 min and then incubated overnight with mouse monoclonal antihuman VEGF and anti-COX-2 antibodies (1 : 60 and 1 : 80, resp.). After the incubation, the slides were washed and then incubated with biotinylated link universal antiserum followed by horseradish peroxidase-streptavidin conjugate (LSAB + kit). The slides were rinsed, and color was developed using 3,3′-diaminobenzidine hydrochloride as a chromogen. Finally, sections were rinsed in distilled water, counterstained with haematoxylin and mounted with DPX mounting medium for evaluation. Pictures were captured with a Photometrics CoolSNAP color camera (Nikon, Lewisville, TX) and MetaMorph version 4.6.5 software (Universal Imaging, Downingtown, PA).

2.12. Western Blot Analysis. Pancreatic tumor tissues (75–100 mg/mouse) from control and experimental mice were minced and incubated with ice for 1 h in 0.5 mL of ice-cold Lysis Buffer (10 mM Tris, ph 8.0, 130 mM Nacl, 1% Triton X-100, 10 mM NaF, 10 mM sodium phosphate, 10 mM sodium pyrophosphate, 2 μg/mL aprotinin, 2 μg/mL leupeptin, and 2 μg/mL pepstatin). The minced tissue was Homogenized using a Dounce homogenizer and centrifuged at 16,000 ×g at 4°C for 10 min. Western blotting analysis was performed as described previously [17]. β-Actin was used as loading control.

3. Results

3.1. Curcumin Inhibits Proliferation and Enhanced Apoptosis of Pancreatic Cancer Cells In Vitro. We first determined whether curcumin inhibits the proliferation of human pancreatic cancer cells by performing *in vitro* assays on MPanc-96, Panc-1, and MIA PaCa-2 cells. Wound healing assay demonstrated that curcumin (50 μM), inhibits the proliferation of pancreatic cancer cell lines at 48 h (Figures 1(a)–1(f)). These results were also confirmed by MTT assay (Figure 1(g)). In order to asses if curcumin enhances the apoptosis in pancreatic cancer cells, we also performed *in vitro* apoptosis assay by flow cytometry. Our results showed that the percentage of apoptosis of MIA PaCa-2 cells treated

with curcumin was higher with respect to controls and to MPanc-96 and Panc-1 cells (Figure 1(h)). Since the effects of curcumin were more evident in MIA PaCa-2 cells, we selected this pancreatic cancer cell line for further experiments. It has been demonstrated that curcumin modulates the activation of the transcription factor nuclear factor-κB (NF-κB) for this reason, we performed a nuclear NF-κB DNA binding assay on MIA PaCA-2 cells treated with curcumin and controls, and we demonstrated that curcumin downregulated NF-κB activation in MIA PaCa-2 cells (Figure 1(i)). To test the hypothesis that inhibition of NF-κB would increase the sensitivity of MIA PaCa-2 cells to curcumin-mediated apoptosis, we used small interfering RNA (siRNA) to knock down p65/relA (a form of NF-κB). Silencing was confirmed by reporter assays as well as western blotting (data not shown). Next, we transiently silenced expression of p65/relA in MIA PaCa-2 cells and examined the effects on the apoptosis alone and in presence of curcumin. We demonstrated that silencing of NF-κB is not able to potentiate the apoptotic effects of curcumin on MIA PaCa-2 cells (Figure 1(j)).

3.2. Curcumin Inhibits the Tumor Growth in Orthotopic Mouse Model of Pancreatic Cancer. In order to study the role curcumin on the tumor growth *in vivo*, we generated a mouse model of pancreatic cancer by injection of MIA PaCa-2-RFP cells in the pancreas of nude mice. Based on the MacroFluo images, 2 weeks later of cell injection, the mice were randomized into two groups: control group (normal diet) and curcumin group (feed added with 0.6% curcumin). The treatment with feed added with 0.6% curcumin was started after the tumor cell implantation and continued for 6 weeks. We also monitored the body weight of mice twice a week until the end of treatment. No difference was observed between the body weight of two groups of animals, indicating that mice eat normally complete fed with curcumin. Mice were sacrificed at the end of treatment. The images were performed on days 10, 17, 24, and 31 after the start of treatment (Figure 2(a)). The bioluminescence imaging results indicated a gradual increase in tumor volume in the curcumin group compared with treatment groups. The final tumor volumes on day 35 after the start of treatment showed a significant decrease in the curcumin group compared with control (Figure 2(b)). These data were also confirmed on tumor measurements performed at the end of the experiment at autopsy using digital Caliper and calculated using the formula $V = 2/3\pi r3$ ($n = 6$) (data not shown).

3.3. Curcumin Inhibits NF-κB Activation and Down-Regulates NF-κB-Regulated Gene Products in Orthotopic Pancreatic Tumors. Since it has been demonstrated that curcumin potentiates the antitumor activity of gemcitabine in pancreatic cells by downregulating NF-κB-regulated gene products [17], we performed DNA binding to detect NF-κB expression in orthotopic tumor tissue samples from control and treated mice. Our results showed the inhibition of NF-κB activation by curcumin (Figure 3(a), lane 2). Since it has been demonstrated that NF-κB regulates the expression of several markers involved in proliferation (COX-2, cyclin D1), in invasion (MMP-9), and in angiogenesis (VEGF), we performed an immunohistochemical analysis and Western blotting on orthotopic tumor tissue samples from control and treated mice. Immunoistochemical analysis indicates that, in tumors of curcumin-treated group, there are significant reductions in the expression of COX-2 and VEGF, compared with the control group (Figure 3(b)). Western blotting analysis revealed that curcumin, significantly decreased the expression of all of these molecules compared with the control treatment in pancreatic tumor tissues (Figure 3(c)). We finally performed a western blot analysis with IKKα and IKKβ in order to understand how curcumin inhibits NF-κB activation in MIA PaCa-2 cells. Our data indicated that there is a reduced expression of IKKα and IKKβ in tumor of mice treated with curcumin with respect to controls, indicating that curcumin inhibits NF-κB activation through suppression of IKK (Figure 3(c)). Figure 4 shows a schematic diagram which contextualizes the various signalling cascades affected by curcumin in pancreatic cancer cells. Altogether, these data indicate that curcumin inhibits NF-κB activation and downregulates NF-κB-regulated gene products in orthotopic pancreatic tumors.

4. Discussion

Pancreatic cancer is a malignant neoplasm originating from transformed cells arising in tissues forming the pancreas. Gemcitabine is the best chemotherapeutic agent available for treatment of pancreatic cancer. However, it is noted that patients with this cancer treated with gemcitabine, showed several side effects and developed drug resistance over time [3]. In order to bypass these problems, novel strategies involving less toxic agents that can sensitize pancreatic cancer cells to chemotherapy, are necessary. Curcumin, a component of turmeric (*Curcuma longa*), is one such agent which inhibit the cell survival, proliferation, angiogenesis of a wide variety of tumor cells, through the modulation of various cell signalling pathways. It has been demonstrated that curcumin in different pancreatic cancer cell lines inhibited proliferation, potentiated the apoptosis induced by gemcitabine, and inhibited constitutive NF-κB activation. Our aim was to determine whether curcumin, inhibits the growth and angiogenesis of MIA PaCa-2 human pancreatic cancer cells in *in vitro* and *in vivo* conditions. It has been largely demonstrated that curcumin is able to suppress the growth of several tumor cell lines, including drug-resistant lines. It suppresses the expression of cyclin D1, which is involved in progression of cell through cell cycle and is deregulated in many tumors [19]. Curcumin potentiates the apoptosis in tumor cells by activation of caspase enzymes and suppresses the activation of many transcription factors involved in tumorigenesis [20]. Recently it has been demonstrated that curcumin potentiates antitumor activity of gemcitabine in an orthotopic model of pancreatic cancer trough suppression of proliferation, angiogenesis, NF-κB, and inhibition of NF-κB-regulated gene products [17]. According to published data, we demonstrated, by *in vitro* experiments, that curcumin inhibits proliferation and enhances apoptosis in MIA PaCa-2 human pancreatic cancer cells. In addition to these *in vitro* results, we found

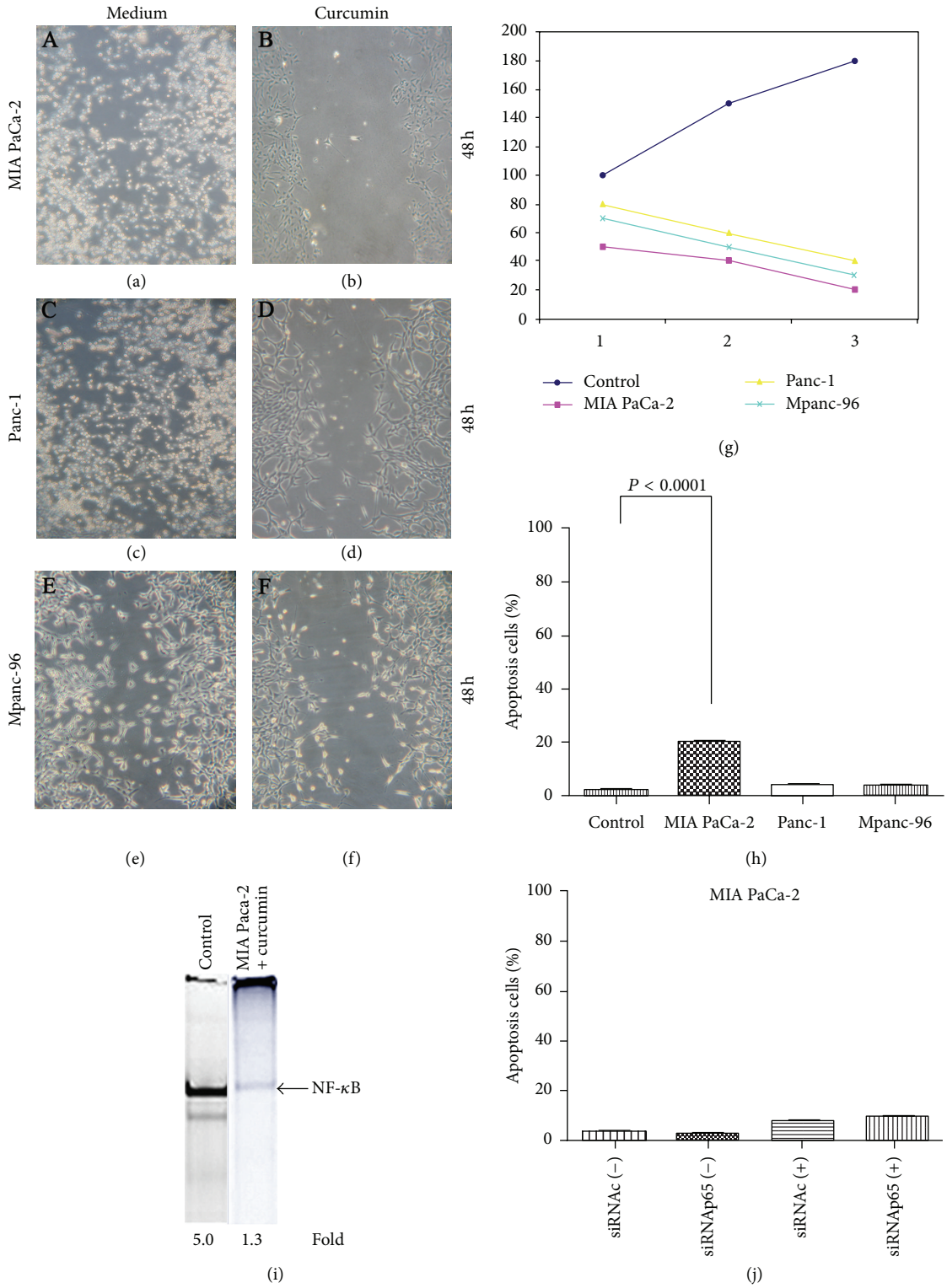

Figure 1: Curcumin inhibits proliferation and enhances apoptosis in MIA PaCa-2 cells. (a)–(f) Wound assay results show suppression of MIA PaCa-2 cell proliferation induced by curcumin at 48 h (b) With respect to controls. The results are the mean of total invaded areas of three distinct sections on the slide per 48 h. ($P = 0.02$, Mann-Whitney U test). (g) MTT assay results show a suppression of proliferation in pancreatic cancer cells treated with curcumin respect to control cells. Data are representative of two independent experiments (P value <0.05). (h) *In vitro* apoptosis assay by flow cytometry indicated that curcumin enhances apoptosis in MIA PaCa-2 cells. (i) EMSA results showes that curcumin suppresses activation of NF-κB in MIA PACA-2 cells. (j) *In vitro* apoptosis assay by flow cytometry indicates that silencing of NF-κB using siRNA κB is not able to potentiate the apoptotic effects of curcumin on MIA PaCa-2 cells.

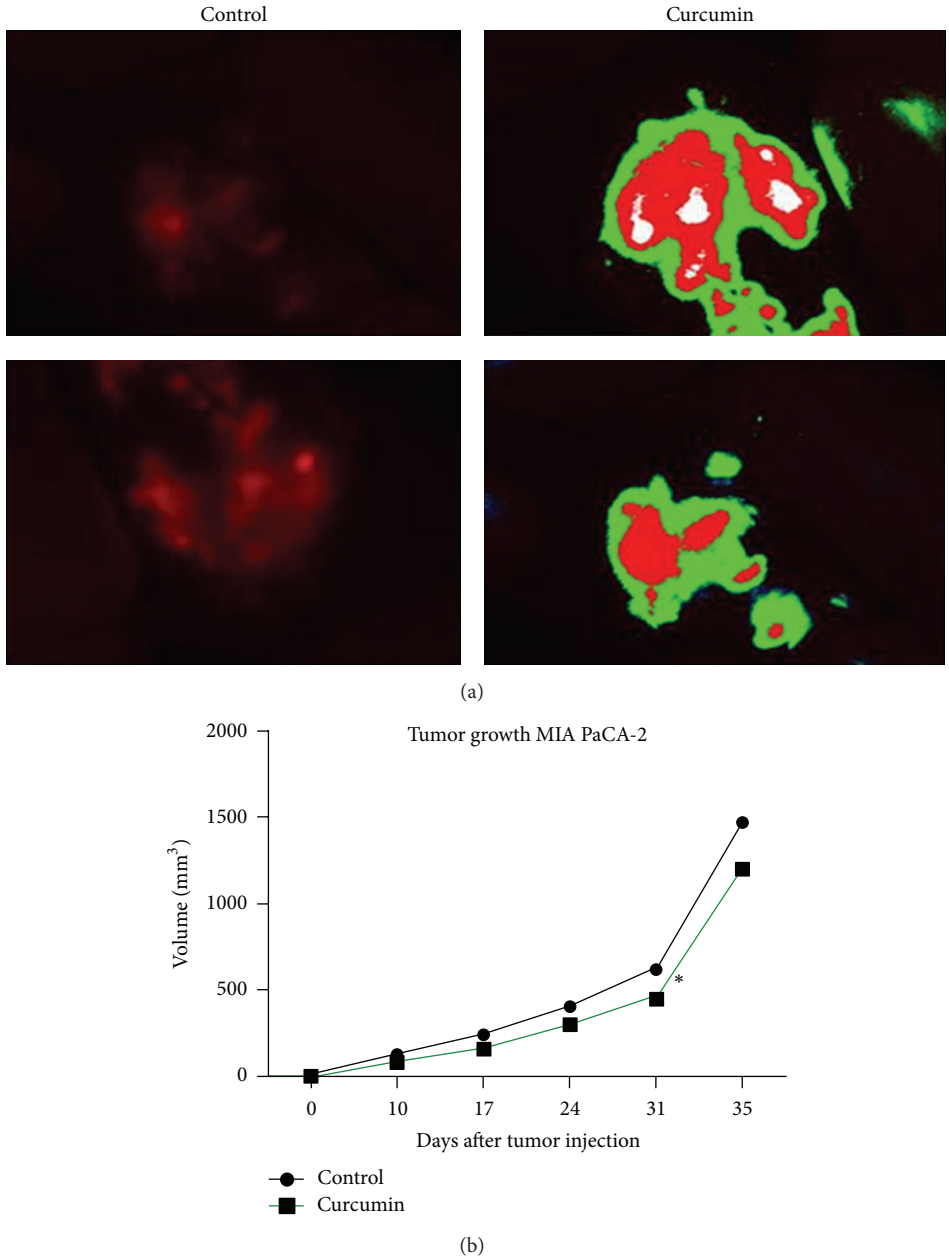

Figure 2: Curcumin inhibits the tumor growth in orthotopic mouse model of pancreatic cancer. (a) MacroFluo images of fluorescent analysis tumor area images control and treated mice. (b) Measurements of fluorescence per second depicting tumor volume at different time points using Macrofluo images, showed that the final tumor volumes on day 35 after the start of treatment is significantly decreased in the curcumin group compared with control ($P = 0.00393$).

that curcumin, administrated in mice with diet, inhibits tumor growth and angiogenesis in an orthotopic model of pancreatic cancer as indicated by a decrease in tumor volume of curcumin-treated mice, compared to controls. By EMSA assay, we demonstrated that curcumin suppressed constitutive NF-κB activation in pancreatic cancer tissues according to previous data [17]. Our data also showed that curcumin inhibited the expression of several important proteins regulated by NF-κB; in particular, we demonstrated that there is a reduced expression of IKKα and IKKβ in tumor of mice treated with curcumin with respect to controls, indicating that curcumin inhibits NF-κB activation through suppression of IKK in MIA PaCa-2 cells. Taken together, our results showed that that curcumin has antitumor effects in an orthotopic mouse model of human pancreatic cancer by inhibiting NF-κB and its downstream targets. Since curcumin is a very well tolerated in human subjects and is assumed by food, our mouse model demonstrated curcumin can be used as an alternative agent to chemotherapy in treatment of human pancreatic cancer. Several *in vitro* and *in vivo* studies are on-going in our laboratory in order to test if a combination of curcumin (administrated by diet of loaded by

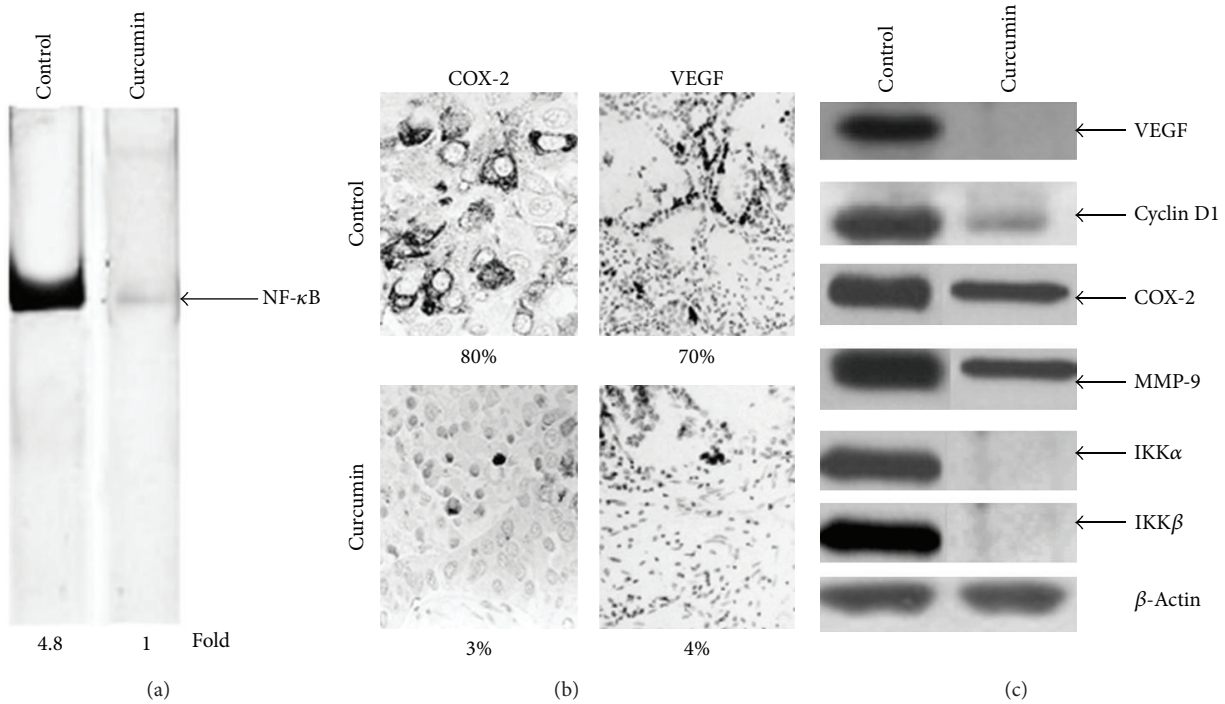

Figure 3: Curcumin inhibits NF-κB activation and downregulates NF-κB-regulated gene products in orthotopic pancreatic tumors. (a) EMSA assay performed on orthotopic tumor tissue samples showed the inhibition of NF-κB by curcumin. (b) Immunohistochemical analysis for nuclear COX-2 and VEGF showed the inhibition of COX-2 and VEGF expression in curcumin-treated group, compared to controls (Figure 3(b), lower panels). Percentages indicate the positive staining for the given biomarker. (c) Western blot showing that curcumin inhibits the expression of NF-κB-dependent gene products VEGF, cyclin D1, MMP-9, COX-2, IKKα, and IKKβ in pancreatic tumor tissues. Samples from three animals in each group were analysed, and representative data are shown. β-Actin was used as loading control.

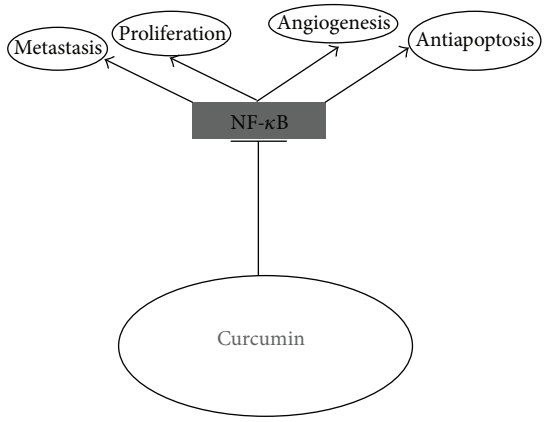

Figure 4: Molecular targets of curcumin in pancreatic cancer cells.

nanoparticles) and gemcitabine can be used as possible and novel therapeutic schedule for pancreatic cancer.

Conflict of Interests

The authors have no other relevant affiliations or financial interest with any organization or entity. No writing assistance was used in the production of paper.

Acknowledgments

The authors thank Massimiliano Spinelli, for kindly help in providing informatics assistance. We also thank Dr. Sonia Petta for her technical support. This work was supported by the 5x mille and current research programs of Institute National of Tumors, IRCCS "Foundation G. Pascale", Naples, Italy.

References

[1] A. Jemal, R. Siegel, E. Ward et al., "Cancer statistics, 2006," *Ca: A Cancer Journal for Clinicians*, vol. 56, no. 2, pp. 106–130, 2006.

[2] J. P. Duffy, G. Eibl, H. A. Reber, and O. J. Hines, "Influence of hypoxia and neoangiogenesis on the growth of pancreatic cancer," *Molecular Cancer*, vol. 2, article no. 12, 2003.

[3] H. A. Burris III, M. J. Moore, J. Andersen et al., "Improvements in survival and clinical benefit with gemcitabine as first-line therapy for patients with advanced pancreas cancer: a randomized trial," *Journal of Clinical Oncology*, vol. 15, no. 6, pp. 2403–2413, 1997.

[4] C. D. Lao, M. T. Ruffin IV, D. Normolle et al., "Dose escalation of a curcuminoid formulation," *BMC Complementary and Alternative Medicine*, vol. 6, article 10, 2006.

[5] B. B. Aggarwal, "Nuclear factor-κB: the enemy within," *Cancer Cell*, vol. 6, no. 3, pp. 203–208, 2004.

[6] A. Arlt, A. Gehrz, S. Müerköster et al., "Role of NF-κB and Akt/PI3K in the resistance of pancreatic carcinoma cell lines

against gemcitabine-induced cell death," *Oncogene*, vol. 22, no. 21, pp. 3243–3251, 2003.

[7] S. Liptay, C. K. Weber, L. Ludwig, M. Wagner, G. Adler, and R. M. Schmid, "Mitogenic and antiapoptotic role of constitutive NF-κB/Rel activity in pancreatic cancer," *International Journal of Cancer*, vol. 105, no. 6, pp. 735–746, 2003.

[8] S. Fujioka, G. M. Sclabas, C. Schmidt et al., "Function of nuclear factor κB in pancreatic cancer metastasis," *Clinical Cancer Research*, vol. 9, no. 1, pp. 346–354, 2003.

[9] F. R. Greten, C. K. Weber, T. F. Greten et al., "Stat3 and NF-κB activation prevents apoptosis in pancreatic carcinogenesis," *Gastroenterology*, vol. 123, no. 6, pp. 2052–2063, 2002.

[10] H. Q. Xiong, J. L. Abbruzzese, E. Lin, L. Wang, L. Zheng, and K. Xie, "NF-κB activity blockade impairs the angiogenic potential of human pancreatic cancer cells," *International Journal of Cancer*, vol. 108, no. 2, pp. 181–188, 2004.

[11] M. Yebra, E. J. Filardo, E. M. Bayna, E. Kawahara, J. C. Becker, and D. A. Cheresh, "Induction of carcinoma cell migration on vitronectin by NF-κB-dependent gene expression," *Molecular Biology of the Cell*, vol. 6, no. 7, pp. 841–850, 1995.

[12] J. L. Arbiser, N. Klauber, R. Rohan et al., "Curcumin is an in vivo inhibitor of angiogenesis," *Molecular Medicine*, vol. 4, no. 6, pp. 376–383, 1998.

[13] D. Thaloor, A. K. Singh, G. S. Sidhu, P. V. Prasad, H. K. Kleinman, and R. K. Maheshwari, "Inhibition of angiogenic differentiation of human umbilical vein endothelial cells by curcumin," *Cell Growth and Differentiation*, vol. 9, no. 4, pp. 305–312, 1998.

[14] R. Mohan, J. Sivak, P. Ashton et al., "Curcuminoids inhibit the angiogenic response stimulated by fibroblast growth factor-2, including expression of matrix metalloproteinase gelatinase B," *Journal of Biological Chemistry*, vol. 275, no. 14, pp. 10405–10412, 2000.

[15] L. Li, B. B. Aggarwal, S. Shishodia, J. Abbruzzese, and R. Kurzrock, "Nuclear factor-κB and IκB are constitutively active in human pancreatic cells, and their down-regulation by curcumin (Diferuloylmethane) is associated with the suppression of proliferation and the induction of apoptosis," *Cancer*, vol. 101, no. 10, pp. 2351–2362, 2004.

[16] L. Li, F. S. Braiteh, and R. Kurzrock, "Liposome-encapsulated curcumin: in vitro and in vivo effects on proliferation, apoptosis, signaling, and angiogenesis," *Cancer*, vol. 104, no. 6, pp. 1322–1331, 2005.

[17] A. B. Kunnumakkara, S. Guha, S. Krishnan, P. Diagaradjane, J. Gelovani, and B. B. Aggarwal, "Curcumin potentiates antitumor activity of gemcitabine in an orthotopic model of pancreatic cancer through suppression of proliferation, angiogenesis, and inhibition of nuclear factor-κB-regulated gene products," *Cancer Research*, vol. 67, no. 8, pp. 3853–3861, 2007.

[18] M. M. Chaturvedi, A. Mukhopadhyay, and B. B. Aggarwal, "Assay for redox-sensitive transcription factor," *Methods in Enzymology*, vol. 319, pp. 585–602, 2000.

[19] A. Mukhopadhyay, S. Banerjee, L. J. Stafford, C. Xia, M. Liu, and B. B. Aggarwal, "Curcumin-induced suppression of cell proliferation correlates with down-regulation of cyclin D1 expression and CDK4-mediated retinoblastoma protein phosphorylation," *Oncogene*, vol. 21, no. 57, pp. 8852–8861, 2002.

[20] B. B. Aggarwal, A. Kumar, and A. C. Bharti, "Anticancer potential of curcumin: preclinical and clinical studies," *Anticancer Research*, vol. 23, no. 1A, pp. 363–398, 2003.

Hindawi Publishing Corporation
BioMed Research International
Volume 2013, Article ID 392434, 10 pages
http://dx.doi.org/10.1155/2013/392434

Research Article

17β-Estradiol Attenuates Poststroke Depression and Increases Neurogenesis in Female Ovariectomized Rats

Yifan Cheng,[1] Qiaoer Su,[1] Bei Shao,[1,2] Jianhua Cheng,[1] Hong Wang,[1] Liuqing Wang,[1] Zhenzhen Lin,[1] Linhui Ruan,[1] Qichuan ZhuGe,[1] and Kunlin Jin[1,3]

[1] *Zhejiang Provincial Key Laboratory of Aging and Neurological Disorder Research, First Affiliated Hospital, Wenzhou Medical University, Wenzhou 35000, China*
[2] *Department of Neurology, First Affiliated Hospital, Wenzhou Medical University, Wenzhou 325000, China*
[3] *Department of Pharmacology and Neuroscience, Institute for Aging and Alzheimer's Disease Research, University of North Texas Health Science Center at Fort Worth, 3500 Camp Bowie Boulevard, Fort Worth, TX 76107, USA*

Correspondence should be addressed to Bei Shao; shao_bei@yahoo.com.cn and Kunlin Jin; kunlin.jin@unthsc.edu

Received 14 July 2013; Revised 11 September 2013; Accepted 18 September 2013

Academic Editor: Monica Fedele

Studies have linked neurogenesis to the beneficial actions of specific antidepressants. However, whether 17β-estradiol (E_2), an antidepressant, can ameliorate poststroke depression (PSD) and whether E_2-mediated improvement of PSD is associated with neurogenesis are largely unexplored. In the present study, we found that depressive-like behaviors were observed at the first week after focal ischemic stroke in female ovariectomized (OVX) rats, as measured by sucrose preference and open field test, suggesting that focal cerebral ischemia could induce PSD. Three weeks after middle cerebral artery occlusion (MCAO), rats were treated with E_2 for consecutive 14 days. We found that E_2-treated rats had significantly improving ischemia-induced depression-like behaviors in the forced-swimming test and sucrose preference test, compared to vehicle-treated group. In addition, we also found that BrdU- and doublecortin (DCX)-positive cells in the dentate gyrus of the hippocampus and the subventricular zone (SVZ) were significantly increased in ischemic rats after E_2 treatment, compared to vehicle-treated group. Our data suggest that focal cerebral ischemia can induce PSD, and E_2 can ameliorate PSD. In addition, newborn neurons in the hippocampus may play an important role in E_2-mediated antidepressant like effect after ischemic stroke.

1. Introduction

Poststroke depression (PSD) is the most frequent and important neuropsychiatric consequence of stroke, which occurs about 33% of all stroke survivors [1, 2]. Compared to stroke patients without depression, patients with PSD were found to be associated with increases in physical disability, cognitive impairment, mortality, and risk of falling, as well as with worsened rehabilitation outcome [3]. Although there have been abundant papers focused on PSD regarding epidemiological features and impact of PSD both on functional outcome, the evidence for effective treatments for PSD remains largely under developed [2].

Estrogens are a group of steroid compounds that functions in the reproductive system, as well as in nonreproductive tissue such as the skeletal and cardiovascular systems. Estrogen treatment to ovariectomized (OXV) female rats significantly reduced the infarct volume [4] and improved sensorimotor dysfunction after focal ischemia [5–7]. In addition to its action on neuroprotection, estrogen is also demonstrated to be beneficial for improving depressive mood in women with reproductive-related mood disorders, including postpartum depression [8] and perimenopausal depressive disorders [9]. Animal studies suggest that estrogen administration can reduce immobility time in the forced swimming test, a paradigm used to test the efficacy of antidepressants and immobility means of depression. Interestingly, recent studies also reveal that estrogen may play a significant role in modulating adult neurogenesis [10, 11]. Administration of 17β-estradiol after ischemic stroke profoundly enhanced neurogenesis by increasing the number of newborn neurons in the subventricular zone (SVZ) and facilitating migration of newborn neurons to ischemic regions [12].

Neurogenesis is a continuous process of the generation of new neurons, which occurs throughout adulthood primarily in the dentate gyrus (DG) of the hippocampus and the SVZ. Current evidence indicate that there is a link between adult hippocampal neurogenesis and depression [13, 14]. Several risk factors for clinical depression, such as chronic stress [15], alcohol abuse [16], infection [17], and neurodegenerative disorders [18], also suppress neurogenesis in the adult hippocampus. Although it is controversial whether impaired neurogenesis is sufficient to cause depressive phenotype, the role of neurogenesis in mediating therapeutic efficacy of antidepressants in depression is recognized [19]. It is well accepted that the behavioral effects of antidepressants is partly mediated by the stimulation of hippocampal neurogenesis. Most antidepressants that confer antidepressant-like behavioral effects induce adult hippocampal neurogenesis by upregulating molecular pathways involving monoamine release [20], activation of serotonin 1A receptor [19], and neurotrophic factor expression [21]. These findings led us to investigate whether estrogen can improve the PSD symptom and its underlying mechanisms.

In this study, we examined the therapeutic potential of 17β-estradiol (E_2) in poststroke depression. We found that E_2 treatment reduced depressive-like behavior and significantly promoted neurogenesis in the DG of the hippocampus and the SVZ after focal cerebral ischemia. Our data suggest that estrogen-induced neurogenesis may play a critical role in antidepressant therapy in PSD.

2. Material and Methods

2.1. Experimental Animals. Female Sprague-Dawley (SD) rats (250–300 g) were housed four per cage under conditions of constant temperature (23 ± 1°C) and humidity (50%) in a 12:12 hr light-dark cycle with ad libitum access to food and water. Four groups of ovariectomized female SD rats were used in our experiment: (1) sham-operated rats treated with vehicle (sham + vehicle); (2) sham-operated rats treated with 17β-estradiol (sham + E_2); (3) left middle cerebral artery occlusion (MCAO) rats treated with vehicle (MCAO + vehicle); (4) MCAO rats treated with 17β-estradiol (MCAO + E_2). All procedures were conducted in accordance with the Guidelines of the Chinese Council on Animal Care and approved beforehand by the Institutional Animal Care and Use Committee of Wenzhou Medical University.

2.2. Ovariectomy and 17β-Estradiol Treatment. Female SD rats were bilaterally OVX under chloral hydrate anesthesia and aseptic conditions. Briefly, a single midline incision was made in the low abdominal area to expose the ovary; oviducts were bilaterally ligated and ovaries removed. After suturing their muscles and skin, the animals were returned to their home cages to recover for one week. The hormone therapy began 3 weeks after surgery. 17β-Estradiol (E_2; sigma; 10 μg) was dissolved in 0.1 mL of soybean oil and administered subcutaneously for consecutive 14 days.

2.3. Behavioral Testing

2.3.1. Sucrose Preference Test (SPT). The SPT was performed as described by Benelli et al. [22]. Briefly, before testing, rats were exposed to a solution of 1% sucrose for 24 hr without any food and get habituated to consuming sucrose solution, during the subsequent 24 hr, one bottle contained the sucrose solution, the other contained tap water. After 23 hr of deprivation of food and water, each rat was provided with two identical bottles, one with 1% sucrose solution and another with tap water. The amount of water and 1% sucrose solution intake was recorded after a 1 hr test. Data were expressed as percentage of 1% sucrose consumption from total consumption.

2.3.2. Open Field Test (OFT). The OFT was performed to evaluate general locomotor and rearing activity of the rats as described by Wang et al. [23]. The apparatus consisted of a dark varnished wooden box (100 × 100 × 40 cm^3) with the floor divided into 25 equal squares. Rats were gently placed on the center square and left to explore the floor for 3 min. The measurement parameters of this test include locomotor activity registered as the number of times the animal crosses squares and the rearing activity, which was registered as the number of times the animal stands upright on its hind legs. Both locomotor activity and rearing activity were manually recorded over a 3 min period by trained observers who were blind to the experimental design.

2.3.3. Forced Swimming Test (FST). The modified FST was performed essentially as described by Detke and his colleague [24]. On the first day, the rats were individually placed in a glass cylinder (45 cm height × 18 cm diameter) containing 30 cm of water at 23–25°C for 15 min. The rats were then removed from the cylinder, dried with tissue paper, and returned to their home cage. On the second day, the rats were placed in the cylinder for 5 min again, and behaviors were scored by observers unaware of experimental groups. Three different behaviors were scored: (1) climbing—presenting active movements with the forepaws in and out of the water, usually directed against the wall of tank; (2) swimming—showing active movements using forepaws and hindpaws within the tank that mimicked swimming motions; (3) Immobility—floating in the water without struggling and doing only those movements necessary to keep the head above the water.

Sucrose preference test and open field test were performed weekly to assess endogenous depressive-like behavior after focal ischemia for three weeks. Likewise, sucrose preference test and forced swimming test were performed weekly to assess behavioral changes after E_2 administration. As the same subjects were used for the behavioral tests, we performed sucrose preference test, and animals were allowed to recover for a day.

2.4. Transient Focal Cerebral Ischemia. Female SD rats were anesthetized with 8% chloral hydrate. The rectal temperature was maintained at 37.0–37.5°C with a heating blanket throughout the operation. Transient focal cerebral ischemia

was induced by occlusion of the left middle cerebral artery (MCA) as described previously [25]. After a midline incision in the neck, the left external carotid artery was ligated and dissected distally, and the left internal carotid was isolated from the vagus nerve. The embolus, made up of nylon suture with rounded tip, was inserted into the left internal carotid through a small incision into the external carotid artery and was gently advanced 20-21 mm past the carotid bifurcation to occlude the left MCA. The embolus was left in place for 90 min and then removed to allow reperfusion. Sham-operated animals were treated identically except that the MCA was not occluded after the neck incisions.

2.5. Measurement of Infarct Volume. The rat brains were removed, and 50 μm coronal sections were cut and stained with cresyl violet. Contralateral and ipsilateral hemisphere areas were measured by a blinded observer using the NIH Image program, and areas were multiplied by the distance between sections to obtain the respective volumes. Volume loss (mm^3) was calculated as a percentage of the volume of the structures in the control hemispheres according the following formula: $(100 \times (V_C - V_L)/V_C\,(V_C$ = control hemisphere volume, V_L = lesioned hemisphere volume)), as described previously [25].

2.6. BrdU Administration. BrdU (50 mg kg^{-1} in saline) was administered intraperitoneally twice daily for 3 consecutive days before rats were euthanized. The rats were perfused transcardially with 4% PFA in PBS, and brains were postfixed overnight and embedded in paraffin.

2.7. Immunohistochemistry. Immunohistochemistry (5-6 animals per group) was performed as described previously [25]. Primary antibodies were mouse monoclonal anti-BrdU (2 μg/mL; Roche) and affinity-purified goat anti-DCX (1 : 200; Santa Cruz Biotechnology); secondary antibodies were biotinylated donkey anti-goat or biotinylated horse anti-mouse IgG (both 1 : 200; Santa Cruz Biotechnology). Sections were examined with a Nikon E800 epifluorescence microscope. Controls included omitting the primary and secondary antibodies.

2.8. Dual-Label Immunohistochemistry. Dual-label immunohistochemistry (5-6 animals per group) was performed as described elsewhere [26]. Primary antibodies were those listed above; secondary antibodies were Alexa Fluor 488-, 594-, or 647-conjugated donkey anti-mouse or anti-goat IgG (1 : 200–500; Molecular Probes). Fluorescence signals were detected using an LSM 510 NLO Confocal Scanning System mounted on an Axiovert 200 inverted microscope (Carl Zeiss) equipped with a two-photon Chameleon laser (Coherent), and images were acquired using LSM 510 Imaging Software (Carl Zeiss). Two- or three-color images were scanned using Ar, 543 HeNe, 633 HeNe, and Chameleon lasers. Selected images were viewed at high magnification. Controls included omitting either the primary or secondary antibody or preabsorbing the primary antibody.

2.9. Cell Counting. BrdU- and DCX-positive cells in SVZ and DG were counted in five to seven 50 μm coronal sections per animal (n = 6 per group), spaced 200 μm apart, by an observer blind to the experimental condition using a Zeiss microscope in bright field mode and a 40X objective. Confocal microscopy was used to count double-labeled cells. In SVZ, DCX- or BrdU-labeled cells were counted along the lateral walls of the lateral ventricles for a total of five to six sections per rat. For the DG, all DCX- or BrdU-labeled cells within two cell diameters from the inner edge of the granule cell layer (GCL) of the DG were included in the analysis. Results were expressed as the average number of BrdU- and DCX-positive cells in SVZ and DG per section.

2.10. Statistical Analysis. All quantitative data were expressed as mean ± SEM. Behavioral data were analyzed by a repeated measurement analysis of variance (ANOVA). The neurogenesis cell count data was analyzed by one way ANOVA followed by LSD *post hoc* test. P values < 0.05 were considered statistically significant.

3. Results

3.1. Depressive-Like Behaviors Were Observed in Poststroke Rats. To determine whether focal cerebral ischemia could induce depressive-like behaviors, behavioral tests were performed in rat after focal ischemia. Compared with the sham-operated group, the ischemic rats displayed a reduction in sucrose preference ($F(1, 38) = 80.688$, $P < 0.001$), which reached statistical significance at the first week and persisted at least over 3 weeks (Figure 1(a)). In addition, the poststroke rats also showed a reduction in locomotor activity ($F(1, 38) = 10.695$, $P < 0.05$) and rearing activity ($F(1, 38) = 12.699$, $P < 0.05$) at first week after MCAO, which continued to decline in the following sessions, compared with sham-operated animals, indicating that the depressive-like behaviors were developed at 1 week in poststroke rats (Figures 1(b) and 1(c)).

3.2. Administration of E_2 Attenuated Poststroke Depressive-Like Behaviors. To investigate whether E_2 has effects on depressive-like behaviors in poststroke rats, we performed sucrose preference test and forced swimming test. In the sucrose preference test, we found that estradiol have increased sucrose preference index in E_2 + MCAO group since the first week administration, compared to vehicle + MCAO group (1 W, $F(3, 36) = 7.715$, 2 W, $F(3, 36) = 7.093$, all $^{*}P < 0.05$). In addition, sucrose preference indexes in both vehicle + sham group (1 W, $P < 0.001$; 2 W, $P < 0.05$) and E_2 + sham group (1 W, 2 W, all $^{**}P < 0.001$) were higher than the vehicle + MCAO group (Figure 2). In the forced swimming test, the longest immobility time was observed in vehicle + MCAO group, compared to the E_2 + MCAO group (1 W, $F(3, 36) = 11.127$, 2 W, $F(3, 36) = 7.177$, all $^{*}P < 0.05$), the vehicle + sham group (1 W, $^{**}P < 0.001$, 2 W, $^{*}P < 0.05$), and the E_2 + sham (1 W, 2 W, all $^{*}P < 0.001$) after E_2 treatment for one week. However, these differences disappear at 2 weeks after E_2 treatment, which was mainly due to an increase in swimming behavior (1 W, $F(3, 36) = 4.741$, 2 W, $F(3, 36) = 3.664$ $^{*}P < 0.05$) (Figure 2).

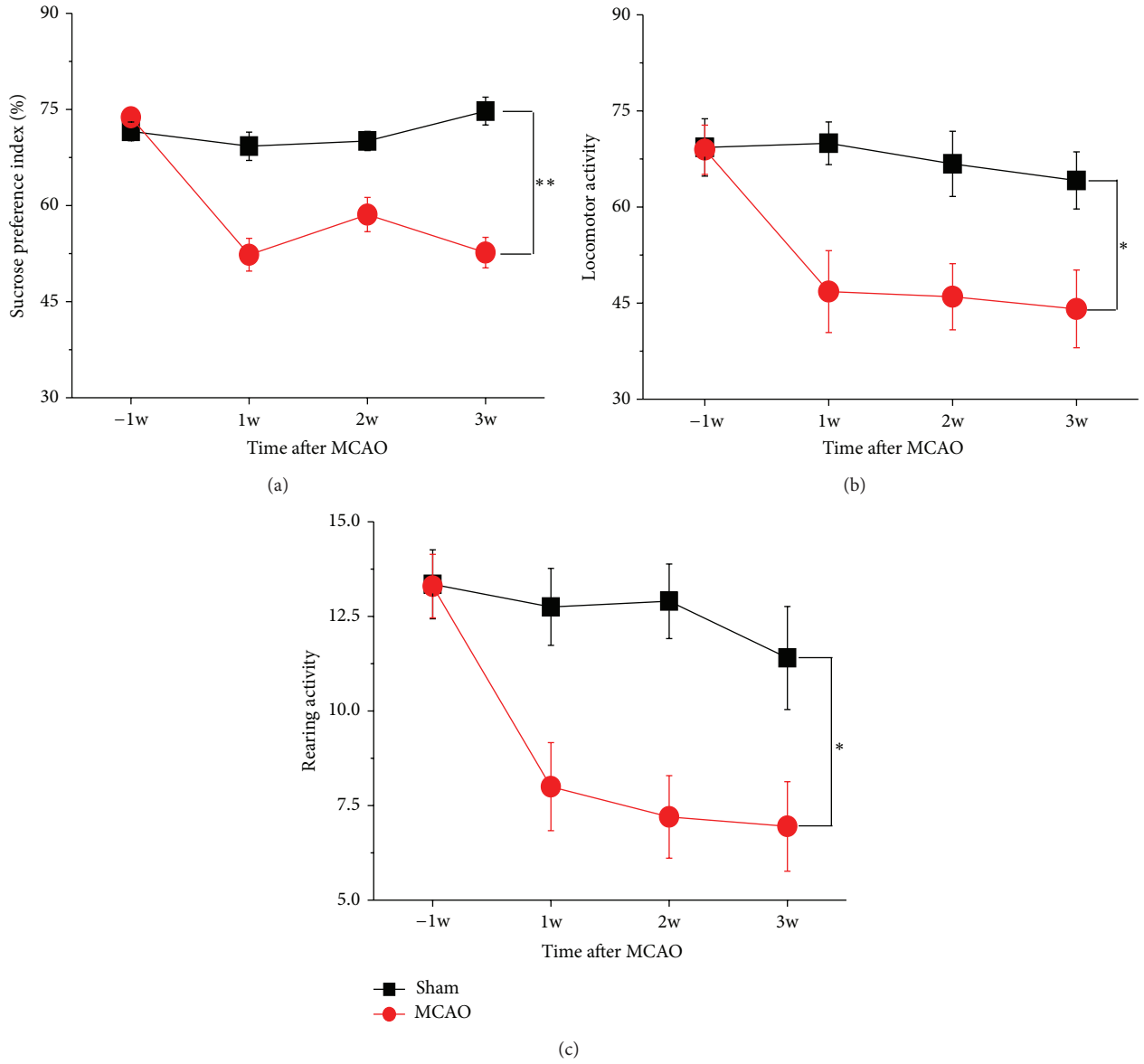

Figure 1: PSD is observed in OVX rats after focal ischemia ($n = 20$). (a) The percentage of sucrose intake was significantly decreased in OVX rats after MCAO, compared to the controls. Locomotor activity (b) and rearing activity (c) were also reduced in the MCAO animals, compared with sham-operated animals. Data were presented as mean ± SEM. $^{*}P < 0.05$, $^{**}P < 0.001$.

3.3. E_2 Treatment Did Not Affect Infarct Volumes after MCAO. To investigate whether the ischemic infarct volumes could be attenuated by E_2 administration, rats were sacrificed 2 weeks after E_2 administration, and the brains were removed and stained with cresyl violet. As shown in Figure 3, there was no significant reduction in infarction volume of E_2-treated ischemic rats, compared with vehicle-treated group.

3.4. E_2 Increased Neurogenesis after Ischemic Stroke. To determine whether E_2 administration could enhance neurogenesis in the SVZ and DG of ischemic brain, rats were treated for 3 days with BrdU, which labels cells that undergo DNA replication in S-phase and therefore reflects the current rate of cell division. As shown in Figure 4, BrdU- and DCX-positive cells in the SVZ and DG were significantly increased in E_2-treated rats compared with control animals ($^{*}P < 0.05$). An increase of BrdU- and DCX-positive cells in the SVZ was also observed in E_2 + MCAO group, compared to vehicle + sham group. Interestingly, BrdU- and DCX-positive cells in the DG were decreased after focal ischemia, compared to the sham-operated rats ($^{*}P < 0.05$), which was reversed after E_2 administration ($^{*}P < 0.05$). Confocal images show that BrdU-positive cells expressed DCX, suggesting that these BrdU-positive cells were proliferative neuronal progenitor cells, and double-labeled cells in E_2-treated group were significantly increased compared to vehicle-treated group after ischemia ($^{**}P < 0.001$) (Figure 5).

4. Discussion

In the present study, we developed a rat model of PSD using left MCAO and found that E_2-treated PSD rats showed

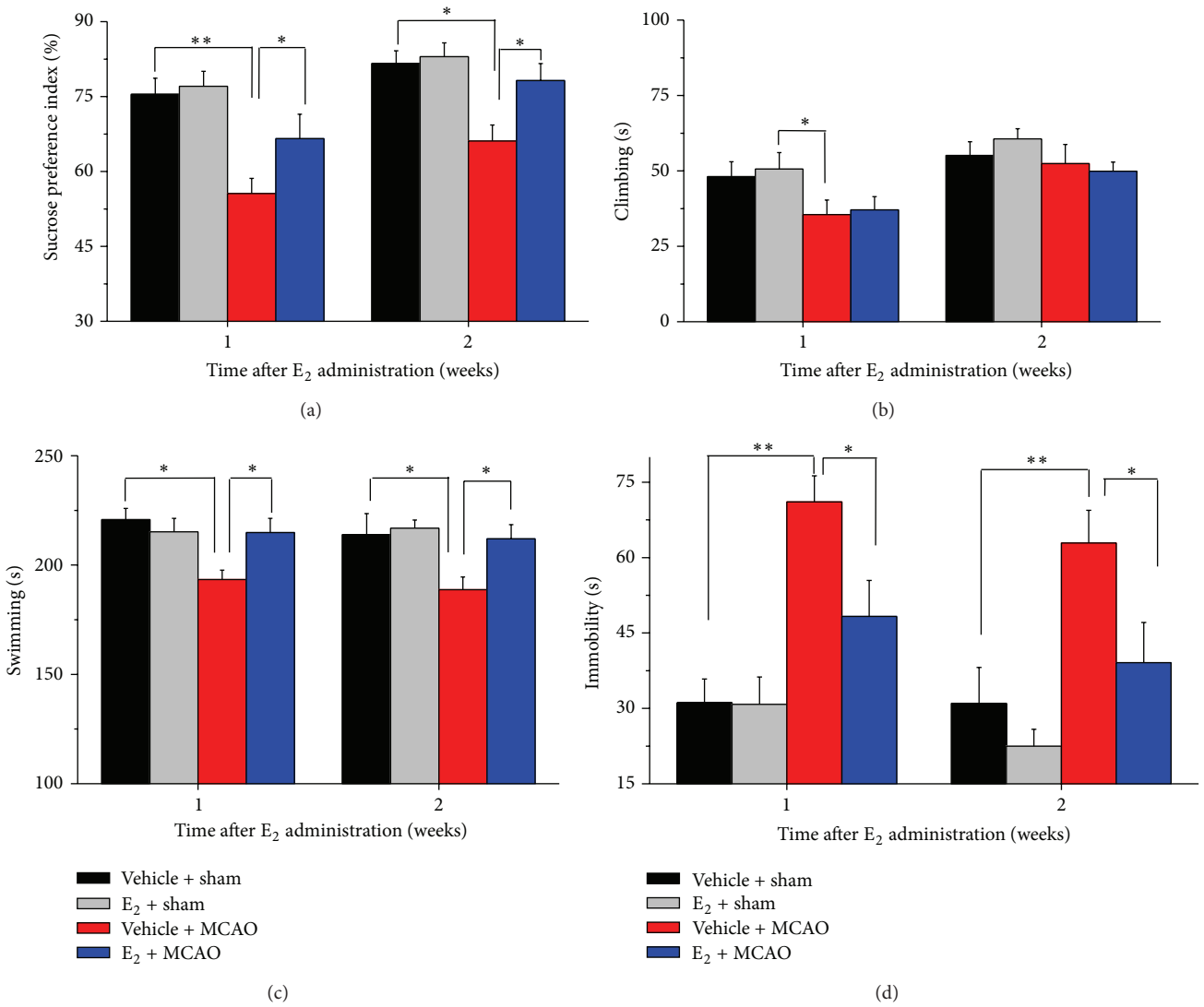

FIGURE 2: E_2 administration after ischemic stroke reverses depressive-like behavior ($n = 10$). (a) E_2-treated animals showed increased percentage of sucrose consumption at 1 week and 2 weeks after E_2 administration, compared to vehicle-treated animals. (b) E_2-treated animals showed no significant differences to vehicle-treated on climbing ability. E_2-treated rats showed increased swimming behavior (c) and decreased immobility (d) after focal ischemia, compared to vehicle-treated ischemic animals. Data were presented as mean ± SEM. $^*P < 0.05$, $^{**}P < 0.001$.

significant improvement in their behavioral performance, as measured by the sucrose preference test and the forced swimming test, suggesting that administration of E_2 induces antidepressant like effect in PSD rats. In addition, our results also showed that the E_2-mediated depressive-like behavioral improvements were concomitant with a significantly increased neurogenesis in the DG after focal ischemia, suggesting that neurogenesis may play a critical role in E_2-mediated antidepressant effect after focal ischemia.

Clinical evidence show that the susceptibility to develop depression in women increases when the estrogen levels fluctuate during their life [27, 28]. Estrogen replacement therapy in these women may reduce depressive symptoms during the premenopausal and postpartum periods [29]. E_2 also induces antidepressant like effects in animal models of depression [30–32]. Furthermore, it has been suggested that E_2 can enhance and shorten the antidepressant-like action of various antidepressants, when combined with these antidepressants [33, 34]. However, whether E_2 produces antidepressant effect in animal model of poststroke depression remains unknown. Here, we applied two behavioral tests, including the sucrose preference test and the force swimming test, which have been developed as straightforward tests for screening the efficacy of antidepressants, to investigate whether E_2 induces antidepressant effect. We observed that E_2 treatment reversed depressive-like behavior in PSD rats, by increasing sucrose consumption in the sucrose preference test, decreasing the immobility time and increasing swimming time in the force swim test, which is consistent with the suggested antidepressant-like effect of E_2.

Previous studies have shown that neurogenesis plays a critical role in the antidepressant-mediated behavioral effects

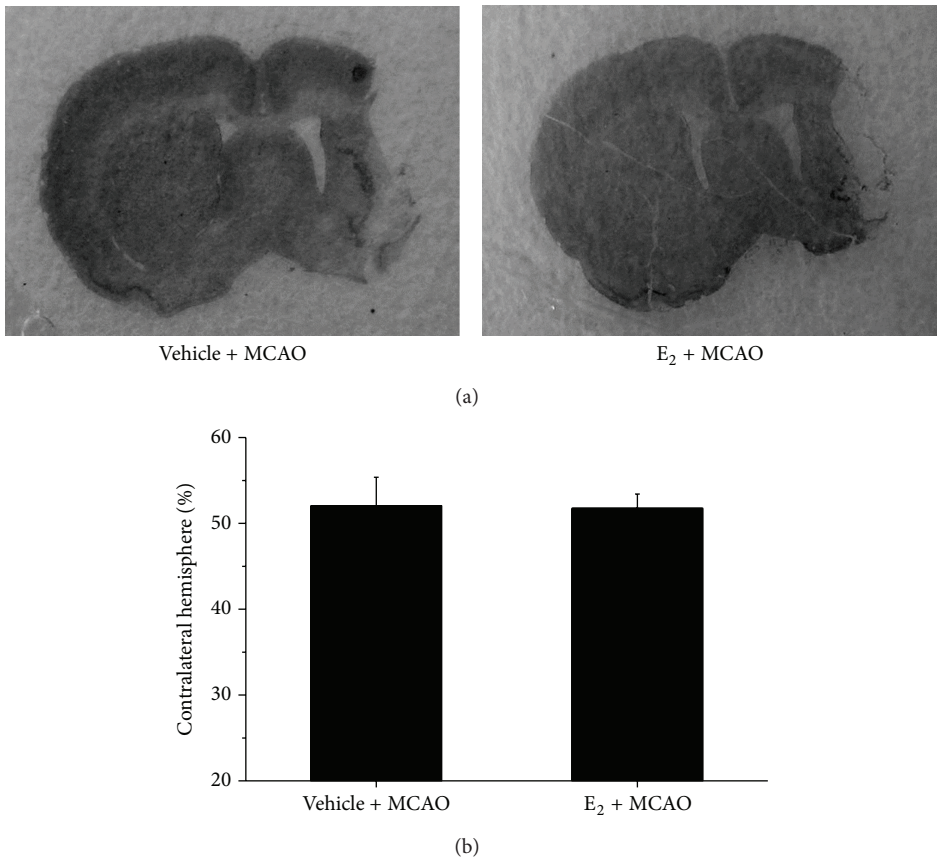

Figure 3: Infarct volume after MCAO with and without E_2 treatment ($n = 5$). (a) Representative images of cresyl violet-stained coronal brain sections from vehicle- and E_2-treated rats. (b) Quantification of infarct volumes in vehicle- and E_2-treated rats. There were no significant differences between vehicle- and E_2-treated groups.

[19]. Therefore, we hypothesized that the antidepressant effects produced by E_2 may also correlate with increased neurogenesis. Our data in this study supported this hypothesis. After 2 weeks of E_2 treatment, the increased neurogenesis in the DG and SVZ was observed by immunohistochemistry analysis. Increased BrdU/DCX-expressing cells in the DG and SVZ suggest that newborn neurons were generated in these regions. Our results are consistent with a recent finding that E_2 treatment enhanced neurogenesis in the SVZ and DG and improved behavioral recovery after ischemic stroke [12]. Suzuki and his coworker also found that pretreatment with physiological doses of E_2 promoted neurogenesis in the SVZ in female rats after ischemic stroke [35]. McClure and her colleagues showed that rats injected with E_2 showed significantly higher levels of activation of new neurons in response to spatial memory compared to controls, suggesting that E_2 plays a role in activation of new neurons in the hippocampus in response to spatial memory in adult female rats [36]. The fate of stem cells in the SVZ remains unclear; some may migrate into the olfactory bulb (OB) via the rostral migratory stream (RMS) and differentiate, where upon they differentiate into local interneurons. As focal ischemia damages cortex and striatum, but does not affect hippocampus neurons, the new born cells migrate into the damaged regions and differentiate into functional neurons for repair. The newborn cells in the SGZ migrate into the granular layer of DG and differentiate into mature neurons. Growing evidence shows that hippocampal adult neurogenesis is important for learning and memory. Most likely, E_2 induced neurogenesis in the SGZ mainly contributes PSD recovery.

Although our data did not provide direct evidence to show that the effects of E_2, on neurogenesis and antidepression, are linked, the role of neurogenesis in E_2-mediated antidepressant effects is further suggested by the following observations: (1) depletion of neurogenesis in the mouse hippocampus by X-irradiation blocks antidepressant effects of two classes of antidepressants [19]; (2) chronic cannabinoid HU210 treatment produces antidepressant effects that depend on hippocampal neurogenesis [37]; (3) the antidepressant effect induced by fluoxetine also requires increased neurogenesis [38]. The underlying mechanism by which E_2 acts to increase neurogenesis remains unclear, but likely involves participation of estrogen receptors and neurotrophic factors. Both estrogen receptor α (ERα) and estrogen receptor β (ERβ) have been detected in the DG of hippocampus in the rat, suggesting that these receptors could influence estradiol's effects on neurogenesis [39, 40] as knocking out either of these receptors blocks the ability of estradiol to increase

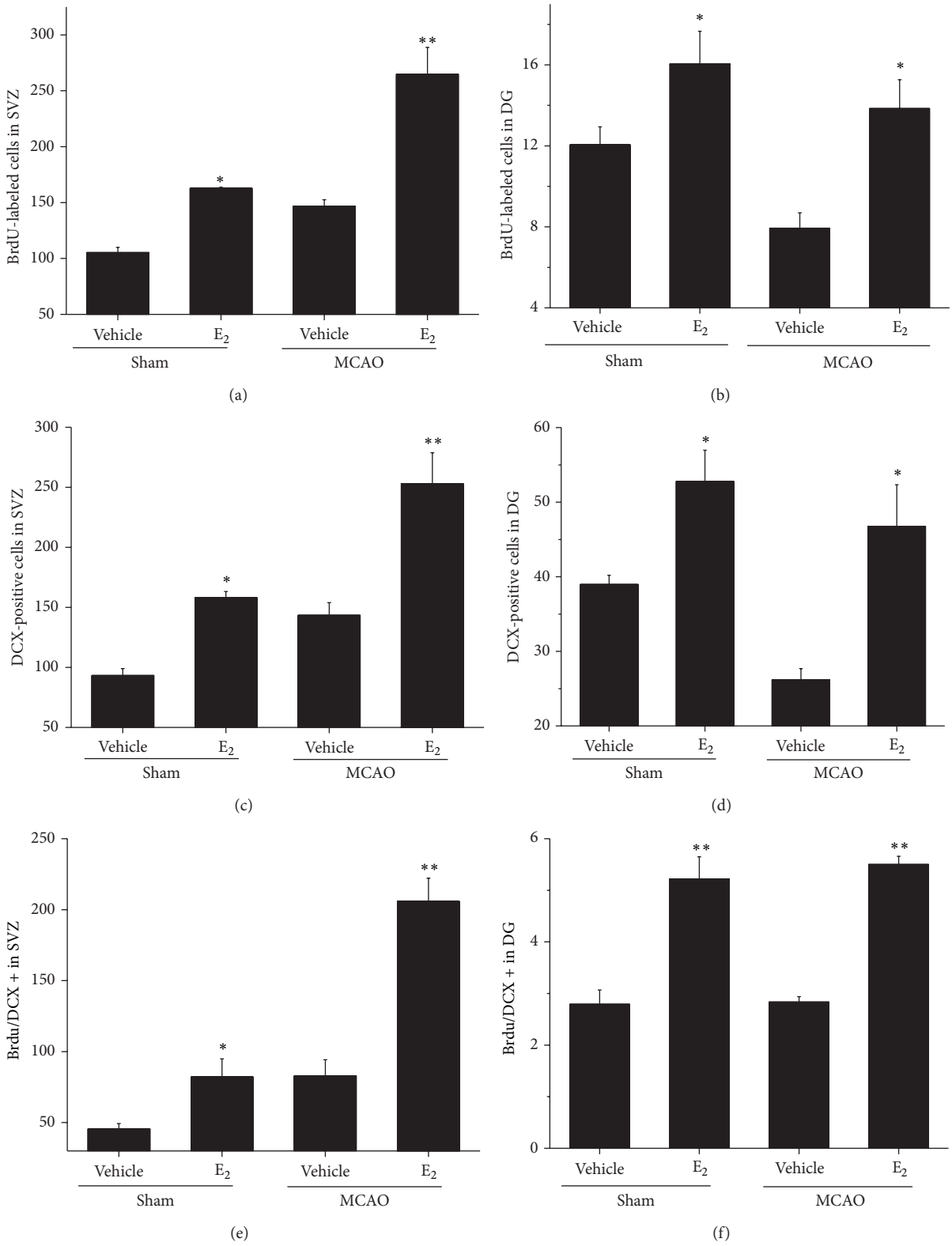

Figure 4: Effect of E_2 on neurogenesis after focal ischemia ($n = 4$). ((a)-(b)) Quantification of BrdU-immunoreactive cells in the SVZ and the DG at the 5 weeks after sham-operated or MCAO rats treated with vehicle or E_2. Data were presented as mean ± SEM. $^{*}P < 0.05$; $^{**}P < 0.01$ compared to vehicle. ((c)-(d)) Quantification of DCX-immunoreactive cells in SVZ and DG at the 5 weeks after sham-operated or MCAO rats treated with vehicle or E_2. Data were presented as mean ± SEM. $^{*}P < 0.05$; $^{**}P < 0.01$ compared to vehicle-treated group. ((e)-(f)) Quantification of BrdU-immunoreactive cells in the SVZ and DG at the 5 weeks after sham-operated or MCAO rats treated with vehicle or E_2. Data were presented as mean ± SEM. $^{*}P < 0.05$; $^{**}P < 0.01$ compared to vehicle.

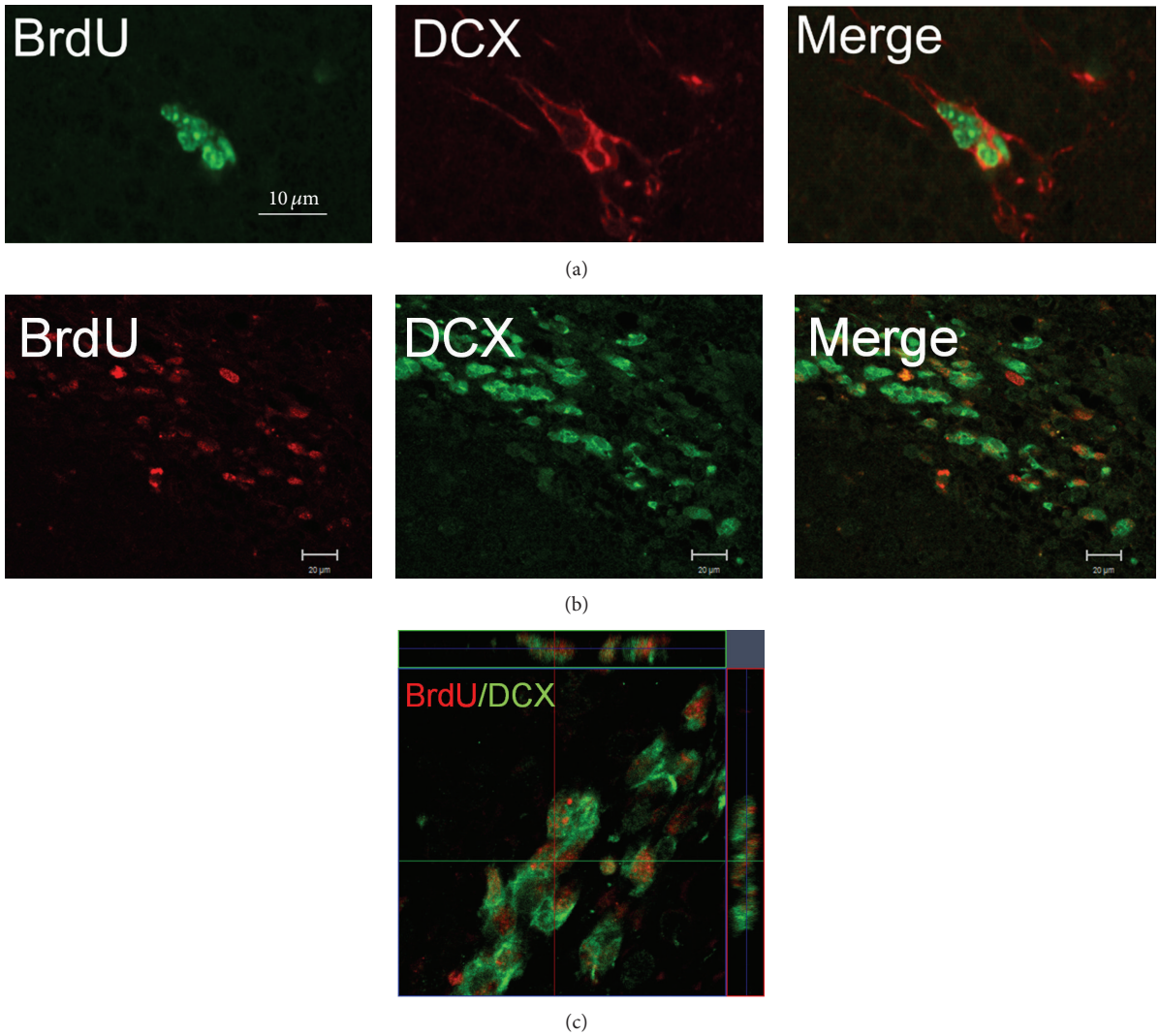

Figure 5: BrdU/DCX-positive cells in the DG and SVZ detected by confocal microscope. (a) Double-immunostaining shows that the BrdU (green) is co-localized with the DCX (red). Representative confocal images of BrdU/DCX-positive cells in the DG of hippocampus. (b) Representative confocal images of BrdU/DCX-positive cells in the SVZ in rat. (c) Confocal image stacks confirmed that BrdU-positive cells (red) expresses DCX (green) in the SVZ.

neurogenesis, indicating that both receptors could directly mediate estradiol's effects on neurogenesis [12, 35]. One of candidate growth factors involved in estradiol's neurogenic effect is brain-derived neurotrophic factor (BDNF), as studies have shown that estrogens regulate the BDNF expression [41, 42] and promote the survival of young granule neurons by stimulating expression of BDNF and its receptor in the hippocampus [43]. Notably, our neurogenesis data shown here are different from other reports [44], the possible reasons include the different animal species, different stroke models, different duration and time to inject BrdU, and whether ovariectomy surgery was performed. Interestingly, a recent study shows that FST increased immobility and corticosterone levels in OVX but not in rats in proestrus. In addition, FST did not affect cell proliferation but significantly decreased the number of BrdU-labeled cells at 2 hr only in OVX-rats, an effect that remained for 3 and 14 days after FST, suggesting that acute stress further decreases the effect of ovariectomy on immobility behavior and hippocampal cell survival in rats [45].

Taken together, all these lines of evidence support the notion that increased neurogenesis in DG and SVZ appears to underlie the mechanism of antidepressant effects produced by E_2 treatment in poststroke depression rats. However, whether increased neurogenesis is sufficient to produce the entire antidepressant effects of E_2 remains to be addressed.

Conflict of Interests

The authors declare no conflict of interests.

Acknowledgments

This work was partially supported by the Projects of International Cooperation and Exchanges of Wenzhou Science and Technology Bureau (no. H20090067), by the Foundation of

Zhejiang Provincial Top Key Discipline of Surgery, and by the National Natural Science Foundation of China (81171088 and 81371395).

References

[1] M. L. Hackett, C. Yapa, V. Parag, and C. S. Anderson, "Frequency of depression after stroke: a systematic review of observational studies," *Stroke*, vol. 36, no. 6, pp. 1330–1340, 2005.

[2] I. Loubinoux, G. Kronenberg, M. Endres et al., "Post-stroke depression: mechanisms, translation and therapy," *Journal of Cellular and Molecular Medicine*, vol. 16, pp. 1961–1969, 2012.

[3] R. G. Robinson, "Poststroke depression: prevalence, diagnosis, treatment, and disease progression," *Biological Psychiatry*, vol. 54, no. 3, pp. 376–387, 2003.

[4] A. Selvamani and F. Sohrabji, "Reproductive age modulates the impact of focal ischemia on the forebrain as well as the effects of estrogen treatment in female rats," *Neurobiology of Aging*, vol. 31, no. 9, pp. 1618–1628, 2010.

[5] X. Li, K. K. Blizzard, Z. Zeng, A. C. DeVries, P. D. Hurn, and L. D. McCullough, "Chronic behavioral testing after focal ischemia in the mouse: functional recovery and the effects of gender," *Experimental Neurology*, vol. 187, no. 1, pp. 94–104, 2004.

[6] L. M. Garcia-Segura, I. Azcoitia, and L. L. DonCarlos, "Neuroprotection by estradiol," *Progress in Neurobiology*, vol. 63, no. 1, pp. 29–60, 2001.

[7] S. Suzuki, C. M. Brown, and P. M. Wise, "Neuroprotective effects of estrogens following ischemic stroke," *Frontiers in Neuroendocrinology*, vol. 30, no. 2, pp. 201–211, 2009.

[8] E. L. Moses-Kolko, S. L. Berga, B. Kalro, D. K. Y. Sit, and K. L. Wisner, "Transdermal estradiol for postpartum depression: a promising treatment option," *Clinical Obstetrics and Gynecology*, vol. 52, no. 3, pp. 516–529, 2009.

[9] C. De Novaes Soares, O. P. Almeida, H. Joffe, and L. S. Cohen, "Efficacy of estradiol for the treatment of depressive disorders in perimenopausal women: a double-blind, randomized, placebo-controlled trial," *Archives of General Psychiatry*, vol. 58, no. 6, pp. 529–534, 2001.

[10] J. M. Barker and L. A. M. Galea, "Repeated estradiol administration alters different aspects of neurogenesis and cell death in the hippocampus of female, but not male, rats," *Neuroscience*, vol. 152, no. 4, pp. 888–902, 2008.

[11] C. Westenbroek, J. A. Den Boer, M. Veenhuis, and G. J. Ter Horst, "Chronic stress and social housing differentially affect neurogenesis in male and female rats," *Brain Research Bulletin*, vol. 64, no. 4, pp. 303–308, 2004.

[12] J. Li, M. Siegel, M. Yuan et al., "Estrogen enhances neurogenesis and behavioral recovery after stroke," *Journal of Cerebral Blood Flow & Metabolism*, vol. 31, no. 2, pp. 413–425, 2011.

[13] R. M. Thomas, G. Hotsenpiller, and D. A. Peterson, "Acute psychosocial stress reduces cell survival in adult hippocampal neurogenesis without altering proliferation," *The Journal of Neuroscience*, vol. 27, no. 11, pp. 2734–2743, 2007.

[14] A. Dranovsky and R. Hen, "Hippocampal neurogenesis: regulation by stress and antidepressants," *Biological Psychiatry*, vol. 59, no. 12, pp. 1136–1143, 2006.

[15] K. Pham, J. Nacher, P. R. Hof, and B. S. McEwen, "Repeated restraint stress suppresses neurogenesis and induces biphasic PSA-NCAM expression in the adult rat dentate gyrus," *European Journal of Neuroscience*, vol. 17, no. 4, pp. 879–886, 2003.

[16] K. Nixon and F. T. Crews, "Temporally specific burst in cell proliferation increases hippocampal neurogenesis in protracted abstinence from alcohol," *The Journal of Neuroscience*, vol. 24, no. 43, pp. 9714–9722, 2004.

[17] Z. Guan and J. Fang, "Peripheral immune activation by lipopolysaccharide decreases neurotrophins in the cortex and hippocampus in rats," *Brain, Behavior, and Immunity*, vol. 20, no. 1, pp. 64–71, 2006.

[18] C. Zhang, E. McNeil, L. Dressler, and R. Siman, "Long-lasting impairment in hippocampal neurogenesis associated with amyloid deposition in a knock-in mouse model of familial Alzheimer's disease," *Experimental Neurology*, vol. 204, no. 1, pp. 77–87, 2007.

[19] L. Santarelli, M. Saxe, C. Gross et al., "Requirement of hippocampal neurogenesis for the behavioral effects of antidepressants," *Science*, vol. 301, no. 5634, pp. 805–809, 2003.

[20] J. M. Brezun and A. Daszuta, "Serotonin may stimulate granule cell proliferation in the adult hippocampus, as observed in rats grafted with foetal raphe neurons," *European Journal of Neuroscience*, vol. 12, no. 1, pp. 391–396, 2000.

[21] M. Sairanen, G. Lucas, P. Ernfors, M. Castrén, and E. Castrén, "Brain-derived neurotrophic factor and antidepressant drugs have different but coordinated effects on neuronal turnover, proliferation, and survival in the adult dentate gyrus," *The Journal of Neuroscience*, vol. 25, no. 5, pp. 1089–1094, 2005.

[22] A. Benelli, M. Filaferro, A. Bertolini, and S. Genedani, "Influence of S-adenosyl-L-methionine on chronic mild stress-induced anhedonia in castrated rats," *British Journal of Pharmacology*, vol. 127, no. 3, pp. 645–654, 1999.

[23] S. H. Wang, Z. J. Zhang, Y. J. Guo, H. Zhou, G. J. Teng, and B. A. Chen, "Anhedonia and activity deficits in rats: impact of post-stroke depression," *Journal of Psychopharmacology*, vol. 23, no. 3, pp. 295–304, 2009.

[24] M. J. Detke, M. Rickels, and I. Lucki, "Active behaviors in the rat forced swimming test differentially produced by serotonergic and noradrenergic antidepressants," *Psychopharmacology*, vol. 121, no. 1, pp. 66–72, 1995.

[25] R. A. Swanson, M. T. Morton, G. Tsao-Wu, R. A. Savalos, C. Davidson, and F. R. Sharp, "A semiautomated method for measuring brain infarct volume," *Journal of Cerebral Blood Flow & Metabolism*, vol. 10, no. 2, pp. 290–293, 1990.

[26] K. Jin, M. Minami, J. Q. Lan et al., "Neurogenesis in dentate subgranular zone and rostral subventricular zone after focal cerebral ischemia in the rat," *Proceedings of the National Academy of Sciences of the United States of America*, vol. 98, no. 8, pp. 4710–4715, 2001.

[27] V. Hendrick, L. L. Altshuler, and R. Suri, "Hormonal changes in the postpartum and implications for postpartum depression," *Psychosomatics*, vol. 39, no. 2, pp. 93–101, 1998.

[28] L. S. Cohen, C. N. Soares, A. F. Vitonis, M. W. Otto, and B. L. Harlow, "Risk for new onset of depression during the menopausal transition: the harvard study of moods and cycles," *Archives of General Psychiatry*, vol. 63, no. 4, pp. 385–390, 2006.

[29] L. S. Cohen, C. N. Soares, J. R. Poitras, J. Prouty, A. B. Alexander, and J. L. Shifren, "Short-term use of estradiol for depression in perimenopausal and postmenopausal women: a preliminary report," *American Journal of Psychiatry*, vol. 160, no. 8, pp. 1519–1522, 2003.

[30] E. Estrada-Camarena, A. Fernández-Guasti, and C. López-Rubalcava, "Antidepressant-like effect of different estrogenic compounds in the forced swimming test," *Neuropsychopharmacology*, vol. 28, no. 5, pp. 830–838, 2003.

[31] A. A. Walf, J. J. Paris, and C. A. Frye, "Chronic estradiol replacement to aged female rats reduces anxiety-like and depression-like behavior and enhances cognitive performance," *Psychoneuroendocrinology*, vol. 34, no. 6, pp. 909–916, 2009.

[32] M. Romano-Torres and A. Fernández-Guasti, "Estradiol valerate elicits antidepressant-like effects in middle-aged female rats under chronic mild stress," *Behavioural Pharmacology*, vol. 21, no. 2, pp. 104–111, 2010.

[33] E. Estrada-Camarena, A. Fernández-Guasti, and C. López-Rubalcava, "Interaction between estrogens and antidepressants in the forced swimming test in rats," *Psychopharmacology*, vol. 173, no. 1, pp. 139–145, 2004.

[34] E. Estrada-Camarena, N. M. Vega Rivera, C. Berlanga, and A. Fernández-Guasti, "Reduction in the latency of action of antidepressants by 17 β-estradiol in the forced swimming test," *Psychopharmacology*, vol. 201, no. 3, pp. 351–360, 2008.

[35] S. Suzuki, L. M. Gerhold, M. Böttner et al., "Estradiol enhances neurogenesis following ischemic stroke through estrogen receptors α and β," *Journal of Comparative Neurology*, vol. 500, no. 6, pp. 1064–1075, 2007.

[36] R. E. McClure, C. K. Barha, and L. A. Galea, "17beta-Estradiol, but not estrone, increases the survival and activation of new neurons in the hippocampus in response to spatial memory in adult female rats," *Hormones and Behavior*, vol. 63, pp. 144–157, 2013.

[37] W. Jiang, Y. Zhang, L. Xiao et al., "Cannabinoids promote embryonic and adult hippocampus neurogenesis and produce anxiolytic- and antidepressant-like effects," *The Journal of Clinical Investigation*, vol. 115, no. 11, pp. 3104–3116, 2005.

[38] R. D. Airan, L. A. Meltzer, M. Roy, Y. Gong, H. Chen, and K. Deisseroth, "High-speed imaging reveals neurophysiological links to behavior in an animal model of depression," *Science*, vol. 317, no. 5839, pp. 819–823, 2007.

[39] N. Weiland, C. Orikasa, S. Hayashi, and B. McEwen, "Distribution and hormone regulation of estrogen receptor immunoreactive cells in the hippocampus of male and female rats," *Journal of Comparative Neurology*, vol. 388, pp. 603–612, 1997.

[40] S. P. Herrick, E. M. Waters, C. T. Drake, B. S. McEwen, and T. A. Milner, "Extranuclear estrogen receptor beta immunoreactivity is on doublecortin-containing cells in the adult and neonatal rat dentate gyrus," *Brain Research*, vol. 1121, no. 1, pp. 46–58, 2006.

[41] F. Sohrabji, R. C. G. Miranda, and C. D. Toran-Allerand, "Identification of a putative estrogen response element in the gene encoding brain-derived neurotrophic factor," *Proceedings of the National Academy of Sciences of the United States of America*, vol. 92, no. 24, pp. 11110–11114, 1995.

[42] M. Singh, E. M. Meyer, and J. W. Simpkins, "The effect of ovariectomy and estradiol replacement on brain-derived neurotrophic factor messenger ribonucleic acid expression in cortical and hippocampal brain regions of female Sprague-Dawley rats," *Endocrinology*, vol. 136, no. 5, pp. 2320–2324, 1995.

[43] B. K. Ormerod, T. T.-Y. Lee, and L. A. M. Galea, "Estradiol enhances neurogenesis in the dentate gyri of adult male meadow voles by increasing the survival of young granule neurons," *Neuroscience*, vol. 128, no. 3, pp. 645–654, 2004.

[44] K. Türeyen, R. Vemuganti, K. A. Sailor, K. K. Bowen, and R. J. Dempsey, "Transient focal cerebral ischemia-induced neurogenesis in the dentate gyrus of the adult mouse," *Journal of Neurosurgery*, vol. 101, no. 5, pp. 799–805, 2004.

[45] N. M. Vega-Rivera, A. Fernandez-Guasti, G. Ramirez-Rodriguez, and E. Estrada-Camarena, "Acute stress further decreases the effect of ovariectomy on immobility behavior and hippocampal cell survival in rats," *Psychoneuroendocrinology*, vol. 38, pp. 1407–1417, 2013.

Hindawi Publishing Corporation
BioMed Research International
Volume 2013, Article ID 180453, 12 pages
http://dx.doi.org/10.1155/2013/180453

Research Article

A Posteriori Comparison of Natural and Surgical Destabilization Models of Canine Osteoarthritis

Maxim Moreau,[1,2] Jean-Pierre Pelletier,[1] Bertrand Lussier,[1,3] Marc-André d'Anjou,[4] Laurent Blond,[5] Johanne-Martel Pelletier,[1] Jérôme R. E. del Castillo,[1,2] and Eric Troncy[1,2]

[1] *Osteoarthritis Research Unit, Université de Montréal Hospital Centre, Notre-Dame Hospital, 1560 Sherbrooke St. East, Montreal, QC, Canada H2L 4M1*
[2] *GREPAQ, Department of Veterinary Biomedical Sciences, Faculty of Veterinary Medicine (FVM), Université de Montréal, P.O. Box 5000, Saint-Hyacinthe, QC, Canada J2S 7C6*
[3] *Department of Clinical Sciences, FVM, Université de Montréal, P.O. Box 5000, Saint-Hyacinthe, QC, Canada J2S 7C6*
[4] *Hôpital Vétérinaire Rive-Sud, 7415 Taschereau, Brossard, QC, Canada J4Y 1A2*
[5] *Clinique Vétérinaire Languedocia, 395 Ruc Maurice Béjart, 34080 Montpellier, France*

Correspondence should be addressed to Eric Troncy; eric.troncy@umontreal.ca

Received 5 July 2013; Accepted 10 September 2013

Academic Editor: Oreste Gualillo

For many years *Canis familiaris*, the domestic dog, has drawn particular interest as a model of osteoarthritis (OA). Here, we optimized the dog model of experimental OA induced by cranial cruciate ligament sectioning. The usefulness of noninvasive complementary outcome measures, such as gait analysis for the limb function and magnetic resonance imaging for structural changes, was demonstrated in this model. Relationships were established between the functional impairment and the severity of structural changes including the measurement of cartilage thinning. In the dog model of naturally occurring OA, excellent test-retest reliability was denoted for the measurement of the limb function. A criterion to identify clinically meaningful responders to therapy was determined for privately owned dogs undergoing clinical trials. In addition, the recording of accelerometer-based duration of locomotor activity showed strong and complementary agreement with the biomechanical limb function. The translation potential of these models to the human OA condition is underlined. A preclinical testing protocol which combines the dog model of experimental OA induced by cranial cruciate ligament transection and the Dog model of naturally occurring OA offers the opportunity to further investigate the structural and functional benefits of disease-modifying strategies. Ultimately, a better prediction of outcomes for human clinical trials would be brought.

1. Introduction

Biomedical research is the broad area of science that investigates the biological processes and the causes of diseases mainly through experimentation and testing. Enticing this vision, the use of animal models is required to advance medical knowledge and overall health benefits. In the field of rheumatic diseases such as osteoarthritis (OA), animal models contribute to the understanding of the basic biology of OA and help to develop potent therapeutic approaches for the benefits of human medicine [1]. Unfortunately, a consensus regarding the ideal animal model for studying OA has not been established [2–4]. Actually, there is a need to optimize current models of OA and to propose avenues to enhance preclinical drug development.

The canine stifle is similar to a human's knee, sharing anatomical components and histological aspects [5]. To give a deep insight in the OA mechanisms, the dogs have been subjected to several approaches over the years to induce the structural changes of OA, including cartilage scarification (or groove model) [6], transarticular impact [7], tibial osteotomy [8], and meniscal lesions [9]. Another well-described dog model of OA is the cranial (or anterior) cruciate ligament (CCL) transection. Surgical CCL transection (CCLT) alters the amount and distribution of biomechanical forces. Over days to months, the joint features structural changes that

mimic OA, including synovitis, osteophyte growth, cartilage depletion, and bone marrow lesions (BMLs) development [10].

The conventional scientific outputs (i.e., joint structural changes) of the experimental dog model of OA induced by CCLT have been recently coupled to peak vertical force (PVF) measurement using kinetic gait analysis to document concomitant potential benefits on the pain-related functional impairment [11–13]. The first aim of this study was to optimize the experimental CCLT-induced dog OA model by further exploring the translational relationship between the level of structural changes and the limb disability.

Developmental arthropathies and joint trauma predispose dog to structural changes of OA, which like in human beings lead to crippling pain and disability [14–16]. The potential of pharmaceutical as well as complementary and alternative medicines has been tested in different randomized controlled trials (RCTs) in naturally occurring OA dogs using PVF as an outcome measure of pain-related functional impairment [17–20]. Naturally occurring models of OA have been proposed even to accelerate the development of human therapeutics [10]. As a second aim, this study would characterize different outcome measures in a manner to optimize the use of naturally occurring OA dogs in research and to improve the quality of RCT in this translational natural model.

2. Materials and Methods

2.1. Dog Model of Experimental OA

2.1.1. Specific Research Objectives. The evolution of the PVF measurement and its relationship with the progression of structural changes evaluated on magnetic resonance imaging (MRI) scans (i.e., cartilage volume loss, focal changes of the articular cartilage, BMLs, osteophytes, joint effusion size, and meniscal lesions) was documented over a period of 26 weeks in CCL-deficient dogs. In addition, the relationship between PVF recording and the macroscopic measurements of cartilage thinning performed at eight weeks following CCLT was documented cross-sectionally. Such relationship served to determine the level of *in vivo* structural changes to be predicted based on a given PVF measurement. To this end, data were selected from previous studies involving PVF measurement and structural changes on MRI (internal data, 2005) [21–23] and macroscopic measurement of cartilage thinning (internal data 2005, 2007) [11, 12] (Figure 1(a)).

All experiments were approved by the Institutional Animal Care and Use Committee in accordance with the guidelines of the Canadian Council on Animal Care. All dogs were acclimated, housed, and then subjected to surgical CCLT of the right knee under preemptive (transdermal fentanyl 50 or 75 μg/h; Janssen Ortho, Markham, ON, Canada) and multimodal (intra-articular block combined with opioid administration) analgesia as previously described [11]. Food was given once daily and removed overnight. Body weight was monitored weekly and was kept constant throughout the study duration. Throughout the study, all dogs were actively exercised in exterior runs (1.35 m × 9.15 m) for a 2-hour period, 5 days a week, under the supervision of an animal care technician.

2.1.2. Peak Vertical Force Measurement. Recognized as a reference method of functional outcome in dog [24–26], the PVF measurement was done at the trot (1.9–2.2 meter/second) using a floor mat-based plantar force measurement system (Walkway with four Matscan sensors 3150; Tekscan Inc., Boston, MA, USA), as previously described [11]. Data were acquired at four successive time points (Figure 1(a)). For the CCL-deficient hind limb, the first stride PVF was acquired. Data from the first five valid trials were averaged and expressed as a percentage of body weight (% BW) and used to describe the change over time in PVF measurement.

2.1.3. Magnetic Resonance Imaging. Structural changes were evaluated at four successive time points (Figure 1(a)) using MRI scans (Echospeed LX; General Electric Healthcare, Waukesha, WI, USA) and settings as previously described [21]. Previous publications detailed the quantification of cartilage volume (mm^3) [21] and the scoring system used for focal changes of the articular cartilage (0–4, maximum score of 44) [21], BMLs (0–3, maximum score of 27) [23], osteophytes (0–3, maximum score of 45) [22], joint effusion size (0–3) [22], and meniscal lesions (0–3, maximum score of 6) [27]. Cartilage volume and structural changes were evaluated using the following sequences: (1) three-dimensional spoiled gradient recalled sequence (SPGR) with fat suppression, (2) T1-weighted three-dimensional fast gradient recalled echo (T1w-GRE), and (3) T2-weighted fast spin echo sequence with fat saturation (T2w-FS). Bone marrow lesions were scored independently in T1w-GRE and T2w-FS sequences as ill-defined areas of hypointensity or hyperintensity, respectively. Evaluation of cartilage volume and structural changes was for the entire (global) joint, except otherwise stated.

2.1.4. Macroscopic Measurement of Cartilage Thinning. Cartilage thinning was quantified at eight weeks following CCLT (Figure 1(a)) using a dissecting microscope (Stereozoom; Bausch & Lomb, Rochester, NY, USA) as previously described [28]. Macroscopic measurement of cartilage thinning (mm^2) was for the medial and lateral femoral condyles and medial and lateral tibial plateaus.

2.2. Dog Model of Naturally Occurring OA

2.2.1. Specific Research Objectives. The repeatability, standard error of measurement (SEM), and minimal detectable change (MDC) of PVF measured in privately owned dogs affected by naturally occurring OA were defined over a four-week period. Moreover, the PVF measurement was tested for its relationship with accelerometer-based duration of daily locomotor activity. The goal of testing such relationship was to determine the level of PVF measurement exceeding the MDC to be predicted based on a change in daily locomotor

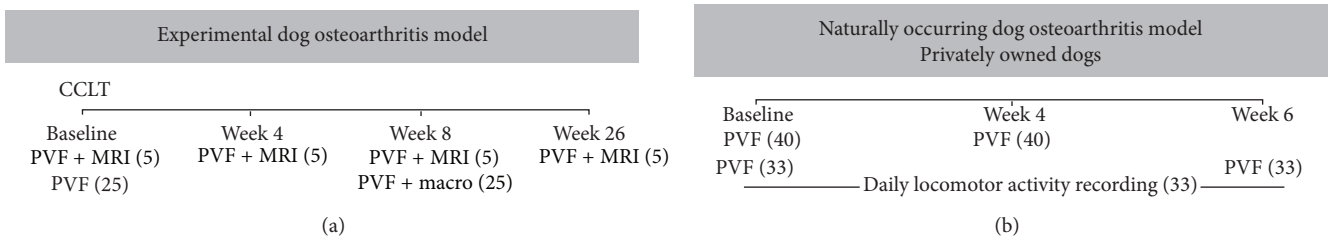

Figure 1: Schematic view of the data reported in (a) the dog model of experimental osteoarthritis and (b) the dog model of naturally occurring osteoarthritis. PVF (peak vertical force), MRI (magnetic resonance imaging), macro (macroscopic structural measurement of cartilage thinning), CCLT (cranial cruciate ligament transection). Numbers of dogs are specified in parenthesis.

activity, which would represent a practical outcome of animal welfare determinant at home [29]. To this end, data were selected from previous studies involving PVF measurement (40 placebo-treated dogs followed up over four weeks) [17, 19, 30] or PVF measurement coupled to daily locomotor activity recording over six weeks (33 dogs, from which 14 were placebo-treated) (internal data, 2007) [17] (Figure 1(b)). All studies were approved by the Institutional Animal Care and Use Committee in accordance with the guidelines of the Canadian Council on Animal Care. All owners gave informed consent for their participation in each RCT.

2.2.2. Naturally Occurring OA Dogs. Seventy-three privately owned adult dogs weighing more than 20 kg having radiographic evidence of OA exclusively at the hip and/or stifle joints were considered, as previously described [17, 19, 30]. All dogs had OA-related hind limb disability according to orthopedic examinations and PVF measurements. Specific washout periods were respected for eventual OA treatment (including pharmaceuticals, natural health products, and therapeutic diets).

2.2.3. Peak Vertical Force Measurement. The PVF measurement was done at the trot (1.9–2.2 meter/second) using a force platform (Model OR6-6, Advanced Mechanical Technology Inc, Watertown, Massachusetts, USA), as previously described [17, 19, 29, 30]. Measurements were done at different time points (Figure 1(b)). Averaged data from the first five valid trials were expressed as % BW. In each dog, the hind limb with the lowest PVF measurement was used for statistical analyses purpose.

2.2.4. Daily Locomotor Activity Recording. Accelerometer-based daily locomotor activity recording was done using Actical system (Bio-Lynx Scientific Equipment Inc., Montreal, QC, Canada) as previously described [17]. Collar-mounted accelerometers were worn by 33 dogs for six weeks, 24 hour/day (Figure 1(b)). The duration of motion was continuously monitored as counts every two minutes, giving 720 counts per day. Daily duration of active period was referred to the time spent (expressed in minutes) when the count exceeded 30 in terms of intensity. This cut-off value was based on internal data (2004) in comparison to video-analysis and was previously used to discern movement in active (intensity > 30) from inactive (intensity < 30) period [17]. Data used were the area under the curve (AUC) which represents the integral of the daily duration of active period over six weeks and the mean of the first three days, and of the last seven days, which defined Baseline and week six data, respectively [31].

2.3. Statistical Analyses. To describe the evolution of limb function in CCL-deficient dogs, a Friedman test was used using Dunn's tests for *post hoc* analyses. To describe the relationship between the limb function with MRI structural changes, data were analyzed with Spearman correlation test and presented as Spearman coefficient (r_s). This coefficient shows by its magnitude the strength of the linear association. An r_s close to one (or minus one) indicates a strong positive (negative) linear correlation. To describe the relationship between the limb function (explanatory variable) with macroscopic measurement of cartilage thinning (response variable), data were analyzed with mixed linear model using studies as random effect. Random-effect models attempt to generalize findings beyond the included studies by assuming that the selected studies are random samples from a larger population. Such models incorporate a component of between-study variation into the uncertainty of the estimates [32]. The general equation of the linear regression was $y = mx + b$, where m refers to the slope and b refers to the y-intercept (i.e., the value of y when x = zero). To describe the natural fluctuation in limb function of placebo-treated (negative control) privately-owned dogs, absolute reliability (test-retest) was calculated using intraclass coefficient of correlation (ICC) and related 95% confidence intervals (95% CI). Two-way random single measures model (ICC 2.1) was used. An ICC close to one indicates "excellent" reliability [33]. The SEM quantifies the precision of individual PVF measurement and defines the boundaries around which a subject's value is expected to lie according to a given confident interval [34]. The SEM at 95% CI was calculated as follows:

$$\text{SEM} = \text{SD} * \sqrt{1} - \text{ICC}, \quad (1)$$

where SD referred to the within-subject standard deviation [35]. The MDC in PVF measurement that can be recorded

Table 1: Correlation analyses of the change in peak vertical force measurement and magnetic resonance imaging over the different phases of functional impairment before (Baseline) and following cranial cruciate ligament transection in five dogs.

	Osteophytes	Joint effusion	Focal cartilage changes	BMLs		Meniscal tears	Cartilage volume loss
				T2w-FS	T1w-GRE		
Phase of functional impairment nadir							
r_s	−0.05	−0.26	−0.70	−0.70	−0.70	0.01	−0.40
P	NS	NS	NS	NS	NS	NS	NS
Phase of remission							
r_s	−0.90	−0.95	−0.97	−0.70	−0.99	0.79	0.60
P	0.037	0.013	0.004	NS	<0.001	$P = 0.1$	$P = 0.1$

Nonsignificant at 5% level (NS).
Spearman coefficients (r_s).
Probability value (P).
Bone marrow lesions (BMLs).
T1-weighted three-dimensional fast gradient recalled echo (T1w-GRE).
T2-weighted fast spin echo sequence with fat saturation (T2w-FS).
The changes in the phase of functional impairment nadir were calculated using week four values minus Baseline. The changes in the phase of remission were calculated using week 26 values minus week four.

confidently (95% CI) between test sessions is referred to as the MDC_{95} and was calculated as follows:

$$MDC_{95} = SEM * 1.96 * \sqrt{2}. \quad (2)$$

The MDC_{95} can be interpreted as the magnitude of change, below which there is more than a 95% chance that change has occurred as a result of measurement error [36]. Outside this change, value does reflect a real alteration in the functional impairment toward improvement or worsening in privately-owned dog with naturally occurring OA. To describe the relationship between the limb function (response variable) with daily locomotor activity recording (explanatory variable), data were analyzed with mixed linear model using study arms (placebo or tested agent) as fixed factor and studies as random factor. All analyses were performed with SPSS, version 20.0 (SPSS Inc., Chicago, IL, USA). Values are presented as mean (standard deviation). Significant level was set at $P < 0.05$.

3. Results

3.1. Dog Model of Experimental OA

3.1.1. Measurement of the PVF. Peak vertical force measurement changed over time ($P < 0.003$) following CCLT (Figure 2(a)). Based on medians, there was a significant decrease at week four and at week eight when compared to Baseline. Then, PVF increased at week 26, reaching values significantly different than week four only. The individual changes over time involved different degrees of functional impairment characterized by a decrease in PVF measurement from Baseline reaching a nadir (at week four) followed by a phase of remission (from week four to week 26, Figure 2(a)).

3.1.2. Relationship between PVF and Structural Changes on MRI. During the phase of functional impairment nadir (from Baseline to week four), the decrease in PVF measurement did not correlate in a significant manner with the development of structural changes as evaluated using MRI (Table 1). Of note, the dogs having the more severe limb disability at week four (Figure 2(b)) were those with the highest level of focal changes of the articular cartilage.

The increase in PVF measured during the phase of remission (from week four to week 26) correlated inversely with the score for osteophytes, joint effusion, hypointense BMLs (Figure 3) and focal changes of the articular cartilage (Table 1). These negative correlations mean an abrogated remission in the presence of severe chondral and subchondral lesions and MRI-scored joint effusion.

The measurement of PVF did not correlate with cartilage volume loss, hyperintense BMLs, or meniscal tears. Only a trend was seen for a positive correlation with medial cartilage volume loss (the more PVF remission was, the more cartilage volume loss was) and medial tears score of the meniscus (Table 1).

3.1.3. Relationship with Macroscopic Measurement of Cartilage Thinning. Twenty-five dogs undergoing PVF measurement before and after CCLT were used. At Baseline, PVF measurement was 70.4 (10.9)% BW and was 26.6 (12.4)% BW and 33.9 (15.8)% BW at week four and eight, respectively. The PVF measured at week eight did not demonstrate significant relationship with cartilage thinning observed on the lateral condyle and plateau and medial plateau (Table 2). However, a significant relationship was observed with the severity of the thinning at the medial condyle, which means higher PVF value in the presence of more severe cartilage thinning. According to the regression parameters (see Table 2), for a group of CCL-deficient dogs weighing 25.0 (2.3) kg, a PVF measured at week eight of 33.9 (15.8)% BW is expected to correspond to an extent of cartilage thinning on the medial condyle of 27.3 mm^2 (95% CI: 10.4–44.2).

3.2. Dog Model of Naturally Occurring OA

3.2.1. Characteristics of PVF Measurement. Forty privately owned dogs affected by OA who received a placebo

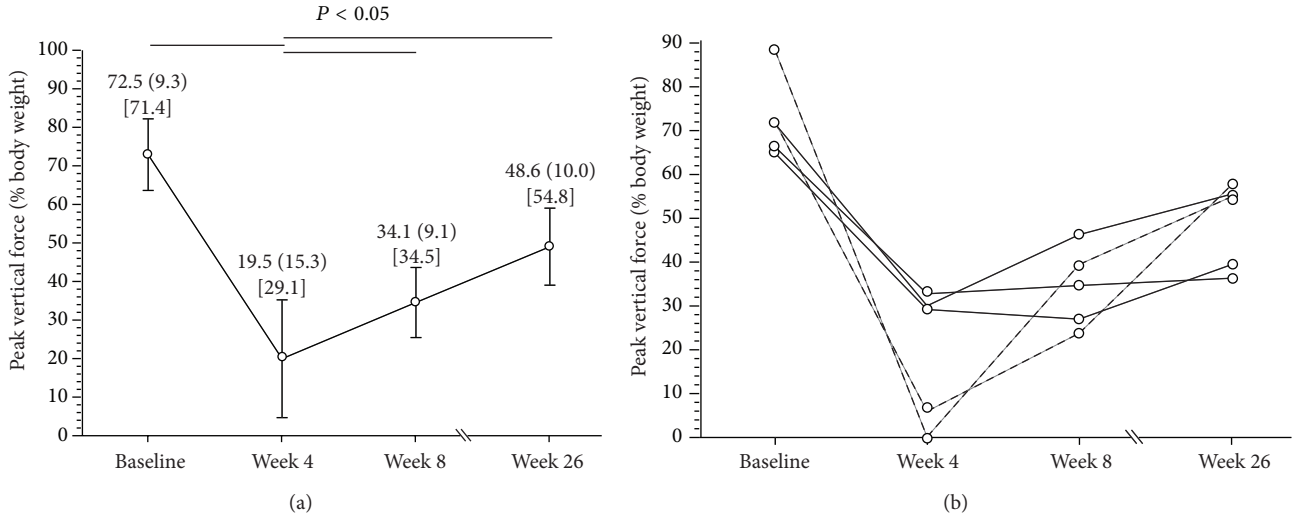

Figure 2: (a) Averaged peak vertical force values measured before (Baseline) and four, eight, and 26 weeks after cranial cruciate ligament transection in dogs. At each time point, group values are presented as mean (standard deviation) (median). Dunn's test identified which medians were significantly different. (b) Individual peak vertical force values measured before (Baseline) and four, eight, and 26 weeks after cranial cruciate ligament transection in dogs. Dotted lines identify dogs having the highest limb disability at week four and the highest levels of focal changes of the articular cartilage.

Table 2: Regression analyses between the recording of the peak vertical force and macroscopic measurement of cartilage thinning at eight weeks following cranial cruciate ligament transection in 25 dogs.

Compartments			
Lateral condyle	Lateral plateau	Medial condyle	Medial plateau
NS	NS	$P = 0.002$ $m = 0.8$ [95% CI: 0.3–1.3] $b = 0.2$ [95% CI: −25.7–26.0]	NS

Nonsignificant at 5% level (NS).
Regression slope (m).
Regression y-intercept (b).
95% confidence intervals (95% CI).

(negative control) served to determine the test-retest reliability of PVF measurement over a period of four weeks (Table 3). Standard error of measurement was determined and served for the calculation of MDC_{95}. The MDC_{95} was consistent with an increase or a decline in the magnitude of 2.0% BW across this group of OA dogs. When expressed relatively to Baseline value, the MDC_{95} represented 3.6%. Figure 4 presents individual changes in PVF measured from Baseline to week four. According to the MDC_{95}, 22 dogs had clinically meaningful changes, which were positive in five dogs and negative in 17 others.

3.2.2. Relationship with Daily Locomotor Activity Recording. Thirty-three privately-owned dogs affected by OA that had PVF measurement and daily locomotor activity recorded over a six-week period were used. The PVF measurement in OA dogs demonstrated a significant relationship with the integral (AUC) of the daily duration of active period recorded during the 26-week period ($P = 0.001$), which means a higher PVF in the presence of higher locomotor activity. The change in the PVF measurement demonstrated a significant relationship with the change in daily duration of active period ($P = 0.003$, $m = 0.03$ (95% CI: 0.01–0.05), $b = 2.8$ (95% CI: 0.4–5.1)) regardless of the study arms (i.e., placebo or tested agents). According to the regression parameters, for an increase in daily duration of active period by 54 minutes in OA dogs, the change in PVF measurement was predicted to be 4.4% BW (95% CI: 2.1–6.8). This by far exceeds the previously defined MDC_{95} (i.e., 2.0% BW), meaning a significant positive effect in PVF measurement (limb function) related to the increase in locomotor activity.

4. Discussion

4.1. Dog Model of Experimental OA. The CCLT dog model of OA involves structural changes that mimic those encountered in human OA [2, 10, 37]. This model was further optimized keeping in mind the three Rs' principles of replacement, reduction, and refinement [38]. The present study demonstrated the usefulness of complementary outcome measures. Hence, PVF measurement, which echoes pain-related functional impairment, can be successfully combined to

Table 3: Characteristics of peak vertical force measurement in 40 privately owned dogs affected by naturally occurring osteoarthritis.

Baseline	Week 4	ICC [95% CI]	SEM	MDC_{95}
56.0% BW (7.5) [26.1–66.1]	54.5% BW (8.4) [23.6–64.9]	91 [80–95]	0.7% BW	2.0% BW

Values are presented as mean (standard deviation) (minimal value–maximal value).
Intraclass coefficient of correlation (ICC).
Standard error of measurement (SEM).
Minimal detectable change at the 95% confidence level (MDC_{95}).
Percentage of body weight (% BW).

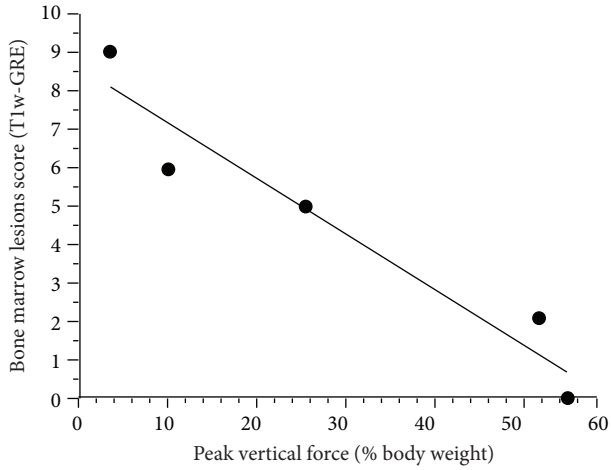

Figure 3: Significant correlation ($r_s = -0.99$, $P < 0.001$) for the differences of hypointense bone marrow lesions on T1-weighted three-dimensional fast gradient recalled echo images (T1w-GRE) scores during the remission phase (week 26 minus week four), with the concurrent difference in peak vertical force measurement. Linear regression trend is illustrated.

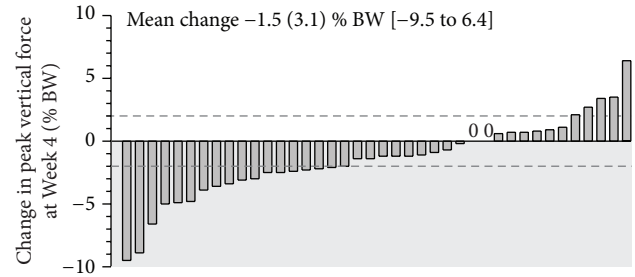

Figure 4: Individual changes in peak vertical force measured at week four in 40 privately owned dogs receiving a placebo in randomized controlled trials. Changes were the difference between week four versus Baseline. Grey zone represents a decrease in peak vertical force measurement compared to Baseline. Dashed lines represent the MDC_{95}. Peak vertical force data are expressed in % BW (body weight) and presented as mean (standard deviation) (minimal value to maximal value).

the common structural outcomes in the CCLT dog model of OA. To maximize the information gained from CCL-deficient dogs, researchers can document in a noninvasive manner the pain-related disability, which comprises a phase of functional impairment with a nadir preceding a remission process. At the preclinical stage of drug development, such information has a clinically meaningful potential for disease-modifying compounds proposed to confer pain and functional improvement in addition to structural benefits. As PVF measurement data were detailed, power and sample size can be determined *a priori*, again supporting the principle of reduction by providing statistical estimates. The principle of refinement is also addressed by documenting individual variability (per dog data) that occurs over an extended duration [39].

Anterior cruciate ligament (human counterpart of CCL) transection leads to rotational and translational changes that induce mechanical stresses on articular surfaces unaccustomed for such loading solicitation [40–44]. This phenomenon generates loss of tissue integrity, involving abnormal architecture and components known as structural changes. Using MRI, which is a non-invasive imaging technique, the present study supports the use of the CCLT dog model of OA for its potential to corroborate the relationship between structural changes and clinical signs observed in human. Hence, a recent systematic review indicated that OA knee pain is associated with BMLs and effusion/synovitis [45]. In line with findings observed in humans [46, 47], severe limb impairment was denoted in dogs with the highest level of focal changes of the articular cartilage during the phase of limb disability (from Baseline to week four). When BMLs evolved minimally, these manifestations were concomitant to lesser limb disability (Figure 3). Such benefits are in accordance with the report of Zhang et al. [48] who observed a fluctuation of pain when BMLs were modulated. We also observed that CCL-deficient dogs had better limb functional remission when osteophyte growth and joint effusion size were minimal. These findings were suggestive of higher pain in the presence of osteophyte and effusion/synovitis as reported in human [45, 49, 50]. In face of the present results, we propose to integrate the pain-related functional impairment to the presence of severe chondral and subchondral lesions. We suggest that a more unstable joint (i.e., devoid of adaptive neuromuscular strategies to palliate for the excessive displacement) could be responsible for the more severe chondral and subchondral changes observed. As an attempt to restore limb function, marked expressions of secondary strategies, such as osteophytes growth and joint effusion, are suggested to develop for providing stability and cushioning, in a manner to minimize the deleterious knee joint load in CCL-deficient dogs.

Although we did not reach statistically significant levels, our findings are suggestive of a role of mechanical environment in cartilage volume loss and meniscus insult in CCL-deficient dogs. Hence, we found a trend to have more severe

cartilage loss and meniscal tears in the medial part of the joint in dogs having recovered well their limb function (i.e., with the highest PVF measurement). In addition, the extent of medial cartilage thinning was greater in dogs having the highest limb function at eight weeks following CCLT. Those findings were in line with those of Smith jr. et al. [13], which reported a link between the level of knee joint chondropathy and increasing limb function in this model. Furthermore, meniscal lesions have been linked with the progression of OA cartilage loss in humans [51, 52] while a strong relationship exists between high joint loading and meniscal lesions [53]. These findings are of major importance, not only because of their correspondence to findings in human knee OA, but also because the presence of meniscal lesions has an impact on the response to disease-modifying OA drug (DMOAD) treatment in human knee OA [46, 51], a finding that likely also applies to the CCLT dog model of OA.

Despite its burgeoning importance, translation of DMOAD therapies from the laboratory into clinical practice has slowed. Differences between the OA models studied preclinically and the disease evaluated in human clinical trials contribute to this failure [54]. First, a general concern is the use of quadruped animals as knee models for the bipedal human, particularly given their range of motion differences noted in a study comparing large animal (cow, sheep, goat, dog, pig, and rabbit) to human cadaveric knees [55]. The disappearance of many of the observed differences in the cruciate and meniscal anatomy after normalization with the tibial plateau width suggested an overall conservation of relative size among species for the cruciates and menisci [55]. This anatomical and biomechanical analogy, while reviewing the different OA animal models, led Gregory et al. [3] to state that the canine model is probably the closest to a gold-standard animal model for OA currently available. The present study adds the structure-function relationship translated from the dog CCLT model to the human pain OA condition.

Second, most animal models of OA induce disease through chemical insult or surgical or mechanical disruption of joint biomechanics in young individuals rather than the spontaneous development of the disease. This instability-induced joint disease in animals best models the structural changes that develops in humans after an injurious event, known as posttraumatic OA [54]. The poor translational predictability to therapy response is particularly high with the rodent preclinical models. Studies in genetically modified mice suggest that post-traumatic OA has a distinct molecular pathophysiology compared with that of spontaneous OA, which might explain the poor translation from preclinical to clinical OA therapeutic trials [54]. On the contrary, molecular changes observed in a past study with the canine CCLT model suggest that dog cartilage responds to post-traumatic OA and degenerative conditions by regulating the same genes in a similar direction as that observed for chondrocytes in post-traumatic and late human OA [56]. Finally, the recent finding about the DMOAD effects of strontium ranelate [57] late in the CCLT dog model of OA being confirmed in a Phase III clinical trial in knee OA patients [58] is of the utmost importance in the context of this publication. Previously, many DMOADs have demonstrated efficacy in the dog OA model, including the matrix metalloproteinase inhibitor doxycycline [59, 60], the viscosupplementation *via* local hyaluronan [61, 62], the antiresorptive agents such as bisphosphonate [11, 63] and calcitonin [64], the anti-inflammatory properties of diacerhein [65], licofelone [28], and NSAIDs (such as carprofen). All these products but calcitonin (probably related to a deficient formulation) demonstrated similar efficacy in human OA [51, 66–73]. To the best of authors' knowledge, no other preclinical animal OA model presents a better translational predictability record, partly because species differences with respect to the relative contribution of various mediators, receptors, or enzymes to the pathology and xenobiotics metabolism are common.

In accordance with the three Rs' principles, the predictive character of the cartilage thinning based upon PVF measurement opens the idea of limiting the requirement of post-mortem analysis for future research aimed to gain insight in joint cartilage integrity in this model. Based on the regression parameters, the limb disability observed at eight weeks following CCLT predicted an extent of macroscopic lesions surface by 27.3 mm^2. This level of lesions represents 12% of the total surface of the medial condyle when based on MRI cartilage surface mapping in dogs of similar BW (ArthroVision, personal communication, 2013). As the characterization of full-thickness cartilage thinning in end-stage OA in humans was shown to range between 10 and 23% at this joint compartment [74], the translational potential (macroscopical structural argument) of this model to human OA is further supported.

It should be pointed out that the statistical method used to correlate structural changes on MRI with PVF measurement does not pinpoint the sequence of events and did not take into account the potential role of confounding factors, interrelationship, and dependency. Findings of the pilot study reported herein will help to promote future research of a more mechanistic (structure-function) approach based on a higher sample size. The complementary outcome measures proposed herein to optimize the use of the dog in OA research are not restricted to the CCLT model. Other experimental avenues should be explored for their potential to induce structural changes in close relationship with functional impairment.

4.2. Dog Model of Naturally Occurring OA. The recent interest in natural models of OA [10] puts more emphasis on the need to improve the rigor of RCT using functional outcome measures, such as PVF, in naturally occurring OA dogs. This study optimized the use of naturally occurring OA dogs in research by characterizing the PVF measurement with regards to the high value of this outcome to address pain/biomechanics-related joint alterations in the dog. Here test-retest PVF measurement values demonstrated excellent between-session reliability with an ICC of 91 (95% CI: 80–95) in placebo-treated dogs followed up over a four-week period. The SEM provides an absolute index of reliability and refers to the precision of individual measurements. Determining magnitude of an intervention benefit is a critical

methodological step in the design of a clinical trial. For the PVF, the MDC_{95} indicated that a change of at least 2.0% BW needs to occur to be confident, at the 95% level, that a change in PVF measurement reflects a real change and not a difference that is within what might be reasonably expected given the measurement error (noise). As PVF measurement characteristics were provided, such as standard deviation, SEM, and the MCD_{95}, such data should help researchers to estimate power and sample size, thus contributing to the principle of refinement.

Randomized controlled trials in naturally occurring OA dogs usually focus on testing mean changes across groups of treated (test article) and control (placebo-treated) animals. This practice often obscures the individual change, which may be very informative in clinical studies [75]. Moreover, reporting the percentages of subjects who met the MDC_{95} requirements provides additional insightful interpretations other than considering only the overall mean change scores [76]. Accordingly, researchers have a tool to distinguish improved (or worsened) dogs by using the proposed MDC_{95} value as a cutoff. Of note, the level of 2.0% BW was in line with the improvement observed following therapeutic modalities in previous clinical RCT in OA dogs [17–20, 30, 77–80].

The results of the current study show that different levels of change in limb function reflected by PVF measurement were observed in privately-owned dogs afflicted by OA (Figure 4). Among the 40 dogs evaluated, 22 (55%) had clinically meaningful changes, which were positive (placebo effect) in five (12.5%) or negative (nocebo effect) in 17 (42.5%) dogs. The high proportion of dogs having a worsening of their condition contributes mainly to the overall decrease in PVF recording by −1.5 (3.1)% BW. A phenomenon known as the maturation effect may be suggested as being involved in changes exceeding the measurement error.

In a recent multicenter RCT in naturally occurring OA, an arbitrary cut-off value (i.e., 2.8% BW or ≥5% of Baseline measurement) was used to distinguish clinically meaningful responders from measurement error [81]. Of note, the global rate of responders reported according to this value was 20.7% whereas it was higher in our study (55%) by applying the MDC_{95} (calculated to be 2.0% BW or ≥3.6% of Baseline measurement). The latter finding is important, as applying the higher arbitrary cut-off value rather than the MDC_{95} proposed herein would lead to a high false negative rate of responders (being indeed considered as nonresponders). This type II error overestimates the required sample size and leads to an unnecessary high number of dogs affected by OA to be recruited in the RCT. It should be noted that the low placebo responder's rate (12.5% in the current study, 12.1% [81]) observed according to the objective PVF measurement again contributes to a judicious use of privately owned dogs in RCT. This is a huge advantage compared to subjective assessment completed by either veterinarians or owners, for whom the placebo responder's rate was oscillating between 25 and 44.8% [81, 82].

As previously demonstrated in naturally occurring OA dogs [17, 29, 31, 77] the usefulness of continuous monitoring of daily locomotor activity recording was sustained in the current study. Particularly, we denoted that continuous activity recording showed strong similarities with PVF measurement, being sensitive to functional improvement. This tool is therefore highly recommended to be used as a complement to punctual PVF measurement in a way to improve the detection of therapeutic benefits in OA dogs. In addition, the present results support the relevance of naturally occurring OA dogs for their potential to respond similarly to the human OA condition. This was illustrated in recent studies in which an anti-inflammatory drug, licofelone, was tested positively both in the dog model of experimental OA [28] naturally occurring OA [30] as well as in a clinical Phase III study in patients with knee OA [51]. Similar concordance in efficacy was observed with doxycycline [59, 60, 71].

Hence, dogs with the most severe limb impairment were those with the lowest degree of daily activity. This was in line with findings in human OA reporting lower physical activity in more afflicted patients [83]. Present data also give a first impression of potential benefits of an increase by 54 minutes in daily life activity being mirrored confidently with an increase in PVF that exceeded the measurement error. This was recently supported in dogs with hip OA, showing a better condition when more than an hour of exercise was performed daily [84]. Human data are also in accordance with this finding as physical activity programs are supported to reduce pain, to improve physical performance, and to delay disability among persons with knee OA [85–87].

4.3. Conclusion. Biomedical research and testing often faces criticism and protestation against the use of dogs for research purposes. As for any animal experiments, the three Rs' principles must apply. In addition, findings from ideal animal models have to be rapidly translated to human characteristic with the ultimate hope to better predict outcomes for human clinical trials. With this idea in mind, we present an optimization of the outcomes gained from the dog model of OA induced by CCLT. The relationship between structural changes and functional impairment denoted strong similarities with the human OA condition. This adds to the recognized anatomical and biomechanical, genomic, molecular, histological, and macroscopical structural similarities to human OA, as well as to the access of yet validated and performing functional and imaging outcome measures, as reported in the present paper.

Regarding the dog model of naturally occurring OA, the present analysis provides compelling evidence to better interpret complementary outcome measures assessing the OA condition. The PVF measurement data particularly is robust, precise, and reliable for determining whether a change has taken place as a result of an intervention. Moreover, the data support the huge interest and applicability of monitoring the level of daily locomotor activity in clinical RCT with privately-owned OA dogs. Such natural model of OA in dog represents a spontaneous model of the disease, different and complementary to the post-traumatic OA model. At the difference of the standardized preclinical CCLT dog model, the conditions are close to those of a population pharmacological study integrating, in addition to the previously listed advantages, the genomics and environmental (such as the physical activity and the nutrition) influences of the disease.

Preclinical testing protocol combining the dog model of OA induced by CCLT and the dog model of naturally occurring OA could better predict outcomes for human clinical trials in a close future, as is supported by the high translational pharmacological responsiveness.

Conflict of Interests

The authors declare that they have no conflict of interest in the research.

Acknowledgments

Authors are grateful to Dr. Jean-Pierre Raynauld, M.D., for his valuable and insightful comments throughout the writing process of the paper. M. Maxim Moreau received a doctoral scholarship from the Canadian Institutes of Health Research—Strategic Training Program (MENTOR) and a doctoral scholarship from the Fonds de recherche du Québec-Santé. This work was supported in part by an ongoing New Opportunities Fund Grant (no. 9483) and a Leader Opportunity Fund Grant (no. 24601) from the Canada Foundation for Innovation (Eric Troncy) for the pain/function equipment, by the Osteoarthritis Chair of the University of Montreal Hospital Centre, Université de Montréal, and a Discovery Grant (no. 327158-2008) from the Natural Sciences and Engineering Research Council of Canada (Eric Troncy) for the bioanalyses and salaries.

References

[1] J.-P. Pelletier, C. Boileau, R. D. Altman, and J. Martel-Pelletier, "Experimental models of osteoarthritis: usefulness in the development of disease-modifying osteoarthritis drugs/agents," *Therapy*, vol. 7, no. 6, pp. 621–634, 2010.

[2] K. Lampropoulou-Adamidou, P. Lelovas, E. V. Karadimas et al., "Useful animal models for the research of osteoarthritis," *European Journal of Orthopaedic Surgery & Traumatology*, 2013.

[3] M. H. Gregory, N. Capito, K. Kuroki, A. M. Stoker, J. L. Cook, and S. L. Sherman, "A review of translational animal models for knee osteoarthritis," *Arthritis*, vol. 2012, Article ID 764621, 14 pages, 2012.

[4] U. G. Longo, M. Loppini, C. Fumo et al., "Osteoarthritis: new insights in animal models," *The Open Orthopaedics Journal*, vol. 6, pp. 558–563, 2012.

[5] H. De Rooster, T. De Bruin, and H. Van Bree, "Morphologic and functional features of the canine cruciate ligaments," *Veterinary Surgery*, vol. 35, no. 8, pp. 769–780, 2006.

[6] L. N. Frost-Christensen, S. C. Mastbergen, M. E. Vianen et al., "Degeneration, inflammation, regeneration, and pain/disability in dogs following destabilization or articular cartilage grooving of the stifle joint," *Osteoarthritis and Cartilage*, vol. 16, no. 11, pp. 1327–1335, 2008.

[7] A. Lahm, M. Uhl, M. Edlich, C. Erggelet, J. Haberstroh, and P. C. Kreuz, "An experimental canine model for subchondral lesions of the knee joint," *Knee*, vol. 12, no. 1, pp. 51–55, 2005.

[8] H. E. Panula, H. J. Helminen, and I. Kiviranta, "Slowly progressive osteoarthritis after tibial valgus osteotomy in young beagle dogs," *Clinical Orthopaedics and Related Research*, no. 343, pp. 192–202, 1997.

[9] H. Troyer, "Experimental models of osteoarthritis: a review," *Seminars in Arthritis and Rheumatism*, vol. 11, no. 3, pp. 362–374, 1982.

[10] J. P. Pelletier, C. Boileau, R. D. Altman, and J. Martel-Pelletier, "Animal models of osteoarthritis," in *Rheumatology*, M. C. Hochberg et al., Ed., pp. 1731–1739, Mosby; Elsevier, 5th edition, 2010.

[11] M. Moreau, P. Rialland, J.-P. Pelletier et al., "Tiludronate treatment improves structural changes and symptoms of osteoarthritis in the canine anterior cruciate ligament model," *Arthritis Research and Therapy*, vol. 13, no. 3, article R98, 2011.

[12] C. Boileau, J. Martel-Pelletier, J. Caron et al., "Oral treatment with a Brachystemma calycinum D don plant extract reduces disease symptoms and the development of cartilage lesions in experimental dog osteoarthritis: inhibition of protease-activated receptor 2," *Annals of the Rheumatic Diseases*, vol. 69, no. 6, pp. 1179–1184, 2010.

[13] G. N. Smith Jr., S. L. Myers, K. D. Brandt, E. A. Mickler, and M. E. Albrecht, "Effect of intraarticular hyaluronan injection on vertical ground reaction force and progression of osteoarthritis after anterior cruciate ligament transection," *Journal of Rheumatology*, vol. 32, no. 2, pp. 325–334, 2005.

[14] S. A. Johnston, "Overview of pain in the lame patient," *Veterinary Clinics of North America*, vol. 31, no. 1, pp. 39–53, 2001.

[15] S. A. Martinez, "Congenital conditions that lead to osteoarthritis in the dog," *The Veterinary Clinics of North America*, vol. 27, no. 4, pp. 735–758, 1997.

[16] S. A. Martinez and G. S. Coronado, "Acquired conditions that lead to osteoarthritis in the dog," *The Veterinary Clinics of North America*, vol. 27, no. 4, pp. 759–775, 1997.

[17] M. Moreau, B. Lussier, J. P. Pelletier et al., "Brachystemma calycinum D. don effectively reduces the locomotor disability in dogs with naturally occurring osteoarthritis: a randomized placebo-controlled trial," *Evidence-Based Complementary and Alternative Medicine*, vol. 2012, Article ID 646191, 9 pages, 2012.

[18] D. J. Imhoff, W. J. Gordon-Evans, R. B. Evans, A. L. Johnson, D. J. Griffon, and K. S. Swanson, "Evaluation of S-adenosyl l-methionine in a double-blinded, randomized, placebo-controlled, clinical trial for treatment of presumptive osteoarthritis in the dog," *Veterinary Surgery*, vol. 40, no. 2, pp. 228–232, 2011.

[19] M. Moreau, J. Dupuis, N. H. Bonneau, and M. Desnoyers, "Clinical evaluation of a nutraceutical, carprofen and meloxicam for the treatment of dogs with osteoarthritis," *Veterinary Record*, vol. 152, no. 11, pp. 323–329, 2003.

[20] S. C. Budsberg, S. A. Johnston, P. D. Schwarz, C. E. DeCamp, and R. Claxton, "Efficacy of etodolac for the treatment of osteoarthritis of the hip joints in dogs," *Journal of the American Veterinary Medical Association*, vol. 214, no. 2, pp. 206–210, 1999.

[21] C. Boileau, J. Martel-Pelletier, F. Abram et al., "Magnetic resonance imaging can accurately assess the long-term progression of knee structural changes in experimental dog osteoarthritis," *Annals of the Rheumatic Diseases*, vol. 67, no. 7, pp. 926–932, 2008.

[22] M.-A. D'Anjou, M. Moreau, É. Troncy et al., "Osteophytosis, subchondral bone sclerosis, joint effusion and soft tissue thickening in canine experimental stifle osteoarthritis: comparison between 1.5 T magnetic resonance imaging and computed radiography," *Veterinary Surgery*, vol. 37, no. 2, pp. 166–177, 2008.

[23] M.-A. d'Anjou, E. Troncy, M. Moreau et al., "Temporal assessment of bone marrow lesions on magnetic resonance imaging

in a canine model of knee osteoarthritis: impact of sequence selection," *Osteoarthritis and Cartilage*, vol. 16, no. 11, pp. 1307–1311, 2008.

[24] C. L. Aragon, E. H. Hofmeister, and S. C. Budsberg, "Systematic review of clinical trials of treatments for osteoarthritis in dogs," *Journal of the American Veterinary Medical Association*, vol. 230, no. 4, pp. 514–521, 2007.

[25] M. M. Quinn, N. S. Keuler, Y. Lu, M. L. E. Faria, P. Muir, and M. D. Markel, "Evaluation of agreement between numerical rating scales, visual analogue scoring scales, and force plate gait analysis in dogs," *Veterinary Surgery*, vol. 36, no. 4, pp. 360–367, 2007.

[26] R. M. McLaughlin, "Kinetic and kinematic gait analysis in dogs," *Veterinary Clinics of North America*, vol. 31, no. 1, pp. 193–201, 2001.

[27] L. Blond, D. E. Thrall, S. C. Roe, N. Chailleux, and I. D. Robertson, "Diagnostic accuracy of magnetic resonance imaging for meniscal tears in dogs affected with naturally occuring cranial cruciate ligament rupture," *Veterinary Radiology and Ultrasound*, vol. 49, no. 5, pp. 425–431, 2008.

[28] M. Moreau, C. Boileau, J. Martel-Pelletier, J. Brunet, S. Laufer, and J.-P. Pelletier, "Licofelone reduces progression of structural changes in a canine model of osteoarthritis under curative conditions: effect on protease expression and activity," *Journal of Rheumatology*, vol. 33, no. 6, pp. 1176–1182, 2006.

[29] P. Rialland, S. Bichot, M. Moreau et al., "Clinical validity of outcome pain measures in naturally occurring canine osteoarthritis," *BMC Veterinary Research*, vol. 8, no. 1, article 162, 2012.

[30] M. Moreau, B. Lussier, M. Doucet, G. Vincent, J. Martel-Pelletier, and J.-P. Pelletier, "Efficacy of licofelone in dogs with clinical osteoarthritis," *Veterinary Record*, vol. 160, no. 17, pp. 584–588, 2007.

[31] D. C. Brown, R. C. Boston, and J. T. Farrar, "Use of an activity monitor to detect response to treatment in dogs with osteoarthritis," *Journal of the American Veterinary Medical Association*, vol. 237, no. 1, pp. 66–70, 2010.

[32] M. W.-L. Cheung, R. C. M. Ho, Y. Lim, and A. Mak, "Conducting a meta-analysis: basics and good practices," *International Journal of Rheumatic Diseases*, vol. 15, no. 2, pp. 129–135, 2012.

[33] G. Atkinson and A. M. Nevill, "Statistical methods for assessing measurement error (reliability) in variables relevant to sports medicine," *Sports Medicine*, vol. 26, no. 4, pp. 217–238, 1998.

[34] J. P. Weir, "Quantifying test-retest reliability using the intraclass correlation coefficient and the SEM," *Journal of Strength and Conditioning Research*, vol. 19, no. 1, pp. 231–240, 2005.

[35] J. M. Bland and D. G. Altman, "Measurement error," *British Medical Journal*, vol. 313, no. 7059, article 744, 1996.

[36] F. M. Kovacs, V. Abraira, A. Royuela et al., "Minimum detectable and minimal clinically important changes for pain in patients with nonspecific neck pain," *BMC Musculoskeletal Disorders*, vol. 9, article 43, 2008.

[37] K. D. Brandt, "Transection of the anterior cruciate ligament in the dog: a model of osteoarthritis," *Seminars in Arthritis and Rheumatism*, vol. 21, no. 3, pp. 22–32, 1991.

[38] W. M. Russell, "The development of the three Rs concept," *Alternatives to Laboratory Animals*, vol. 23, no. 3, pp. 298–304, 1995.

[39] A. Manciocco, F. Chiarotti, A. Vitale, G. Calamandrei, G. Laviola, and E. Alleva, "The application of Russell and Burch 3R principle in rodent models of neurodegenerative disease: the case of Parkinson's disease," *Neuroscience and Biobehavioral Reviews*, vol. 33, no. 1, pp. 18–32, 2009.

[40] T. P. Andriacchi, S. Koo, and S. F. Scanlan, "Gait mechanics influence healthy cartilage morphology and osteoarthritis of the knee," *Journal of Bone and Joint Surgery A*, vol. 91, no. 1, pp. 95–101, 2009.

[41] T. P. Andriacchi, P. L. Briant, S. L. Bevill, and S. Koo, "Rotational changes at the knee after ACL injury cause cartilage thinning," *Clinical Orthopaedics and Related Research*, no. 442, pp. 39–44, 2006.

[42] T. P. Andriacchi and A. Mündermann, "The role of ambulatory mechanics in the initiation and progression of knee osteoarthritis," *Current Opinion in Rheumatology*, vol. 18, no. 5, pp. 514–518, 2006.

[43] T. P. Andriacchi, A. Mündermann, R. L. Smith, E. J. Alexander, C. O. Dyrby, and S. Koo, "A framework for the in vivo pathomechanics of osteoarthritis at the knee," *Annals of Biomedical Engineering*, vol. 32, no. 3, pp. 447–457, 2004.

[44] S. Tashman, W. Anderst, P. Kolowich, S. Havstad, and S. Arnoczky, "Kinematics of the ACL-deficient canine knee during gait: serial changes over two years," *Journal of Orthopaedic Research*, vol. 22, no. 5, pp. 931–941, 2004.

[45] E. Yusuf, M. C. Kortekaas, I. Watt, T. W. J. Huizinga, and M. Kloppenburg, "Do knee abnormalities visualised on MRI explain knee pain in knee osteoarthritis? a systematic Review," *Annals of the Rheumatic Diseases*, vol. 70, no. 1, pp. 60–67, 2011.

[46] L. M. Wildi, J.-P. Raynauld, J. Martel-Pelletier et al., "Chondroitin sulphate reduces both cartilage volume loss and bone marrow lesions in knee osteoarthritis patients starting as early as 6 months after initiation of therapy: a randomised, double-blind, placebo-controlled pilot study using MRI," *Annals of the Rheumatic Diseases*, vol. 70, no. 6, pp. 982–989, 2011.

[47] A. Anandacoomarasamy, G. Smith, S. Leibman et al., "Cartilage defects are associated with physical disability in obese adults," *Rheumatology*, vol. 48, no. 10, pp. 1290–1293, 2009.

[48] Y. Zhang, M. Nevitt, J. Niu et al., "Fluctuation of knee pain and changes in bone marrow lesions, effusions, and synovitis on magnetic resonance imaging," *Arthritis and Rheumatism*, vol. 63, no. 3, pp. 691–699, 2011.

[49] G. Zhai, F. Cicuttini, C. Ding, F. Scott, P. Garnero, and G. Jones, "Correlates of knee pain in younger subjects," *Clinical Rheumatology*, vol. 26, no. 1, pp. 75–80, 2007.

[50] L. Torres, D. D. Dunlop, C. Peterfy et al., "The relationship between specific tissue lesions and pain severity in persons with knee osteoarthritis," *Osteoarthritis and Cartilage*, vol. 14, no. 10, pp. 1033–1040, 2006.

[51] J.-P. Raynauld, J. Martel-Pelletier, P. Bias et al., "Protective effects of licofelone, a 5-lipoxygenase and cyclo-oxygenase inhibitor, versus naproxen on cartilage loss in knee osteoarthritis: a first multicentre clinical trial using quantitative MRI," *Annals of the Rheumatic Diseases*, vol. 68, no. 6, pp. 938–947, 2009.

[52] M.-J. Berthiaume, J.-P. Raynauld, J. Martel-Pelletier et al., "Meniscal tear and extrusion are strongly associated with progression of symptomatic knee osteoarthritis as assessed by quantitative magnetic resonance imaging," *Annals of the Rheumatic Diseases*, vol. 64, no. 4, pp. 556–563, 2005.

[53] M. L. Davies-Tuck, A. E. Wluka, A. J. Teichtahl et al., "Association between meniscal tears and the peak external knee adduction moment and foot rotation during level walking in postmenopausal women without knee osteoarthritis: a cross-sectional study," *Arthritis Research and Therapy*, vol. 10, no. 3, article R58, 2008.

[54] C. B. Little and D. J. Hunter, "Post-traumatic osteoarthritis: from mouse models to clinical trials," *Nature Reviews Rheumatology*, vol. 9, pp. 485–497, 2013.

[55] B. L. Proffen, M. McElfresh, B. C. Fleming, and M. M. Murray, "A comparative anatomical study of the human knee and six animal species," *Knee*, vol. 19, no. 4, pp. 493–499, 2012.

[56] H. Lorenz, W. Wenz, M. Ivancic, E. Steck, and W. Richter, "Early and stable upregulation of collagen type II, collagen type I and YKL40 expression levels in cartilage during early experimental osteoarthritis occurs independent of joint location and histological grading," *Arthritis Research & Therapy*, vol. 7, no. 1, pp. R156–R165, 2005.

[57] J. P. Pelletier, M. Kapoor, H. Fahmi et al., "Strontium ranelate reduces the progression of experimental dog osteoarthritis by inhibiting the expression of key proteases in cartilage and of IL-1beta in the synovium," *Annals of the Rheumatic Diseases*, vol. 72, no. 2, pp. 250–257, 2013.

[58] J. Y. Reginster, J. Badurski, N. Bellamy et al., "Efficacy and safety of strontium ranelate in the treatment of knee osteoarthritis: results of a double-blind, randomised placebo-controlled trial," *Annals of the Rheumatic Diseases*, vol. 72, no. 2, pp. 179–186, 2013.

[59] S. Jauernig, A. Schweighauser, M. Reist, B. Von Rechenberg, P. Schawalder, and D. Spreng, "The effects of doxycycline on nitric oxide and stromelysin production in dogs with cranial cruciate ligament rupture," *Veterinary Surgery*, vol. 30, no. 2, pp. 132–139, 2001.

[60] L. P. Yu Jr., G. N. Smith Jr., K. D. Brandt, S. L. Myers, B. L. O'Connor, and D. A. Brandt, "Reduction of the severity of canine osteoarthritis by prophylactic treatment with oral doxycycline," *Arthritis and Rheumatism*, vol. 35, no. 10, pp. 1150–1159, 1992.

[61] K. W. Marshall, V. Manolopoulos, K. Mancer, J. Staples, and A. Damyanovich, "Amelioration of disease severity by intraarticular hylan therapy in bilateral canine osteoarthritis," *Journal of Orthopaedic Research*, vol. 18, no. 3, pp. 416–425, 2000.

[62] W. Wenz, S. J. Breusch, J. Graf, and U. Stratmann, "Ultrastructural findings after intra-articular application of hyaluronan in a canine model of arthropathy," *Journal of Orthopaedic Research*, vol. 18, no. 4, pp. 604–612, 2000.

[63] S. L. Myers, K. D. Brandt, D. B. Burr, B. L. O'Connor, and M. Albrecht, "Effects of a bisphosphonate on bone histomorphometry and dynamics in the canine cruciate deficiency model of osteoarthritis," *Journal of Rheumatology*, vol. 26, no. 12, pp. 2645–2653, 1999.

[64] D. H. Manicourt, R. D. Altman, J. M. Williams et al., "Treatment with calcitonin suppresses the responses of bone, cartilage, and synovium in the early stages of canine experimental osteoarthritis and significantly reduces the severity of the cartilage lesions," *Arthritis and Rheumatism*, vol. 42, no. 6, pp. 1159–1167, 1999.

[65] G. N. Smith, Jr, S. L. Myers, K. D. Brandt, E. A. Mickler, and M. E. Albrecht, "Diacerhein treatment reduces the severity of osteoarthritis in the canine cruciate-deficiency model of osteoarthritis," *Arthritis and Rheumatism*, vol. 42, no. 3, pp. 545–554, 1999.

[66] B. A. McArthur, C. J. Dy, P. D. Fabricant, and A. G. Valle, "Long term safety, efficacy, and patient acceptability of hyaluronic acid injection in patients with painful osteoarthritis of the knee," *Patient Preference and Adherence*, vol. 6, pp. 905–910, 2012.

[67] E. Nüesch, A. W. Rutjes, S. Trelle, S. Reichenbach, and P. Jüni, "Doxycycline for osteoarthritis of the knee or hip," *Cochrane Database of Systematic Reviews*, no. 4, Article ID CD007323, 2009.

[68] R. C. Hamdy and D. N. Daley, "Oral calcitonin," *International Journal of Women's Health*, vol. 4, pp. 471–479, 2012.

[69] J. Iwamoto, T. Takeda, Y. Sato, and H. Matsumoto, "Effects of risedronate on osteoarthritis of the knee," *Yonsei Medical Journal*, vol. 51, no. 2, pp. 164–170, 2010.

[70] E. M. Bartels, H. Bliddal, P. K. Schøndorff, R. D. Altman, W. Zhang, and R. Christensen, "Symptomatic efficacy and safety of diacerein in the treatment of osteoarthritis: a meta-analysis of randomized placebo-controlled trials," *Osteoarthritis and Cartilage*, vol. 18, no. 3, pp. 289–296, 2010.

[71] K. D. Brandt, S. A. Mazzuca, B. P. Katz et al., "Effects of doxycycline on progression of osteoarthritis: results of a randomized, placebo-controlled, double-blind trial," *Arthritis and Rheumatism*, vol. 52, no. 7, pp. 2015–2025, 2005.

[72] N. Bellamy, J. Campbell, V. Robinson, T. Gee, R. Bourne, and G. Wells, "Viscosupplementation for the treatment of osteoarthritis of the knee," *Cochrane Database of Systematic Reviews*, no. 2, Article ID CD005321, 2005.

[73] M. Dougados, M. Nguyen, L. Berdah et al., "Evaluation of the structure-modifying effects of diacerein in hip osteoarthritis: ECHODIAH, a three-year, placebo-controlled trial. Evaluation of the chondromodulating effect of diacerein in OA of the Hip," *Arthritis and Rheumatism*, vol. 44, no. 11, pp. 2539–2547, 2001.

[74] W. C. Bae, M. M. Payanal, A. C. Chen et al., "Topographic patterns of cartilage lesions in knee osteoarthritis," *Cartilage*, vol. 1, no. 1, pp. 10–19, 2010.

[75] L. Tesio, "Outcome measurement in behavioural sciences: a view on how to shift attention from means to individuals and why," *International Journal of Rehabilitation Research*, vol. 35, no. 1, pp. 1–12, 2012.

[76] J. S. Schmitt and R. P. Di Fabio, "Reliable change and minimum important difference (MID) proportions facilitated group responsiveness comparisons using individual threshold criteria," *Journal of Clinical Epidemiology*, vol. 57, no. 10, pp. 1008–1018, 2004.

[77] P. Rialland, S. Bichot, B. Lussier et al., "Effect of a green-lipped mussel-enriched diet on pain behaviours and functioning in dogs with clinical osteoarthritis," *Canadian Journal of Veterinary Research*, vol. 77, no. 1, pp. 66–74, 2013.

[78] M. Moreau, E. Troncy, J. R. Del Castillo, C. Bedard, D. Gauvin, and B. Lussier, "Effects of feeding a high omega-3 fatty acids diet in dogs with naturally occurring osteoarthritis," *Journal of Animal Physiology and Animal Nutrition*, vol. 97, no. 5, pp. 830–837, 2013.

[79] A. Hielm-Bjorkman, R. M. Tulamo, H. Salonen, and M. Raekallio, "Evaluating complementary therapies for canine osteoarthritis—Part II: a homeopathic combination preparation (Zeel)," *Evidence-Based Complementary and Alternative Medicine*, vol. 6, no. 4, pp. 465–471, 2009.

[80] M. Moreau, J. Dupuis, N. H. Bonneau, and M. Lécuyer, "Clinical evaluation of a powder of quality elk velvet antler for the treatment of osteoarthrosis in dogs," *Canadian Veterinary Journal*, vol. 45, no. 2, pp. 133–139, 2004.

[81] M. G. Conzemius and R. B. Evans, "Caregiver placebo effect for dogs with lameness from osteoarthritis," *Journal of the American Veterinary Medical Association*, vol. 241, no. 10, pp. 1314–1319, 2012.

[82] B. KuKanich, "Outpatient oral analgesics in dogs and cats beyond nonsteroidal antiinflammatory drugs," *Veterinary Clinics of North America*, vol. 43, no. 5, pp. 1109–1125, 2013.

[83] J. N. Farr, S. B. Going, T. G. Lohman et al., "Physical activity levels in patients with early knee osteoarthritis measured by accelerometry," *Arthritis and Rheumatism*, vol. 59, no. 9, pp. 1229–1236, 2008.

[84] L. M. Greene, D. J. Marcellin-Little, and B. D. Lascelles, "Associations among exercise duration, lameness severity, and hip joint range of motion in Labrador Retrievers with hip dysplasia," *Journal of the American Veterinary Medical Association*, vol. 242, no. 11, pp. 1528–1533, 2013.

[85] B. W. J. H. Penninx, W. J. Rejeski, J. Pandya et al., "Exercise and depressive symptoms: a comparison of aerobic and resistance exercise effects on emotional and physical function in older persons with high and low depressive symptomatology," *Journals of Gerontology B*, vol. 57, no. 2, pp. P124–P132, 2002.

[86] B. W. J. H. Penninx, S. P. Messier, W. J. Rejeski et al., "Physical exercise and the prevention of disability in activities of daily living in older persons with osteoarthritis," *Archives of Internal Medicine*, vol. 161, no. 19, pp. 2309–2316, 2001.

[87] W. H. Ettinger Jr., R. Burns, S. P. Messier et al., "A randomized trial comparing aerobic exercise and resistance exercise with a health education program in older adults with knee osteoarthritis: the Fitness Arthritis and Seniors Trial (FAST)," *Journal of the American Medical Association*, vol. 277, no. 1, pp. 25–31, 1997.

Hindawi Publishing Corporation
BioMed Research International
Volume 2013, Article ID 208912, 10 pages
http://dx.doi.org/10.1155/2013/208912

Research Article

Modification of a Rodent Hindlimb Model of Secondary Lymphedema: Surgical Radicality versus Radiotherapeutic Ablation

Hyung Sub Park,[1,2] In Mok Jung,[1,3] Geum Hee Choi,[2] Soli Hahn,[2] Young Sun Yoo,[4] and Taeseung Lee[1,2]

[1] *Department of Surgery, Seoul National University College of Medicine, Seoul 110-799, Republic of Korea*
[2] *Department of Surgery, Seoul National University Bundang Hospital, 166 Gumi-ro, Bundang-gu, Seongnam-si, Gyeonggi-do 463-707, Republic of Korea*
[3] *Department of Surgery, Seoul Metropolitan Government Seoul National University Boramae Medical Center, Seoul 156-707, Republic of Korea*
[4] *Department of Surgery, Chosun University Hospital, Chosun University College of Medicine, Gwangju 501-717, Republic of Korea*

Correspondence should be addressed to Taeseung Lee; tslee@snubh.org

Received 11 July 2013; Revised 7 September 2013; Accepted 9 September 2013

Academic Editor: Monica Fedele

Secondary lymphedema is an intractable disease mainly caused by damage of the lymphatic system during surgery, yet studies are limited by the lack of suitable animal models. The purpose of this study was to create an improved model of secondary lymphedema in the hindlimbs of rodents with sustained effects and able to mimic human lymphedema. This was achieved by combining previously reported surgical methods and radiation to induce chronic lymphedema. Despite more radical surgical destruction of superficial and deep lymphatic vessels, surgery alone was not enough to sustain increased hindlimb volume. Radiotherapy was necessary to prolong these effects, with decreased lymphatic flow on lymphoscintigraphy, but hindlimb necrosis occurred after 4 weeks due to radiation toxicity. The applicability of this model for studies of therapeutic lymphangiogenesis was subsequently tested by injecting muscle-derived stem cells previously cocultured with the supernatant of human lymphatic endothelial cells in vitro. There was a tendency for increased lymphatic flow which significantly increased lymphatic vessel formation after cell injection, but attenuation of hindlimb volume was not observed. These results suggest that further refinement of the rodent hindlimb model is needed by titration of adequate radiation dosage, while stem cell lymphangiogenesis seems to be a promising approach.

1. Introduction

Lymphedema is defined as the accumulation of tissue fluid as a consequence of impaired lymphatic drainage [1]. Its etiology may be either congenital or acquired, and it is estimated to affect approximately 140 to 250 million people worldwide [2]. The acquired form of lymphedema is more common and is mainly caused by destruction of the lymphatic system during surgery or radiation therapy. Unfortunately there is no known definite cure for lymphedema and most of the current treatment strategies are focused on conservative measures with treatment of secondary complications such as cellulitis/lymphangitis or malignant tumors.

Our understanding about the pathologic mechanisms of this disease and therapeutic approaches is limited by the lack of suitable animal models. The importance of animal models for preclinical studies is indisputable, and many researchers have proposed several animal models in the last several decades, which include canine, rabbit, and rodent models, but none of them have been able to reliably reproduce a sustained chronic effect similar to that found in human secondary (postsurgical) lymphedema [3]. The first models were created in dogs as early as 1888 by ligation of the lymphatic trunks in the hindlimb [4], and many modifications have been made since then, but none of the methods gained great acceptance because of the complexity of the procedure and the long

latency before the appearance of chronic lymphedema [5]. An alternative model was the rabbit ear model, first proposed in 1977, which had the anatomic advantage of having superficially located lymphatics and nonexistent deep lymphatic systems, making model creation easier and more reliable [6]. However, this method had problems regarding difficult reproducibility by other researchers with high dependence on the animals and conditions used. The rodent model was first introduced in the 1980s and is most widely used nowadays because of its easy accessibility, low cost, and shorter duration to obtain clinically relevant observations. Additionally, the rodent lymphatics present muscular patterns that are similar to humans than any other species, making physiologic studies more feasible [5]. There are two models of lymphedema in rodents: the tail model and the hindlimb model. The tail model is being used in most recent studies because of its procedural simplicity and its effectiveness in providing information about the molecular aspects of lymphangiogenesis. The hindlimb model, on the other hand, is more complex to create but is physiologically and anatomically more similar to human postsurgical lymphedema than the tail model and has the advantage of providing abundant tissue for harvesting.

These animal models can be used for studies of therapeutic lymphangiogenesis, which involves the regeneration of lymphatic vessels to restore lymphatic flow and improve lymphedema. Lymphangiogenesis has been shown to occur in adult tissues during inflammation, wound healing, and tumor metastasis [7]. Research in lymphangiogenesis has been possible due to identification of regulatory molecules and markers specific to the lymphatic endothelium, which include Prox-1, lymphatic vessel hyaluronan receptor-1 (LYVE-1), vascular endothelial growth factor receptor-3 (VEGFR-3 or Flt-4), and podoplanin. These markers are now specifically used as markers of lymphatic vessels.

In this study, we set out to determine whether a sustainable model of lymphedema can be created by more radical destruction of the lymphatic vessels using surgical and radiotherapeutic methods in rodent hindlimbs. The applicability of this model for studies of therapeutic lymphangiogenesis was investigated by injecting lymphatic endothelial cell (LEC) precursors previously differentiated from muscle-derived stem cells in vitro into the hindlimbs, and the potential role of stem cell therapy was assessed.

2. Materials and Methods

2.1. Animal Model for Lymphedema and Study Design. Under the approval of the Institutional Animal Care and Use Committee (IACUC) of Seoul National University Bundang Hospital for the whole study, Balb/c mice (male, 4 weeks old) were anesthetized using an intraperitoneal injection of 0.2 mL tiletamine/zolazepam (Zoletil, Virbac) and 0.15 mL xylazine (Rompun, Bayer). For detection of the lymphatic system, 0.05 mL of methylene blue was injected subcutaneously in the right distal hindlimb and the limb was intermittently flexed and extended for 30 min. A circumferential incision was made on the right hindlimb and a 1 cm wide circumferential strip of skin and subcutaneous tissue was resected. During the procedure, the medial neurovascular bundle was saved by meticulous dissection and gentle retraction to separate it from the surrounding tissue (Figure 1(a)). Further resection of the underlying muscle was done to destroy the deep lymphatic system (Figure 1(b)), and electrocauterization of the stained lymphatics as well as circumferentially along the proximal and distal margins was performed. The inguinal lymph nodes were also removed surgically using a surgical microscope system (Carl Zeiss) and remnant lymphatics were electrocauterized (Figure 1(c)). The resected muscle was restored by fixation to the surrounding tissue using a 5-0 polyglactin suture and the wound was covered with a strip of surgical glove to protect the wound from external damage or dehydration.

A total of 24 mice underwent this procedure for creation of lymphedema and were divided into 3 groups. In the Surgery group ($n = 8$), the above described surgical procedure was performed only, while, in the Surgery+RT group ($n = 8$), mice were exposed to 4500 cGy/3 fractions of radiotherapy at day 5 after surgery. Fractional doses of 1500 cGy were given to the inguinal area for 3 consecutive times with intervals between each fraction using a 6 MeV electron (Varian 21 EX linear accelerator), while the rest of the mouse body (except for the inguinal area) was shielded from radiation using lead blocks. In a third group, named the Cell therapy group ($n = 8$), the same surgical and RT procedures were performed, and injection of 1×10^7 cells of LEC precursors obtained from in vitro MDSC cocultured with HLEC (50% sup.) was given at 3 different locations in the hindlimb at day 5 immediately after RT. The same volume of saline was injected in the hindlimbs (both operated and contralateral nonoperated limbs) of the other groups to correct for volume discrepancies during subsequent volumetric analyses.

2.2. Water Displacement Volumetric Analysis. The degree of lymphedema was quantified by measuring the volume of the right (operated) hindlimb using a water displacement volumetry method. A 1.8 mL polypropylene tube (Nalge Nunc) was fully filled with saline and the right hindlimb was inserted into the tube up to the most proximal margin of the circumferentially excised wound. The overflowed saline was refilled using a 1 mL syringe and the volume of saline needed to fully refill the tube was indirectly used as an indicator of hindlimb volume. All mice were anesthetized during this procedure and the contralateral left limb was used as a control for normal hindlimb volume. Measurement was performed at 1, 3, and 5 days and 1, 2, 4, and 8 weeks and each measurement was performed 3 times by a single researcher to obtain a mean value.

2.3. Lymphoscintigraphy. Lymphoscintigraphy was performed at 8 weeks using a NanoSPECT/CT device (Bioscan). After intraperitoneal anesthesia, technetium-99m antimony sulfur colloid (Tc-99m ASC) was injected subcutaneously in the right foot and frames were taken at a speed of 15 seconds per frame for the first 5 minutes. A delayed frame was taken 40 minutes after injection. All necessary safety measures regarding radioactivity issues were taken.

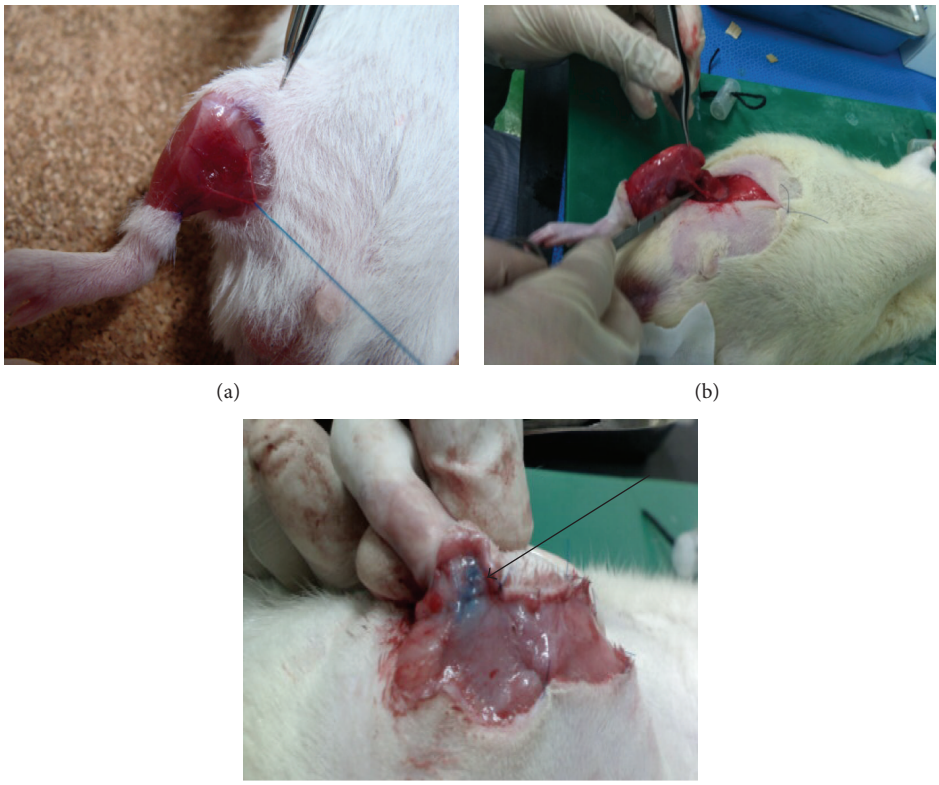

(a) (b)

(c)

Figure 1: Formation of lymphedema in the right hindlimb of Balb/c mice. (a) Meticulous dissection and preservation of the neurovascular bundle by gentle retraction. (b) Circumferential resection of strip of skin, subcutaneous tissue, and muscle to obliterate deep lymphatics. (c) Staining of lymph nodes and lymphatics after injection of methylene blue (black arrow) for lymphatic obliteration and lymph node dissection.

2.4. LYVE-1 IHC Staining of Lymphatic Capillaries. Tissue specimens from the right hindlimb were obtained at 1, 2, 4, and 8 weeks for immunohistochemical (IHC) staining and RT-PCR of lymphatic markers. For LYVE-1 3,3′-diaminobenzidine (DAB) IHC, tissues were fixed in 4% formalin, embedded in paraffin, and sectioned into 5–7 μm slices. After deparaffinization, rehydration, and blocking, the tissues were incubated with primary antibody for LYVE-1 (1 : 100, Abcam) at 4°C overnight. The next day, DAB staining was performed with the REAL Envision Detection System, Peroxidase/DAB+, and Rabbit/Mouse (Dako) according to the manufacturer's instructions, which sequentially conjugates secondary goat antigen and stains for DAB. LYVE-1 positive tubular structures were counted by from 4 random high-power microscope fields with Image Pro Plus 4.5 (Cybernetics Inc.) and the mean value was calculated.

2.5. In Vitro Lymphatic Differentiation of MDSCs and Lymphatic Marker Expression. The injected cells in the Cell therapy group were obtained by isolation of MDSCs from the gastrocnemius muscle of 4–6-week-old Balb/c mice using a modified preplate technique, as previously described [8, 9]. Human lymphatic endothelial cells (HLEC, ScienCell Research Laboratories) were cultured for 3 days until 80% confluence was achieved and the supernatant was moved to a new tube. Isolated MDSCs (50%) and the supernatant of HLECs (50%) were placed in a new culture medium and cocultured for 4 weeks for lymphatic differentiation.

To determine the differentiation of MDSCs to LEC precursors, the lymphangiogenic characteristics of MDSCs cocultured with 50% supernatant of HLECs were compared with native MDSCs and HLECs. The respective cells were seeded on plate slides (Nalge Nunc), fixed with cold methanol, and blocked for 30 min with 5% blocking solution (Dako). The primary antibody Prox-1 (1 : 100, Abcam) was added and incubated overnight at 4°C. For DAB staining, the REAL Envision Detection System, Peroxidase/DAB+, and Rabbit/Mouse (Dako) were used as described previously. Counterstaining with hematoxylin and mounting with DAPI were then performed and the slides were observed under microscopy. For immunofluorescence (IF) staining, the respective fluorescein isothiocyanate-(FITC-labeled) secondary antibody was incubated for 3 h at 4°C and mounted with DAPI and the slides were observed under microscopy. The expression of Prox-1 was quantified for the three different cell types by counting the number of positive cells from 4 random high-power fields, and the relative expression rate of native MDSCs and cocultured MDSCs against HLECs was determined.

Reverse transcriptase polymerase chain reaction (RT-PCR) was performed for lymphatic markers Prox-1, Flt-4, and podoplanin. Total RNA from the respective cells were

Table 1: RT-PCR primer sequences and product size.

Gene	Accession number	Primer sequence (forward, reverse)	Temp (°C)	Size (bp)
Prox-1	NM_002763.3	5′-GGAGATGGCTGAGAACAAGC-3′ 5′-AGACTTTGACCACCGTGTCC-3′	53	232
Flt-4	NM_182925	5′-GCTGTTGGTTGGAGAGAAGC-3′ 5′-TGCTGGAGAGTTCTGTGTGG-3′	53	213
Podoplanin	BC022812	5′-GCCAGTGTTGTTCTGGGTTT-3′ 5′-AGAGGTGCCTTGCCAGTAGA-3′	53	209
Actin	NM_001101.3	5′-GAGTCAACGGATTTGGTCGT-3′ 5′-TTGATTTTGGAGGGATCTCG-3′	51	200

extracted using the RNeasy Mini Kit (Qiagen) according to the manufacturer's instructions, and the quantity and quality of the extracted RNA were determined by absorbance at 260 nm and 280 nm wavelengths using the SmartSpec Plus Spectrophotometer (Bio-Rad). An oligonucleotide deoxythymidine primer was added to 2 μg of the extracted total RNA and incubated at 65°C for 10 min. The denatured RNA was mixed with 4 μL of 5x reaction buffer, 1 mM dNTP, 20 U of RNase inhibitor, and reverse transcriptase BioScript (Bioline) to make a final volume of 20 μLcDNA. For PCR amplification, cDNA equivalent to 500 ng of starting RNA was mixed with 20 pmol of forward and reverse primers with 10x PCR buffer (MangoMix, Bioline). The sequences of the PCR primers for lymphatic markers are shown in Table 1. PCR amplification was performed with PTC-200 PCR Thermal Cycler (MJ Research) using the following cycling conditions: 94°C for 2 min (initial denaturation), 94°C for 30 s, 53–55°C for 45 s, 72°C for 30 s (35 cycles), and 72°C for 10 min (final extension). PCR products were subjected to electrophoresis on 1-2% agarose gels containing ethidium bromide. Images were captured with a camera and the relative band intensities were analyzed with a computer-assisted bioimaging analyzer (EXT-20MX; Vilber Lourmat) after normalization against actin.

2.6. Statistical Analysis. All data are presented as means ± SE. Multiple comparisons were performed using a one-way ANOVA with post hoc test using Tukey's method. IBM SPSS Statistics 20 (IBM) was used for analysis, and differences were considered statistically significant when $P < 0.05$.

3. Results

3.1. Assessment of Animal Model for Lymphedema Formation. The degree of lymphedema in our animal model was measured by volumetric analysis using a water displacement method. The Surgery group showed a significant increase in volume of the operated right hindlimb compared to the contralateral normal hindlimb (used as control) at day 5, and there was a tendency for this difference to be maintained up to 1 week (Figure 2(a)). However, there was a decline in volume after 1 week, becoming similar to the normal contralateral hindlimb at 4 weeks, thus demonstrating that surgery alone was not able to produce a sustained effect for the study of chronic lymphedema. With the addition of radiotherapy at day 5, the Surgery+RT group showed a sustained volume increase after 1 week which was maintained up to 4 weeks compared to the Surgery group, although this difference failed to achieve statistical significance. Unfortunately, there was a high incidence of necrosis in hindlimbs of mice from the Surgery+RT group between 4 and 8 weeks, probably due to the toxicity of radiation exposure, which led to significant tissue loss, causing a dramatic decrease in volume during this period.

Lymphoscintigraphic findings between the Surgery and Surgery+RT groups demonstrate that, in the Surgery group, there was partial radioactive uptake in the inguinal area in the delayed images which was not observed in the Surgery+RT group (Figure 2(b)). In the Surgery+RT group, there was barely any movement of radioactive substance from the foot. These results have two implications: (1) RT was probably able to ablate the remnant lymphatics that were not fully destroyed by surgical methods, and (2) RT was able to suppress spontaneous regeneration of lymphatic vessels, thus completely obstructing lymphatic flow leading to increased hindlimb volume.

3.2. MDSCs Cocultured with HLEC. In order to assess the applicability of our animal model for studies of lymphangiogenesis, we differentiated stem cells into LEC precursors in vitro. MDSCs cocultured with the 50% supernatant of HLECs showed a change in cell morphology from a spindled shape to round shape under light microscopy, resembling the appearance of HLECs (Figure 3(a)). DAB staining of cells with lymphatic marker Prox-1 showed that native MDSCs had no expression, while cocultured MDSCs showed positive brown staining of the cytoplasm in morphologically MDSC-like cells (as shown by the same morphology of the nucleus). IF staining for Prox-1 also revealed a similar pattern, with MDSCs showing only DAPI stained nuclei while the coculture, as well as HLECs, showed a positive green fluorescence of the cytoplasm. Quantification of Prox-1 expression demonstrated that MDSCs had no expression while the coculture showed an expression rate of around 70% relative to HLECs (100%) (Figure 3(b)). At the genetic level, RT-PCR also showed a similar pattern, with native MDSCs showing no gene expression for lymphatic markers Prox-1, Flt-4, and podoplanin, while the coculture showed around 60% expression of these lymphatic markers with respect to HLECs (Figures 4(a) and 4(b)). These in vitro studies

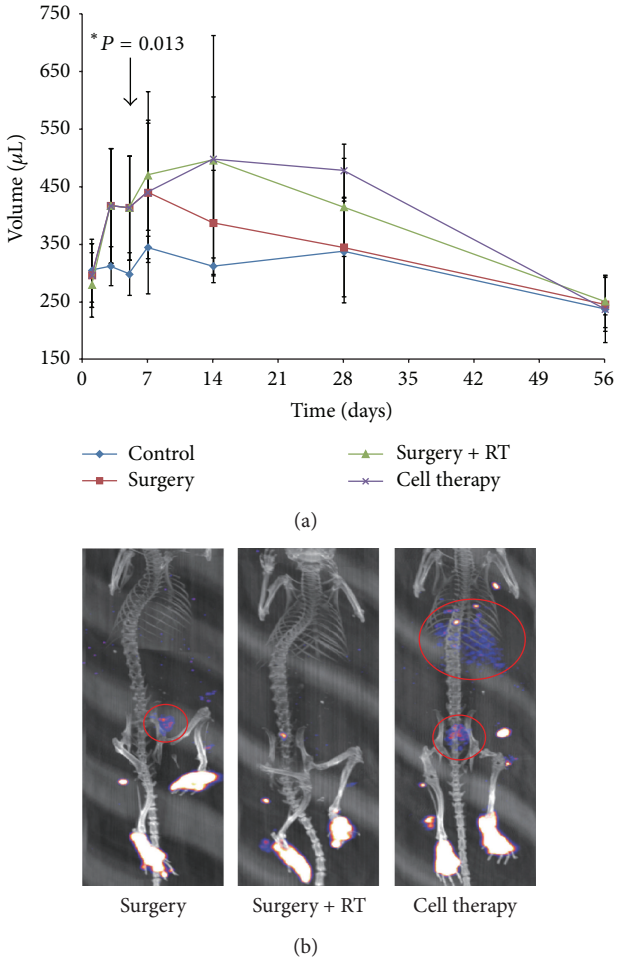

Figure 2: In vivo measurement of hindlimb volume and lymphatic flow. (a) Volume measurements of hindlimbs at different time intervals and compared against the normal left hindlimb. There is an overall increase in volume compared to the normal hindlimb, with statistical significance at day 5. This volume increase tends to be maintained after radiotherapy at 14 days, but this difference is lost at 56 days. (b) Lymphoscintigraphy shows an improvement in lymphatic flow after cell therapy as demonstrated by the collection of radioactive materials (red circles) in the proximal parts of the body compared to the other groups.

demonstrate that a coculture of MDSCs with the supernatant of HLECs can drive differentiation of MDSCs towards the lymphoendothelial lineage, showing expression of lymphatic markers at the genetic and cellular levels while maintaining the morphologic characteristics of MDSCs.

3.3. Effect of Cell Therapy on Lymphedema Attenuation. Injection of lymphoendothelial precursor cells derived from MDSCs into the hindlimbs after RT did not cause any attenuation of hindlimb volume during the whole study period (Figure 2(a)). Volumetric analysis of the Cell therapy group showed a similar pattern of volume to that of the Surgery+RT group, with a steep decline in volume after 4 weeks due to tissue loss. Lymphoscintigraphy, on the other hand, showed increased radioactive substances in the upper part of the body in the delayed frame images (Figure 2(b)), suggesting that lymphatic flow may be restored after cell therapy.

At the histological level, IHC for LYVE-1, a cell surface receptor on lymphatic endothelial cells, was performed from the specimens obtained at 1, 2, 4, and 8 weeks. The results showed that the Cell therapy group had an overall higher expression of brown stained tubular structures compared to the Surgery+RT or Surgery group (Figure 5(a)). Quantification of the lymphatic structures showed that at 1 week the Surgery+RT and Cell therapy groups had significantly lower number of lymphatics compared to the Surgery group (Figure 5(b)). This finding can be explained by the fact that radiotherapy and cell injection were done at day 5 and therefore there was immediate destruction of lymphatics by radiation without enough time for the effects of cell therapy to appear. However from 2 weeks, the Cell therapy group had higher lymphatic formation than the other groups which becomes statistically significant at 8 weeks.

4. Discussion

In this study we attempted to create a modified, more radical animal model of chronic lymphedema. Our animal model was similar to the prototype model proposed by Olszewski et al. [10] in canine limbs, which was first modified by Wang and Zhong [11] to be performed in rodents. Wang's rat hindlimb model involved circumferential incision and excision of a circular strip of skin and all subcutaneous tissue, identification and ligation of the main lymphatic trunks after dye injection, popliteal node excision, and suturing of the skin edges to the muscles. Lymphedema persisted up to 15 days postoperatively, but the difference was lost by 30 days, and the difference became significant again after 180 days. Despite the late reappearance of lymphedema after 6 months, this model was only partially successful in producing a sustained effect needed to study chronic lymphedema. In our study, we performed a more radical surgical ablation of the lymphatics, especially the deep lymphatic system, which may not have been fully ablated in Wang's model. To achieve this, we also resected the muscle down to the periosteum to fully divide all underlying deep lymphatics, and, after meticulous electrocauterization of any stained lymphatics, the muscle was sutured again to its original location. We also performed electrocauterization around the upper and lower circumferential resection margins, and the inguinal lymph nodes were removed using microsurgical techniques. Despite this radical surgical approach, our results showed that the edematous state did not persist beyond 1 week. Addition of radiation therapy was therefore performed in an attempt to fully destroy any remnant lymphatics that may not have been destroyed under surgical methods and to suppress spontaneous lymphatic vascular regeneration that may occur after surgery. Both Lee-Donaldson et al. [12] and Kanter et al. [13] used radiotherapy to induce lymphedema, but, in these studies, the degree of surgical ablation of the lymphatics was less radical, ranging from regional groin

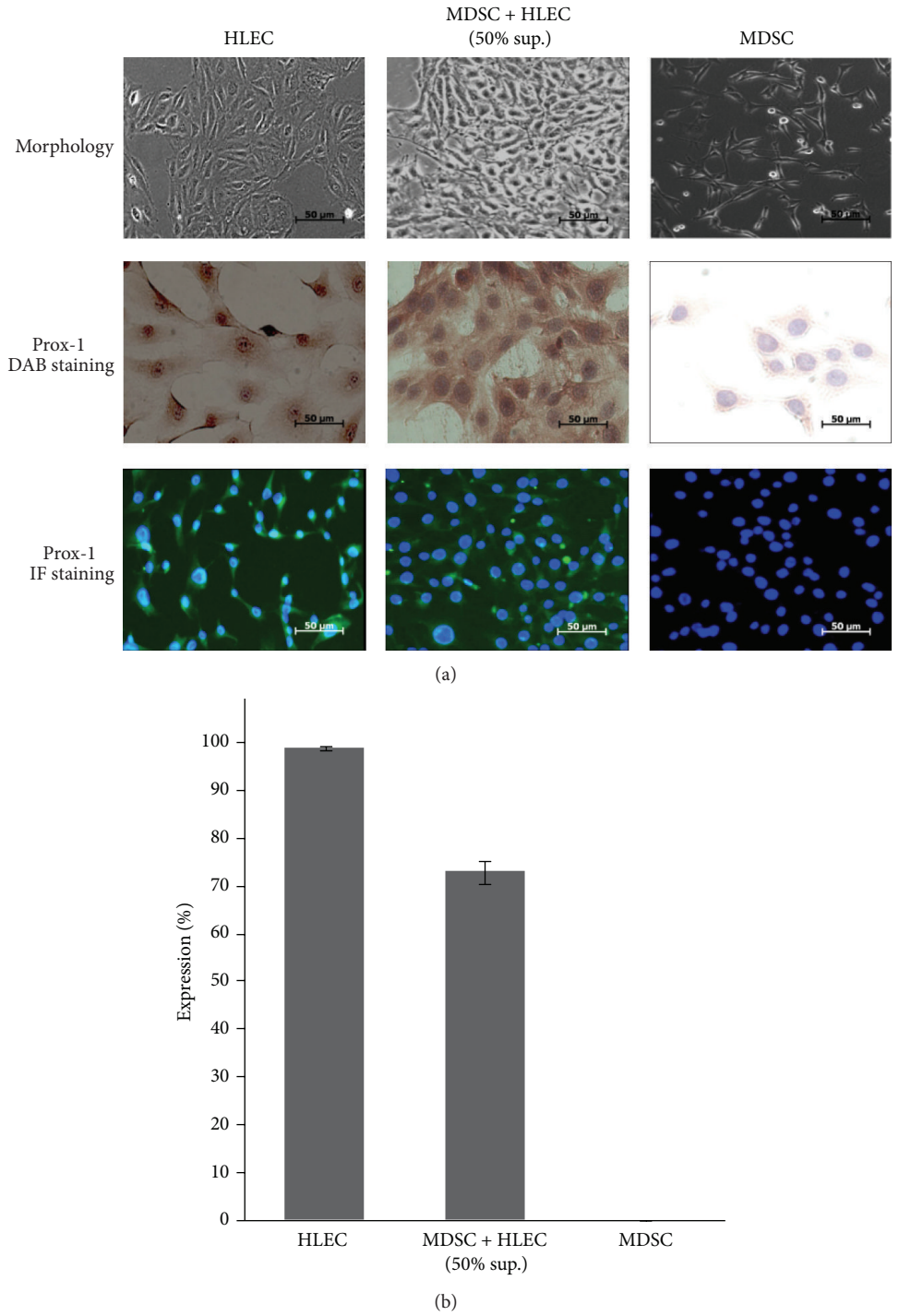

Figure 3: Coculture of MDSCs with the supernatant of HLECs demonstrates differentiation of MDSCs towards the lymphatic lineage. (a) The coculture MDSC + HLEC (50% sup.) shows a change in morphology, as shown by the change from a spindled shape (MDSC) to a rounder shape, resembling the morphology of HLECs. The coculture also shows positive expression of Prox-1 under DAB and IF staining, while native MDSCs show negative expression (400x magnification). (b) Graphical representation of Prox-1 expression rate showing 70% expression in the coculture compared to negative expression in native MDSCs.

lymphatic ablation with lymph node dissection only (Lee-Donaldson) to circumferential excision of skin and subcutaneous tissue and deep lymphatic ablation after dye injection but without muscle resection or lymph node dissection (Kanter). The radiation dose used in our study was 4500 rads, which was the same dose used by the previous studies on rodents. Lymphedema was sustained for a longer period of time after radiotherapy, but necrosis of the hindlimb after

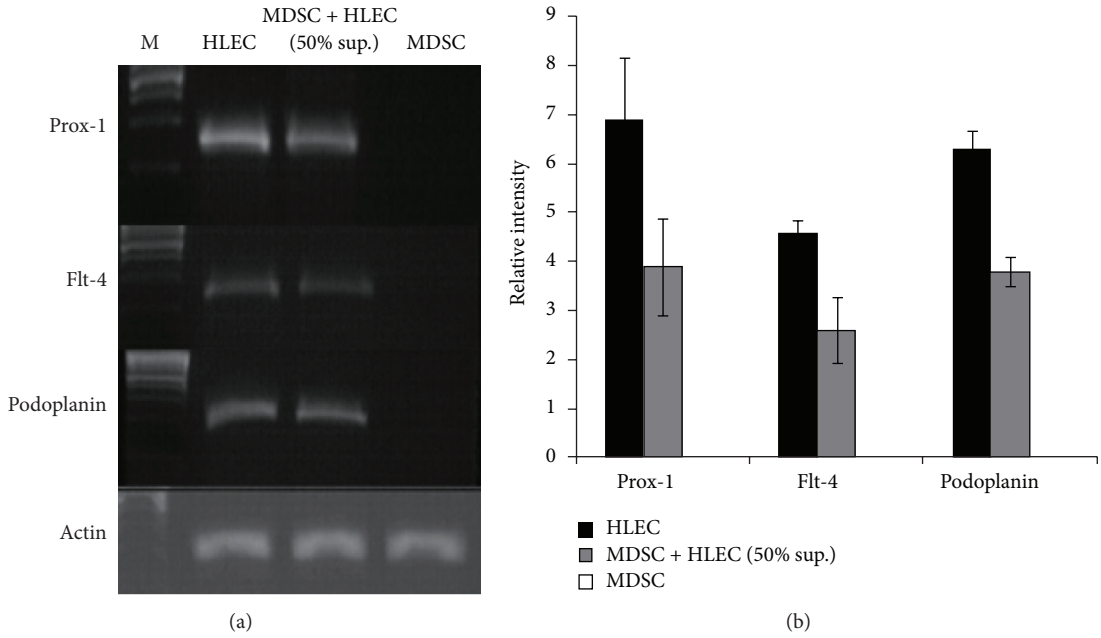

Figure 4: Upregulation of lymphatic specific genes after coculture of MDSCs with the supernatant of HLECs. (a) RT-PCR demonstrates negative expression of genes for Prox-1, FLt-4, and podoplanin in native MDSCs, while the coculture demonstrates upregulation of these genes. (b) Graphical representation of gene expression rate normalized against actin. There is upregulation of genes for Prox-1, FLt-4, and podoplanin after coculture compared to native MDSCs.

4 weeks was found, probably due to the toxicity of radiation, making further volumetric analyses inappropriate. The same problems were also faced in the previous studies, suggesting that an adjustment of the radiation dose is necessary to overcome this problem. In fact, previous studies in canine models have used radiation doses of 1200 to 1500 rads [14, 15], suggesting that the dose of 4500 rads in smaller rodents may be too toxic. Yet, our results are in accordance with previous studies in that RT is a necessary procedure to induce sustained lymphedema after surgery. The fact that the radicality of the surgical procedure to destroy potential deep lymphatics did not affect the duration of lymphedema may suggest that the role of RT is greater in the suppression of lymphatic regeneration and collateral circulation rather than total ablation of remnant lymphatics.

In terms of the applicability of our model for the study of therapeutic lymphangiogenesis, the necrosis of the hindlimb tissue after RT made volumetric analysis studies inappropriate. A refinement of the model is necessary, yet it is also possible that the cell therapy effect may not have been enough to produce substantial changes in volume. One possible explanation may be that the therapeutic dose may not have been achieved by a single injection. A previous study of stem cell lymphangiogenesis achieved lymphedema regression by performing weekly injections of stem cells [16]. Despite these problems, the lymphoscintigraphic findings and the increased lymphatic vessel formation in our IHC studies after cell therapy suggest that the model can be used to analyze functional aspects of lymphatic flow and provide for histopathologic information, the latter being an advantage of the rodent hindlimb model compared to the tail model (abundant tissue for harvesting).

In our study, we did not investigate the histopathologic characteristics associated with chronic lymphedema, which include findings such as increased number of fibroblasts, adipocytes, keratinocytes, mononuclear inflammatory cells, and ultimately skin thickening with subcutaneous tissue fibrosis [17]. However, we found that calgranulin (both A and B) genetic expression was increased from RT-PCR studies of harvested hindlimb tissues at 4 and 8 weeks in the Surgery+RT group and even higher in Cell therapy group (data not shown). Calgranulin is a gene known to be related to inflammation and it has been reported to be expressed with high specificity in microarray studies of lymphedema [18]. RT has the effect of producing an inflammatory response which is needed to produce the effects observed in human chronic lymphedema, and a higher inflammatory response in the Cell therapy group can be explained by the fact that inflammatory response to lymph stasis acts as an important trigger for postnatal lymphangiogenesis [19, 20].

With regard to therapeutic lymphangiogenesis, we have proposed a different approach using stem cells instead of the more commonly used VEGF-C. Previous studies have mainly used VEGF-C administered either as single injections [21] or by gene transfer into plasmid DNAs encoding human VEGF-C [22]. Other growth factors such as HGF [23] and PDGF-BB [24] have also been reported. However, stem cells have the advantage that they have potential for multilineage differentiation and self-regeneration [25], which can be used to increase lymphangiogenesis effectively. The

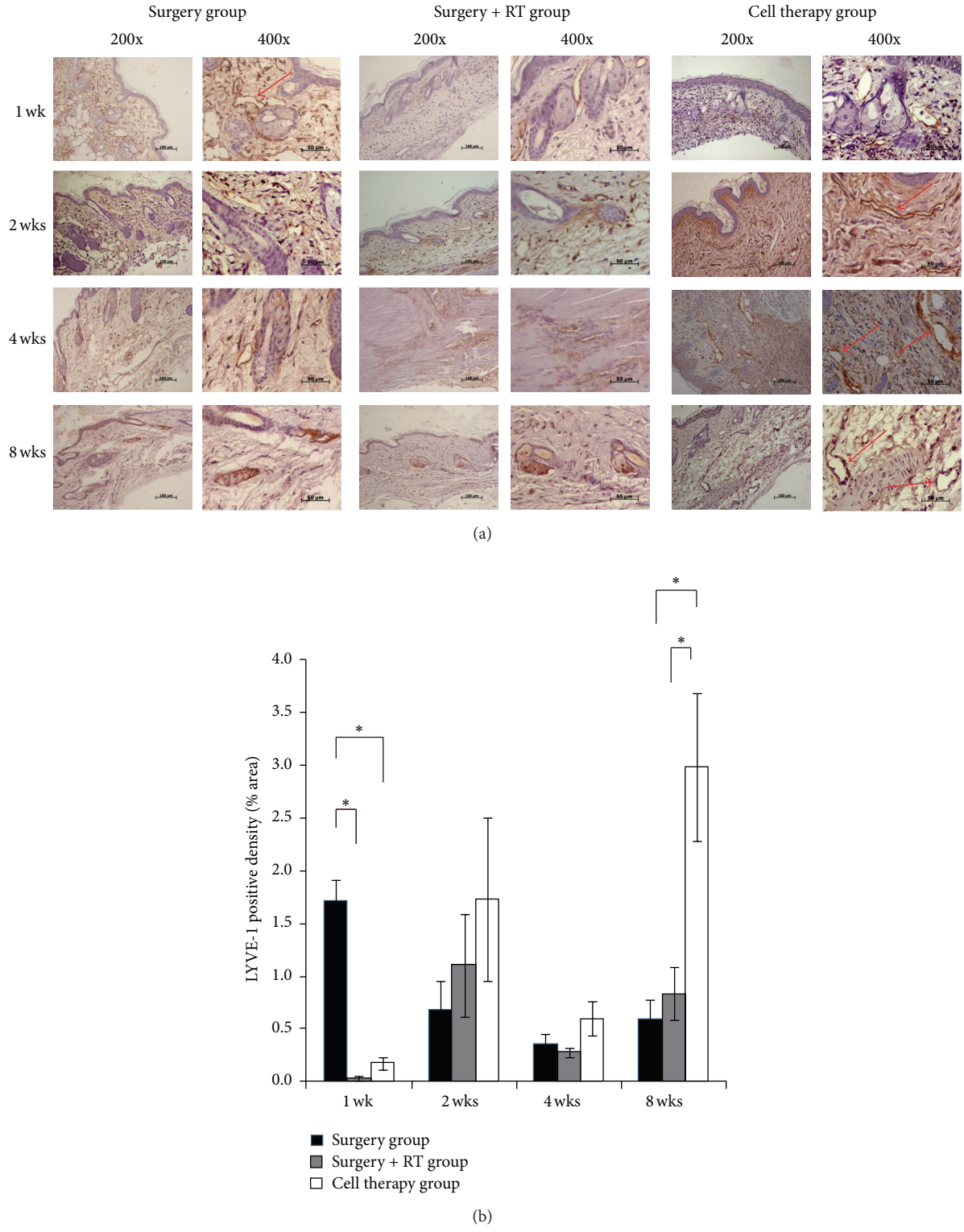

FIGURE 5: Increase in formation of LYVE-1 positive lymphatic structures after injection of differentiated stem cells (a) LYVE-1 IHC staining from harvested tissues at 1, 2, 4, and 8 weeks, showing increased formation of LYVE-1 positive lymphatic structures (arrows) in the Cell therapy group. (b) Graphical representation of LYVE-1 positive lymphatic structure density, showing an overall increased density at 2, 4, and 8 weeks in the Cell therapy group. Asterisk (∗) represents $P < 0.05$.

role of stem cells in lymphangiogenesis was first described by Liersch et al. [26] by use of embryonic stem cells stimulated with both VEGF-C and VEGF-A, but, since then, only few reports on the potential role of stem cells for treatment of lymphedema can be found [16, 27–29]. Our study is one of the few studies that have used adult somatic stem cells, with the advantage that MDSCs originate from one of the most abundant and easily obtainable sources, and its efficacy and freedom from malignant transformation have been widely studied [30].

Overall, we were not able to create a reliable model of chronic lymphedema despite our more radical approach using both surgical and radiotherapeutic methods. Our study was also limited by a short study period of only 8 weeks, and thus late effects such as delayed reappearance of lymphedema could not be assessed. The effects of cell therapy on attenuation of lymphedema were not evident from a volumetric approach, which demonstrates the need for a refined animal model, especially a titration for optimal radiation dosage. However, the tendency for functional improvement of lymphatic flow and increased lymphatic vessel formation suggest that there is still room for improvement of this model and that stem cells can be a promising tool for use in therapeutic lymphangiogenesis.

Conflict of Interests

There is no conflict of interests.

Authors' Contribution

Hyung Sub Park and In Mok Jung have contributed equally to this work as co-first author.

Acknowledgments

This study was supported by the 2010 Lee Yong Kak-Astellas Research Grant from the Korean Society for Vascular Surgery. This study was presented orally at Vascular 2012 Conference, held in Melbourne, Australia, in October 20–23, 2012.

References

[1] A. Szuba and S. G. Rockson, "Lymphedema: classification, diagnosis and therapy," *Vascular Medicine*, vol. 3, no. 2, pp. 145–156, 1998.

[2] J. E. Zuther, *Lymphedema Management: The Comprehensive Guide for Practitioners*, Thieme, New York, NY, USA, 2nd edition, 2009.

[3] W. S. Shin, A. Szuba, and S. G. Rockson, "Animal models for the study of lymphatic insufficiency," *Lymphatic Research and Biology*, vol. 1, no. 2, pp. 159–169, 2003.

[4] B. Delius, *Uber die Regeneration der Lymphdrusen [Dissertation]*, 1888, quoted by A. W. Meyer, "An experimental study on the recurrence of lymphatic glands and the regeneration of lymphatic vessels in the dog," *Bulletin of the Johns Hopkins Hospital*, vol. 17, p. 185, 1906.

[5] C. Hadamitzky and R. Pabst, "Acquired lymphedema: an urgent need for adequate animal models," *Cancer Research*, vol. 68, no. 2, pp. 343–345, 2008.

[6] J. R. Casley Smith, L. Clodius, and M. Foldi, "Experimental blood vascular and lymphatic occlusion in the rabbit ear and the effect of benzopyrones," *Arzneimittel-Forschung*, vol. 27, no. 2, pp. 379–382, 1977.

[7] T. Tammela and K. Alitalo, "Lymphangiogenesis: molecular Mechanisms and Future Promise," *Cell*, vol. 140, no. 4, pp. 460–476, 2010.

[8] H. S. Park, S. Hahn, G. H. Choi, Y. S. Yoo, J. Y. Lee, and T. Lee, "Muscle-Derived stem cells promote angiogenesis and attenuate intimal hyperplasia in different murine vascular disease models," *Stem Cells and Development*, vol. 22, no. 6, pp. 866–877, 2013.

[9] H. S. Park, G. H. Choi, S. Hahn, Y. S. Yoo, J. Y. Lee, and T. Lee, "Potential role of vascular smooth muscle cell-like progenitor cell therapy in the suppression of experimental abdominal aortic aneurysms," *Biochemical Biophysical Research Communications*, vol. 431, no. 2, pp. 326–331, 2013.

[10] W. Olszewski, Z. Machowski, J. Sokolowski, and J. Nielubowicz, "Experimental lymphedema in dogs," *Journal of Cardiovascular Surgery*, vol. 9, no. 2, pp. 178–183, 1968.

[11] G.-Y. Wang and S.-Z. Zhong, "A model of experimental lymphedema in rats' limbs," *Microsurgery*, vol. 6, no. 4, pp. 204–210, 1985.

[12] L. Lee-Donaldson, M. H. Witte, M. Bernas, C. L. Witte, D. Way, and B. Stea, "Refinement of a rodent model of peripheral lymphedema," *Lymphology*, vol. 32, no. 3, pp. 111–117, 1999.

[13] M. A. Kanter, S. A. Slavin, and W. Kaplan, "An experimental model for chronic lymphedema," *Plastic and Reconstructive Surgery*, vol. 85, no. 4, pp. 573–580, 1990.

[14] S. K. Das, J. D. Franklin, B. M. O'Brien, and W. A. Morrison, "A practical model of secondary lymphedema in dogs," *Plastic and Reconstructive Surgery*, vol. 68, no. 3, pp. 422–428, 1981.

[15] H.-C. Chen, J. J. Pribaz, B. M. O'Brien, K. R. Knight, and W. A. Morrison, "Creation of distal canine limb lymphedema," *Plastic and Reconstructive Surgery*, vol. 83, no. 6, pp. 1022–1026, 1989.

[16] C. Conrad, H. Niess, R. Huss et al., "Multipotent mesenchymal stem cells acquire a lymphendothelial phenotype and enhance lymphatic regeneration in vivo," *Circulation*, vol. 119, no. 2, pp. 281–289, 2009.

[17] S. G. Rockson, "Lymphedema," *American Journal of Medicine*, vol. 110, no. 4, pp. 288–295, 2001.

[18] R. Tabibiazar, L. Cheung, J. Han et al., "Inflammatory manifestations of experimental lymphatic insufficiency," *PLoS Medicine*, vol. 3, no. 7, article e254, 2006.

[19] A. Ristimäki, K. Narko, B. Enholm, V. Joukov, and K. Alitalo, "Proinflammatory cytokines regulate expression of the lymphatic endothelial mitogen vascular endothelial growth factor-C," *Journal of Biological Chemistry*, vol. 273, no. 14, pp. 8413–8418, 1998.

[20] C. Mouta and M. Heroult, "Inflammatory triggers of lymphangiogenesis," *Lymphatic research and biology*, vol. 1, no. 3, pp. 201–218, 2003.

[21] A. Szuba, M. Skobe, M. J. Karkkainen et al., "Therapeutic lymphangiogenesis with human recombinant VEGF-C," *The FASEB Journal*, vol. 16, no. 14, pp. 1985–1987, 2002.

[22] Y.-S. Yoon, T. Murayama, E. Gravereaux et al., "VEGF-C gene therapy augments postnatal lymphangiogenesis and ameliorates secondary lymphedema," *Journal of Clinical Investigation*, vol. 111, no. 5, pp. 717–725, 2003.

[23] Y. Saito, H. Nakagami, R. Morishita et al., "Transfection of human hepatocyte growth factor gene ameliorates secondary lymphedema via promotion of lymphangiogenesis," *Circulation*, vol. 114, no. 11, pp. 1177–1184, 2006.

[24] R. Cao, M. A. Björndahl, P. Religa et al., "PDGF-BB induces intratumoral lymphangiogenesis and promotes lymphatic metastasis," *Cancer Cell*, vol. 6, no. 4, pp. 333–345, 2004.

[25] B. M. Deasy, R. J. Jankowski, and J. Huard, "Muscle-derived stem cells: characterization and potential for cell-mediated therapy," *Blood Cells, Molecules, and Diseases*, vol. 27, no. 5, pp. 924–933, 2001.

[26] R. Liersch, F. Nay, L. Lu, and M. Detmar, "Induction of lymphatic endothelial cell differentiation in embryoid bodies," *Blood*, vol. 107, no. 3, pp. 1214–1216, 2006.

[27] T. Kono, H. Kubo, C. Shimazu et al., "Differentiation of lymphatic endothelial cells from embryonic stem cells on OP9 stromal cells," *Arteriosclerosis, Thrombosis, and Vascular Biology*, vol. 26, no. 9, pp. 2070–2076, 2006.

[28] K. Harada, T. Yamazaki, C. Iwata et al., "Identification of targets of Prox1 during in vitro vascular differentiation from embryonic stem cells: functional roles of HoxD8 in lymphangiogenesis," *Journal of Cell Science*, vol. 122, no. 21, pp. 3923–3930, 2009.

[29] J. H. Hwang, I. G. Kim, J. Y. Lee et al., "Therapeutic lymphangiogenesis using stem cell and VEGF-C hydrogel," *Biomaterials*, vol. 32, no. 19, pp. 4415–4423, 2011.

[30] B. M. Deasy, B. M. Gharaibeh, J. B. Pollett et al., "Long-term self-renewal of postnatal muscle-derived stem cells," *Molecular Biology of the Cell*, vol. 16, no. 7, pp. 3323–3333, 2005.

Hindawi Publishing Corporation
BioMed Research International
Volume 2013, Article ID 410631, 8 pages
http://dx.doi.org/10.1155/2013/410631

Research Article

A Novel Closed-Chest Porcine Model of Chronic Ischemic Heart Failure Suitable for Experimental Research in Cardiovascular Disease

Giuseppe Biondi-Zoccai,[1] Elena De Falco,[1] Mariangela Peruzzi,[1] Elena Cavarretta,[1] Massimo Mancone,[2] Omar Leoni,[3] Maria Emiliana Caristo,[3] Marzia Lotrionte,[4] Antonino G. M. Marullo,[1] Antonio Amodeo,[5] Luca Pacini,[1] Antonella Calogero,[1] Vincenzo Petrozza,[1] Isotta Chimenti,[1] Fabrizio D'Ascenzo,[6] and Giacomo Frati[1,7]

[1] *Department of Medico-Surgical Sciences and Biotechnologies, Sapienza University of Rome, Corso della Repubblica 79, 04100 Latina, Italy*
[2] *Department of Cardiovascular, Respiratory, Nephrologic, Anesthesiologic and Geriatric Sciences, Sapienza University of Rome, Viale del Policlinico 155, 00161 Rome, Italy*
[3] *Center of Experimental Research, Catholic University of Rome, Largo Agostino Gemelli 8, 00168 Rome, Italy*
[4] *Division of Cardiology, Catholic University of Rome, Largo Agostino Gemelli 8, 00168 Rome, Italy*
[5] *Department of Cardiac Surgery, Bambino Gesù Hospital, Piazza di Sant'Onofrio 4, 00165 Rome, Italy*
[6] *Division of Cardiology, University of Turin, Corso Bramante 88-90, 10126 Turin, Italy*
[7] *IRCCS Neuromed, Via Atinense 18, 86077 Pozzilli, Italy*

Correspondence should be addressed to Giuseppe Biondi-Zoccai; gbiondizoccai@gmail.com

Received 18 July 2013; Accepted 12 August 2013

Academic Editor: Andrea Vecchione

Cardiac pathologies are among the leading causes of mortality and morbidity in industrialized countries, with myocardial infarction (MI) representing one of the major conditions leading to heart failure (HF). Hitherto, the development of consistent, stable, and reproducible models of closed-chest MI in large animals, meeting the clinical realism of a patient with HF subsequent to chronic ischemic necrosis, has not been successful. We hereby report the design and ensuing application of a novel porcine experimental model of closed-chest chronic ischemia suitable for biomedical research, mimicking post-MI HF. We also emphasize the key procedural steps involved in replicating this unprecedented model, from femoral artery and vein catheterization to MI induction by permanent occlusion of the left anterior descending coronary artery through superselective deployment of platinum-nylon coils, as well as endomyocardial biopsy sampling for histologic analysis and cell harvesting. Our model could indeed represent a valuable contribution and tool for translational research, providing precious insights to understand and overcome the many hurdles concerning, and currently quenching, the preclinical steps mandatory for the clinical translation of new cardiovascular technologies for personalized HF treatments.

1. Introduction

Cardiac pathologies are among the leading causes of mortality and morbidity in industrialized countries, with heart failure (HF) representing the final common pathway for many diseases that affect the heart and defining a syndrome characterized by inadequate performance of the heart that negatively affects whole body blood supply [1]. Myocardial infarction (MI) is one of the major conditions leading to HF, having an ominous impact on public health in terms of mortality and morbidity [2]. The hemodynamic overload generated by MI imposes mechanical and neurohumoral modifications on cardiac walls, triggering complex biological responses that culminate in tissue remodeling. This response initially starts as compensatory left ventricular hypertrophy but eventually evolves towards maladaptive remodeling,

possibly triggering transition to HF. The cascade of events that begins with cardiac hypertrophy, attempting to set on a compensatory response and finally leading to HF, is characterized by contractile dysfunction and cell death of stressed cardiomyocytes, reduced capillary density, inflammation and fibrosis [3]. To date available medical treatments aim more at preserving residual, albeit compromised, cardiac function rather than at restoring lost functions. Besides, available drug therapies act by decreasing cardiac workload by reducing heart rate and blood pressure (such as β-blockers), preserving blood flow in coronaries (such as nitrates), and by blocking or reversing the remodeling process (such as angiotensin-converting enzyme (ACE) inhibitors), while not addressing the specific issue of recovering the loss of function due to massive muscular death. Even cardiac surgery remains a palliative management, not always suitable for catastrophic events like large myocardial damage due to huge infarction and cell demise.

However, all research approaches focusing on the improvement of cardiac function by cell therapy have hitherto encountered only incomplete success and generated conflicting results with no clear evidence of heart regeneration potential, which is mainly due to unsolved issues related to low survival and engraftment rate of injected cells, as well as the occurrence of complications such as inflammation or fibrosis [4]. In that sense, the scientific community has now to take a step back as the clinical outcome highlighted by the most recent clinical trials has only partially mirrored the expected results based on preclinical animal models, in terms of actual engraftment, survival, differentiation, and functional recovery.

Thus, the development of a consistent, stable, and reproducible model of closed-chest MI and cell delivery is mandatory as an efficient and realistic tool for the preclinical evaluation of cell therapy procedures. Nowadays, in the scholarly literature, several in vivo animal models reproducing HF are available as a result of genetic modifications, surgical ligature of the coronary arteries (with or without reperfusion), microembolization, cryoinjuries to the epicardium, electrical stimulation at a rapid pace, modifications of load, or toxic pharmacological treatments [5–10]. All these models have certainly allowed us to improve our mechanistic knowledge, but they do not go far enough in meeting the clinical reality of a patient with HF subsequent to chronic ischemia. Indeed, small animal models such as rodents have provided significant insights into human cardiac pathophysiology. Specifically, rodent and human hearts are greatly different in their dimension, structure, heart rate, oxygen consumption, regional and global contractility, protein expression, and even in resident stem cell populations [11], with the consequent and clear need for models of HF in large animals. The emergence of such large animal models in cardiovascular research fields such as MI, HF, valvular disease, heart transplantation, and ventricular assist devices (VAD) reflects the close similarity of these animals to human anatomy and physiology. The size of pigs (e.g., female Landrace pigs, weighing 30–35 kg, aged 3–12 months) allows the use of surgical equipment and imaging modalities similar to those used in humans, aiming at reproducing a real clinical situation with the employment of human-sized instruments while enabling the development and application of a unique model close to the clinical reality of a patient with HF.

In the light of this, our aim was to devise and apply a novel porcine closed-chest experimental model for biomedical research, describing how to perform a full procedure from femoral artery and vein catheterization to MI creation by minimally invasive transcatheter permanent coronary occlusion at the level of the left anterior descending artery (LAD) with selective deployment of intraluminal coils. We also describe transcatheter endomyocardial bioptic sample collection in order to isolate, characterize, and expand autologous resident cardiac progenitor cells [12], representing the basis for the clinical translation of new possible protocols for regenerative medicine. Results from this report aim at proposing a consistent, stable, reproducible, and, most importantly, clinically relevant model of closed-chest MI and ensuing HF, resembling more realistically the medical history of a patient with this condition, and thus representing a more accurate pathophysiological model to test possible cardiac progenitor cell-based technologies for personalized HF treatments closer to clinical translation.

2. Materials and Methods

2.1. In Vivo Experimental Protocol. All animals were handled in compliance with the European Convention on Animal Care and received humane care in accordance with the Principles of Laboratory Animal Care and the Guide for the Care and Use of Laboratory Animals. The experimental protocol was approved by local authorities and by the bioethical committee of the Catholic University, Rome, Italy (Protocol CESA/P/52/2012-13/12/2012).

2.2. Animal Preparation and Anesthesia. Experimental preparation and surgical protocol were performed under sterile conditions. Atropine (0.02 mg/kg IM), ketamine (15 mg/kg IM), and diazepam (0.1 mg/kg IM) were used for premedication, and intravenous access was obtained with a 21- or 22-Gauge needle in the ear vein. Anesthesia was induced by IV injection of ketamine (35 mg/kg) and diazepam (0.1 mg/kg). All animals were intubated with an endotracheal tube of 5 to 7 mm internal diameter, and general anesthesia was maintained with 1% to 2% isoflurane supplemented with oxygen, both supplied by an Aliseo mechanical ventilator (Datex Ohmeda, General Electric, Fairfield, CN, USA) and a constant rate IV infusion of propofol at 6 mg/kg/h for the first two hours and then at 4 mg/kg. Muscle relaxation was obtained with a constant rate IV infusion of atracurium besylate (0.5 mg/kg). Ventilator parameters were set according to each animal body weight (tidal volume 10 mL/kg, respiratory rate 16/minute, I/E 1 : 2, FiO2 40%, heart rate 70/130 bpm, SBP 110–120/70–80 mm Hg, central venous pressure 4–10 mm Hg). During the anesthesia we used a IV infusion of Ringer Lactate crystalloid solution of 10 mL/kg. In order to prevent infection, we administered enrofloxacin (5 mg/kg qd IM for 5 days), whereas for the intra- and postoperatory pain relief we used tramadol at 2/4 mg/kg bid

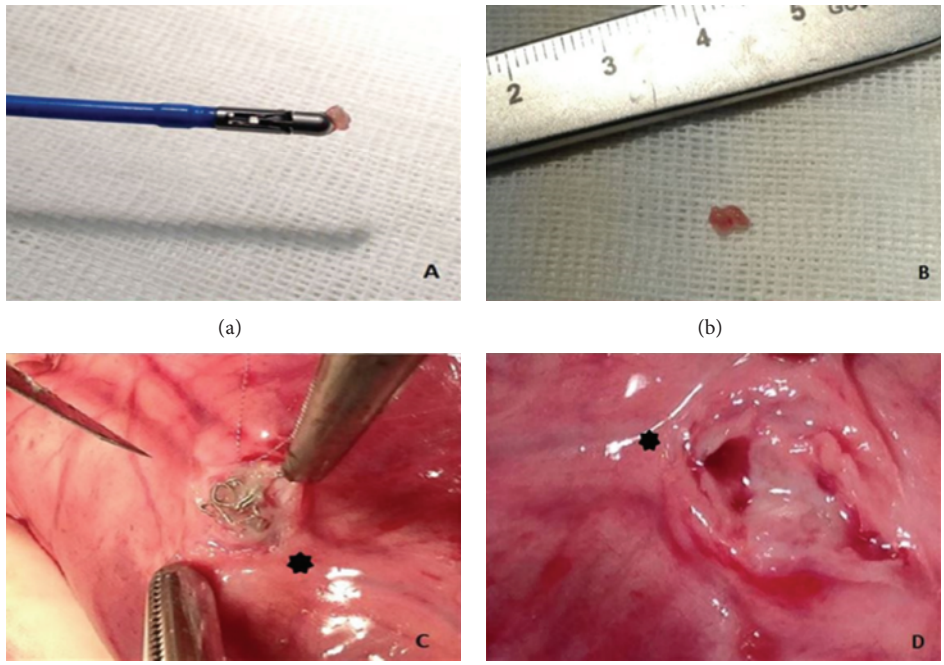

(a) (b)

(c) (d)

Figure 1: ((a) and (b)) Ventricular biopsies obtained using a standard clinical cardiac bioptome introduced through a 7-French sheath. (c) Evidence of the intraluminal platinum-nylon coil (Axium, Covidien, Mansfield, MA, USA) at 1 month followup (distal left anterior descending (LAD) represented by the star). (d) Evidence of the coronary lumen at 1 month highlighting the segment of the coronary vessel distal to the occluded segment (distal LAD represented by the star).

IM/EV for the first 48 h, followed by ketoprofen: 2 mg/kg qd IM for further 3 days. Before starting all the procedures (about 30 minutes prior to the intervention) an IV infusion of 1.0–2.5 mg/kg amiodarone was started in order to prevent possible ventricular arrhythmias, and 2000 IU heparin IV was administered in order to avoid thromboembolic phenomena.

2.3. Ventriculography, Bioptic Sampling, and Coil Deployment. The right femoral artery was willingly punctured in all animals according to Seldinger and cannulated with a short 5-French sheath exchanged for a 90 cm 7-French sheath (Cordis, Miami, FL, USA). Left ventriculography was performed in a right anterior oblique projection, with injection of dye through either a 5-French pigtail catheter (Boston Scientific, Natick, MA, USA), a 5-French Amplatz Right 1 diagnostic catheter (Boston Scientific), deployed by means of a 300 cm 0.035″ angiographic guide wire (Boston Scientific), or the 7-French sheath. Then, endomyocardial biopsy was performed aiming at the interventricular septum with a 7-French device (BiPal, Cordis). After obtaining a suitable number of endomyocardial samples (5 to 7 per animal, each weighing from 10 to 50 mg, see Figure 1), the bioptome was exchanged for an Amplatz Right 1 or Amplatz Left 1 Judkins Right guiding catheters, which were used to cannulate the left coronary artery for selective coronary arteriography and coil deployment. A 0.014″ J-tipped floppy angioplasty guide wire (ChoICE PT floppy, Boston Scientific) was then inserted into the LAD under fluoroscopic guidance, and coronary occlusion was achieved by deploying one or more 4.0 × 10 mm platinum-nylon microcoils (Axium, Covidien, Mansfield, MA, US) distally to the ostium of the first major diagonal branch. To further ensure that the occlusion was permanent, 20 mg of protamine was administered IV after deployment of the coil. Complete cessation of flow into the distal LAD was then confirmed by angiography in all cases (Figure 2). Amiodarone was discontinued 30 minutes after the evidence of ischemia, even if only one case of significant arrhythmias occurred. After all the procedures animals were gradually weaned from anesthesia and allowed to recover in specific single cages. For postoperatory pain relief we used tramadol at 2/4 mg/kg bid IM/IV for the first 48 hours, followed by ketoprofen: 2 mg/kg qd IM for further 3 days. All animals were monitored (4 times/day) and handled in compliance with the European Convention on Animal Care and received humane care in accordance with the Principles of Laboratory Animal Care and the Guide for the Care and Use of Laboratory Animals.

2.4. Electrocardiography and Echocardiography. To assess for signs of acute myocardial injury, continuous monitoring by electrocardiography (ECG) was performed. Changes in 12-lead ECG were also appraised to confirm ongoing MI, recording at 25 mm/s, 40 Hz, and 10 mm/mV in all anesthetized and immobilized animals in a supine position. Catheters and sheaths were removed, with hemostasis achieved with manual compression, while transthoracic echocardiography (1 hour after-procedure) was performed to evaluate wall

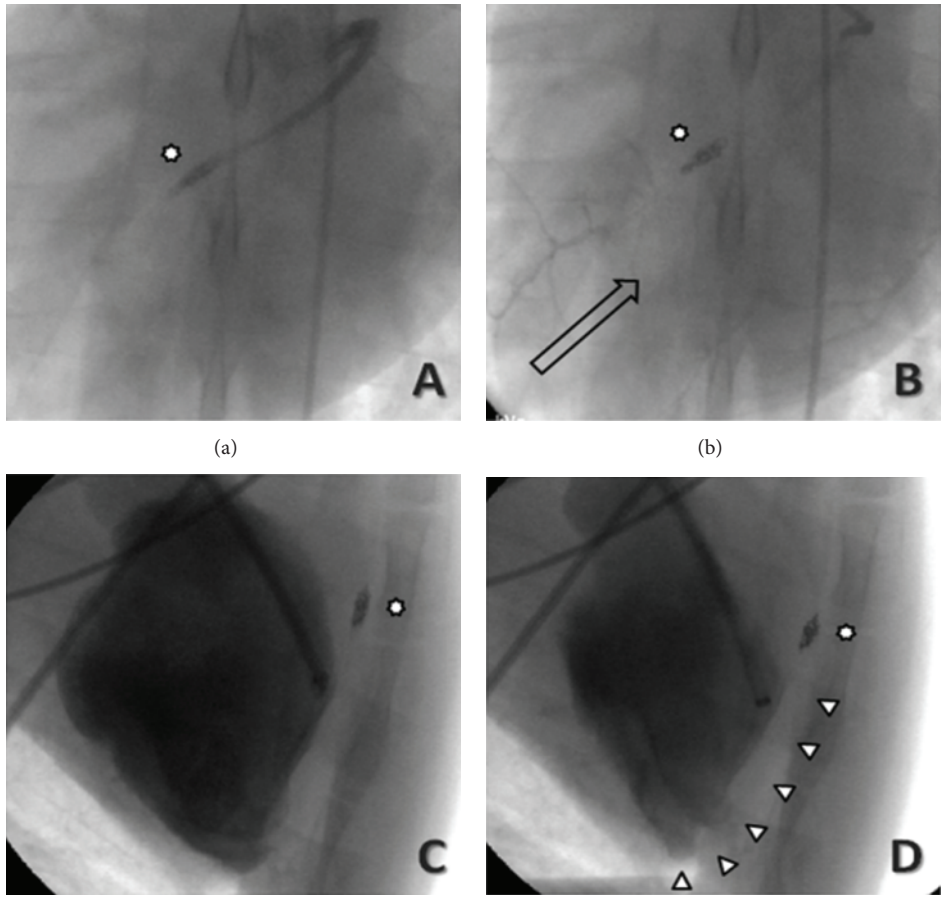

(a) (b)

(c) (d)

Figure 2: Coronary angiography of the occlusion of the mid tract of the left anterior descending coronary leading to myocardial infarction after deploying an intraluminal platinum-nylon coil (Axium, Covidien, Mansfield, MA, USA) at (a) 1 month followup (star represents the coil), with retrograde collateral flow from the left circumflex (b). Follow-up ventriculography showing the diastolic (c) and systolic (d) phases. Arrowheads represent the akinetic segments.

motion abnormalities, confirming in real time the presence of hypokinesia/akinesia of the anterior-lateral wall. Echocardiographic evaluation was performed at baseline, 1 hour after the occlusion, and then at 1-week and 1-month followup. Animals were investigated both in a right and left lateral positions. An experienced cardiologist performed all echocardiographic studies. A commercially available CX-50 machine (Philips, Andover, MA, USA), equipped with a 1–5 MHz probe (S5-1 PureWave sector array), was used for all examinations. Two-dimensional and M-mode data were acquired in parasternal long- and short-axis views at the level of papillary muscles and in apical four-chamber view. At least three consecutive beats were acquired and digitally recorded for off-line analysis performed by two experienced cardiologists with proprietary software (Philips). Left ventricular (LV) diameters, thicknesses, ejection fraction (LVEF), fractional shortening (LVFS), and LV volumes were obtained. The euthanasia was obtained after 30 days with the administration of Tanax (0.3 mL/kg IV; Intervet Italia, Segrate, Italy).

Hearts were explanted, rinsed 8–10 times with saline solution for a total of 5 minutes, prepared by surgical opening of the right and left atria and immediately submerged in a medical grade formaldehyde-buffered solution in sterile conditions for histological and immunohistochemical assessment.

2.5. Tissue Processing and Histology. After sacrifice, hearts were harvested and fixed with formaldehyde 4% (Kaltek, Padua, Italy) for 48 hours. The presence and the location of the infarct area were assessed by two expert clinical pathologists through macroscopic examination. Paraffin sections (2 μm) were then obtained from fixed hearts (PM2255 microtome, Leica, Solms, Germany) and stained with haematoxylin/eosin in the automated station St 5020 (Leica) to microscopically analyse the myocardial tissue. Subsequently, tissue sections were stained with Masson's Trichrome (Menarini, Parma, Italy, cat. N° 04010802), and images were acquired by a DSIGHT Fluo microscope (Menarini).

3. Results

3.1. Functional Evaluation. One out of 5 animals (20%) showed ventricular fibrillation immediately after permanent

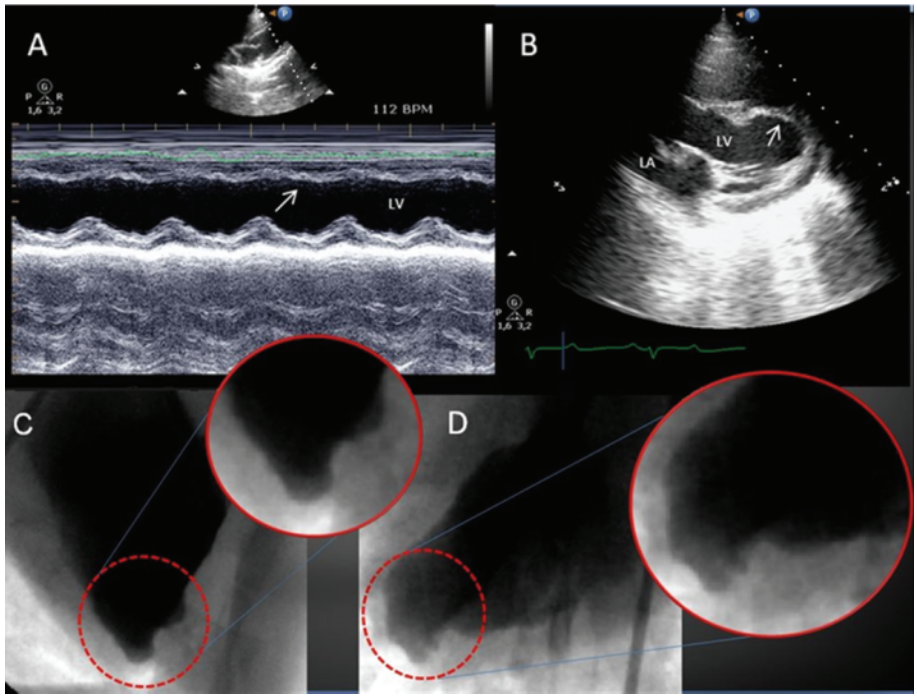

Figure 3: (A) Echocardiography at 1 month: M-mode image of left ventricle (LV); the arrow points at the anterior interventricular septum, which appears severely hypokinetic/akinetic, in comparison with the posterior wall. (B) Two-dimensional parasternal long axis; the LV apex appears remodeled and aneurysmatic (arrow), and wall thickness is markedly reduced in comparison with the basal segment. LA: left atrium. Follow-up ventriculography (1 month), with magnified views, showing a remodeled and aneurysmatic LV apex, in the right oblique (C) and anteroposterior (D) views.

LAD occlusion, and in this case resuscitation was achieved with repeated adrenaline boluses (10 mcg/kg IV) and a single biphasic DC shock at 200 Joules. Heart rates were detected at baseline (79.7 ± 3.5 bpm), soon after the occlusion (100.1 ± 7.3 bpm) and during all the phases of chronic HF subsequent to permanent coronary occlusion (85.3 ± 5.9 bpm). ECG was performed at baseline, continuously during the intervention (pre-, intra-, and postcoronary occlusion), at 1 week and at the end of the experiment confirming in all significant ST-segment elevation in the acute phase and a necrosis pattern afterwards.

Coronary occlusion with the subsequent MI resulted in immediate reduction in LVEF and LVFS, from 62.7 ± 2.3% to 45.3 ± 5.1% and from 33.6 ± 1.6% to 22.1 ± 2.9%, respectively. Ongoing remodeling of the LV was evident by continued reduction in LVEF and LVFS over the following 4 weeks (from 45.3 ± 5.1% to 35.9 ± 3.2% and from 22.1 ± 2.9% to 18.2 ± 4.3%, resp.,) and by an increase in LV end-diastolic diameters and volumes (Table 1). M-mode imaging of left ventricle showed a severely hypokinetic/akinetic anterior interventricular septum, in comparison with the posterior wall (Figure 3). Two-dimensional parasternal long-axis view evidenced an aneurysmatic left ventricular apex, with the distal and median wall thicknesses markedly reduced in comparison with the basal segment that resulted normokinetic (Figure 3). This seems to mirror the LV remodeling observed in humans after a MI.

Coronary angiography (Figure 2) performed at 1 month highlighted the completeocclusion of the mid tract of the LAD consequent to the deployment of the intraluminal platinum-nylon coil. In two out of five animals (20%), selective coronary angiography of the LAD at 1-month followup showed a faint retrograde collateral flow from the left circumflex (Figure 2). Follow-up ventriculography performed at 1 month confirmed the presence of akinetic segments corresponding to the lateral wall of LV and a remodeled and aneurysmatic apex (Figures 2 and 3).

Mortality in this series was 0% likely in reason of the fact that, after the set-up stage, we always deployed the platinum-nylon microcoils distally to the ostium of the first major diagonal branch. Indeed, deployment of the microcoil proximally to the ostium of the first major diagonal branch resulted in immediate ventricular fibrillation unresponsive to pharmacological and/or electrical treatment, in keeping with prior experiences with very proximal LAD balloon occlusion [9].

3.2. Histological Analysis. All hearts showed transmural scar and massive fibrosis consistent with acute coronary occlusion due to thrombosis [13]. The infarct area was white, shrunken, thin, and firm. The average of total infarct area corresponds to 31.8 ± 1.5 cm^2 (Figure 4). Healed infarcts displayed a white scar surrounded by small areas with congestion and vasodilatation. The ventricular wall was thinned as it appears in transmural infarction. Indeed the infarcts occupied more than 60% of the LV wall, from the subendocardial to the epicardial surface. Microscopic

Table 1: Basal and postacute myocardial infarction echocardiographic data.

Echocardiographic data	Basal	Post-AMI 1 hour	Post-AMI 1 week	Post-AMI 1 month
LV end-diastolic diameter (mm)	41.6 ± 1.7	40.8 ± 1.9	42.8 ± 1.2	46.7 ± 1.3
LV end-systolic diameter (mm)	27.6 ± 1.2	31.7 ± 0.8	33.7 ± 3.3	38.3 ± 1.3
LV end-diastolic volume (mL)	77.1 ± 7.2	73.5 ± 8.2	84.3 ± 8.3	99.9 ± 4.6
LV end-systolic volume (mL)	28.7 ± 3.6	40.2 ± 2.5	47.3 ± 2.6	63.2 ± 5.1
LV ejection fraction (%)	62.7 ± 2.3	45.3 ± 5.1	42.8 ± 1.7	35.9 ± 3.2
LV fractional shortening (%)	33.6 ± 1.6	22.1 ± 2.9	21.2 ± 6.9	18.2 ± 4.3

LV: left ventricle.

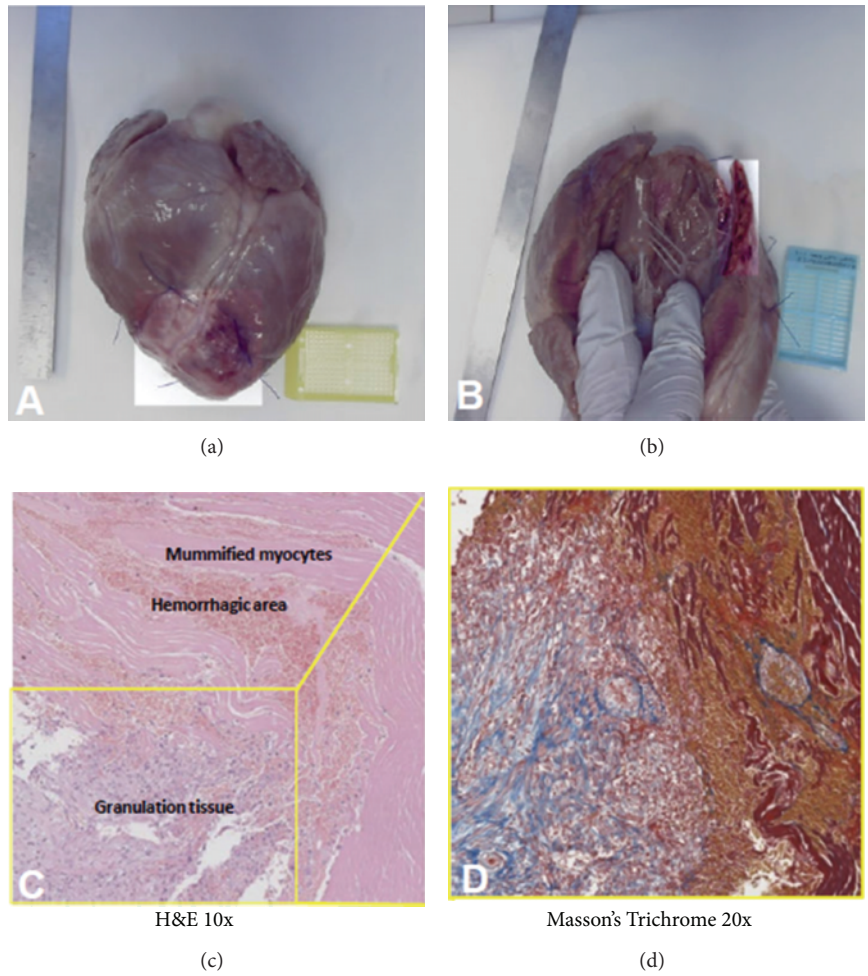

Figure 4: (a) Macroscopic analysis of the porcine heart showing the infarcted area, which appears brighter than the rest of the myocardium. (b) Ventricular wall appears thinned in the area of transmural infarction. (c) Hematoxylin/eosin (H&E) staining of the porcine model showing the haemorrhagic and the necrotic zones in the infarcted area. Infiltration of granulation tissue and fibroblastic/macrophagic cells is also observed (10x magnification). (d) Masson's Trichrome staining on a selected area of the section confirming both fibrotic connective and granulation tissues (20x magnification).

findings demonstrate the presence of granulation tissue with a large number of macrophages often engulfed with debris of the necrotic myocytes and hemosiderin. Fibroblasts actively producing collagen were found in the area of healing as well as angiogenesis. Rare eosinophils were also present within the chronic inflammatory areas. The central area of infarction showed a small unhealed zone with mummified myocytes and limited necrosis. Hemorrhagic areas were also present. Masson's Trichrome staining confirmed the presence of fibrotic area evenly distributed in the tissue sections. Representative images of histology analysis are displayed in Figure 4.

4. Discussion

In the last two decades, rapid advances have been made in understanding genetic, molecular, and pathophysiological pathways involved in the development and homeostasis of the mammalian heart, as well as perturbations that may influence cardiac physiology. Despite all this, to date reliable animal models, both suitable for research purposes and closely resembling human heart failure, still do not exist. The importance to develop such models is based on major limitations that occur particularly with murine in vivo models, which show relevant physiological differences with human hearts [11], although very useful and less expensive than large animals.

Among large animals, pigs are certainly preferred, due to the collateral coronary circulation and arterial anatomy very similar to humans and most importantly because it is even possible to predict the infarct size [14–16]. Moreover, animal models of HF, as opposed to isolated cells or organs, permit a more accurate, realistic, and complete analysis of the physiological effects of cardiac dysfunction, which are of great importance in the overall HF epiphenomenon.

In this study we have attempted to address the key issue of creating an animal model of HF which could simplify an extremely complex and challenging syndrome into manageable cardiovascular research questions. Specifically, the major novelty of our model lies in the fact that for the first time we propose a chronic post-MI HF model with a real LV remodeling, based on a closed-chest technique [17], combined with the permanent occlusion of the LAD. This model has been conceived to allow the possibility of safely performing afterward a surgical operation such as a VAD implantation or a stem cells delivery without the jeopardy of a redo procedure, consequently avoiding all related complications such as surgical adherences, bleeding, and prolonged surgical times. The present model, once optimized the coil deployment site, seems also to have the advantage of dramatically reduced mortality (nihil in our current experience), possibly reducing also the overall cost of research. The validation of our model has been confirmed by the histological analysis, showing pathological features of a 4-week-old MI, very similar to nonreperfused or delayed-reperfused MI (6 to 12 hours). Accordingly, other models exploiting a transient coronary occlusion followed by reperfusion (opposed to our model of a permanent coronary occlusion) do not reflect the current clinical practice, in reason of the fact that the vast majority of patients with acute MI does not receive a reperfusion therapy before 3 to 4 hours from symptoms onset or does not receive it at all [9]. Therefore, this technique might help to more easily mimic the pathophysiology of nonreperfused or delayed-reperfused MI.

In the future, we envision exploiting further this model and evaluating whether it can also prove useful and suitable for cell therapy applications, by obtaining and injecting autologous cardiac resident stem cells and by implantation of left VAD (LVAD) without the challenges of a redo procedure. All research approaches focusing on the improvement of cardiac function by cell therapy have hitherto encountered only incomplete success and generated conflicting results with no clear evidence of heart regeneration potential, which is mainly due to unsolved issues related to low survival and engraftment rate of injected cells, as well as the occurrence of complications such as inflammation or fibrosis [4, 18–20]. In that sense, the scientific community has now to take a step back as the clinical outcome highlighted by the most recent clinical trials has only partially mirrored the expected results based on preclinical animal models, in terms of actual engraftment, survival, differentiation, and functional recovery. Thus, the development of a consistent, stable, and reproducible model of closed-chest MI and biopsy collection is mandatory as a realistic tool for the preclinical evaluation of cell therapy procedures.

Despite the obvious impossibility of selecting one single swine model as the best fitting or performing for all kinds of research needs, nevertheless compared to current surgical in vivo models, our approach could represent a new promising tool for a more realistic clinical translation of novel regenerative medicine technologies.

This work has several strengths but also some key limitations. The limited sample size, performance by a team of highly skilled clinician investigators, veterinarians, and pathologists, all thoroughly experienced in animal experimental research spanning from small and large sizes, and use of sophisticated equipments and devices may limit the external validity of our results. However, we are confident that applying this model in a similar setting by similarly experienced and skilled operators will yield similarly satisfactory and precise results.

5. Conclusion

It is clear that an intriguing question concerns the choice of the animal model balancing researcher's options between convenience, cost, physiological applicability, and real correspondence to the original human model. We are also aware that a unique animal model cannot exist. Despite all these limitations, large animals still remain the best tool to investigate severe diseases such as cardiovascular diseases.

Conflicts of Interests

All authors declare that they do not have a direct financial relation with the commercial identities mentioned in the present paper that might lead to a conflict of interests.

Authors' Contribution

Giuseppe Biondi-Zoccai and Elena De Falco contributed equally to this work.

Acknowledgments

This study was supported by funds from the Italian Ministry of Health (Programmi di Ricerca Fondi 5 × mille) to Giacomo Frati. Profs. Filippo Crea, Ernesto Greco, Massimo Massetti, and Mauro Rinaldi provided input on developmental aspects of the experimental model. We are also thankful to all

personnel of the Center of Experimental Research, Catholic University, Rome, Italy, for their kind and skilful technical assistance.

References

[1] E. Braunwald, "Heart failure," *Journal of the American College of Cardiology*, vol. 1, no. 1, pp. 1–20, 2013.

[2] A. S. Go, D. Mozaffarian, V. L. Roger et al., "Executive summary: heart disease and stroke statistics—2013 update: a report from the American Heart Association," *Circulation*, vol. 127, no. 1, pp. 143–152, 2013.

[3] D. Carnevale, G. Cifelli, G. Mascio et al., "Placental growth factor regulates cardiac inflammation through the tissue inhibitor of metalloproteinases-3/tumor necrosis factor-α-converting enzyme axis: crucial role for adaptive cardiac remodeling during cardiac pressure overload," *Circulation*, vol. 124, no. 12, pp. 1337–1350, 2011.

[4] S. Koudstaal, S. J. Jansen Of Lorkeers, R. Gaetani et al., "Concise review: heart regeneration and the role of cardiac stem cells," *Stem Cells Translational Medicine*, vol. 2, no. 6, pp. 434–443, 2013.

[5] A. Halapas, A. Papalois, A. Stauropoulou et al., "In vivo models for heart failure research," *In Vivo*, vol. 22, no. 6, pp. 767–780, 2008.

[6] L. Barandon, J. Calderon, P. Réant et al., "Adjustment and characterization of an original model of chronic ischemic heart failure in pig," *Cardiology Research and Practice*, vol. 1, no. 1, Article ID 542451, 2010.

[7] J. D. Schmitto, K. O. Coskun, S. T. Coskun et al., "Hemodynamic changes in a model of chronic heart failure induced by multiple sequential coronary microembolization in sheep," *Artificial Organs*, vol. 33, no. 11, pp. 947–952, 2009.

[8] S.-X. Zhou, J. Lei, C. Fang, Y.-L. Zhang, and J.-F. Wang, "Ventricular electrophysiology in congestive heart failure and its correlation with heart rate variability and baroreflex sensitivity: a canine model study," *Europace*, vol. 11, no. 2, pp. 245–251, 2009.

[9] Y. Suzuki, J. K. Lyons, A. C. Yeung, and F. Ikeno, "In vivo porcine model of reperfused myocardial infarction: in situ double staining to measure precise infarct area/area at risk," *Catheterization and Cardiovascular Interventions*, vol. 71, no. 1, pp. 100–107, 2008.

[10] W. G. Kim, Y. C. Shin, S. W. Hwang, C. Lee, and C. Y. Na, "Comparison of myocardial infarction with sequential ligation of the left anterior descending artery and its diagonal branch in dogs and sheep," *International Journal of Artificial Organs*, vol. 26, no. 4, pp. 351–357, 2003.

[11] R. Breckenridge, "Heart failure and mouse models," *DMM Disease Models and Mechanisms*, vol. 3, no. 3-4, pp. 138–143, 2010.

[12] I. Chimenti, R. Gaetani, L. Barile et al., "Isolation and expansion of adult cardiac stem/progenitor cells in the form of cardiospheres from human cardiac biopsies and murine hearts," *Methods in Molecular Biology*, vol. 879, pp. 327–338, 2012.

[13] A. G. Freifeld, E. H. Schuster, and B. Healy Buckley, "Nontransmural versus transmural myocardial infarction. A morphologic study," *American Journal of Medicine*, vol. 75, no. 3, pp. 423–432, 1983.

[14] Y. Suzuki, A. C. Yeung, and F. Ikeno, "The representative porcine model for human cardiovascular disease," *Journal of Biomedicine and Biotechnology*, vol. 2011, Article ID 195483, 10 pages, 2011.

[15] J. H. Geens, S. Trenson, F. R. Rega, E. K. Verbeken, and B. P. Meyns, "Ovine models for chronic heart failure," *International Journal of Artificial Organs*, vol. 32, no. 8, pp. 496–506, 2009.

[16] M. Bjerre, H. Jensen, J. D. Andersen et al., "Chronic ischemic mitral regurgitation induced in pigs by catheter-based coronary artery occlusion," *The Journal of Heart Valve Disease*, vol. 17, no. 3, pp. 283–289, 2008.

[17] G. A. Krombach, S. Kinzel, A. H. Mahnken, R. W. Günther, and A. Buecker, "Minimally invasive close-chest method for creating reperfused or occlusive myocardial infarction in swine," *Investigative Radiology*, vol. 40, no. 1, pp. 14–18, 2005.

[18] R. Gaetani, G. Rizzitelli, I. Chimenti et al., "Cardiospheres and tissue engineering for myocardial regeneration: potential for clinical application," *Journal of Cellular and Molecular Medicine*, vol. 14, no. 5, pp. 1071–1077, 2010.

[19] E. Forte, I. Chimenti, L. Barile et al., "Cardiac cell therapy: the next (re)generation," *Stem Cell Reviews and Reports*, vol. 7, no. 4, pp. 1018–1030, 2011.

[20] E. Abdelwahid, T. Siminiak, L. C. Guarita-Souza et al., "Stem cell therapy in heart diseases: a review of selected new perspectives, practical considerations and clinical applications," *Current Cardiology Reviews*, vol. 7, no. 3, pp. 201–212, 2011.

Hindawi Publishing Corporation
BioMed Research International
Volume 2013, Article ID 423147, 8 pages
http://dx.doi.org/10.1155/2013/423147

Review Article

Models of Abnormal Scarring

Bommie F. Seo, Jun Yong Lee, and Sung-No Jung

Department of Plastic and Reconstructive Surgery, Uijeongbu St. Mary's Hospital, College of Medicine, Catholic University of Korea, 65-1 Kumoh-Dong, Uijeongbu 480-135, Republic of Korea

Correspondence should be addressed to Sung-No Jung; jsn7190@catholic.ac.kr

Received 23 June 2013; Revised 31 July 2013; Accepted 2 August 2013

Academic Editor: Monica Fedele

Keloids and hypertrophic scars are thick, raised dermal scars, caused by derailing of the normal scarring process. Extensive research on such abnormal scarring has been done; however, these being refractory disorders specific to humans, it has been difficult to establish a universal animal model. A wide variety of animal models have been used. These include the athymic mouse, rats, rabbits, and pigs. Although these models have provided valuable insight into abnormal scarring, there is currently still no ideal model. This paper reviews the models that have been developed.

1. Introduction

Keloids are defined as pathologic scars that grow beyond the confines of the original injury [1]. They occur in areas of cutaneous injury, and they are benign, dermal fibroproliferative tumors, with no malignant potential [2, 3]. They are characterized by an excessive deposition of extracellular matrix components, namely, collage, fibronectin, elastin, proteoglycans, and growth factors. There is a higher incidence among African-Americans, Asian-Americans, Latin-Americans, and other darker pigmented ethnicities. Reports of familial cases and parallelism in identical twins imply a genetic contribution to the pathophysiology [4]. Keloids cause cosmetic deformities but are usually asymptomatic. However, some may grow large enough to cause functional limitations, especially when located along the joint.

The term "keloid" is derived from the Greek word *chele*, which means crab's claw, a comparison to the horizontal growth of the tissue into the normal skin [2]. This characteristic, among others, differentiates them from hypertrophic scars. Hypertrophic scars are fibrous tissue outgrowth with excessive scarring, which are confined to the original wound margins [5]. These scars usually develop within a couple of months after initial wound development, grow rapidly for several months, and then gradually regress over the next few years. Keloids may develop far after initial injury, persist for extensive periods of time, and usually do not regress. Keloids also have increased fibroblast density and proliferation rates, larger, thicker, more wavy collagen fibers, and an increased ratio of type I to type III collagens, unlike hypertrophic scars [6–8]. Hypertrophic scars contain more type III collagen, fibers oriented more parallel to the epidermal surface, with nodules consisting of myofibroblasts. They slowly process through the normal healing cycle of inflammation, proliferation, and maturation, while the keloid scar does not [9].

Keloids and hypertrophic scars are one of the most infuriating clinical problems in wound healing. There is still no single, unified hypothesis that explains the pathogenesis of keloid formation. This fact is underscored by the multiple treatment options for keloids including excision, intralesional steroids, adjuvant radiation therapy, laser, silicone, pressure therapy, and combination therapies [10–15]. Some have advocated that intralesional triamcinolone, surgical excision, and radiation actually promote recurrence [2, 10, 16].

The suggested hypotheses for the derailing of normal scar formation in keloids are alteration in growth factors and extracellular matrix components via epithelial keratinocyte-mesenchymal fibroblast interactions or hypoxia-induced angiogenetic responses, alteration in collagen turnover, alteration in the keloid fibroblast response to various growth factors, mechanical tension-induced fibroblast proliferation and collagen synthesis, genetic immune dysfunction,

and immunological reaction to sebum [17–22]. A multifactorial inheritance model may be the underlying cause of such alterations [4].

Animal models provide valuable translational vehicles for human treatment modalities. However, as these aberrant scars are specific to humans, the development of an animal model for hypertrophic scarring or keloids has been extremely difficult. A major difference between laboratory animals and humans is the presence of the panniculus carnosus in animals, a fibromuscular layer enabling the skin to slide over underlying fascia. This facilitates rapid contraction and faster healing of burn wounds.

The lack of a universal animal model for such scarring has been an obstacle in developing a successful therapeutic strategy. Many groups have attempted to generate animal models, and this collective process has helped to elucidate most of what we now know of this perplexing entity. In this paper, we describe the wide variety of animal models that have been developed and used in the history of scar research.

2. Experimental Models of Abnormal Scarring

Keloid or hypertrophic scars have been extensively studied through two types of basic research approaches, either through animal models or through tissue or cell cultures. In earlier research, combined studies on both hypertrophic and keloid scars were common because differentiation between these two entities had not been established.

2.1. Animal Models. There are two main approaches in the development of the animal model. The earlier approach is to induce an innate keloid-like scar in animals. However, such scars were only maintained for a very limited time period and usually developed characteristics of hypertrophic scars. The other approach is to transplant human keloid or hypertrophic scar tissue into animals. Recent studies have integrated tissue engineering with animal models, transplanting cultured human keloid tissue into animals for longer survival.

2.1.1. Induction of Abnormal Scars. Different methods of wounding have been inflicted upon various animals to induce hypertrophic or keloid scars. In 2001, Sullivan et al. performed a review of the literature to compare the adequacy of laboratory animals as a model for human wound healing. Studies on wound dressings, topical antimicrobials, and growth factors using humans, pigs, rabbits, guinea pigs, rats, and mice were examined. The authors found 78% agreement between humans and pigs, 53% agreement between humans and small mammals, and 57% agreement between humans and *in vitro* studies [23].

(1) Pigs. The first animal model was suggested in 1972 and 1976 by Silverstein who inflicted repeated deep dermal injuries on the backs of twelve red Duroc pigs to induce successful formation of a hypertrophic scar in all the animals. Pigs are tight-skinned animals that have similar skin architecture with humans. They also sustain sunburn and rely on fat for insulation as do humans, unlike other animals that require fur. Both humans and pigs have thick epidermis with similar turnover times. Both have elastic fibers in their epidermis and contain Langerhans cells. Collagen structure is also similar [24].

The first model by Silverstein vanished in the literature after being reported. In 2003, Zhu et al. and, in 2004, Gallant-Behm et al. made full-thickness wounds with Padgett dermatomes on the back of female red Duroc pigs, and showed that this animal model presented hypertrophic scarring up to 5 months after the incisions [25].

Zhu et al., in their 2003 study, reported that red Duroc pigs had skin cones and developed hypertrophic scars histologically similar to humans. Subsequent studies by the group reported that immunohistochemical patterns of decorin, versican, and insulin-like growth factor-1 (IGF-1) were also analogous to hypertrophic scars in humans and that the number of nerve fibers in the scar was similar [26, 27]. Biochemical studies demonstrated that comparable levels of vascular endothelial growth factor and nitric oxide could be found in human and porcine scar tissue, as were the corresponding numbers of mastocytes, collagen nodules, and myofibroblasts [28, 29].

Gallant-Behm et al., in their 2004 study, compared scar formation in the female red Duroc pigs with that in Yorkshire pigs and juvenile castrated male red Duroc pigs. Gross and histologic results were indistinguishable between the male and female red Duroc pigs. However, expression of types I and III collagen, heat shock protein 47, bone morphogenic protein 1, diverse proteoglycans, and osteopontin differed in pattern, with the red Duroc pig exhibiting a unique biphasic pattern, undocumented previously [30]. Subsequent studies by the same group using electric dermatome wounds on the backs of red Duroc pigs revealed characteristics in expression of cytokines, transcription factors, growth factors, and receptors similar to human scars [31]. Stewart et al., also from this group, reported in 2006 that the kinetics of blood flow in the red Duroc model were comparable with the previously observed laser Doppler imaging of human skin wounds and hypertrophic scars [32]. In 2007, Gallant-Behm's group studied first generation offspring between the red Duroc and Yorkshire pigs. They had intermediate scar behavior, supporting growing evidence that wound phenotypes were genetically programmed [33].

While porcine skin resembles human skin in many aspects and may develop scars similar in some characteristics to human hypertrophic scars, there are still many limitations to the porcine model. Skin structure is not identical. Pig epidermis has only three layers as opposed to five in humans, with a thick and compact stratum corneum. The distribution of apocrine and eccrine sweat glands are different, as is the architecture of hair follicles. Pigs are also large, costly to obtain, and difficult to maintain [34].

(2) Mice. In 1983, Ehrlich reported on the hyperplastic wound healing process noted in tight-skin mice. Tight-skin mice (TSM), a mutant mouse strain, have a skin covering tightly adhered to their bodies and were used by the authors to overcome the major contributor to loose skinned animal wound healing: wound contraction. Sharp, full-thickness

excision was done to make square defects on the dorsum of tight-skinned mice; wounds were left undressed and were excised at weekly intervals between 1 and 9 weeks following wounding. Abundant swirls of collagen fibers and hypertrophy of connective tissue and vessels histologically similar to human hypertrophic scars were noted [35]. However, scars failed to maintain these characteristics for prolonged periods of time.

(3) Rabbits. In 1997, a group of surgeons at Northwestern University who had noticed that surgical scars in rabbit ears remained elevated months after wounding standardized a rabbit ear model for biochemical and molecular scarring studies. Forty excisional wounds each 6 mm in diameter were created down to bare cartilage on the ventral surface of young adult female New Zealander white rabbit ears. In the acute model, these wounds were treated with either intralesional triamcinolone or saline at day 16 and histologically analyzed at day 22. In the chronic form, larger excisions were made and accumulation of new collagen and cartilage was observed for over 9 months [36]. This model was used and validated in a variety of studies evaluating the effect of age on scars, efficacy of therapeutic agents, and molecular mechanisms [37–39].

(4) Guinea Pigs. In 2002, Aksoy et al. developed a guinea pig hypertrophic scar model, using albino male guinea pigs and coal tar. They focused on the costly maintenance necessary for immunosuppressed mice or pigs and suggested a cheaper, easier method. Circular skin defects with diameters ranging 1.7~2.0 cm were made on each side of the dorsal thorax, followed by circular defects of the panniculus carnosus with a larger diameter. Any latissimus dorsi muscle remaining between the skin and thoracic wall was removed. The defect on the right was left untouched, and the defect on the right received applications of coal tar every 48 hours, beginning four days after the wounds were made. Scars with erythema and elevated edges developed in 10 out of 12 animals. However, morphological correlation was found in only six of these, and increased glucose-6-phosphate dehydrogenase (G6PD) enzyme activity was only detected in four. G6PD activity is increased in human proliferative scars [36]. Although less costly and easier to conduct than the athymic mouse or pig model, the toxic, carcinogenic effects of coal tar must also be investigated. The longevity of the guinea pigs was not mentioned.

The most critical limitation of the aforementioned models is that they are all animal models that develop characteristics of hypertrophic scars. Keloids are, to date, virtually impossible to induce in animal wounds.

2.1.2. Heterologous Transplantation of Human Keloid or Hypertrophic Scar Tissue. Xenografts of human scar tissue into different wounds of different species have been described. To avoid rejection, either immunodeficient animals such as athymic mice and rats or an immune privileged site such as the cheek pouch of a hamster has been used.

(1) Athymic Mouse. Most studies use variations of the original nude mouse model, incorporating deepithelialized, diced human abnormal scar tissue in the subcutaneous pockets on the back or thorax of nude, athymic mice, with minor alterations. This model is relatively easy to perform; nude athymic mice are relatively easy to maintain, and the implants are easily accessible and visible.

The athymic mouse was first described in 1966 by Flanagan, and it is still extensively used for transplantation and graft studies thanks to its impaired T-cell function [40].

Shetlar et al. first described implantation of human keloid tissue into subcutaneous pockets of athymic mice in 1985 [41]. In 1987, Robb et al. grafted human cadaveric partial thickness skin to full-thickness skin defects on the backs of athymic nude mice, suturing them to the defect margins. Three weeks after grafting, they created burns which resulted in scars of increased collagen. They also grafted human hypertrophic scars from burn patients to full-thickness skin defects on athymic nude mice, and they found that these grafts were able to revascularize in samples up to 3 mm thick and maintained histologic and gross characteristics for up to 6 months, when the animals were sacrificed [42].

In 1989, Kischer et al. reported on implants of human hypertrophic scars and keloids into the subcutaneous pockets above the panniculus muscle on backs of athymic nude mice and observed growth of the implanted tissue for up to 246 days. Microvascular anastamosis between the grafted scar tissue and host vessels was noted within the first several days. Size reduction was noted, with a slope of −0.436 for hypertrophic scars and −0.736 for keloids. This means that in about 67 days the keloid implants have half of their initial volume. Histological analysis confirmed retention of character. Occlusion of microvessels was consistently seen in transmission electron microscopy [43, 44].

In 1991, Waki et al. used the same model to report on the effects of pharmacologic agents. Deepithelialized human keloids were implanted bilaterally in the subcutaneous pouch of the thorax in athymic mice. They noticed an initial growth spurt until the fourth week after implantation, then regression, a pattern that differed from previous studies. Rejection or collagen degradation, outgrowth of vascular supply, or loss of collagen synthesis gene regulator feedback was suggested as the mechanism [45].

In 2004, an *in vivo* model with genetically modified skin-humanized mice was proposed. Previous studies using genetically modified human skin grafted onto mice had focused on time point analysis of graft behavior and take [46–49]. Cultured bioengineered skin equivalent with labeled keratinocytes was transplanted on the backs of nude mice, and a small, circular full-thickness wound was made 9 to 12 weeks after grafting. The study shows that this model recapitulates the features of native human wound healing, using epithelial and stromal markers [50]. Yang et al. also grafted full-thickness human skin onto full-thickness defects measuring 2.0 × 1.5 cm on the backs of nude mice and inflicted burn injuries after complete graft take to induce scarring. Hypertrophic scars similar to human hypertrophic scars were noted [51].

In 2013, Ishiko et al. sutured explanted keloid tissue to the dorsum of the mice to evaluate the effects of chondroitinase injection on keloid tissue. They describe significant reduction

in keloid scar tissue volume. The mechanism proposed was the reorganization of the extracellular matrix with regenerated elastic fibers [52]. This method is also used for studies on hypertrophic scars [53, 54].

The main limitations of the nude mouse model are small animal size, therefore small sample size, along with difficulty of maintenance on an acceptable, isolated pedicle, and limited longevity.

(2) Rat. An athymic hairless mutation in a colony of outbred hooded rats was first observed in 1953 at the Rowett Research Institute in Aberdeen. Homozygous mutants were recovered in 1975, and in 1977, a breeding colony of congenitally athymic, nude rats were developed [55].

Polo et al., noting the limitations of the nude mouse in scar studies, developed a nude rat sandwich flap keloid scar model. They implanted homogeneous sections of human keloid tissue beneath the epigastric island flap of a nude rat and, then, after a 3-week maturation period, elevated the epigastric flap along with the implanted scar tissue. A catheter was inserted into the flap pedicle for future injection purposes. Wrapping the elevated flap around the scar tissue to form a sandwich island flap, the authors passed the flap through a subcutaneous tunnel to the dorsum of the rat. The flap was sutured to two incisions made prior to tunneling [56–58]. This model ensured that the scar tissue was separated from surrounding tissue and supplied, through a single pedicle, the superficial inferior epigastric pedicle. These efforts were made in an attempt to prevent the previously noted absorption of keloid scar tissue, and they resulted in maintenance of the transplanted tissue up to 18 months. Transpositioning to the dorsum allows accurate measurement, isolation of the pedicle allows manipulation of vascular supply, and catheter placement enables intralesional injections minimizing systemic spread [59].

(3) Hamster. In 2005, Hochman et al. implanted keloid scars from the breast of an adult female patient into both cheek pouches of 18 male Syrian golden hamsters (*Mesocricetus auratus*). This small mammal has a normal immune system, but it is endowed with an immune privileged site, the subepithelium of its jugal pouches. The jugal pouches are diverticular structures inside the mouth used for storing and transporting food. The subepithelium lacks lymphatic structures except in its proximal region, and thus this area has been used in various animal models for grafts and neoplasms [60–62]. Because the epithelium is transparent, the keloid specimens were visible from the mouth. The grafts were analyzed 5, 12, 21, 42, 84, and 168 days after implantation. Histological evaluation revealed increased vascularity, deposition of inflammatory infiltrate and collagen analogous with human hypertrophic scarring. They also noted an increase of melanocytes in the groups sacrificed after 42 days. Unfortunately, epithelium integrity was not completely maintained in the groups after 42 days, and the authors suggest that this model may be effective for about 21 days [63].

Transplantation of human keloid or hypertrophic scar xenografts allows us to perform studies on tissue that possesses similar histological structures and biochemical features with *in vivo* scars. However, because the physiological microenvironment differs, such similarities begin to diminish with the passage of time. The human tissue is completely isolated from its *in vivo* environment. Viability is limited, so long term effects of treatment modalities are difficult to assess. The transplanted tissue is usually obtained months or years after injury or onset, so heterogenous material is usually transplanted, and studies on preventive measures are impossible. The cost and energy it takes to maintain and handle immunodeficient rodents is also something to consider [64].

2.2. Tissue or Cell Cultures. The difficulty in developing a universal animal model is reflected in the abundant research upon cell or tissue culture models of abnormal scars.

The cell culture technique is to harvest dermal derived cells such as fibroblasts, endothelial cells, and keratinocytes from human keloid scars and culture them two-dimensionally on a plastic substrate or culture dish [65–67]. Early models used serum containing culture media. Because serum contains growth factors, it was used to sustain cell growth, but it confounded the experimental results. In 1997, Koch et al. developed a serum-free keloid fibroblast culture that did not compromise cell growth, enabling evaluation of various growth factors and wound modulators [67]. The major limitation of such cultures is that the cells grown in monolayer cannot replicate the complex cell-to-cell or cell-to-matrix interactions found in intact tissue.

Tissue cultures have been employed to better study these pathophysiological mechanisms. To better mimic the *in vivo* microenvironmental condition, keloid tissue derived cells have been loaded onto three-dimensional (3D) synthetic scaffolds or grown in a 3D format [68, 69]. Organotypic methods of skin constructs have been used to mimic the *in vivo* environment. Butler et al. cultured a keratinocyte layer upon a fibroblast cell layer to mimic epidermal-dermal interface. They used this model to compare tissue thickness between keloid derived fibroblasts and normal fibroblasts, finding thicker growth of the artificial tissue in the keloid fibroblast group [69]. Artificial tissue constructs using rafts, consisting of fibroblasts embedded in a collagen gel with or without keratinocytes seeded on the surface, have been used in another organotypic culture model. After stratification of the keratinocyte layer, full-thickness incisions were made on the constructs, and these were maintained at air-fluid interface. Evaluation was performed with multiphoton microscopes that obtained serial images of multiple layers of the specimen and phase-contrast microscopy, enabling visualization of biologic activity of the wound [70]. Polylactic acid (PLA), polyglycolic acid (PGA), and their copolymers, polylactic-*co*-glycolic acid (PLGA), and polyhydroxybutyrate are biodegradable materials approved by the United States Food and Drug Administration for application in humans [71, 72]. The selection of the scaffold material, which composes the extracellular matrix of the tissue is a key to success of model establishment. Wang and Luo used PLGA because it is nontoxic, and the porosity rate is similar to human dermal structure [73].

Lee et al. applied the concept of multicellular tumor spheroid culture models to develop 3D organotypic multicellular keloid spheroids (OMSs) derived from freshly isolated keloid tissue and found that keloid characteristics and viability persisted for 7 days [74]. Bagabir et al. recently developed a method of long-term organ culture. Human keloid was dissected into 3,4,5, and 6 mm punch biopsy sizes, embedded in collagen gel, and then either submerged in serum-free and supplemented media (serum-free Dulbecco's modified Eagle's medium/Ham's F12 or William's E medium) or set in an air-liquid interface (ALI). They found that keloid tissue cultures in the ALI set in supplemented William's E (WE) medium most optimally expressed keloid characteristics up to 6 weeks [75].

2.3. Implantation of Tissue Engineered Scar Tissue into Athymic Mice. Merging the techniques of tissue engineering and xenograft transplantation, recent studies have focused on the implantation of tissue engineered keloid tissue scaffolds or engineered skin substitutes into athymic mice.

Yagi et al. developed an *ex vivo* glycosaminoglycan (GAG) deposition model, employing collagen sponges consisting of chemically cross-linked collagen resistant to collagenase digestion *in vivo*. These sponges were seeded with human keloid cells, then implanted in the subcutaneous space of nude mice. Sponges loaded with keloid lesion cells were compared with sponges seeded with fibroblasts harvested from normal skin. A month after implantation, the keloid sponge was significantly heavier than the fibroblast sponge, and this model was subsequently used to evaluate the effect of interleukin 1β or chondroitinase ABC, known to inhibit prostaglandins *in vitro* [22].

Wang and Luo, as previously mentioned, transferred human keloid fibroblasts to PLGA scaffolds sized $5 \times 5 \times 0.5$ mm and cultured these in a rotator cell-culture system for one week. PLGA scaffolds without keloid fibroblasts were used as controls. These cultured scaffolds were implanted in a subcutaneous pouch on the backs of female athymic mice; the cell loaded scaffold on the left and the control in the right. The animals were sacrificed at day 30, 60, 120, and 180 for analysis. Keloid fibroblasts and collagen were observed at all time points, even at day 180 [73].

Supp et al. divided the dermis of a human keloid specimen into deep and superficial dermis, in order to assess the roles of deep and superficial keloid fibroblasts. They inoculated harvested and cultured keloid fibroblasts onto rehydrated bovine collagen-glycosaminoglycan polymer substrates, followed by keratinocytes. These engineered skin substitutes were incubated at the air-liquid interface for two weeks, then cut into 2×2 cm squares, and transplanted to full-thickness excision wounds cut on the right flank of nude athymic female mice. The grafts were sutured to the wounds and dressed with antimicrobial coated gauze, tied over with opposing sutures. The mice were photographed every 2 weeks and sacrificed at 12 weeks for analysis. The authors found that the group with deep fibroblasts had significantly thicker tissue, and that the group with superficial fibroblasts had significantly increased area [76].

Such methods provide a similar microenvironment for keloid tissue growth, and treatment modalities may be evaluated in a setting more closer to the *in vivo* environment. However, the keloid cells transferred to the scaffolds may still be obtained months to years after injury. The largest limitation is probably the requirement of both a sophisticated tissue engineering unit and qualified animal laboratory facilities.

3. Conclusion

This article describes the animal models utilized in abnormal scarring research to date. These models have provided valuable information about the pathogenesis and treatment possibilities of such scars. As with most other animal models, the validity of each of these models depends on the extent of similarity to human characteristics. However, because no model yet exactly replicates the pathophysiological condition *in vivo*, results analyzed from each study must be interpreted in the context of the model used. While recent progress merging tissue engineering with animal studies looks quite promising, there is still much to be done. Induction of keloids, not hypertrophic scars, on human skin grafted onto mice may be developed. Genetic models, which may enable us to finally analyze preventive measures, are likely to show up in the future.

References

[1] B. S. Atiyeh, M. Costagliola, and S. N. Hayek, "Keloid or hypertrophic scar: the controversy: review of the literature," *Annals of Plastic Surgery*, vol. 54, no. 6, pp. 676–680, 2005.

[2] P. D. Butler, M. T. Longaker, and G. P. Yang, "Current progress in Keloid research and treatment," *Journal of the American College of Surgeons*, vol. 206, no. 4, pp. 731–741, 2008.

[3] M. C. Naylor and A. E. Brissett, "Current concepts in the etiology and treatment of keloids," *Facial Plastic Surgery*, vol. 28, no. 5, pp. 504–512, 2012.

[4] A. S. Halim, A. Emami, I. Salahshourifar, and T. Ponnuraj Kannan, "Keloid scarring: understanding the genetic basis, advances, and prospects," *Archives of Plastic Surgery*, vol. 39, no. 3, pp. 184–189, 2012.

[5] J. C. Murray, "Keloids and hypertrophic scars," *Clinics in Dermatology*, vol. 12, no. 1, pp. 27–37, 1994.

[6] H. Nakaoka, S. Miyauchi, and Y. Miki, "Proliferating activity of dermal fibroblasts in keloids and hypertrophic scars," *Acta Dermato-Venereologica*, vol. 75, no. 2, pp. 102–104, 1995.

[7] H. P. Ehrlich, A. Desmoulière, R. F. Diegelmann et al., "Morphological and immunochemical differences between keloid and hypertrophic scar," *American Journal of Pathology*, vol. 145, no. 1, pp. 105–113, 1994.

[8] D. W. Friedman, C. D. Boyd, J. W. Mackenzie, P. Norton, R. M. Olson, and S. B. Deak, "Regulation of collagen gene expression in keloids and hypertrophic scars," *Journal of Surgical Research*, vol. 55, no. 2, pp. 214–222, 1993.

[9] A. Burd and L. Huang, "Hypertrophic response and keloid diathesis: two very different forms of scar," *Plastic and Reconstructive Surgery*, vol. 116, no. 7, pp. 150e–157e, 2005.

[10] A. Al-Attar, S. Mess, J. M. Thomassen, C. L. Kauffman, and S. P. Davison, "Keloid pathogenesis and treatment," *Plastic and Reconstructive Surgery*, vol. 117, no. 1, pp. 286–300, 2006.

[11] P. F. Gadson, J. D. Russell, and S. B. Russel, "Glucocorticoid receptors in human fibroblasts derived from normal dermis and keloid tissue," *Journal of Biological Chemistry*, vol. 259, no. 18, pp. 11236–11241, 1984.

[12] B. Cosman and M. Wolff, "Correlation of keloid recurrence with completeness of local excision. A negative report," *Plastic and Reconstructive Surgery*, vol. 50, no. 2, pp. 163–166, 1972.

[13] S. Luo, M. Benathan, W. Raffoul, R. G. Panizzon, and D. V. Egloff, "Abnormal balance between proliferation and apoptotic cell death in fibroblasts derived from keloid lesions," *Plastic and Reconstructive Surgery*, vol. 107, no. 1, pp. 87–96, 2001.

[14] M. H. Gold, "A controlled clinical trial of topical silicone gel sheeting in the treatment of hypertrophic scars and keloids," *Journal of the American Academy of Dermatology*, vol. 30, no. 3, pp. 506–507, 1994.

[15] M. P. Goldman and R. E. Fitzpatrick, "Laser treatment of scars," *Dermatologic Surgery*, vol. 21, no. 8, pp. 685–687, 1995.

[16] A. L. Van De Kar, M. Kreulen, P. P. M. Van Zuijlen, and F. Oldenburger, "The results of surgical excision and adjuvant irradiation for therapy-resistant keloids: a prospective clinical outcome study," *Plastic and Reconstructive Surgery*, vol. 119, no. 7, pp. 2248–2254, 2007.

[17] M. Ikeda, M. Naitoh, H. Kubota et al., "Elastic fiber assembly is disrupted by excessive accumulation of chondroitin sulfate in the human dermal fibrotic disease, keloid," *Biochemical and Biophysical Research Communications*, vol. 390, no. 4, pp. 1221–1228, 2009.

[18] K. Kashiyama, N. Mitsutake, M. Matsuse et al., "miR-196a downregulation increases the expression of type I and III collagens in Keloid fibroblasts," *Journal of Investigative Dermatology*, vol. 132, no. 6, pp. 1597—1604, 2012.

[19] J. C. Smith, B. E. Boone, S. R. Opalenik, S. M. Williams, and S. B. Russell, "Gene profiling of keloid fibroblasts shows altered expression in multiple fibrosis-associated pathways," *Journal of Investigative Dermatology*, vol. 128, no. 5, pp. 1298–1310, 2008.

[20] O. M. Fasika, "Keloids: a study of the immune reaction to sebum," *East African Medical Journal*, vol. 69, no. 2, pp. 114–116, 1992.

[21] S. Younai, L. S. Nichter, T. Wellisz et al., "Modulation of collagen synthesis by transforming growth factor-β in keloid and hypertrophic scar fibroblasts," *Annals of Plastic Surgery*, vol. 33, no. 2, pp. 148–154, 1994.

[22] Y. Yagi, E. Muroga, and M. Naitoh, "An ex vivo model employing keloid-derived cell-seeded collagen sponges for therapy development," *Journal of Investigative Dermatology*, vol. 133, no. 2, pp. 386–393, 2013.

[23] T. P. Sullivan, W. H. Eaglstein, S. C. Davis, and P. Mertz, "The pig as a model for human wound healing," *Wound Repair and Regeneration*, vol. 9, no. 2, pp. 66–76, 2001.

[24] N. J. Vardaxis, T. A. Brans, M. E. Boon, R. W. Kreis, and L. M. Marres, "Confocal laser scanning microscopy of porcine skin: implications for human wound healing studies," *Journal of Anatomy*, vol. 190, no. 4, pp. 601–611, 1997.

[25] K. Q. Zhu, L. H. Engrav, N. S. Gibran et al., "The female, red Duroc pig as an animal model of hypertrophic scarring and the potential role of the cones of skin," *Burns*, vol. 29, no. 7, pp. 649–664, 2003.

[26] Z. Liang, L. H. Engrav, P. Muangman et al., "Nerve quantification in female red Duroc pig (FRDP) scar compared to human hypertrophic scar," *Burns*, vol. 30, no. 1, pp. 57–64, 2004.

[27] K. Q. Zhu, L. H. Engrav, R. N. Tamura et al., "Further similarities between cutaneous scarring in the female, red Duroc pig and human hypertrophic scarring," *Burns*, vol. 30, no. 6, pp. 518–530, 2004.

[28] K. Q. Zhu, L. H. Engrav, R. Armendariz et al., "Changes in VEGF and nitric oxide after deep dermal injury in the female, red Duroc pig—further similarities between female, Duroc scar and human hypertrophic scar," *Burns*, vol. 31, no. 1, pp. 5–10, 2005.

[29] N. Harunari, K. Q. Zhu, R. T. Armendariz et al., "Histology of the thick scar on the female, red Duroc pig: final similarities to human hypertrophic scar," *Burns*, vol. 32, no. 6, pp. 669–677, 2006.

[30] C. L. Gallant, M. E. Olson, and D. A. Hart, "Molecular, histologic, and gross phenotype of skin wound healing in red Duroc pigs reveals an abnormal healing phenotype of hypercontracted, hyperpigmented scarring," *Wound Repair and Regeneration*, vol. 12, no. 3, pp. 305–319, 2004.

[31] C. L. Gallant-Behm, M. E. Olson, and D. A. Hart, "Cytokine and growth factor mRNA expression patterns associated with the hypercontracted, hyperpigmented healing phenotype of red Duroc pigs: a model of abnormal human scar development?" *Journal of Cutaneous Medicine and Surgery*, vol. 9, no. 4, pp. 165–177, 2005.

[32] C. J. Stewart, C. L. Gallant-Behm, K. Forrester, J. Tulip, D. A. Hart, and R. C. Bray, "Kinetics of blood flow during healing of excisional full-thickness skin wounds in pigs as monitored by laser speckle perfusion imaging," *Skin Research and Technology*, vol. 12, no. 4, pp. 247–253, 2006.

[33] C. L. Gallant-Behm, H. Tsao, C. Reno, M. E. Olson, and D. A. Hart, "Skin wound healing in the first generation (F1) offspring of Yorkshire and red Duroc pigs: evidence for genetic inheritance of wound phenotype," *Burns*, vol. 32, no. 2, pp. 180–193, 2006.

[34] K. Q. Zhu, G. J. Carrougher, N. S. Gibran, F. F. Isik, and L. H. Engrav, "Review of the female Duroc/Yorkshire pig model of human fibroproliferative scarring," *Wound Repair and Regeneration*, vol. 15, no. 1, supplement, pp. S32–S39, 2007.

[35] H. P. Ehrlich and A. L. Needle, "Wound healing in tight-skin mice: delayed closure of excised wounds," *Plastic and Reconstructive Surgery*, vol. 72, no. 2, pp. 190–198, 1983.

[36] D. E. Morris, L. Wu, L. L. Zhao et al., "Acute and chronic animal models for excessive dermal scarring: quantitative studies," *Plastic and Reconstructive Surgery*, vol. 100, no. 3, pp. 674–681, 1997.

[37] J. R. Marcus, J. W. Tyrone, S. Bonomo, Y. Xia, and T. A. Mustoe, "Cellular mechanisms for diminished scarring with aging," *Plastic and Reconstructive Surgery*, vol. 105, no. 5, pp. 1591–1599, 2000.

[38] I. Kim, J. E. Mogford, C. Witschi, M. Nafissi, and T. A. Mustoe, "Inhibition of prolyl 4-hydroxylase reduces scar hypertrophy in a rabbit model of cutaneous scarring," *Wound Repair and Regeneration*, vol. 11, no. 5, pp. 368–372, 2003.

[39] L. Lu, A. S. Saulis, W. R. Liu et al., "The temporal effects of anti-TGF-β1, 2, and 3 monoclonal antibody on wound healing and hypertrophic scar formation," *Journal of the American College of Surgeons*, vol. 201, no. 3, pp. 391–397, 2005.

[40] L. Mecklenburg, M. Nakamura, J. P. Sundberg, and R. Paus, "The nude mouse skin phenotype: the role of Foxn1 in hair follicle development and cycling," *Experimental and Molecular Pathology*, vol. 71, no. 2, pp. 171–178, 2001.

[41] M. R. Shetlar, C. L. Shetlar, L. Hendricks, and C. W. Kischer, "The use of athymic nude mice for the study of human

keloids," *Proceedings of the Society for Experimental Biology and Medicine*, vol. 179, no. 4, pp. 549–552, 1985.

[42] E. C. Robb, J. P. Waymack, and G. D. Warden, "A new model for studying the development of human hypertrophic burn scar formation," *Journal of Burn Care and Rehabilitation*, vol. 8, no. 5, pp. 371–375, 1987.

[43] C. W. Kischer, D. Sheridan, and J. Pindur, "Use of nude (athymic) mice for the study of hypertrophic scars and keloids: vascular continuity between mouse and implants," *Anatomical Record*, vol. 225, no. 3, pp. 189–196, 1989.

[44] C. W. Kischer, J. Pindur, M. R. Shetlar, and C. L. Shetlar, "Implants of hypertrophic scars and keloids into the nude (athymic) mouse: viability and morphology," *Journal of Trauma*, vol. 29, no. 5, pp. 672–677, 1989.

[45] E. Y. Waki, R. L. Crumley, and J. G. Jakowatz, "Effects of pharmacologic agents on human keloids implanted in athymic mice. A pilot study," *Archives of Otolaryngology*, vol. 117, no. 10, pp. 1177–1181, 1991.

[46] S. A. Eming, J. Lee, R. G. Snow, R. G. Tompkin, M. L. Yarmush, and J. R. Morgan, "Genetically modified human epidermis overexpressing PDGF-A directs the development of a cellular and vascular connective tissue stroma when transplanted to athymic mice—implications for the use of genetically modified keratinocytes to modulate dermal regeneration," *Journal of Investigative Dermatology*, vol. 105, no. 6, pp. 756–763, 1995.

[47] S. A. Eming, D. A. Medalie, R. G. Tompkins, M. L. Yarmush, and J. R. Morgan, "Genetically modified human keratinocytes overexpressing PDGF-A enhance the performance of a composite skin graft," *Human Gene Therapy*, vol. 9, no. 4, pp. 529–539, 1998.

[48] D. M. Supp and S. T. Boyce, "Overexpression of vascular endothelial growth factor accelerates early vascularization and improves healing of genetically modified cultured skin substitutes," *Journal of Burn Care and Rehabilitation*, vol. 23, no. 1, pp. 10–20, 2002.

[49] D. M. Supp, A. P. Supp, S. M. Bell, and S. T. Boyce, "Enhanced vascularization of cultured skin substitutes genetically modified to overexpress vascular endothelial growth factor," *Journal of Investigative Dermatology*, vol. 114, no. 1, pp. 5–13, 2000.

[50] M. J. Escamez, M. García, F. Larcher et al., "An in vivo model of wound healing in genetically modified skin-humanized mice," *Journal of Investigative Dermatology*, vol. 123, no. 6, pp. 1182–1191, 2004.

[51] D.-Y. Yang, S.-R. Li, G. Li et al., "Establishment of an animal model of human hyperplastic scar in nude mice," *Chinese Journal of Burns*, vol. 20, no. 2, pp. 82–84, 2004.

[52] T. Ishiko, M. Naitoh, H. Kubota et al., "Chondroitinase injection improves keloid pathology by reorganizing the extracellular matrix with regenerated elastic fibers," *Journal of Dermatology*, vol. 40, no. 5, pp. 380–383, 2013.

[53] H. Eto, H. Suga, N. Aoi et al., "Therapeutic potential of fibroblast growth factor-2 for hypertrophic scars: upregulation of MMP-1 and HGF expression," *Laboratory Investigation*, vol. 92, no. 2, pp. 214–223, 2012.

[54] J. Wang, J. Ding, H. Jiao et al., "Human hypertrophic scar-like nude mouse model: characterization of the molecular and cellular biology of the scar process," *Wound Repair and Regeneration*, vol. 19, no. 2, pp. 274–285, 2011.

[55] M. F. W. Festing, D. May, and T. A. Connors, "An athymic nude mutation in the rat," *Nature*, vol. 274, no. 5669, pp. 365–366, 1978.

[56] M. Polo, Y.-J. Kim, A. Kucukcelebi et al., "An in vivo model of human proliferative scar," *Journal of Surgical Research*, vol. 74, no. 2, pp. 187–195, 1998.

[57] X. Wang, P. Smith, L. L. Q. Pu, Y. J. Kim, F. Ko, and M. C. Robson, "Exogenous transforming growth factor β2 modulates collagen I and collagen III synthesis in proliferative scar xenografts in nude rats," *Journal of Surgical Research*, vol. 87, no. 2, pp. 194–200, 1999.

[58] Y. J. Kim, G. H. Jo, D. M. Chang, P. K. Lee, and P. Lim, "A new animal model of proliferative scarring," *Journal of the Korean Society of Plastic and Reconstructive Surgeons*, vol. 107, pp. 671–676, 1999.

[59] Y. J. Kim, "Modulatory effect of TGF-β^2 to proliferative kinetics of fibroblast in Keloid and hyeprtrophic scar," , *Journal of the Korean Society of Plastic and Reconstructive Surgeons*, vol. 30, no. 2, pp. 194–200, 2003.

[60] K. Ley, K. Schümann, and H. Henrich, "Microvascular permeability and blood flow in atrial homografts in the hamster cheek pouch," *International Journal of Microcirculation, Clinical and Experimental*, vol. 3, no. 1, pp. 29–39, 1984.

[61] S. K. Liao, P. B. Dent, and A. H. Qizilbash, "Characterization of human malignant melanoma cell lines—5. Heterotransplantation in the hamster cheek pouch," *Zeitschrift fur Krebsforschung und Klinische Onkologie*, vol. 88, no. 2, pp. 121–128, 1977.

[62] C. L. Sanders and K. E. McDonald, "Malignancy of proliferative pulmonary lesions in the Syrian hamster following inhalation of 239PuO2," *Journal of Environmental Pathology, Toxicology and Oncology*, vol. 11, no. 3, pp. 151–156, 1992.

[63] B. Hochman, F. C. Vilas Bôas, M. Mariano, and L. M. Ferreiras, "Keloid heterograft in the hamster (*Mesocricetus auratus*) cheek pouch, Brazil," *Acta Cirúrgica Brasileira*, vol. 20, no. 3, pp. 200–212, 2005.

[64] M. P. Hillmer and S. M. MacLeod, "Experimental keloid scar models: a review of methodological issues," *Journal of Cutaneous Medicine and Surgery*, vol. 6, no. 4, pp. 354–359, 2002.

[65] I. J. Lim, T.-T. Phan, B.-H. Bay et al., "Fibroblasts cocultured with keloid keratinocytes: normal fibroblasts secrete collagen in a keloidlike manner," *American Journal of Physiology*, vol. 283, no. 1, pp. C212–C222, 2002.

[66] Y. Wu, Q. Zhang, D. K. Ann et al., "Increased vascular endothelial growth factor may account for elevated level of plasminogen activator inhibitor-1 via activating ERK1/2 in keloid fibroblasts," *American Journal of Physiology*, vol. 286, no. 4, pp. C905–C912, 2004.

[67] R. J. Koch, R. L. Goode, and G. T. Simpson, "Serum-free keloid fibroblast cell culture: an in vitro model for the study of aberrant wound healing," *Plastic and Reconstructive Surgery*, vol. 99, no. 4, pp. 1094–1098, 1997.

[68] M. Sato, O. Ishikawa, and Y. Miyachi, "Distinct patterns of collagen gene expression are seen in normal and keloid fibroblasts grown in three-dimensional culture," *British Journal of Dermatology*, vol. 138, no. 6, pp. 938–943, 1998.

[69] P. D. Butler, D. P. Ly, M. T. Longaker, and G. P. Yang, "Use of organotypic coculture to study keloid biology," *American Journal of Surgery*, vol. 195, no. 2, pp. 144–148, 2008.

[70] B. A. Torkian, A. T. Yeh, R. Engel, C.-H. Sun, B. J. Tromberg, and B. J. F. Wong, "Modeling aberrant wound healing using tissue-engineered skin constructs and multiphoton microscopy," *Archives of Facial Plastic Surgery*, vol. 6, no. 3, pp. 180–187, 2004.

[71] B.-S. Kim and D. J. Mooney, "Development of biocompatible synthetic extracellular matrices for tissue engineering," *Trends in Biotechnology*, vol. 16, no. 5, pp. 224–229, 1998.

[72] S. L. Ishaug, G. M. Crane, M. J. Miller et al., "Bone formation by three-dimensional stromal osteoblast culture in biodegradable polymer scaffolds," *Journal of Biomedical Materials Research*, vol. 36, no. 1, pp. 17–28, 1997.

[73] H. Wang and S. Luo, "Establishment of an animal model for Human Keloid Scars Using Tissue Engineering Method," *Journal of Burn Care & Research*, 2012.

[74] W. J. Lee, I. K. Choi, J. Lee et al., "A novel three-dimensional model system for keloid study: organotypic multicellular scar model," *Wound Repair and Regeneration*, vol. 21, no. 1, pp. 155–165, 2013.

[75] R. Bagabir, F. Syed, R. Paus, and A. Bayat, "Long-term organ culture of keloid disease tissue," *Experimental Dermatology*, vol. 21, no. 5, pp. 376–381, 2012.

[76] D. M. Supp, J. M. Hahn, K. Glaser, K. L. McFarland, and S. T. Boyce, "Deep and superficial keloid fibroblasts contribute differentially to tissue phenotype in a novel in vivo model of keloid scar," *Plastic and Reconstructive Surgery*, vol. 129, no. 6, pp. 1259–1271, 2012.

Hindawi Publishing Corporation
BioMed Research International
Volume 2013, Article ID 624815, 12 pages
http://dx.doi.org/10.1155/2013/624815

Research Article

The Ehrlich Tumor Induces Pain-Like Behavior in Mice: A Novel Model of Cancer Pain for Pathophysiological Studies and Pharmacological Screening

Cassia Calixto-Campos,[1] Ana C. Zarpelon,[1] Mab Corrêa,[1] Renato D. R. Cardoso,[1] Felipe A. Pinho-Ribeiro,[1] Rubens Cecchini,[1] Estefania G. Moreira,[2] Jefferson Crespigio,[1] Catia C. F. Bernardy,[3] Rubia Casagrande,[4] and Waldiceu A. Verri Jr.[1]

[1] *Departamento de Ciências Patológicas, Centro de Ciências Biológicas, Universidade Estadual de Londrina, Rod. Celso Garcia Cid KM480 PR445, 86051-990 Londrina, PR, Brazil*
[2] *Departamento de Ciências Fisiológicas, Centro de Ciências Biológicas, Universidade Estadual de Londrina, Rod. Celso Garcia Cid KM480 PR445, 86051-990 Londrina, PR, Brazil*
[3] *Departamento de Enfermagem, Centro de Ciências da Saúde, Universidade Estadual de Londrina, Avenida Robert Koch 60, 86038-350 Londrina, PR, Brazil*
[4] *Departamento Ciências Farmacêuticas, Centro de Ciências da Saúde, Universidade Estadual de Londrina, Avenida Robert Koch 60, 86038-350 Londrina, PR, Brazil*

Correspondence should be addressed to Waldiceu A. Verri Jr.; waldiceujr@yahoo.com.br

Received 29 April 2013; Accepted 10 July 2013

Academic Editor: Monica Fedele

The Ehrlich tumor is a mammary adenocarcinoma of mice that can be developed in solid and ascitic forms depending on its administration in tissues or cavities, respectively. The present study investigates whether the subcutaneous plantar administration of the Ehrlich tumor cells induces pain-like behavior and initial pharmacological susceptibility characteristics. The Ehrlich tumor cells (1×10^4–10^7 cells) induced dose-dependent mechanical hyperalgesia (electronic version of the von Frey filaments), paw edema/tumor growth (caliper), and flinches compared with the saline group between days 2 and 12. There was no difference between doses of cells regarding thermal hyperalgesia in the hot-plate test. Indomethacin (a cyclooxygenase inhibitor) and amitriptyline hydrochloride (a tricyclic antidepressant) treatments did not affect flinches or thermal and mechanical hyperalgesia. On the other hand, morphine (an opioid) inhibited the flinch behavior and the thermal and mechanical hyperalgesia. These effects of morphine on pain-like behavior were prevented by naloxone (an opioid receptor antagonist) treatment. None of the treatments affected paw edema/tumor growth. The results showed that, in addition to tumor growth, administration of the Ehrlich tumor cells may represent a novel model for the study of cancer pain, specially the pain that is susceptible to treatment with opioids, but not to cyclooxygenase inhibitor or to tricyclic antidepressant.

1. Introduction

Pain is a symptom related to poor quality of life in cancer patients. In fact, in the United States, it is the most frequent cause of disability in these patients [1, 2]. Furthermore, reports of cancer pain have been increasing over the years accompanying the increased survival of patients [3, 4]. Most patients with advanced cancer (60%–85%) and 5-year survivors (40%) report pain [5–8]. In patients with advanced cancer, 62%–85% experience significant pain that is described as moderate to severe in approximately 4%–50% and as very severe in 25%–30% [9]. In fact, approximately 43% of the patients report feeling pain as early as diagnosis [7]. Therefore, pain management in cancer patients is a public health issue, and the mechanisms of cancer pain are not completely understood [7].

In this sense, there are various animal models of cancer pain that are used in an attempt to clarify the nociceptive

pathways involved in cancer-related pain, including skin cancer pain [10], neuropathic cancer pain [11], and bone cancer pain [12, 13]. These models have been important, for instance, in the demonstration of the contribution of transient receptor potential vanilloid receptor 1 (TRPV1), acid-sensing ion channels (ASICs), nerve growth factor (NGF), bradykinin, adenosine triphosphate (ATP), endothelin, and other mediators in the nociceptor sensitization during cancer pain [14]. There is also evidence that the inflammatory response against the tumor cells results in the production of cytokines and chemokines that sensitize the nociceptors by receptor-mediated activation of protein kinase C (PKC) and protein kinase A (PKA) and/or activation of mytogen-activated protein kinases such as p38. The activation of these intracellular pathways results in activation of TRPV1 and tetrodotoxin-resistant sodium channels and increased expression of TRPV1 [15]. Therefore, there are complex mechanisms, which may also vary depending on the cancer type.

The Ehrlich tumor is a spontaneous murine mammary adenocarcinoma [16] adapted to ascites form [17] and carried in mice by serial intraperitoneal (i.p.) passages [18]. The ascitic form of the tumor has been used as experimental model to assess the influence of drugs of different origins on its proliferation and host responses against the tumor cells [19–21]. The characteristic ascites is probably formed as a consequence of the inflammatory response towards tumor cells resulting in increased peritoneal vascular permeability [22]. Other factors that contribute to ascites and lethality of the Ehrlich tumor includes the impaired peritoneal lymphatic drainage by the tumor cells [22], the mechanic pressure exerted by progressive increase of ascitic fluid, peritoneal hemorrhage, and endotoxemia [23–25]. The Ehrlich tumor cells are also used as a model of solid tumor by injection in different sites [26].

Despite the wide use of the Ehrlich tumor cells in the investigation of the mechanisms of tumor proliferation as well as the host inflammatory and oxidative responses against tumor cells, it is yet undetermined whether inoculation of the Ehrlich tumor cells could represent a murine model to study cancer pain. Therefore, the present study standardized a murine model of cancer pain induced by the intraplantar injection of the Ehrlich tumor cells and investigated the pharmacological susceptibility of the model using three classes of analgesics.

2. Materials and Methods

2.1. Animals. The experiments were performed on male Swiss mice (20–25 g, Universidade Estadual de Londrina, Londrina, PR, Brazil) housed in standard clear plastic cages (six per cage) with free access to food and water. The behavioral testing was performed between 9:00 am and 5:00 pm in a temperature-controlled room. Animals' care and handling procedures were in accordance with the International Association for Study of Pain (IASP) guidelines and with the approval of the Ethics Committee of Universidade Estadual de Londrina. All efforts were made to minimize the number of animals used and their suffering.

2.2. The Ehrlich Tumor Cells Inoculation. The Ehrlich tumor cells were collected from ascitic fluid of the peritoneal cavity of mice 10 days after tumor administration. The ascitic fluid was washed in phosphate-buffered saline (PBS, pH 7.4), centrifuged (200 g, 10 min), and washed with PBS three times. The cell viability was determined by the 0.5% trypan blue exclusion method in the Neubauer chamber [27]. The Ehrlich tumor cells were suspended to the final concentrations of 1×10^4, 1×10^5, 1×10^6, and 1×10^7 in 25 μL of saline. Measurements were performed before and after injection of tumor cells between days 0 and 12.

2.3. Drugs. Drugs were obtained from the following sources: indomethacin from Prodome Chemical and Pharmaceutical (Sao Paulo, SP, Brazil), amitriptyline from Germed (Sao Bernardo do Campo, SP, Brazil), morphine sulphate from Cristalia (São Paulo, SP, Brazil), and naloxone hydrochloride from Sigma-Aldrich (St Louis, MO, USA).

2.4. Protocols. Firstly, mice received intraplantar (i.pl.) injection of the Ehrlich tumor cells (1×10^4–10^7 in 25 μL) or saline. Measurements of mechanical and thermal hyperalgesia, paw edema/tumor growth, and overt pain-like behavior were performed on days 0–12. According to the results, the dose of 1×10^6/paw of tumor cells was chosen for next experiments of mechanical hyperalgesia, thermal hyperalgesia, paw edema/tumor growth, and histological analysis at indicated timepoints. The dose of 1×10^7/paw of tumor cells and evaluation at the 8th day after inoculation were chosen for experiments of overt pain. Paw samples were collected for histological analysis and microscopic observation 12 days after tumor injection. To evaluate the hyperalgesic effect of cellular remnants, the Ehrlich tumor cells were inactivated and injected i.pl., and compared with the saline and the viable Ehrlich tumor cells groups; measurements were performed on days 0–12. To evaluate the pharmacological modulation of the Ehrlich tumor-induced pain-like behavior, mice were treated with the cyclooxygenase inhibitor (indomethacin, 0.7, 2, and 6 mg/kg, i.p.) or opioid (morphine, 1, 3, and 10 mg/kg, i.p.) on the 8th day after the Ehrlich tumor cells administration, and the evaluation of mechanical and thermal hyperalgesia, paw edema/tumor growth, and overt pain was performed 3 h or 45 min after the treatment, respectively. Another group of mice was treated with tricyclic antidepressant (amitriptyline, 3, 10, and 30 mg/kg, p.o.) daily during 12 days. The evaluation of mechanical and thermal hyperalgesia, paw edema/tumor growth, and overt pain was performed 3 h after treatment on days 0–12. It is noteworthy that different experimenters prepared the solutions, made the administrations, and performed the evaluation of pain-like behavior.

2.5. The Electronic Pressure Meter Test of Mechanical Hyperalgesia. Mechanical hyperalgesia was tested in mice as previously reported [28]. Briefly, the test consists of evoking a hindpaw flexion reflex with a hand-held force transducer (the electronic von Frey anesthesiometer: Insight, Ribeirão Preto, SP, Brazil) adapted with a 0.5 mm^2 contact area polypropylene tip. The investigator was trained to apply the tip perpendicularly to the central area of the hindpaw, and the endpoint

was characterized by the removal of the paw. The results are expressed by delta (Δ) withdrawal threshold (in g), which was calculated by subtracting the zero-time mean measurements from the mean measurements (indicated timepoints) after stimulus.

2.6. The Hot-Plate Test of Thermal Hyperalgesia. Thermal hyperalgesia was evaluated before and at indicated timepoints after injection of the Ehrlich tumor cells. In brief, mice were placed in a 10 cm wide glass cylinder on a hot plate (Hot Plate HP-2002, Insight Equipamentos, Ribeirao Preto, SP, Brazil) maintained at 55°C. The reaction time was scored when the animal jumped, flinched, and/or licked its paws. A maximum latency (cutoff) was set at 30 s to avoid tissue damage [29].

2.7. Evaluation of Paw Edema/Tumor Growth. The paw edema/tumor growth was determined before and at indicated timepoints (at 48 h intervals) after the injection of the Ehrlich tumor cells using an analog caliper. Paw edema/tumor growth was presented as Δ mm [29].

2.8. Overt Pain-Like Behavior Evaluation. Mice were placed in clear glass compartments at room temperature. After an acclimation period of 15 min, mice were observed for 10 min, and the cumulative number of flinches was measured [27].

2.9. Histopathological Analysis. On the 12th day after injection of tumor cells, mice were killed, and the paws were removed and fixed in the Bowen solution (75% picric acid, 25% formaldehyde, and 5% acetic acid) for 21 days. The samples were embedded in paraffin, sectioned into 5 μm sections, and stained with hematoxylin and eosin for light microscopic observation.

2.10. Inactivation of the Ehrlich Tumor Cells by Thermal Alteration. The Ehrlich tumor cells were inactivated to evaluate the involvement of cellular remnants in pain induced by the Ehrlich tumor cells. For this, the cells were inactivated by the process of freezing and heating. The Ehrlich tumor cells were first suspended to the final concentration of 1×10^6 or 1×10^7; next cell suspension was submerged in liquid nitrogen for 5 min and then heated in water-bath (80°C) during 5 min (EvLab, Londrina, PR, Brazil). This process was repeated 5 times, followed by assessment of cell viability by the trypan blue test, in order to confirm that cells were not viable. Mice received the equivalent to 1×10^6 or 1×10^7 inactivated tumor cells, viable cells, or saline (25 μL) i.pl. The evaluation of mechanical and thermal hyperalgesia and paw edema/tumor growth was performed between days 0 and 12 and, the evaluation of the overt pain was performed in 8th day.

2.11. Statistical Analysis. Results are presented as mean ± SEM of measurements made on 6 animals in each group in each experiment and are representative of two independent experiments. The two-way analysis of variance (ANOVA) was used to compare the groups and doses at all times (curves) when the hyperalgesic responses were measured at different times after the stimulus injection. The analyzed factors were treatment, time, and time *versus* treatment interaction. When there was a significant time *versus* treatment interaction, one-way ANOVA followed by Tukey's *t*-test was performed for each time. On the other hand, when the hyperalgesic responses were measured once after the stimulus injection, the differences between responses were evaluated by one-way ANOVA followed by Tukey's *t*-test. Additionally, comparative statistical analysis between two groups was done using the *t*-test. Statistical differences were considered to be significant at $P < 0.05$.

3. Results

3.1. The Subcutaneous Injection of the Ehrlich Cells Induces Mechanical and Thermal Hyperalgesia, Paw Edema/Tumor Growth, and Overt Pain-Like Behavior in a Dose-Dependent Manner. The Ehrlich tumor cells (1×10^4–10^7 in 25 μL per paw), or the vehicle group (PBS), were subcutaneously injected in the mouse hindpaw (i.pl.), and mechanical hyperalgesia was evaluated 2, 4, 6, 8, 10, and 12 days after cell injection, Figure 1(a). The mechanical hyperalgesia induced by tumor cells was dose and time dependent. All doses of tumor cells tested induced significant mechanical hyperalgesia on day 8, which remained on days 10 and 12. There was no statistical difference between the doses of 10^6 and 10^7 tumor cells regarding mechanical hyperalgesia, Figure 1(a). There was no difference between the doses in the hot-plate test (data not shown); therefore, for clear presentation, only the results on thermal hyperalgesia and the dose of 10^6 are shown in Figure 1(b). The injection of tumor cells induced a progressive and dose-dependent increase in paw edema/tumor growth, Figure 1(c), which corroborates the progressive increase of mechanical hyperalgesia in Figure 1(a). The dose of 10^4 did not induce significant paw edema/tumor growth, while 10^5 induced at days 10 and 12, Figure 1(c). The paw edema/tumor growth was significant between 2 and 12 days for the doses of 10^6 and 10^7 (Figure 1(c)). Spontaneous nociceptive behavior was quantified by the number of flinches, Figure 1(d). The doses of 10^4 and 10^5 did not induce paw flinch, the dose of 10^6 induced paw flinch at days 10–12, and 10^7 induced a significant number of flinches at days 4–12 with a peak at day 8 (Figure 1(d)). Considering these results, the dose of the 10^6 Ehrlich tumor cells was chosen for histological analysis and behavioral experiments evaluating mechanical and thermal hyperalgesia and paw edema/tumor growth, while the dose of 10^7 was chosen for overt pain-like behavior evaluation.

3.2. Histopathological Analysis. Mice were sacrificed at day 12 after injection of the Ehrlich tumor cells or saline (25 μL), and the paws were collected for histological analysis performed with hematoxylin/eosin staining (Figure 2). There was no histological abnormality in mice that received i.pl. injection of saline (Figure 2(a)), presenting normal epithelium (arrow 1) and normal bone cartilage (arrow 2). Mice that received i.pl. injection of the Ehrlich tumor cells (10^4–10^7) showed malignant neoplasm and poor differentiation, characterized by the presence of tumor cells, with nucleus showing frequent aberrant mitosis. Considering that there was no difference between the different doses of tumor cells

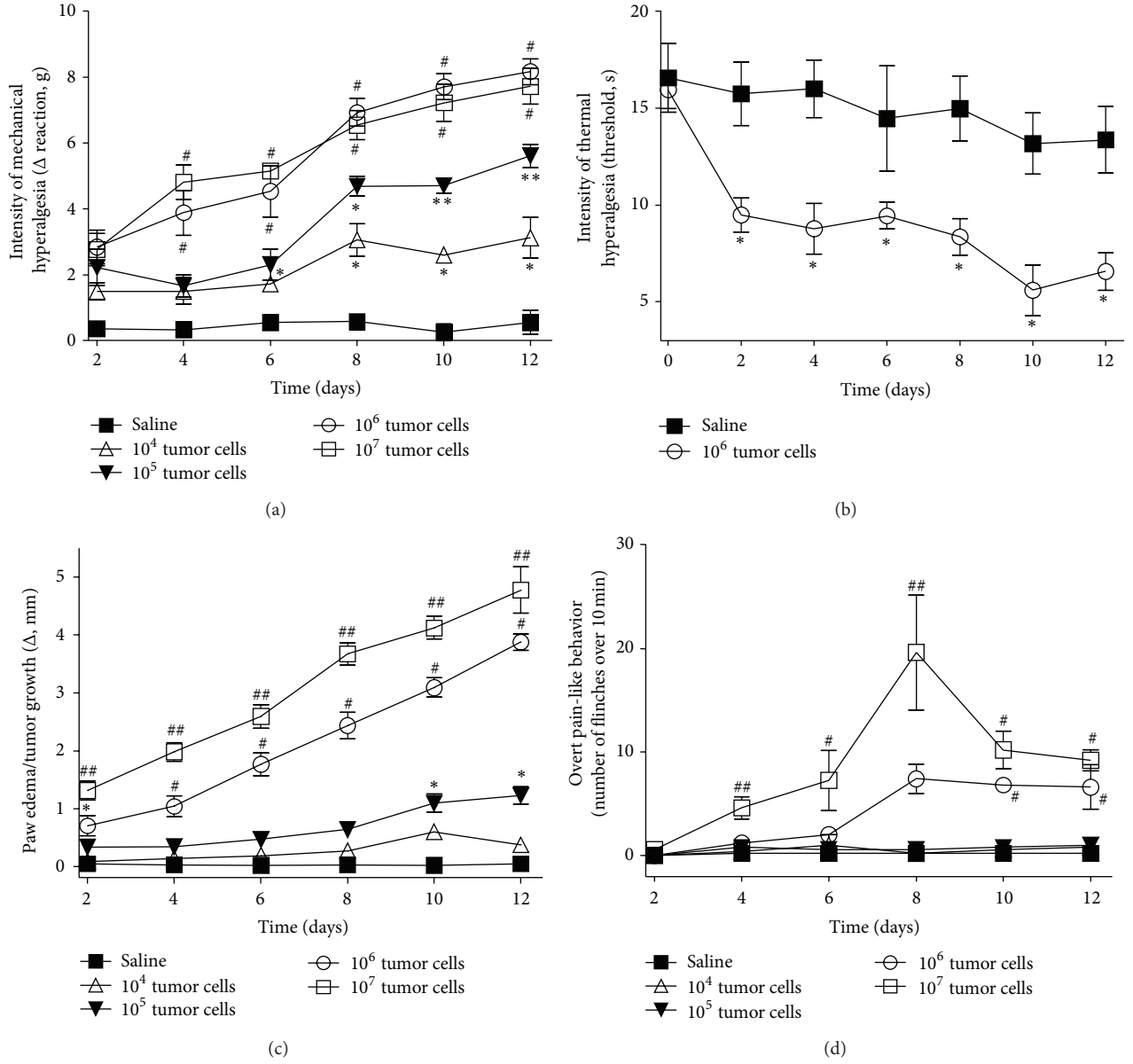

FIGURE 1: The Ehrlich tumor induces pain and paw edema/tumor growth in a dose-dependent manner. The Ehrlich tumor cells ($1 \times 10^{4-7}$) or saline (25 μL) was injected subcutaneously in the paw. (a) The intensity of mechanical hyperalgesia, (b) thermal hyperalgesia, (c) paw edema/tumor growth, and (d) overt pain-like behavior was evaluated between 0 and 12 days at every-other-day intervals after injection of tumor cells or saline; $n = 6$, representative of two experiments. $^{*}P < 0.05$ compared with saline; $^{**}P < 0.05$ compared with saline and the dose of 10^4; $^{\#}P < 0.05$ compared with saline and the doses of 10^4 and 10^5; $^{\#\#}P < 0.05$ compared with saline and the doses of $1 \times 10^{4-6}$.

regarding the tumor characteristics, the figures represent the dose of the 10^6 Ehrlich tumor cells that was used in most of the evaluations (Figures 2(b)–2(h)). Figure 2(b) shows bone cartilage destruction induced by tumor cells (arrow 4). Figure 2(c) shows at 4x magnification the epithelium (arrow 1) and the presence of tumor cells (arrow 3) with intense areas of necrosis (arrow 5). Figure 2(d) shows areas of necrosis (arrow 5) induced by the Ehrlich tumor cells. Figure 2(e) shows at 10x magnification the presence of tumor cells (arrow 3) in a paw tissue, and Figure 2(f) shows tumor cells (arrow 3), areas of necrosis (arrow 5), and a presence of mitosis (arrow 6). Figure 2(g) shows the presence of atypical mitosis (arrow 6), and Figure 2(h) shows at 40x magnification mitosis (arrow 6) and tumor cells with atypical nucleus (arrow 7). Therefore, the histopathological analysis confirmed the presence of the tumor cells (Figures 2(b) and 2(h)), together with an extensive area of necrosis (Figures 2(c), 2(d), and 2(f)) characterized by neutrophilic infiltration, associated with the presence of fibrin and red blood cells, which gives an eosinophilic coloration (Figure 2(d)), tumor cells with aberrant mitosis (Figure 2(g)), and bone/cartilage destruction (Figure 2(b)).

3.3. Inactivation of the Ehrlich Tumor Cells by Thermal Alteration Abolishes the Nociceptive Responses. Mice received i.pl.

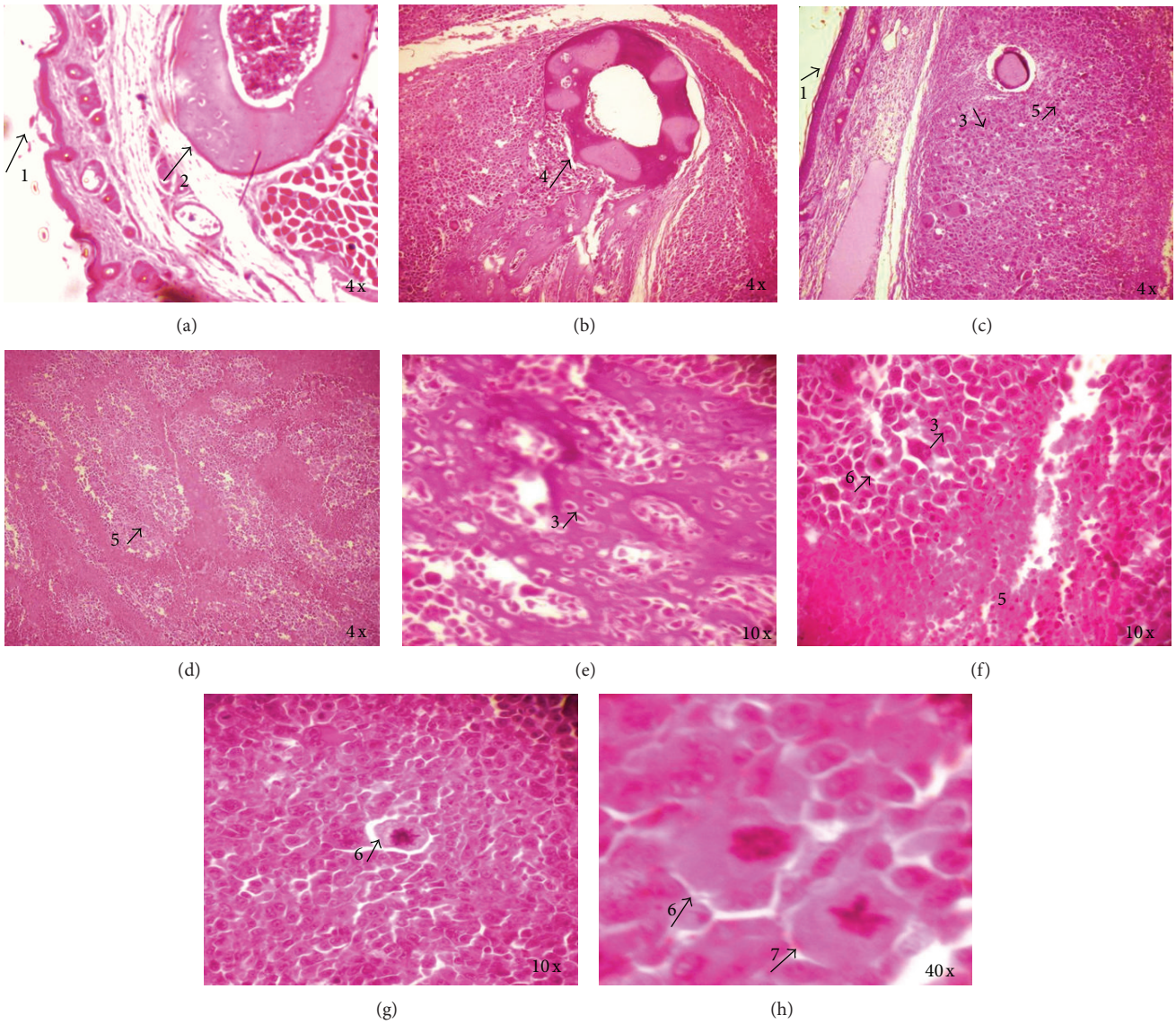

FIGURE 2: Histopathological analysis of paw injected with the Ehrlich tumor. The Ehrlich tumor cells (1×10^6) or saline (25 μL) was injected subcutaneously into the hindpaws of the mice. Panel (a) indicates histological sections of normal paw that received saline, and panels (b)–(h) indicate the paw that received the Ehrlich tumor cells stained by hematoxylin/eosin. Arrows (1) indicate normal epithelium; (2) normal bone cartilage; (3) tumor cells; (4) destroyed bone cartilage; (5) extensive area of necrosis; (6) tumor cells with mitosis or atypical mitosis; (7) and tumor cells with atypical nucleus.

injection of saline (25 μL), the viable Ehrlich tumor cells (10^6 or 10^7/paw), or the inactivated Ehrlich tumor cells (equivalent to 10^6 or 10^7 cells). Mechanical and thermal hyperalgesia and paw edema/tumor growth were evaluated between 0 and 12 days, and overt pain-like behavior was evaluated on day 8 after stimulus. The inactivation of the 10^6 Ehrlich tumor cells was able to abolish the mechanical (Figure 3(a)) and thermal (Figure 3(b)) hyperalgesia and paw edema/tumor growth (Figure 3(c)) compared with the viable cells. Inactivation of the 10^7 tumor cells also resulted in abolishment of overt pain-like behavior (Figure 3(d)) compared with the viable cells. Thus, the cellular remnants of the Ehrlich tumor cells were not capable of inducing paw edema/tumor growth and nociceptive responses, which suggests that these responses depend on the proliferation of tumor cells and their activities and interactions with the host immune responses.

3.4. Effect of Indomethacin Treatment on the Nociceptive Responses and Paw Edema/Tumor Growth Induced by the Ehrlich Tumor Cells. Mice received the 10^6 or 10^7 Ehrlich tumor cells, and on the 8th day, they were treated with indomethacin (0.7, 2, or 6 mg/Kg i.p.) or Tris buffer, and 3 h after the treatment mechanical, and thermal hyperalgesia, paw edema/tumor growth, and overt pain-like behavior were measured (Figure 4). The Ehrlich tumor cells induced significant mechanical (Figure 4(a)) and thermal (Figure 4(b)) hyperalgesia, paw edema/tumor growth (Figure 4(c)), and overt pain-like behavior (Figure 4(d)) compared with the

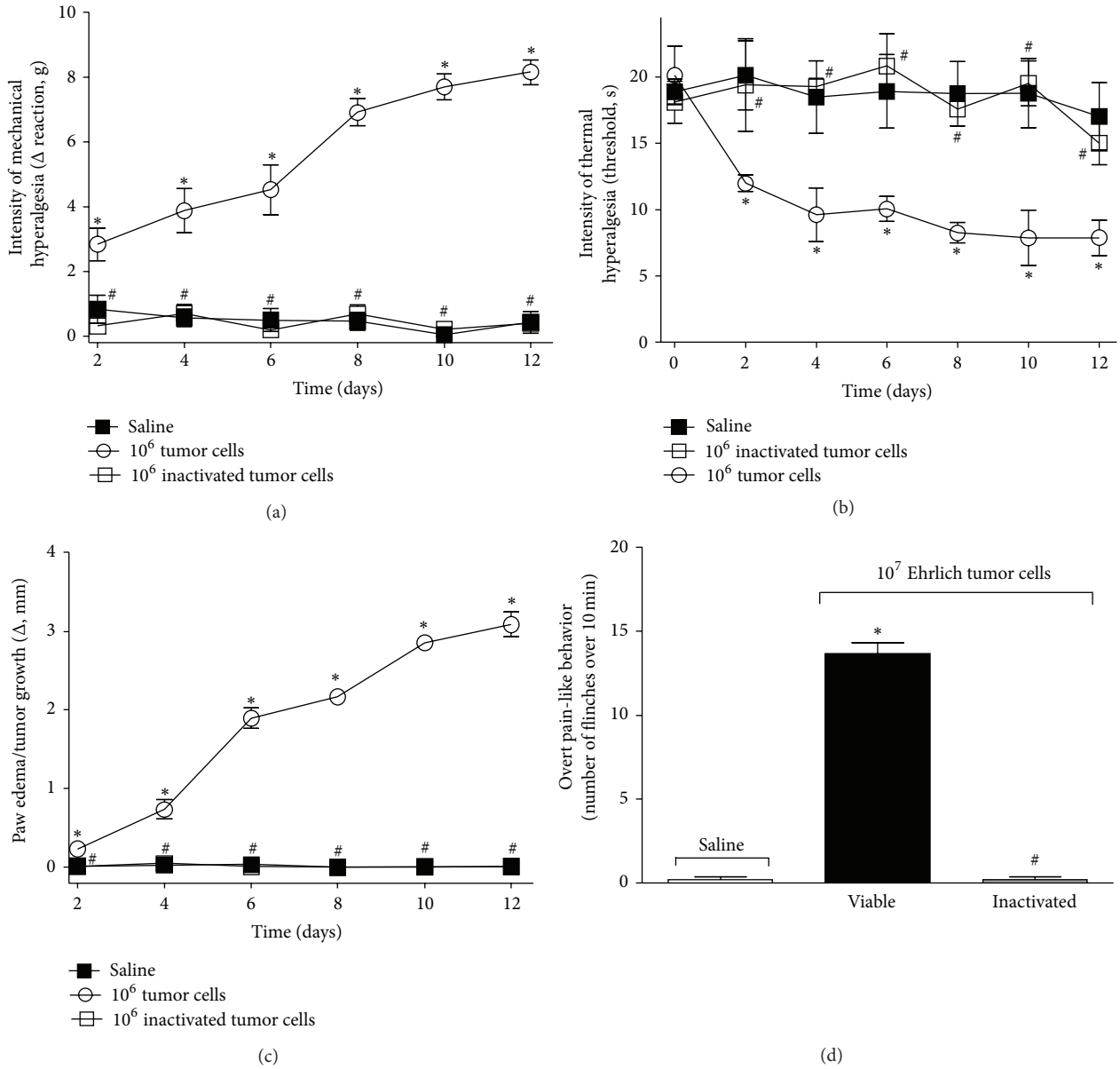

Figure 3: Thermal inactivation of the Ehrlich tumor cells abolishes pain and paw edema/tumor growth. The Ehrlich tumor cells (1×10^6) were inactivated by cold followed by heat. Mice received 25 μL of inactivated tumor cells, viable tumor cells (1×10^6), or saline. (a) The intensity of mechanical hyperalgesia, (b) thermal hyperalgesia, and (c) paw edema/tumor growth was evaluated on days 2–12 after injection of the inactivated Ehrlich tumor cells, viable tumor cells, or saline. Mice received 1×10^7 of inactivated tumor cells, viable cells, or saline and (d) the overt pain was evaluated on the 8th day after injection; $n = 6$, representative of two experiments. $^*P < 0.05$ compared with the saline, and $^\#P < 0.05$ compared with the viable 1×10^6 or 1×10^7 tumor cells.

saline group. However, the treatment with indomethacin did not affect those parameters induced by the Ehrlich tumor cells (Figure 4), indicating that they do not depend on the production of prostanoids.

3.5. Effect of Amitriptyline Treatment on the Nociceptive Responses and Paw Edema/Tumor Growth Induced by the Ehrlich Tumor Cells. After inoculation of the 10^6 or 10^7 Ehrlich tumor cells, mice were treated with amitriptyline (3, 10, and 30 mg/kg) or water via oral gavage (per oral: p.o.) once a day during 12 days, and 3 h after treatment, mechanical and thermal hyperalgesia, paw edema/tumor growth, and overt pain-like behavior were evaluated (Figure 5). None of the doses of amitriptyline affected the Ehrlich tumor cells-induced mechanical hyperalgesia (Figure 5(a)), thermal hyperalgesia (Figure 5(b)), paw edema/tumor growth (Figure 5(c)), or overt pain (Figure 5(d)). These results suggest that the inhibition of serotonin and/or norepinephrine reuptake does not affect the maintenance of cancer pain in this model.

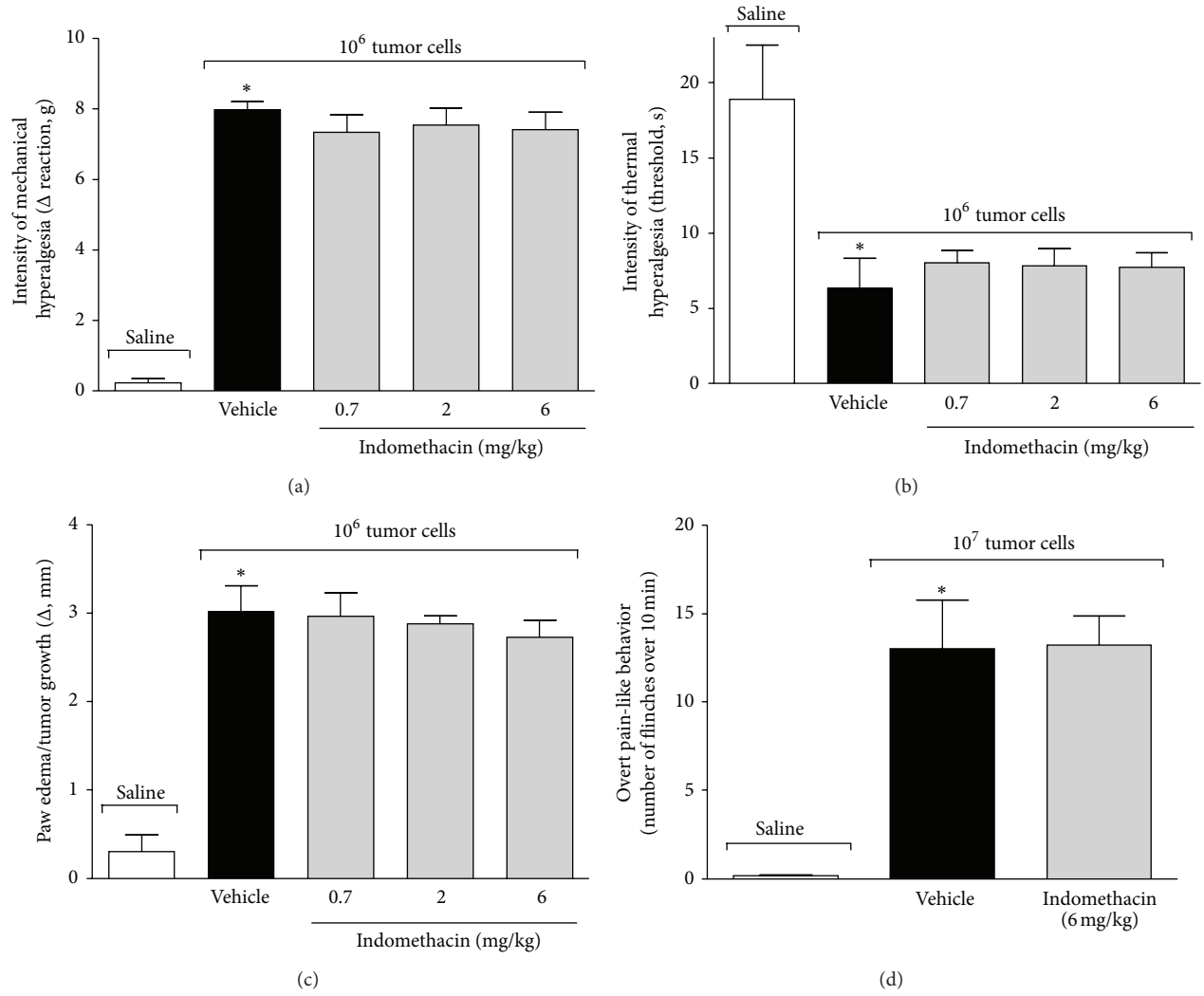

Figure 4: Effect of indomethacin treatment on pain and paw edema/tumor growth induced by the Ehrlich tumor cells. Mice received the 1×10^6 Ehrlich tumor cells or saline, and on the 8th day, they were treated with indomethacin (0.7–6 mg/kg, i.p.) or Tris buffer. (a) The intensity of mechanical hyperalgesia, (b) thermal hyperalgesia, and (c) paw edema/tumor growth was evaluated 3 h after the treatment. Mice received the 1×10^7 Ehrlich tumor cells or saline, and on 8th day, they were treated with indomethacin (6 mg/kg i.p.) or Tris buffer, and (d) overt pain was assessed 3 h after treatment; $n = 6$, representative of two experiments. $^*P < 0.05$ vehicle group compared with the saline.

3.6. Effect of Morphine Treatment on the Nociceptive Responses and Paw Edema/Tumor Growth Induced by the Ehrlich Tumor Cells. Mice were treated with morphine (1–10 mg/kg, i.p.) or saline on the 8th day after the Ehrlich tumor (10^6 or 10^7 cells) injection in which the peak of hyperalgesia was detected. After the treatment (45 min) with morphine, mechanical (Figure 6(a)) and thermal (Figure 6(b)) hyperalgesia and paw edema/tumor growth (Figure 6(c)) were evaluated. The morphine dose dependently inhibited Ehrlich tumor-induced mechanical (Figure 6(a)) and thermal (Figure 6(b)) hyperalgesia, but it did not affect the paw edema/tumor growth, which indicates that morphine presents analgesic effect not related to inhibition of tumor proliferation. The dose of 3 mg/kg of morphine reduced the Ehrlich tumor-induced mechanical hyperalgesia compared with the positive control, while the dose of 10 mg/kg of morphine presented significant inhibition compared with the Ehrlich tumor-positive control and the doses of 1 and 3 mg/kg of morphine (Figure 6(a)). The Ehrlich tumor-induced thermal hyperalgesia was inhibited by the dose of 10 mg/kg of morphine without significant inhibition with the doses of 1 and 3 mg/kg (Figure 6(b)). To confirm the receptor-dependent effect of morphine and that an opioid-receptor-dependent inhibition of the Ehrlich tumor-induced hyperalgesia was being observed, mice were treated with naloxone (1 mg/kg, i.p.) 1 h before morphine (10 mg/kg) treatment, and after additional 45 min, measurements of mechanical (Figure 6(d)) and thermal (Figure 6(e)) hyperalgesia were performed. Again, the Ehrlich tumor-induced (10^6 cells) mechanical and thermal hyperalgesia were inhibited by morphine, and this inhibition was prevented by naloxone treatment. Furthermore, the Ehrlich tumor induced (10^7 cells) spontaneous flinches at the 8th day

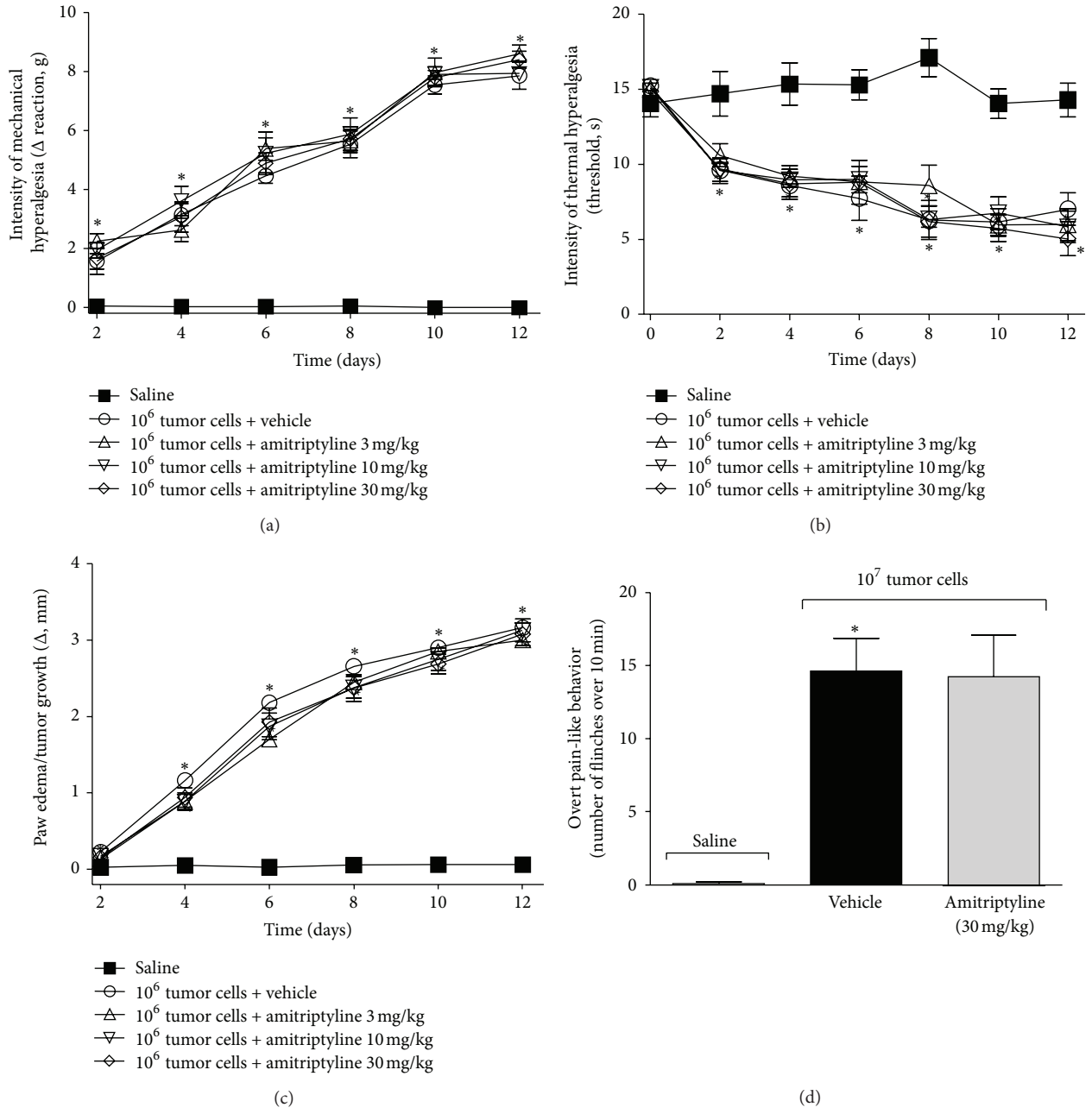

FIGURE 5: Effect of amitriptyline treatment on pain and paw edema/tumor growth induced by the Ehrlich tumor cells. Mice received the 1×10^6 Ehrlich tumor cells or saline, and they were treated with amitriptyline (3–30 mg/kg, p.o.) or water every day after subcutaneous injection of tumor cells. (a) The intensity of mechanical hyperalgesia, (b) thermal hyperalgesia, and (c) paw edema/tumor growth was evaluated 3 h after the treatment on days 2, 4, 6, 8, 10, and 12 after injection of the cells. Mice received the 1×10^7 Ehrlich tumor cells or saline and were treated daily with amitriptyline (30 mg/kg, p.o.) or water and after 8 days; (d) the overt pain was assessed 3 h after the treatment; $n = 6$, representative of two experiments. $^*P < 0.05$ compared with the saline.

of cancer development, which were also inhibited by morphine treatment (10 mg/kg), and the analgesic effect of morphine was prevented by naloxone treatment (Figure 6(f)). Therefore, the Ehrlich tumor induces mechanical and thermal hyperalgesia and overt pain-like behavior susceptible to opioid-receptor analgesia (Figure 6).

4. Discussion

Cancer pain directly affects the quality of life and survival of patients with cancer [11, 30]. Cancer pain is characterized by the presence of hyperalgesia, allodynia, and/or spontaneous pain. Tactile allodynia and mechanical hyperalgesia

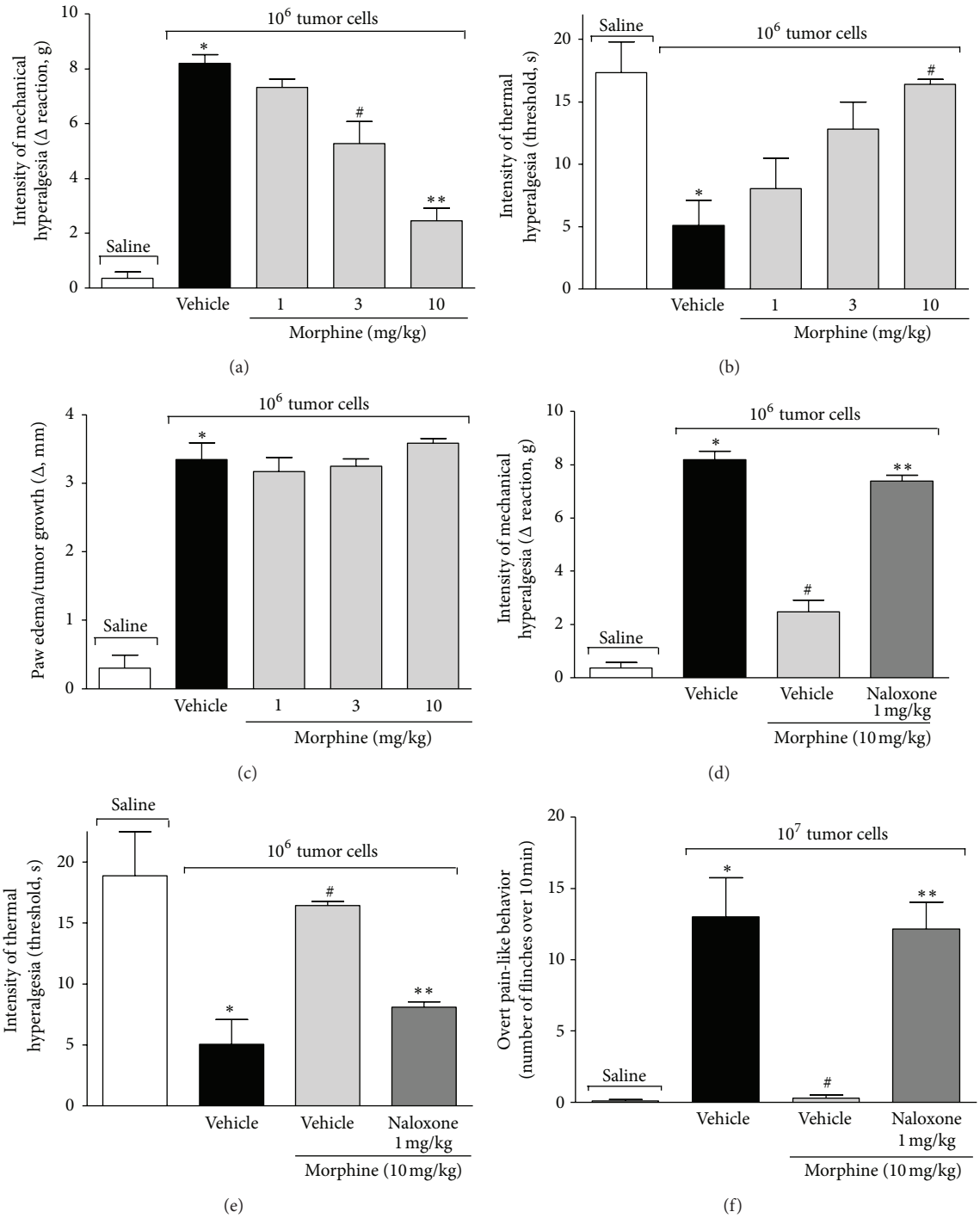

FIGURE 6: Effect of morphine treatment on pain and paw edema/tumor growth induced by the Ehrlich tumor cells. Mice that received the 1×10^6 Ehrlich tumor cells were treated with morphine (1–10 mg/Kg, i.p.) or saline on the 8th day after tumor cells injection. (a) The intensity of mechanical hyperalgesia, (b) thermal hyperalgesia, and (c) paw edema/tumor growth was evaluated 45 minutes after treatment with morphine. In another set, mice were treated with naloxone (1 mg/kg, i.p.) 1 hour before the treatment with morphine (10 mg/kg i.p.), and (d) 45 minutes after morphine treatment, the intensity of mechanical hyperalgesia and (e) thermal hyperalgesia was evaluated. Mice received the 1×10^7 Ehrlich tumor cells or saline, and after 8 days, they were treated with naloxone (1 mg/kg i.p.) 1 h before treatment with morphine (10 mg/kg i.p.), and (f) 45 min after the treatment with morphine, the overt pain was assessed; $n = 6$, representative of two experiments. $^{*}P < 0.05$ vehicle group compared with the saline; $^{\#}P < 0.05$ compared with the tumor or compared with the treatment with naloxone plus morphine, and $^{**}P < 0.05$ compared with the doses of 1 and 3 mg/kg morphine.

are important features of cancer pain and decrease the life quality of patients. Considering the importance of pain in cancer, several experimental models, including neuropathic cancer pain [11], bone cancer pain [12, 31, 32], and cancer pain induced by orthotopic tumor inoculation in mice [10, 33], have been developed and contributed to the characterization of the pathophysiology of cancer pain.

Several experimental studies have shown that marked nociceptive reactions induced by malignant tumor vary with animal species, tumor types, and localizations of the tumor [10–12, 33–36]. In the present study, we develop a model of pain characterized by mechanical and thermal hyperalgesia and spontaneous pain-like behavior, for example, flinching of the paw. The mechanical hyperalgesia and flinches were dependent on the number of the Ehrlich tumor cells injection and were progressive over time. The time- and dose-dependent features of the present model argue in its favor as a good model to investigate the effect of novel analgesics and mechanisms involved in cancer pain regarding mechanical hyperalgesia and overt pain-like behavior. It is noteworthy that, in the case of thermal hyperalgesia, it was significant and increased over time, but there were no differences in the responses induced by different number of the Ehrlich tumor cells injected.

It is important to understand the mechanisms involved in the model used to investigate the action of novel drugs and to have a clear view of the possible mechanisms to be addressed. Nevertheless, as a first insight into the mechanisms involved in the Ehrlich tumor-induced nociception, it was determined its susceptibility to three classes of analgesics; nonsteroidal anti-inflammatory drug, tricyclic antidepressant, and opioid. The acute treatment with nonsteroidal anti-inflammatory drug, indomethacin, a cyclooxygenase inhibitor, did not affect the nociceptive responses and paw edema/tumor growth induced by the Ehrlich tumor. Indomethacin did not affect pain in a model of femur cancer pain induced by fibrosarcoma cells in mice [37]. On the other hand, in a model of bone cancer pain induced by injection of osteolytic murine sarcoma into the femur, the oral administration of indomethacin reduced pain behavior in mice [38]. These controversial data may be due to the different routes of administration that were used, the different doses of treatment, and mainly the different models of cancer pain.

Chronic treatment with amitriptyline, a tricyclic antidepressant inhibitor of reuptake of serotonin and norepinephrine, did not inhibit the nociception induced by the Ehrlich tumor cells. Others have shown that amitriptyline reduced only spontaneous pain behavior at sedative doses [37]. Tricyclic antidepressants have been extensively studied because there is evidence of their analgesic properties in several chronic diseases [37], and neuropathic pain [39]. However, the reuptake of serotonin and norepinephrine seems not to be related to the maintenance of cancer pain induced by the Ehrlich tumor.

The treatment with morphine dose dependently reduced the nociception induced by the Ehrlich tumor. Additionally, it was observed that the effect of morphine was receptor specific, because the opioid receptor antagonist naloxone reversed the effect of morphine. Despite the reduction of nociception promoted by morphine, there was no change in tumor growth, which indicates that morphine inhibited nociceptive responses rather than reduced nociception by decreasing tumor growth.

Despite all of the research performed in an attempt to inhibit cancer pain, it cannot be stated the exact mechanisms involved in the maintenance and chronicity of cancer pain. In fact, cancer patients still face inadequate analgesia. One major reason is that, despite some similarities, each model of cancer pain has its peculiar mechanisms similarly to each type of cancer in humans. Thus, it is conceivable that a great variety of cancer pain models are necessary to line up with varied human conditions. Bone cancer pain models are considered particularly interesting since during metastasis tumor cells may reach the bones. In the present study, there was bone cartilage destruction in the foci of tumor injected, indicating that there might be a bone pain component in this model. Nevertheless, models that evaluate the pain before metastasis are also important. To exemplify conditions in which cancer pain before metastasis is important, it is noteworthy to mention that a third of breast cancer patients will report pain in the lump spontaneously or upon examination [40]. The present model using the injection of cells of a murine mammary adenocarcinoma presents a condition resembling the preoperative breast cancer pain since there is spontaneous pain-like behavior in the paw and hyperalgesia upon stimulation of the lump (foci of tumor injection in the paw). Importantly, there is a significant relation between preoperative breast pain and phantom breast pain syndrome [41], and treatment of pain prior to mastectomy is an important clinical approach to reduce the incidence of phantom breast pain syndrome. Therefore, the present model might contribute as a model to study preoperative breast cancer pain mechanisms.

5. Conclusion

We have characterized a cancer pain model induced by subcutaneous injection of the Ehrlich tumor cells into the hindpaw of mice. This model is characterized by robust tumor growth and rapid development of mechanical and thermal hyperalgesia and overt pain-like behavior, rendering it as convenient to study the mechanisms of cancer pain and tumor growth and to test new treatments.

Conflict of Interests

The authors declare that they have no conflict of interests.

Acknowledgments

The authors appreciate the technical support of Jesus Vargas, Pedro Dionísio Filho, Talita P. Domiciano (received a SETI/Fundação Araucária and Parana State Government fellowship), and Miriam S. N. Hohmann for the English editing. This work was supported by grants from SETI/Fundação Araucária, Parana State Government, Fundo de Apoio ao Ensino Pesquisa e Extensão/Universidade Estadual de Londrina (FAEPE/UEL 01/2011 and 02/2011), Conselho Nacional

de Desenvolvimento Científico e Tecnológico (CNPq), and Coordenadoria de Aperfeiçoamento de Pessoal de Nível Superior (CAPES), Brazil. W. A. Verri Jr. received a senior research fellowship from CNPq, and R. Cecchini, E. G. Moreira and R. Casagrande received senior research fellowship from SETI/Fundação Araucária and Parana State Government.

References

[1] P. E. Greenberg, S. A. Leong, H. G. Birnbaum, and R. L. Robinson, "The economic burden of depression with painful symptoms," *Journal of Clinical Psychiatry*, vol. 64, no. 7, pp. 17–23, 2003.

[2] C. R. Green, S. K. Ndao-Brumblay, and T. Hart-Johnson, "Sleep problems in a racially diverse chronic pain population," *Clinical Journal of Pain*, vol. 25, no. 5, pp. 423–430, 2009.

[3] W. F. Stewart, J. A. Ricci, E. Chee, D. Morganstein, and R. Lipton, "Lost productive time and cost due to common pain conditions in the US workforce," *Journal of the American Medical Association*, vol. 290, no. 18, pp. 2443–2454, 2003.

[4] D. C. Turk, "Clinical effectiveness and cost-effectiveness of treatments for patients with chronic pain," *Clinical Journal of Pain*, vol. 18, no. 6, pp. 355–365, 2002.

[5] K. O. Anderson, T. R. Mendoza, V. Valero et al., "Minority cancer patients and their providers: pain management attitudes and practice," *Cancer*, vol. 88, no. 8, pp. 1929–1938, 2000.

[6] J. E. Nelson, D. E. Meier, E. J. Oei et al., "Self-reported symptom experience of critically ill cancer patients receiving intensive care," *Critical Care Medicine*, vol. 29, no. 2, pp. 277–282, 2001.

[7] A. Caraceni, "Evaluation and assessment of cancer pain and cancer pain treatment," *Acta Anaesthesiologica Scandinavica*, vol. 45, no. 9, pp. 1067–1075, 2001.

[8] C. R. Green, T. Hart-Johnson, and D. R. Loeffler, "Cancer-related chronic pain," *Cancer*, vol. 117, no. 9, pp. 1994–2003, 2011.

[9] M. H. J. van den Beuken-van Everdingen, J. M. de Rijke, A. G. Kessels, H. C. Schouten, M. van Kleef, and J. Patijn, "Prevalence of pain in patients with cancer: a systematic review of the past 40 years," *Annals of Oncology*, vol. 18, no. 9, pp. 1437–1449, 2007.

[10] T. Sasamura, S. Nakamura, Y. Iida et al., "Morphine analgesia suppresses tumor growth and metastasis in a mouse model of cancer pain produced by orthotopic tumor inoculation," *European Journal of Pharmacology*, vol. 441, no. 3, pp. 185–191, 2002.

[11] M. Shimoyama, K. Tanaka, F. Hasue, and N. Shimoyama, "A mouse model of neuropathic cancer pain," *Pain*, vol. 99, no. 1-2, pp. 167–174, 2002.

[12] M. J. Schwei, P. Honore, S. D. Rogers et al., "Neurochemical and cellular reorganization of the spinal cord in a murine model of bone cancer pain," *Journal of Neuroscience*, vol. 19, no. 24, pp. 10886–10897, 1999.

[13] P. W. Wacnik, L. J. Eikmeier, T. R. Ruggles et al., "Functional interactions between tumor and peripheral nerve: morphology, algogen identification, and behavioral characterization of a new murine model of cancer pain," *Journal of Neuroscience*, vol. 21, no. 23, pp. 9355–9366, 2001.

[14] P. W. Mantyh, "Mechanisms of malignant bone pain," in *Cancer Pain: From Molecules to Suffering*, A. J. Paice, R. F. Bell, E. A. Kalso, and O. A. Soyannwo, Eds., chapter 3, pp. 45–62, IASP Press, Washington, DC, USA, 1st edition, 2010.

[15] M. Kress, "Cytokines and cancer pain," in *Cancer Pain: From Molecules to Suffering*, A. J. Paice, R. F. Bell, E. A. Kalso, and O. A. Soyannwo, Eds., chapter 4, pp. 63–84, IASP Press, Washington, DC, USA, 1st edition, 2010.

[16] P. Ehrlich and H. Apolant, "Beobachtungen uber maligne mausetumoren," *Berliner Klinische Wochenschrift*, vol. 42, pp. 871–874, 1905.

[17] H. Loewenthal and G. Jahn, "Übertragunsversuche mit carcinomatöser Mäuse-Ascitesflüssigkeit und ihr Verhalten gegen physikalische und chemische Einwirkungen," *Zeitschrift für Krebsforschung*, vol. 37, no. 1, pp. 439–447, 1932.

[18] H. Ahmed, B. P. Chatterjee, and A. K. Debnath, "Interaction and in vivo growth inhibition of Ehrlich ascites tumor cells by jacalin," *Journal of Biosciences*, vol. 13, no. 4, pp. 419–424, 1988.

[19] S. Kametani, T. Oikawa, A. Kojima-Yuasa et al., "Mechanism of growth inhibitory effect of cape aloe extract in Ehrlich ascites tumor cells," *Journal of Nutritional Science and Vitaminology*, vol. 53, no. 6, pp. 540–546, 2007.

[20] E. Balamurugan, B. V. Reddy, and V. P. Menon, "Antitumor and antioxidant role of Chrysaora quinquecirrha (sea nettle) nematocyst venom peptide against ehrlich ascites carcinoma in Swiss Albino mice," *Molecular and Cellular Biochemistry*, vol. 338, no. 1-2, pp. 69–76, 2009.

[21] A. Kumar, S. S. D'Souza, S. R. Mysore Nagaraj, S. L. Gaonkar, B. P. Salimath, and K. M. L. Rai, "Antiangiogenic and antiproliferative effects of substituted-1,3,4-oxadiazole derivatives is mediated by down regulation of VEGF and inhibition of translocation of HIF-1α in Ehrlich ascites tumor cells," *Cancer Chemotherapy and Pharmacology*, vol. 64, no. 6, pp. 1221–1233, 2009.

[22] J. Fastaia and A. E. Dumont, "Pathogenesis of ascites in mice with peritoneal carcinomatosis," *Journal of the National Cancer Institute*, vol. 56, no. 3, pp. 547–550, 1976.

[23] F. Hartveit, "The immediate cause of death in mice with Ehrlich's ascites carcinoma," *Acta Pathologica et Microbiologica Scandinavica*, vol. 65, no. 3, pp. 359–365, 1965.

[24] K. D. Mayer, "The pathogenicity of the Ehrlich ascites tumour," *British Journal of Experimental Pathology*, vol. 47, no. 5, pp. 537–544, 1966.

[25] J. Vieira, P. Matsuzaki, M. K. Nagamine et al., "Inhibition of ascitic Ehrlich tumor cell growth by intraperitoneal injection of Pfaffia paniculata (Brazilian ginseng) butanolic residue," *Brazilian Archives of Biology and Technology*, vol. 53, no. 3, pp. 609–613, 2010.

[26] X. Zhu, H. Wu, J. Xia, M. Zhao, and Z. Xianyu, "The relationship between ^{99m}Tc-MIBI uptakes and tumor cell death/proliferation state under irradiation," *Cancer Letters*, vol. 182, no. 2, pp. 217–222, 2002.

[27] P. Brigatte, S. C. Sampaio, V. P. Gutierrez et al., "Walker 256 tumor-bearing rats as a model to study cancer pain," *Journal of Pain*, vol. 8, no. 5, pp. 412–421, 2007.

[28] T. M. Cunha, W. A. Verri Jr., G. G. Vivancos et al., "An electronic pressure-meter nociception paw test for mice," *Brazilian Journal of Medical and Biological Research*, vol. 37, no. 3, pp. 401–407, 2004.

[29] D. A. R. Valério, T. M. Cunha, N. S. Arakawa et al., "Anti-inflammatory and analgesic effects of the sesquiterpene lactone budlein A in mice: inhibition of cytokine production-dependent mechanism," *European Journal of Pharmacology*, vol. 562, no. 1-2, pp. 155–163, 2007.

[30] S. J. Medhurst, K. Walker, M. Bowes et al., "A rat model of bone cancer pain," *Pain*, vol. 96, no. 1-2, pp. 129–140, 2002.

[31] D. R. Clohisy, C. M. Ogilvie, and M. L. R. Ramnaraine, "Tumor osteolysis in osteopetrotic mice," *Journal of Orthopaedic Research*, vol. 13, no. 6, pp. 892–897, 1995.

[32] L. Menendéz, L. Juárez, V. García, A. Hidalgo, and A. Baamond, "Involvement of nitric oxide in the inhibition of bone cancer-induced hyperalgesia thought the activation of peripheral opioid receptors in mice," *Neuropharmacology*, vol. 53, no. 1, pp. 71–80, 2007.

[33] Y. Kuraishi, Y. Iida, H. Zhang et al., "Suppression by gabapentin of pain-related mechano-responses in mice given orthotopic tumor inoculation," *Biological and Pharmaceutical Bulletin*, vol. 26, no. 4, pp. 550–552, 2003.

[34] N. M. Luger, P. Honore, M. A. C. Sabino et al., "Osteoprotegerin diminishes advanced bone cancer pain," *Cancer Research*, vol. 61, no. 10, pp. 4038–4047, 2001.

[35] R. K. Portenoy and G. Frager, "Pain management: pharmacological approaches," *Cancer Treatment and Research*, vol. 100, pp. 1–29, 1999.

[36] M. Shimoyama, H. Tatsuoka, S. Ohtori, K. Tanaka, and N. Shimoyama, "Change of dorsal horn neurochemistry in a mouse model of neuropathic cancer pain," *Pain*, vol. 114, no. 1-2, pp. 221–230, 2005.

[37] M. E. Mouedden and T. F. Meert, "Pharmacological evaluation of opioid and non-opioid analgesics in a murine bone cancer model of pain," *Pharmacology Biochemistry and Behavior*, vol. 86, no. 3, pp. 458–467, 2007.

[38] O. Saito, T. Aoe, and T. Yamamoto, "Analgesic effects of non-steroidal antiinflammatory drugs, acetaminophen, and morphine in a mouse model of bone cancer pain," *Journal of Anesthesia*, vol. 19, no. 3, pp. 218–224, 2005.

[39] K. Vissers, V. Hoffmann, F. Geenen, R. Biermans, and T. Meert, "Is the second phase of the formalin test useful to predict activity in chronic constriction injury models? A pharmacological comparison in different species," *Journal of World Institute of Pain*, vol. 3, no. 4, pp. 298–309, 2003.

[40] W. G. Harris, E. A. Benson, D. Cartwright et al., "Symptoms and signs of operable breast cancer," *The Journal of the Royal College of General Practitioners*, vol. 33, pp. 473–476, 1983.

[41] K. Kroner, B. Krebs, J. Skov, and H. S. Jorgensen, "Immediate and long-term phantom breast syndrome after mastectomy: incidence, clinical characteristics and relationship to premastectomy breast pain," *Pain*, vol. 36, no. 3, pp. 327–334, 1989.

Hindawi Publishing Corporation
BioMed Research International
Volume 2013, Article ID 258141, 4 pages
http://dx.doi.org/10.1155/2013/258141

Review Article

The Role of Morphine in Animal Models of Human Cancer: Does Morphine Promote or Inhibit the Tumor Growth?

Sabrina Bimonte,[1] Antonio Barbieri,[1] Giuseppe Palma,[1,2] and Claudio Arra[1]

[1] *Istituto Nazionale per lo Studio e la Cura dei Tumori, "Fondazione G. Pascale," IRCCS, Via Mariano Semmola, 80131 Naples, Italy*
[2] *Istituto di Endocrinologia e Oncologia Sperimentale del Consiglio Nazionale delle Ricerche, Dipartimento di Biologia e Patologia Cellulare e Molecolare "L. Califano," Università degli Studi di Napoli "Federico II," Via Pansini 5, 80131 Napoli, Italy*

Correspondence should be addressed to Sabrina Bimonte; s.bimonte@istitutotumori.na.it

Received 16 July 2013; Accepted 29 July 2013

Academic Editor: Monica Fedele

Morphine, a highly potent analgesic agent, is widely used to relieve pain and suffering of patients with cancer. Additionally, it has been reported that morphine is important in the regulation of cancerous tissue. Morphine relieves pain by acting directly on the central nervous system, although its activities on peripheral tissues are responsible for many adverse side effects. For these reasons, it is very important also to understand the role of morphine in cancer treatment. The published literature reporting the effect of morphine on tumor growth presents some discrepancies, with reports suggesting that morphine may either promote or inhibit the tumor growth. It has been also demonstrated that morphine modulates angiogenesis which is important for primary tumour growth, invasiveness, and the development of metastasis. This review will focus on the latest findings on the role of morphine in the regulation of cancer cell growth and angiogenesis.

1. Introduction

Morphine is used to relieve pains of patients with cancer in terminal phases, in order to improve quality of life [1]. Morphine is an opiate-based drug isolated for the first time in 1803 by Friedrich W. Sertürner [2]. It has been shown that morphine explains its function by acting through opioid receptors, μ, δ, and κ, which are localized in the brain [3, 4]. Morphine relieves pain by acting directly on central nervous system (CNS), although its activity on peripheral tissue leads to many secondary complications, including addiction, respiratory depression, and tolerance. Apart from these severe effects, morphine is still considered the most effective drug clinically available for the management of severe pain associated with cancer [5]. Several experimental studies performed on cancer cell lines and mouse models showed that morphine can also play a role in the regulation of cancer cell growth. Unfortunately, the results obtained by these studies are still contradictory. Some reports demonstrated that morphine inhibited the growth of various human cancer cell lines [6–12] or animal models [13–16]. On the contrary, other studies proved that morphine increased tumor cell growth in *in vivo* [17, 18] or *in vitro* [19] models. According to some studies, morphine at clinically relevant doses stimulated angiogenesis *in vitro* [20] and tumour growth in breast cancer mouse model [21]. It has been demonstrated that morphine modulates angiogenesis which is important for primary tumour growth, invasiveness, and the development of metastasis. For these reasons, there is a dilemma about the effects of morphine on cancer cell growth and angiogenesis.

This review will focus on the latest findings on the role of morphine in the regulation of cancer cell growth and angiogenesis.

2. Morphine Affects Tumor Growth and Apoptosis

The role of morphine in the regulation of tumor cell growth is not yet correctly established. Several xenograft mouse models were generated to study cancer cell growth-promoting or inhibiting effects of morphine. Tegeder et al. [13] generated mouse models of breast cancer by subcutaneous injection of MCF-7 and MDA-MB231 cells in NMRI-nu/nu mice. In these

mice, morphine, intraperitoneally injected, significantly reduced tumor growth through a p53-dependent mechanism. Additionally, in these mice, naloxone, an opioid inverse agonist, increased the growth-inhibitory effects of morphine. Similar results were obtained in rat model of colon cancer generated by intraperitoneal injection of colon cancer cells in Fisher 244 rats. In these animals, subcutaneous administration of morphine leads to significant decrease in the hepatic tumor burden. Morphine inhibited not only tumor growth but also metastasis in melanoma mouse model generated by subcutaneous injection of B16-BL6 cells into the hind paws of C57BL mice [15]. Another group, demonstrated that morphine inhibited tumor metastasis formation when it was administered intraperitoneally in mouse model of colon cancer [16]. On the contrary, several experimental studies demonstrated that morphine increased tumor growth. Gupta et al., in orthotropic mouse model of breast cancer obtained by injection of MCF-7 cells into the mammary fat pads of nude mice, demonstrated that morphine, in clinically relevant doses, increased tumor growth. This was associated with increased angiogenesis and inhibition of apoptosis and promotion of cell cycle progression [20]. In this study, it was also reported that naloxone itself had no significant effect on angiogenesis. Our preliminary data, obtained by *in vitro* and *in vivo* experiments using MDA.MB231 breast cancer cells, seems to validate this hypothesis (Bimonte et al., unpublished data). According to these results, in another study, it was demonstrated that morphine, subcutaneously administrated in mice, increased the tumor growth in mouse model of leukaemia and sarcoma. In these mice, morphine played also a general immunosuppressive role [22].

These contrasting results are probably associated with different concentration and/or time of administration of morphine. In fact, *in vitro* and *in vivo* studies demonstrated that tumor-enhancing effects with morphine occur after administration of low daily doses or single dose of morphine [23], while tumor suppression occurs after chronic high doses of morphine [11, 15, 16].

It has also been demonstrated that the μ-opioid receptor, by which morphine exerts its action, directly regulates tumor growth and metastasis. On the basis of these results, different mechanisms of opioid receptor-mediated influence of morphine on tumor growth have been proposed. Morphine, as mentioned above, after binding to the μ-opioid receptor, regulates cell cycle progression by stimulating mitogen-activated protein kinase (MAPK)/extracellular growth factor (Erk) pathways [20]. Alternatively, morphine can mediate apoptosis by activating phosphatidylinositol 3-kinase (PI3K)/protein kinase B (Akt) pathway [24]. Additionally, morphine, by the upregulation of urokinase plasminogen activator (uPA) expression, induces metastasis formation [25], while, by transactivation of VEGF receptor, it induces angiogenesis [26]. Finally, morphine affects also the function of T lymphocytes, leading to immunosuppression [27].

It has been proposed that morphine plays also a role in tumor apoptosis. Apoptosis is a form of cell death in which a programmed sequence of events leads to the elimination of cells without releasing harmful substances into the surrounding area. It is noted that apoptosis is regulated by two pathways: the mitochondrial-mediated pathway (intrinsic) [28] and death receptor-mediated pathway (extrinsic) [29]. It is noted that in cancer cells apoptosis is deregulated, and this leads to quick proliferation and tumor growth [30, 31]. Morphine was shown to induce apoptosis of macrophages, T lymphocytes, and human endothelial cells [32, 33]. Experiments performed on human tumor cell lines demonstrated that morphine in high concentration induces apoptosis and inhibits cancer cell growth by activation of different signal pathways involving caspase 3/9, cytochrome c, and sigma-2 receptor. On the contrary, it has been demonstrated that morphine can inhibit apoptosis. Additionally in SH-SY5Y cells, morphine has antiapoptotic effect by antagonizing doxorubicin [34]. These discrepancies, also in these cases, are associated with different cell line tumor type used and/or *in vivo* dose/time of morphine administrated.

3. Morphine Regulates Angiogenesis and Metastasis Formation

Recent data demonstrated a role of morphine in angiogenesis. Angiogenesis is required for invasive tumor growth and metastasis and represents an important point in the control of cancer progression. Proangiogenic activity of morphine was demonstrated in the MCF-7 breast cancer model. In these mice, morphine at clinically relevant concentrations enhanced tumor neovascularization [20]. In an animal model of hormone-dependent breast cancer, it has also been demonstrated that morphine promoted activation of vascular endothelial growth factor (VEGF) receptor and increased metastasis [21, 27]. It has been proposed that morphine explains its proangiogenic activity by the stimulation of mitogen-activated protein kinase (MAPK) signalling pathway via G protein-coupled receptors and nitric oxide (NO). Alternatively, several *in vivo* studies provided evidence that morphine can induce tumor growth by the upregulation of cyclooxygenase-2 (COX-2) [35–38] and/or prostaglandin E2-mediated stimulation of angiogenesis [39–42]. On the contrary, several *in vivo* and *in vitro* studies demonstrated that morphine can inhibit angiogenesis by the regulation of different pathways [8, 32, 43, 43–50]. These different results can be due to different experimental conditions (cell line tumor type used and/or dose/time of morphine). Morphine plays a role not only in tumor cell growth but also in metastasis formation, which is the main process related to most cancer deaths and failure in cancer treatment [51, 52]. The process which leads to metastasis formation initiated with migration of cancer cells through the extracellular matrix (ECM). Both pro- and antimigratory effects have been reported for morphine. Specifically, it has been shown that morphine significantly reduces the adhesion, invasion, and metastasis of metastatic colon 26-L5 carcinoma cells [16], by the regulation of matrix metalloproteinases (MMPs). On the contrary, morphine can promote invasion, metastasis formation and migration of cancer cells by the upregulation of MMPs in breast and lung cancer [52, 53]. Finally, in MCF-7 breast cancer cells [50, 54] and in H729 cancer cells [55], morphine treatments lead to the upregulation of urokinase plasminogen activator (uPA) which promotes migration of cancer cells through the ECM.

4. Conclusions

Several studies provided evidence that morphine can affect tumor growth by acting with different mechanisms, including tumor cells or endothelial cells or growth factors secreted by meditation of CNS. Unfortunately, the results obtained from both *in vitro* and *in vivo* studies are so far conflicting. Some reports suggested that morphine may promote the tumor growth by inhibiting apoptosis and by promoting angiogenesis and migration of tumor cells. On the contrary, it has been demonstrated that morphine may also exert proapoptotic and antiangiogenic effects. These different results can be associated with the different doses of morphine administrated, with different models used and different cancer. For these reasons, it is very important for the management of severe pain associated with cancer to consider accurately the dose and route of administration of morphine. Further studies will be necessary to establish if morphine is an inhibitor of tumor growth or whether it promotes cancer.

Disclosure

The authors have no other relevant affiliations or financial interests with any organization or entity. No writing assistance was used in the production of the paper.

Acknowledgments

The authors thank Massimiliano Spinelli for kind help in providing informatics assistance. This work was supported by the 5x mille and current research programs of the Istituto Nazionale per lo Studio e la Cura dei Tumori, "Fondazione G. Pascale," IRCCS, Naples, Italy.

References

[1] J. N. Lickiss, "Approaching cancer pain relief," *European Journal of Pain*, vol. 5, pp. 5–14, 2001.

[2] R. Schmitz, "Friedrich Wilhelm Sertürner and the discovery of morphine," *Pharmacy in history*, vol. 27, no. 2, pp. 61–74, 1985.

[3] G. W. Pasternak, "Pharmacological mechanisms of opioid analgesics," *Clinical Neuropharmacology*, vol. 16, no. 1, pp. 1–18, 1993.

[4] B. L. Kieffer and C. Gavériaux-Ruff, "Exploring the opioid system by gene knockout," *Progress in Neurobiology*, vol. 66, no. 5, pp. 285–306, 2002.

[5] P. W. Mantyh, "Cancer pain and its impact on diagnosis, survival and quality of life," *Nature Reviews Neuroscience*, vol. 7, no. 10, pp. 797–809, 2006.

[6] N. Sueoka, E. Sueoka, S. Okabe, and H. Fujiki, "Anti-cancer effects of morphine through inhibition of tumour necrosis factor-α release and mRNA expression," *Carcinogenesis*, vol. 17, no. 11, pp. 2337–2341, 1996.

[7] R. Maneckjee and J. D. Minna, "Opioids induce while nicotine suppresses apoptosis in human lung cancer cells," *Cell Growth and Differentiation*, vol. 5, no. 10, pp. 1033–1040, 1994.

[8] A. Pasi, B. Qu, R. Steiner, H.-J. Senn, W. Bar, and F. S. Messiha, "Angiogenesis: modulation with opioids," *General Pharmacology*, vol. 22, no. 6, pp. 1077–1079, 1991.

[9] A. Hatzoglou, E. Bakogeorgou, E. Papakonstanti, C. Stournaras, D. S. Emmanouel, and E. Castanas, "Identification and characterization of opioid and somatostatin binding sites in the opossum kidney (OK) cell line and their effect on growth," *Journal of Cellular Biochemistry*, vol. 63, no. 4, pp. 410–421, 1996.

[10] A. Hatzoglou, L. Ouafik, E. Bakogeorgou, K. Thermos, and E. Castanas, "Morphine cross-reacts with somatostatin receptor SSTR2 in the T47D human breast cancer cell line and decreases cell growth," *Cancer Research*, vol. 55, no. 23, pp. 5632–5636, 1995.

[11] R. Maneckjee, R. Biswas, and B. K. Vonderhaar, "Binding of opioids to human MCF-7 breast cancer cells and their effects on growth," *Cancer Research*, vol. 50, no. 8, pp. 2234–2238, 1990.

[12] M. Kampa, E. Bakogeorgou, A. Hatzoglou, A. Damianaki, P.-M. Martin, and E. Castanas, "Opioid alkaloids and casomorphin peptides decrease the proliferation of prostatic cancer cell lines (LNCaP, PC3 and DU145) through a partial interaction with opioid receptors," *European Journal of Pharmacology*, vol. 335, no. 2-3, pp. 255–265, 1997.

[13] I. Tegeder, S. Grösch, A. Schmidtko et al., "G protein-independent G1 cell cycle block and apoptosis with morphine in adenocarcinoma cells: involvement of p53 phosphorylation," *Cancer Research*, vol. 63, no. 8, pp. 1846–1852, 2003.

[14] M. P. Yeager and T. A. Colacchio, "Effect of morphine on growth of metastatic colon cancer in vivo," *Archives of Surgery*, vol. 126, no. 4, pp. 454–456, 1991.

[15] T. Sasamura, S. Nakamura, Y. Iida et al., "Morphine analgesia suppresses tumor growth and metastasis in a mouse model of cancer pain produced by orthotopic tumor inoculation," *European Journal of Pharmacology*, vol. 441, no. 3, pp. 185–191, 2002.

[16] Y. Harimaya, K. Koizumi, T. Andoh, H. Nojima, Y. Kuraishi, and I. Saiki, "Potential ability of morphine to inhibit the adhesion, invasion and metastasis of metastatic colon 26-L5 carcinoma cells," *Cancer Letters*, vol. 187, no. 1-2, pp. 121–127, 2002.

[17] R. H. Simon and T. E. Arbo, "Morphine increases metastatic tumor growth," *Brain Research Bulletin*, vol. 16, no. 3, pp. 363–367, 1986.

[18] J. W. Lewis, Y. Shavit, and G. W. Terman, "Apparent involvement of opioid peptides in stress-induced enhancement of tumor growth," *Peptides*, vol. 4, no. 5, pp. 635–638, 1983.

[19] M. G. Sergeeva, Z. V. Grishina, and S. D. Varfolomeyev, "Morphine effect on proliferation of normal and tumor cells of immune origin," *Immunology Letters*, vol. 36, no. 2, pp. 215–218, 1993.

[20] K. Gupta, S. Kshirsagar, L. Chang et al., "Morphine stimulates angiogenesis by activating proangiogenic and survival-promoting signaling and promotes breast tumor growth," *Cancer Research*, vol. 62, no. 15, pp. 4491–4498, 2002.

[21] M. Farooqui, Y. Li, T. Rogers et al., "COX-2 inhibitor celecoxib prevents chronic morphine-induced promotion of angiogenesis, tumour growth, metastasis and mortality, without compromising analgesia," *British Journal of Cancer*, vol. 97, no. 11, pp. 1523–1531, 2007.

[22] M. Ishikawa, K. Tanno, A. Kamo, Y. Takayanagi, and K.-I. Sasaki, "Enhancement of tumor growth by morphine and its possible mechanism in mice," *Biological and Pharmaceutical Bulletin*, vol. 16, no. 8, pp. 762–766, 1993.

[23] J. Zong and G. M. Pollack, "Morphine antinociception is enhanced in mdr1a gene-deficient mice," *Pharmaceutical Research*, vol. 17, no. 6, pp. 749–753, 2000.

[24] M. Iglesias, M. F. Segura, J. X. Comella, and G. Olmos, "μ-opioid receptor activation prevents apoptosis following serum

withdrawal in differentiated SH-SY5Y cells and cortical neurons via phosphatidylinositol 3-kinase," *Neuropharmacology*, vol. 44, no. 4, pp. 482–492, 2003.

[25] K. Gach, J. Szemraj, J. Fichna, M. Piestrzeniewicz, D. S. Delbro, and A. Janecka, "The influence of opioids on urokinase plasminogen activator on protein and mRNA level in MCF-7 breast cancer cell line," *Chemical Biology and Drug Design*, vol. 74, no. 4, pp. 390–396, 2009.

[26] P. A. Singleton and J. Moss, "Effect of perioperative opioids on cancer recurrence: a hypothesis," *Future Oncology*, vol. 6, no. 8, pp. 1237–1242, 2010.

[27] C. Chen, M. Farooqui, and K. Gupta, "Morphine stimulates vascular endothelial growth factor-like signaling in mouse retinal endothelial cells," *Current Neurovascular Research*, vol. 3, no. 3, pp. 171–180, 2006.

[28] D. R. Green and J. C. Reed, "Mitochondria and apoptosis," *Science*, vol. 281, no. 5381, pp. 1309–1312, 1998.

[29] A. Ashkenazi and V. M. Dixit, "Apoptosis control by death and decoy receptors," *Current Opinion in Cell Biology*, vol. 11, no. 2, pp. 255–260, 1999.

[30] D. Hanahan and R. A. Weinberg, "The hallmarks of cancer," *Cell*, vol. 100, no. 1, pp. 57–70, 2000.

[31] M. O. Hengartner, "The biochemistry of apoptosis," *Nature*, vol. 407, no. 6805, pp. 770–776, 2000.

[32] P.-N. Hsiao, M.-C. Chang, W.-F. Cheng et al., "Morphine induces apoptosis of human endothelial cells through nitric oxide and reactive oxygen species pathways," *Toxicology*, vol. 256, no. 1-2, pp. 83–91, 2009.

[33] A. A. Kapasi, S. A. Coscia, M. P. Pandya, and P. C. Singhal, "Morphine modulates HIV-1 gp160-induced murine macrophage and human monocyte apoptosis by disparate ways," *Journal of Neuroimmunology*, vol. 148, no. 1-2, pp. 86–96, 2004.

[34] X. Lin, Q. Li, Y.-J. Wang et al., "Morphine inhibits doxorubicin-induced reactive oxygen species generation and nuclear factor κB transcriptional activation in neuroblastoma SH-SY5Y cells," *Biochemical Journal*, vol. 406, no. 2, pp. 215–221, 2007.

[35] R. Arerangaiah, N. Chalasani, A. M. Udager et al., "Opioids induce renal abnormalities in tumor-bearing mice," *Nephron—Experimental Nephrology*, vol. 105, no. 3, pp. e80–e89, 2007.

[36] D. Salvemini, T. P. Misko, J. L. Masferrer, K. Seibert, M. G. Currie, and P. Needleman, "Nitric oxide activates cyclooxygenase enzymes," *Proceedings of the National Academy of Sciences of the United States of America*, vol. 90, no. 15, pp. 7240–7244, 1993.

[37] E. Nédélec, A. Abid, C. Cipolletta et al., "Stimulation of cyclooxygenase-2-activity by nitric oxide-derived species in rat chondrocyte: lack of contribution to loss of cartilage anabolism," *Biochemical Pharmacology*, vol. 61, no. 8, pp. 965–978, 2001.

[38] M. Farooqui, Z. H. Geng, E. J. Stephenson, N. Zaveri, D. Yee, and K. Gupta, "Naloxone acts as an antagonist of estrogen receptor activity in MCF-7 cells," *Molecular Cancer Therapeutics*, vol. 5, no. 3, pp. 611–620, 2006.

[39] D. Salvemini, K. Seibert, J. L. Masferrer, T. P. Misko, M. G. Currie, and P. Needleman, "Endogenous nitric oxide enhances prostaglandin production in a model of renal inflammation," *Journal of Clinical Investigation*, vol. 93, no. 5, pp. 1940–1947, 1994.

[40] R. J. Griffin, B. W. Williams, R. Wild, J. M. Cherrington, H. Park, and C. W. Song, "Simultaneous inhibition of the receptor kinase activity of vascular endothelial, fibroblast, and platelet-derived growth factors suppresses tumor growth and enhances tumor radiation response," *Cancer Research*, vol. 62, no. 6, pp. 1702–1706, 2002.

[41] K. M. Leahy, R. L. Ornberg, Y. Wang, B. S. Zweifel, A. T. Koki, and J. L. Masferrer, "Cyclooxygenase-2 inhibition by celecoxib reduces proliferation and induces apoptosis in angiogenic endothelial cells in vivo," *Cancer Research*, vol. 62, no. 3, pp. 625–631, 2002.

[42] S. H. Chang, C. H. Liu, R. Conway et al., "Role of prostaglandin E2-dependent angiogenic switch in cyclooxygenase 2-induced breast cancer progression," *Proceedings of the National Academy of Sciences of the United States of America*, vol. 101, no. 2, pp. 591–596, 2004.

[43] C.-F. Lam, Y.-C. Liu, F.-L. Tseng et al., "High-dose morphine impairs vascular endothelial function by increased production of superoxide anions," *Anesthesiology*, vol. 106, no. 3, pp. 532–537, 2007.

[44] J. Blebea, J. E. Mazo, T. K. Kihara et al., "Opioid growth factor modulates angiogenesis," *Journal of Vascular Surgery*, vol. 32, no. 2, pp. 364–373, 2000.

[45] C.-F. Lam, P.-J. Chang, Y.-S. Huang et al., "Prolonged use of high-dose morphine impairs angiogenesis and mobilization of endothelial progenitor cells in mice," *Anesthesia and Analgesia*, vol. 107, no. 2, pp. 686–692, 2008.

[46] J. L. Martin, R. Charboneau, R. A. Barke, and S. Roy, "Chronic morphine treatment inhibits LPS-induced angiogenesis: implications in wound healing," *Cellular Immunology*, vol. 265, no. 2, pp. 139–145, 2010.

[47] S. Roy, S. Balasubramanian, J. Wang, Y. Chandrashekhar, R. Charboneau, and R. Barke, "Morphine inhibits VEGF expression in myocardial ischemia," *Surgery*, vol. 134, no. 2, pp. 336–344, 2003.

[48] L. Koodie, S. Ramakrishnan, and S. Roy, "Morphine suppresses tumor angiogenesis through a HIF-1α/p38MAPK pathway," *American Journal of Pathology*, vol. 177, no. 2, pp. 984–997, 2010.

[49] N. Faramarzi, A. Abbasi, S. M. Tavangar, M. Mazouchi, and A. R. Dehpour, "Opioid receptor antagonist promotes angiogenesis in bile duct ligated rats," *Journal of Gastroenterology and Hepatology*, vol. 24, no. 7, pp. 1226–1229, 2009.

[50] R. L. Shapiro, J. G. Duquette, D. F. Roses et al., "Induction of primary cutaneous melanocytic neoplasms in urokinase-type plasminogen activator (uPA)-deficient and wild-type mice: cellular blue nevi invade but do not progress to malignant melanoma in uPA-deficient animals," *Cancer Research*, vol. 56, no. 15, pp. 3597–3604, 1996.

[51] J. A. Engbring and H. K. Kleinman, "The basement membrane matrix in malignancy," *Journal of Pathology*, vol. 200, no. 4, pp. 465–470, 2003.

[52] M. S. Widel and M. Widel, "Mechanisms of metastasis and molecular markers of malignant tumor progression. I. Colorectal cancer," *Postępy Higieny i Medycyny Doświadczalnej*, vol. 60, pp. 453–470, 2006.

[53] C. C. Lynch and L. M. Matrisian, "Matrix metalloproteinases in tumor-host cell communication," *Differentiation*, vol. 70, no. 9-10, pp. 561–573, 2002.

[54] K. Gach, J. Szemraj, A. Wyrębska, and A. Janecka, "The influence of opioids on matrix metalloproteinase-2 and -9 secretion and mRNA levels in MCF-7 breast cancer cell line," *Molecular Biology Reports*, vol. 38, no. 2, pp. 1231–1236, 2011.

[55] G. Nylund, A. Pettersson, C. Bengtsson, A. Khorram-Manesh, S. Nordgren, and D. S. Delbro, "Functional expression of μ-opioid receptors in the human colon cancer cell line, HT-29, and their localization in human colon," *Digestive Diseases and Sciences*, vol. 53, no. 2, pp. 461–466, 2008.

Hindawi Publishing Corporation
BioMed Research International
Volume 2013, Article ID 824682, 8 pages
http://dx.doi.org/10.1155/2013/824682

Research Article

Gastric Tissue Damage Analysis Generated by Ischemia: Bioimpedance, Confocal Endomicroscopy, and Light Microscopy

Nohra E. Beltran,[1,2] Laura E. Garcia,[3] and Mario Garcia-Lorenzana[4]

[1] *Departamento de Procesos y Tecnologia, Universidad Autonoma Metropolitana, Cuajimalpa. Artificios 40, Colonia Hidalgo, 01120 Ciudad de Mexico, DF, Mexico*
[2] *Centro Nacional de Investigación en Instrumentacion e Imagenologia Medica, Universidad Autonoma Metropolitana, Iztapalapa. Avenida San Rafael Atlixco 186, Colonia Vicentina, 09340 Ciudad de Mexico, DF, Mexico*
[3] *Departamento de Ingenieria Electrica, Universidad Autonoma Metropolitana, Iztapalapa. Avenida San Rafael Atlixco 186, Colonia Vicentina, 09340 Ciudad de Mexico, DF, Mexico*
[4] *Departamento de Biologia de la Reproduccion, Universidad Autonoma Metropolitana, Iztapalapa. Avenida San Rafael Atlixco 186, Colonia Vicentina, 09340 Ciudad de Mexico, DF, Mexico*

Correspondence should be addressed to Nohra E. Beltran; nbeltran@correo.cua.uam.mx

Received 2 May 2013; Accepted 4 June 2013

Academic Editor: Andrea Vecchione

The gastric mucosa ischemic tissular damage plays an important role in critical care patients' outcome, because it is the first damaged tissue by compensatory mechanism during shock. The aim of the study is to relate bioimpedance changes with tissular damage level generated by ischemia by means of confocal endomicroscopy and light microscopy. Bioimpedance of the gastric mucosa and confocal images were obtained from Wistar male rats during basal and ischemia conditions. They were anesthetized, and stain was applied (fluorescein and/or acriflavine). The impedance spectroscopy catheter was inserted and then confocal endomicroscopy probe. After basal measurements and biopsy, hepatic and gastric arteries clamping induced ischemia. Finally, pyloric antrum tissue was preserved in buffered formaldehyde (10%) for histology processing using light microscopy. Confocal images were equalized, binarized, and boundary defined, and infiltrations were quantified. Impedance and infiltrations increased with ischemia showing significant changes between basal and ischemia conditions ($P < 0.01$). Light microscopy analysis allows detection of general alterations in cellular and tissular integrity, confirming gastric reactance and confocal images quantification increments obtained during ischemia.

1. Introduction

Shock is a critical condition in which oxygen availability becomes restricted, and tissues will consume as much oxygen as is available. Compensated shock occurs when systemic delivery of oxygen (DO_2) decreases and the tissues turn to anaerobic sources of energy. Under these conditions, cellular function is maintained as long as the combined yield of aerobic and anaerobic sources of energy provides sufficient ATP for protein synthesis and contractile processes. Some tissues are more resistant to hypoxia than others [1]. The intestinal and gastric mucosae show evidence of anaerobic metabolism before decreases in systemic oxygen consumption (VO_2) is detected [2]. Uncompensated shock resulting in irreversible tissue damage occurs when the combined aerobic and anaerobic supplies of ATP are not sufficient to maintain cellular function. Failure of membrane-associated ion transport pumps, in particular those associated with the regulation of calcium and sodium, results in the loss of membrane integrity and in cellular swelling [3, 4]. Among other mechanisms that lead to irreversible cellular injury during hypoxia are depletion of cellular energy, cellular acidosis, and oxygen free radical generation [1].

An important objective in the care of critically ill patients is to ensure the adequacy of tissue oxygenation, since tissue hypoxia may result in anaerobic metabolism, cellular

acidosis, and death [5]. Emerging data suggest that early aggressive resuscitation of critically ill patients may limit and/or reverse tissue hypoxia, progression to organ failure, and improve outcome [6]. In critical illness, blood flow to the splanchnic tissues is frequently reduced and redirected to other vital organs such as the brain, heart, and kidneys. Inadequately oxygenated, the splanchnic tissues may become prone to ischemia-related complications [7]. However, at present, there is no clinically useful method to directly monitor the level of gastric tissue dysoxia injury.

After a certain period of ischemia, the gastrointestinal tissue becomes vulnerable to damage due to reperfusion, in which restored oxygen supply produces free radical species, which lead to further tissue injury [8]. For an effective and correctly timed therapy, it may be very useful to know the ischemic level and the tissue damage in a continuous and simple manner [9].

Electric impedance measurements in tissues and biological systems have been used for decades in a wide variety of applications [10]. Impedance spectroscopy is the study of the passive electrical properties of biological tissues as a function of frequency. The impedance of biological tissues results from the interaction of an electrical current with the tissue at the cellular and molecular level. Impedance is the total effect of two separate orthogonal dimensions: the electrical resistance which restricts the flow of electrons and dissipates energy and the electrical reactance which is the capacity to store and release energy.

On a conceptual level, the cell cytoplasm and extracellular space act as conductive media isolated from each other by the cell membrane. The conductivity of the extra- and intracellular space contributes to the overall resistance of the tissue while the cell membrane contributes to the capacitive effect [10, 11]. For instance, in a normoxic condition, a significant amount of low frequency current is able to flow through the extracellular spaces; when dysoxia occurs, the cells are not capable to generate enough energy to feed the ion pumps and extracellular water penetrates into the cell. As a consequence, the cells grow and invade the extracellular space causing a reduction of the current in extracellular fluids and are seen as a low frequency impedance increase [12]. Also the closure of gap junctions contributes to the impedance increment at these low frequencies. At high frequencies, impedance changes are influenced by intracellular and extracellular fluid impedances and ion permeability of cellular membranes [11, 13]. The electrical impedance of a living tissue can be continuously measured to determine its pathophysiological evolution. Some pathologies like ischemia, infarct, or necrosis cause cellular alterations that are reflected as impedance changes [14].

Our group developed an instrument that measures the impedance spectrum of the gastric mucosa in the range of 215 Hz to 1 MHz [15]. Along with the technique, an impedance spectrometry probe and nasogastric tube (ISP/NGT) [16] allow the direct acquisition of an electric impedance spectrum of the mucosa. Most of the authors in the bioimpedance field use the Cole-Cole equation to describe their experimental results characterizing the tissue bioimpedance with four parameters. For our device, an adaptation of Cole-Cole model was performed to develop an algorithm to calculate the 6 characteristic electrical values that best describe human gastric impedance measurements [17]. The device has been tested and validated during the last 12 years. The results confirm the potential of this technology for critical care monitoring. However, some studies are required to determine actual tissue damage levels via impedance spectroscopy in critical care patients in order to guide therapy and improve outcome. The objective of the study was to relate bioimpedance changes with tissular damage level generated during induced hypovolemic shock in a rat model, using confocal endomicroscopy and light microscopy.

2. Materials and Methods

2.1. Animals. Healthy adult male rats of Wistar strain, aged 3 months and weighting 350–400 g at the beginning of the experiment, were used. Animals were bred and kept at the Animal Facility of the Autonomous Metropolitan University in a temperature-controlled environment on a 12 : 12 h light-dark cycle and were fasted 12 h before experiment started. All procedures used in the study complied with the guide for care and use of laboratory animals. The experimental protocol was approved by the National Center for Medical Instrumentation and Imaging Research Ethical Committee.

2.2. Ischemia Induced Procedure. The surgical procedures were performed under clean conditions. Rats were deeply anesthetized using 1.5 mL intraperitoneal anesthesic cocktail (0.05 mL ketamine, 0.25 mL propionylpromazine, and 0.1 mL xylazine in 0.6 mL saline solution per mL). Another 1 mL of the ketamine/propionylpromazine/xylazine combination was kept for further maintenance anesthesia as needed.

The animals were mounted on a dissection frame with attached limbs. After the onset of general anesthesia, 10 μL/g of fluorescein (Alcon Pharma, Novartis Pharmaceuticals, Mexico) was injected in the tail vein. The rats underwent a 5 cm midline laparotomy from the xiphoid process to just above the penis. After opening the abdomen, the abdominal cavity was carefully inspected, and stomach was exposed (Figure 1).

Using a 0.5 mL syringe containing heparin, blood samples were taken from the femoral artery immediately after opening the abdomen and 30 min after isquemia. pH and lactate concentration were assessed with a blood gas analyzer (GEM Premier 3000; Instrumentation Laboratory, Lexington, MA).

Based on duodenum, a 1 cm incision was made over the greater curvature. Then a biopsy was obtained, and impedance measurements were taken during 15 minutes. When it was necessary, for topical staining, some drops of a 0.02% solution of acriflavine (Merck KGaA, Darmstadt, Germany) in saline were applied to the tissue surface, and excess dye was washed away with phosphate buffered saline. Then a collection of endomicroscopy images was stored. Afterwards, hepatic and gastric arteries were isolated and clamped (Figure 2). Bioimpedance measurements, confocal images, and biopsy were taken. After 30 min of ischemia, Evan's blue solution (1.5 mL of 0.1%) was injected into the

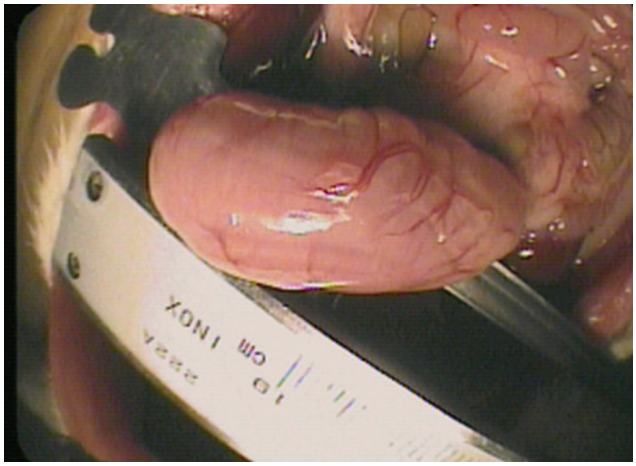

Figure 1: Stomach exhibition for greater curvature incision.

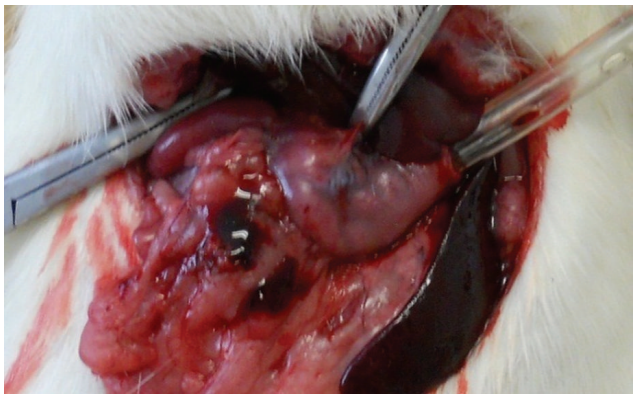

Figure 2: Hepatic and gastric arteries occlusion for ischemia generation.

celiac artery to evaluate perfusion. Once the experiment was concluded a humanitarian sacrifice was developed according to Mexican Official Standard (NOM-033-ZOO-1995).

2.3. Impedance Spectra Acquisition. The impedance spectroscopy system consists of three elements: the catheter, the impedance spectrometer, and the control and analysis system. The catheter is a flexible plastic tube that can be inserted in any hollow viscous organ. At the distal tip four electrodes are located that function as ionic current to electronic current transducers, such as Ag/AgCl electrodes. The electrodes are connected to leads that provide an electrical connection to the other end of the catheter along the wall of the tubing or in the lumen. At the proximal end, the leads end in an electrical multichannel connector that can be plugged into the impedance spectrometer [15]. The prototype impedance spectrometer meets the international regulation standards, as the BS EN 60601-1:1990 and ANSI/AAMI ES1:1993. A PC, with special software developed by our research group, controls the impedance spectrometer operations and data acquisition, storage and analysis. Impedance measurements obtained from these animals were automatically recorded every 30 seconds during 15 minutes for each condition.

2.4. Confocal Endomicroscopy Images Acquisition. Confocal endomicroscopy (EC-3870CIFK; Pentax, Tokyo, Japan) provides a 3-dimensional optical biopsy *in vivo* without physically disrupting epithelial integrity. For labeling of tissues fluorescent dyes (fluorescein and acriflavine) are used. Confocal gray scale images with a field of view of 475 × 475 μm can be obtained by gently pressuring the confocal window onto the surface mucosa. The optical slice thickness of a single image is 7 μm with a lateral resolution of 0.7 μm. The range of the z-axis can be varied from the surface to 0–70 μm below the surface layer of the gastric mucosa after topical staining with acriflavine. A single point within the tissue is scanned in a raster pattern, and measurement of light returning to the detector from successive points is digitized to construct an image of the scanned region. Each resultant image is a transverse optical section, 500 × 500 mm in size. Serial images are collected at a scan rate of 0.8 frames per second at a resolution of 1024 × 1024 pixels, approximating a 1000x magnification on a 19-inch screen. Five sets of confocal endomicroscopy images were obtained for each condition.

2.5. Tissue Collection and Histological Analysis. Chemical fixation of the pyloric antrum tissue for light microscopy was developed using buffered formaldehyde (10%) [18]. The pyloric antrum tissue was processed with the conventional histological techniques and included in Paraplast (Oxford Labware, St. Louis, Mo, USA). The pyloric antrum tissue was cut longitudinally and transversally; in each case, 5-micrometer serial sections were obtained and stained using hematoxylin-eosin [19]. The tissues sections were analyzed under a clear field light microscope (Axioskop II, Carl Zeiss) and image analyzer (Axiovision 4.8, Carl Zeiss). Thirty microscopic fields by condition were chosen at random. Micrographs were taken with an AxioCam MRc5 (Carl Zeiss).

2.6. Data Analysis. Impedance measurements were processed to calculate the central resistance and reactance at low frequencies (R_L, and X_L, resp.) and central resistance and reactance at high frequencies (R_H and X_H resp.), as the characteristic gastric impedance parameters of interest, as reported by Beltran et al. [17]. To analyze differences in impedance parameters between the different conditions (basal and ischemia), we calculated the average for each parameter over the monitoring time for each animal. A total of 50 to 100 images were collected per condition with the help of a foot pedal and digitally stored as gray-scale images. Analysis of images was performed using a specific algorithm designed by our group. Confocal endomicroscopy images were grouped by condition and staining type. Difference in the mean of all the values of experimental groups was analyzed using the Student's t-test. A P value < 0.01 was considered statistically significant. Data are presented as mean ± standard deviation (SD).

Table 1: Impedance parameters for acriflavine staining. Difference in the mean parameters by condition was analyzed using the Student's t-test. Data are presented as mean ± standard deviation (SD).

Impedance parameter	Basal	Ischemia	P
R_L [Ohms]	75.4 ± 1.7	91.9 ± 1.4	<0.01*
R_H [Ohms]	34.3 ± 0.7	35.9 ± 0.5	0.053
X_L [-jOhms]	7.4 ± 0.5	11.5 ± 0.4	<0.01*
X_H [-jOhms]	8.9 ± 0.2	18.5 ± 0.1	0.037

*Statistically significant ($P < 0.01$).

Table 2: Impedance parameters for fluorescein staining. Difference in the mean parameters by condition was analyzed using the Student's t-test. Data are presented as mean ± standard deviation (SD).

Impedance parameter	Basal	Ischemia	P
R_L [Ohms]	62.9 ± 3.1	99.1 ± 3.4	<0.01*
R_H [Ohms]	31.5 ± 1.5	39.2 ± 1.6	<0.01*
X_L [-jOhms]	3.1 ± 0.3	6.7 ± 0.4	<0.01*
X_H [-jOhms]	10.9 ± 0.8	17.5 ± 0.8	<0.01*

*Statistically significant ($P < 0.01$).

Table 3: Impedance parameters for the combination of fluorescein and acriflavine. Difference in the mean parameters by condition was analyzed using the Student's t-test. Data are presented as mean ± standard deviation (SD).

Impedance parameter	Basal	Ischemia	P
R_L [Ohms]	70.3 ± 2.1	91.3 ± 1.6	<0.01*
R_H [Ohms]	34.7 ± 0.6	35.6 ± 0.5	0.278
X_L [-jOhms]	7.6 ± 0.4	11.7 ± 0.3	<0.01*
X_H [-jOhms]	9.4 ± 0.4	16.3 ± 0.3	<0.01*

*Statistically significant ($P < 0.01$).

3. Results

The arteries clamping resulted in a significant decrease in blood pH (7.36 ± 0.04 for basal condition versus 7.18 ± 0.01 for ischemia condition). Lactate increased significantly to 5.23 ± 0.51 mmol/L, indicating metabolic acidosis and tissue ischemia.

In order to obtain impedance spectroscopy measurements and evaluate staining effects in spectra measurements, data were obtained using just acriflavine, just fluorescein, and the combination of fluorescein and acriflavine. Impedance parameters: R_L (central resistance at low frequencies), X_L (central reactance at low frequencies), R_H (central resistance at high frequencies), and yX_H (central reactance at high frequencies) were calculated, and Student's t-test was used in order to evaluate changes between basal and isquemia conditions. Table 1 shows impedance parameters for acriflavine staining, Table 2 for fluorescein staining, and Table 3 for the combination of fluorescein and acriflavine. No immediate adverse reactions were noted following topical or systemic dye application.

Table 4: Relationship between impedance parameters and confocal images infiltration numbers. Data are presented as mean ± standard deviation (SD).

	R_L [Ohms]	X_L [-jOhms]	Infiltration number
Acriflavine			
Basal	75.4 ± 1.7	7.4 ± 0.5	4294
Ischemia	91.9 ± 1.4	11.5 ± 0.4	4423
Fluorescein			
Basal	62.9 ± 3.1	3.1 ± 0.3	2349
Ischemia	99.1 ± 3.4	6.7 ± 0.4	4150
Acriflavine and fluorescein			
Basal	70.3 ± 2.1	7.6 ± 0.4	691
Ischemia	91.3 ± 1.6	11.7 ± 0.3	4169

Confocal endomicroscopy images were grouped according to staining type, a set of 6 images was used for each staining, and 2 cut series (basal and ischemia) for the combination of fluorescein and acriflavine. Images were processed using an algorithm developed by our group. Equalization, filtering, and binarization processing were applied in order to enhance image features (Figure 3). The number of imaging infiltrations was calculated in Figure 4 (right corner), which indicate oedema alterations. Table 4 illustrates the relationship between impedance parameters (R_L and X_L) and number of infiltrations grouped by staining and condition. Impedance parameters increase during ischemia and are related to more infiltrations, especially for the combination of fluorescein and acriflavine staining.

3.1. Light Microscopy. In basal condition the gastric mucosa presents simple columnar epithelium with invaginations to form foveolae and glands. A thin lamina propria layer forms packing among many gastric glands (Figures 5(A) and 5(E)).

In ischemic animals evidence of sub-lethal (pale stained) and lethal cell injury (cytoplasmic eosinophilia, and nuclear condensation) are observed in Figures 5(C) and 5(F) respectively. The lethal damage generates cellular death. Few scattered mononuclear cells (neutrophils), mainly localized between the crypts and diffusely distributed through the lamina propria, and vessels dilatation are observed (Figures 5(B), 5(C), and 5(D)). These are events during the initial phases of the acute inflammatory response. Also slightly foveolar epithelium erosion is illustrated in Figures 5(B) and 5(C).

4. Discussion and Conclusion

Up to now, no clinically useful method to directly monitor the level of tissue dysoxia injury is available. We proposed that bioimpedance and particularly gastric reactance is an early indicator of ischemia and we developed some studies that confirm the prognostic and diagnostic value of these measurements [20, 21]. However, before we may advocate the clinical use of this technology we need to first answer the

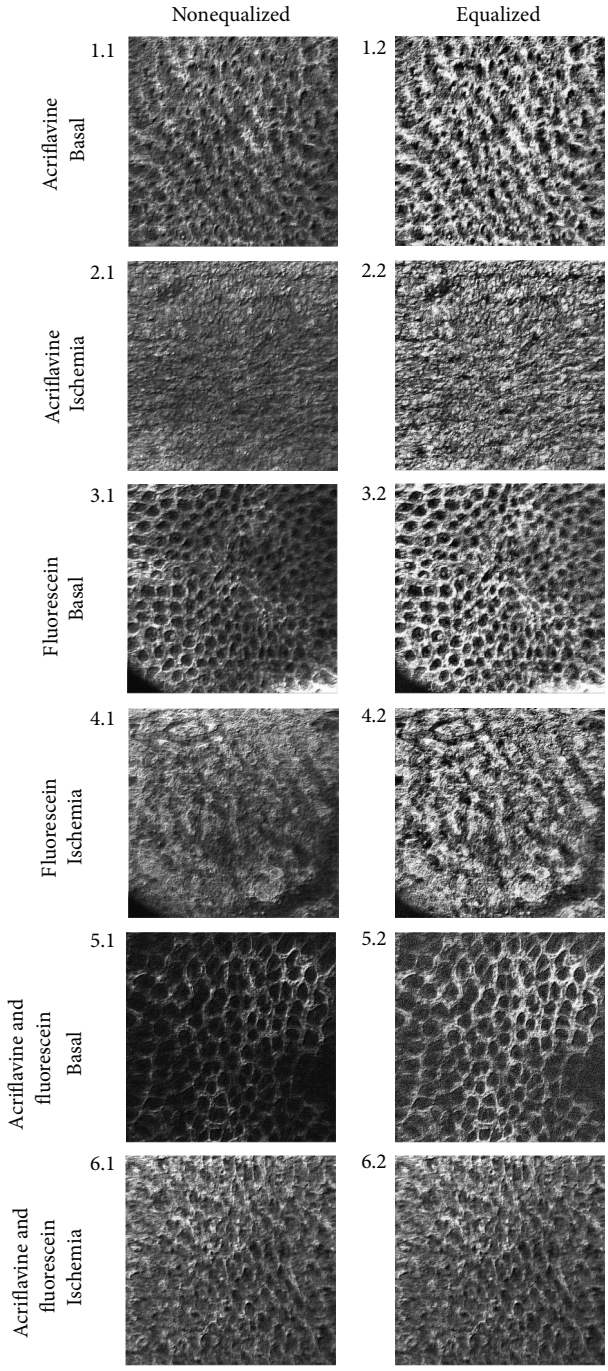

Figure 3: Confocal images comparison between nonequalized and equalized images, after edge enhancement for different staining.

following questions: (1) Can we quantify oedema and tissue damage from impedance parameters?, (2) Can we use this information to improve patient management and treatment? The second question is the hardest to answer and will require further research and experience. This study was designed to answer the first question and relate impedance parameters changes with tissular damage level generated during induced ischemia in a rat model, using confocal endomicroscopy and light microscopy.

This is the first animal model designed to quantify gastric injury generated by ischemia by confocal endomicroscopy imaging and evaluate its relationship with bioimpedance measurements. In this hypovolemic shock model impedance parameters statistically increase during ischemia as Tables 1, 2, and 3 showed. The greater changes are observed in central resistance at low frequencies that reflects tissue oedema caused by prolonged ischemia, causing a net increase in intracellular to extracellular volume ratio. Accumulation of

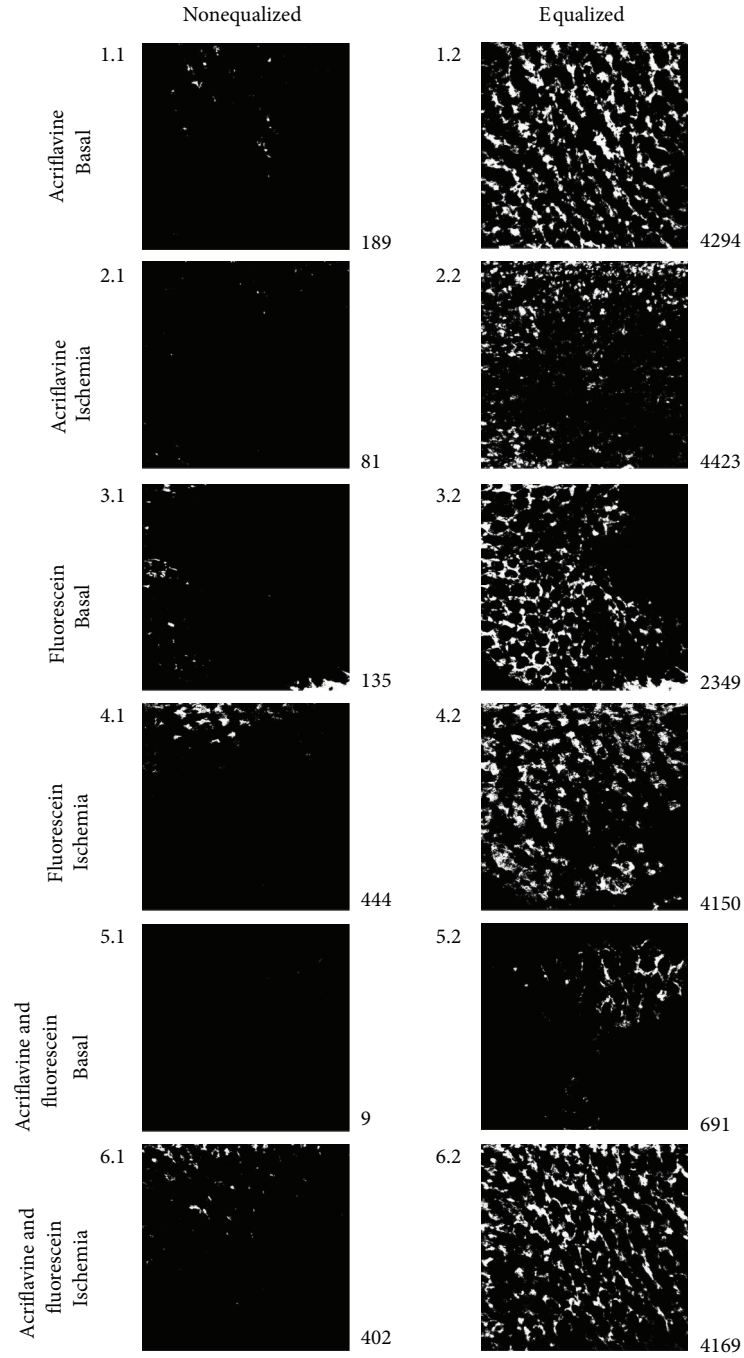

Figure 4: Number of imaging infiltrations according to staining type (right square), after binarization processing.

metabolic products, cell swelling caused by osmosis, and closing gap junctions are important effects which can be detected by means of electrical impedance spectroscopy: at low frequencies (<1 kHz) tissue impedance is influenced mostly by extracellular fluid impedance (extracellular pathway narrowing (caused by cell swelling) and gap junction status can be ascertained), while at high frequencies it is influenced by both intercellular and extracellular fluid impedances [11, 13]. According to confocal endomicroscopy imaging processing we developed an algorithm to quantify indirectly cell swelling by infiltration accumulation. Although acriflavine has been used to highlight nuclei, when it is used alone, no differences in infiltrations were found between basal and ischemia conditions (Table 4). Nuclear staining was diminished in necrotic areas generated during ischemia. Because the inflammatory process was focal rather than homogeneous, *in vivo* microscopy helped to localize the inflammatory infiltrate and necrotic areas. The inflammatory

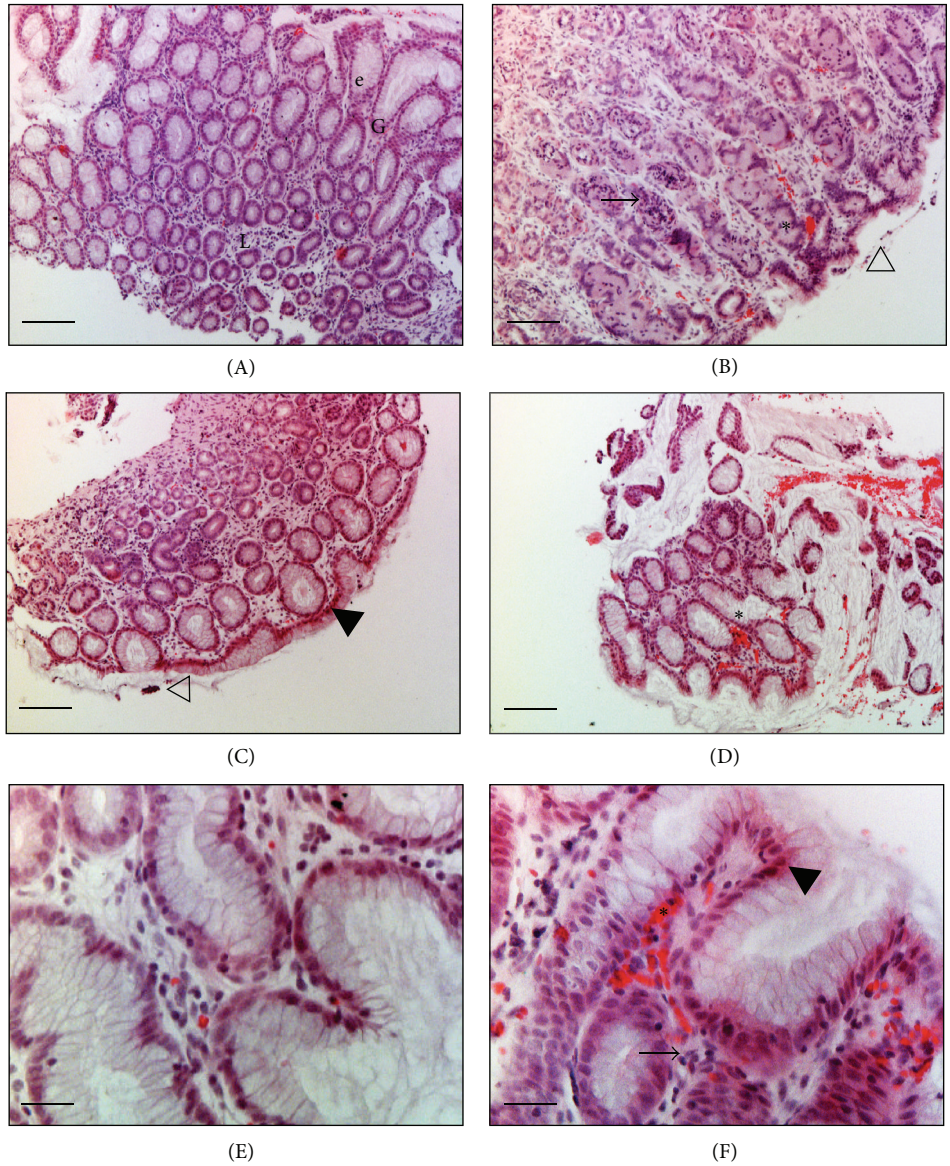

FIGURE 5: Hematoxylin and eosin stained histological sections of rat pyloric antrum tissue under basal and ischemia conditions. (A) and (E) basal condition: normal epithelium (e), lamina propria (L), and gastric glands (G). (B), (C), (D), and (F) ischemia condition: some epithelial cells show histological features of necrosis (▲), and the initial phases of the acute inflammatory response: leukocyte infiltration (→), vascular congestion (∗), and epithelium integrity lost (∇) ((A), (B), (C), and (D) magnification ×100, Bar = 100 μm; H-E) ((E) and (F) magnification ×400, bar = 25 μm).

infiltration and weak nuclear pyloric antrum tissue staining of the foci corresponded well with *ex vivo* histology using hematoxylin and eosin staining as reported in other confocal endomicroscopy studies [22].

Fluorescein staining exhibits significant differences ($P < 0.01$) between basal and ischemic groups; however there were a large number of infiltrations for basal conditions that are not related with the normal pyloric antrum tissue evidenced by histology analysis (Figure 5). The staining that best reflects ischemia condition and that can be quantified properly by our algorithm is the combination of fluorescein and acriflavine. In this case, our algorithm made a clear differentiation between normal and inflammatory infiltrations in pyloric antrum tissue as observed in Table 4. Relatively few studies have therefore successfully used this technique for imaging in animal disease models or in humans *in vivo* [22]. On the other hand, targeted fluorescence technology has been thoroughly exploited but has not been linked to *in vivo* microscopic imaging [23].

Impedance parameters increased during ischemia; however there is not a clear effect of staining type in these measurements. It seems like fluorescein alone lightly decreases R_L, but we did not find a clear relationship between impedance parameters and inflamatory infiltration numbers. Nevertheless, there was a relation between impedance increase and cellular damage observed by light microscopy

(Figure 5), indicating that the impedance spectrometer device proposed will be useful to reflect tissue oedema in critically ill patients. Further studies are necessary in order to understand cellular function and interactions in human diseases to improve patient management and treatment. The results demonstrated that the infiltration number calculated is associated with the tissue injury observed histologically. This method could be a quick evaluation for the tissue status that realizes the concept of electrical biopsy [24].

Conflict of Interests

The authors declare that they have no conflict of interests associated with this paper.

Acknowledgments

The authors wish to thank Saul Gaona for technical assitance. This work was developed in the National Center for Medical Instrumentation and Imaging Research, and the Tissular Neurobiology Laboratory at Autonomous Metropolitan University in Mexico City.

References

[1] G. Gutierrez, H. D. Reines, and M. E. Wulf-Gutierrez, "Clinical review: hemorrhagic shock," *Critical Care*, vol. 8, no. 5, pp. 373–381, 2004.

[2] A. Dubin, E. Estenssoro, G. Murias et al., "Effects of hemorrhage on gastrointestinal oxygenation," *Intensive Care Medicine*, vol. 27, no. 12, pp. 1931–1936, 2001.

[3] S. A. Oakes, J. T. Opferman, T. Pozzan, S. J. Korsmeyer, and L. Scorrano, "Regulation of endoplasmic reticulum Ca^{2+} dynamics by proapoptotic BCL-2 family members," *Biochemical Pharmacology*, vol. 66, no. 8, pp. 1335–1340, 2003.

[4] R. G. Boutilier, "Mechanisms of cell survival in hypoxia and hypothermia," *Journal of Experimental Biology*, vol. 204, no. 18, pp. 3171–3181, 2001.

[5] G. Gutierrez, H. Bismar, D. R. Dantzker, and N. Silva, "Comparison of gastric intramucosal pH with measures of oxygen transport and consumption in critically ill patients," *Critical Care Medicine*, vol. 20, no. 4, pp. 451–457, 1992.

[6] M. M. Levy, W. L. Macias, J. A. Russell et al., "Failure to improve during the first day of therapy is predictive of 28-day mortality in severe sepsis," *Chest*, vol. 124, supplement, p. 120S, 2003.

[7] J. Arnold, J. Hendriks, C. Ince, and H. Bruining, "Tonometry to assess the adequacy of splanchnic oxygenation in the critically ill patient," *Intensive Care Medicine*, vol. 20, no. 6, pp. 452–456, 1994.

[8] D. N. Granger, "Role of xanthine oxidase and granulocytes in ischemia-reperfusion injury," *American Journal of Physiology*, vol. 255, no. 6, p. 24/6, 1988.

[9] G. Gutierrez, F. Palizas, G. Doglio et al., "Gastric intramucosal pH as a therapeutic index of tissue oxygenation in critically ill patients," *The Lancet*, vol. 339, no. 8787, pp. 195–199, 1992.

[10] A. H. Kyle, C. T. O. Chan, and A. I. Minchinton, "Characterization of three-dimensional tissue cultures using electrical impedance spectroscopy," *Biophysical Journal*, vol. 76, no. 5, pp. 2640–2648, 1999.

[11] E. Gersing, "Impedance spectroscopy on living tissue for determination of the state of organs," *Bioelectrochemistry and Bioenergetics*, vol. 45, no. 2, pp. 145–149, 1998.

[12] J. Flores, D. R. DiBona, C. H. Beck, and A. Leaf, "The role of cell swelling in ischemic renal damage and the protective effect of hypertonic solute," *Journal of Clinical Investigation*, vol. 51, no. 1, pp. 118–126, 1972.

[13] B. Rigaud, L. Hamzaoui, N. Chauveau, M. Granie, J.-P. Scotto Di Rinaldi, and J.-P. Morucci, "Tissue characterization by impedance: a multifrequency approach," *Physiological Measurement*, vol. 15, no. 2A, pp. A13–A20, 1994.

[14] A. Ivorra, M. Genescà, A. Sola et al., "Bioimpedance dispersion width as a parameter to monitor living tissues," *Physiological Measurement*, vol. 26, no. 2, pp. S165–S173, 2005.

[15] S. Othman and E. Sacristan, "Complex impedance spectrometer using parallel demodulation and digital conversion," United States Patent US 6,970,738 B1, 2005.

[16] E. Sacristan, "Impedance spectroscopy system and catheter for ischemic mucosal damage monitoring in hollow viscous organs," United States Patent US 6,882,879 B2, 2005.

[17] N. E. Beltran, J. J. M. De Folter, M. M. Godinez, and E. Sacristan Rock, "Systems and methods for characteristic parameter estimation of gastric impedance spectra in humans," United States Patent US 2010/0268110 A1, 2010.

[18] E. B. Prophet, B. Mills, J. B. Arrington, and L. H. Sobin, *AFIP Laboratory Methods in Histotechnology*, American Registry of Pathology, 1992.

[19] J. K. Presnell and M. P. Schreibman, *Animal Techniques*, The John Hopkins University Press, Baltimore, Md, USA, 1997.

[20] N. E. Beltran, G. Sanchez-Miranda, M. Godinez, U. Diaz, and E. Sacristan, "Gastric impedance spectroscopy in elective cardiovascular surgery patients," *Physiological Measurement*, vol. 27, no. 3, pp. 265–277, 2006.

[21] N. E. Beltran, G. Sanchez-Miranda, M. M. Godinez, U. Diaz, and E. Sacristan, "The predictive value of gastric reactance for postoperative morbidity and mortality in cardiac surgery patients," *Physiological Measurement*, vol. 31, no. 11, pp. 1423–1436, 2010.

[22] M. Goetz, C. Footner, E. Schirrmacher et al., "*In vivo* confocal real-time mini-microscopy in animal models of human inflammatory and neoplastic diseases," *Endoscopy*, vol. 39, no. 4, pp. 350–356, 2007.

[23] R. Weissleder, C.-H. Tung, U. Mahmood, and A. Bogdanov Jr., "*In vivo* imaging of tumors with protease-activated near-infrared fluorescent probes," *Nature Biotechnology*, vol. 17, no. 4, pp. 375–378, 1999.

[24] Y.-J. Huang, E.-Y. Huang, and K.-S. Cheng, "The correlation between extracellular resistance by electrical biopsy and the ratio of optical low staining area in irradiated intestinal tissues of rats," *Biomed Eng Online*, vol. 12, p. 23, 2013.